Universität Hamburg

DER FORSCHUNG | DER LEHRE | DER BILDUNG

Ab initio Strong Light-Matter Theoretical Framework for Phenomena in Non-relativistic Quantum Electrodynamics

Dissertation zur Erlangung des Doktorgrades an der Fakultät für Mathematik, Informatik und Naturwissenschaften, Fachbereich Physik, der Universität Hamburg

vorgelegt von

Davis M. Welakuh

Hamburg, Germany
May 2021

MAX-PLANCK-GESELLSCHAFT

Max-Planck-Institut für
Struktur und Dynamik der Materie

Gutachter/innen der Dissertation:	Prof. Dr. Angel Rubio Prof. Dr. Klaus Sengstock
Zusammensetzung der Prüfungskommission:	Prof. Dr. Angel Rubio Dr. Michael Ruggenthaler Prof. Dr. Klaus Sengstock Prof. Dr. Michael Potthoff Prof. Dr. Paola Gori-Giorgi
Vorsitzende/r der Prüfungskommission:	Prof. Dr. Michael Potthoff
Datum der Disputation:	08.06.2021
Vorsitzender Fach-Promotionsausschusses Physik:	Prof. Dr. Günter Hans Walter Sigl
Leiter des Fachbereichs Physik:	Prof. Dr. Wolfgang Hansen
Dekan der Fakultät MIN:	Prof. Dr. Heinrich Graener

EIDESSTATTLICHE VERSICHERUNG/DECLARATION

Hiermit versichere ich an Eides statt, die vorliegende Dissertationsschrift selbst verfasst und keine anderen als die angegebenen Hilfsmittel und Quellen benutzt zu haben.

Die eingereichte schriftliche Fassung entspricht der auf dem elektronischen Speichermedium.

Die Dissertation wurde in der vorgelegten oder einer ähnlichen Form nicht schon einmal in einem früheren Promotionsverfahren angenommen oder als ungenügend beurteilt.

Hamburg, Germany, May 2021

Davis M. Welakuh

"The future is predetermined by the character of those who shape it."

— Oma Desala & Davos, Stargate SG-1 and Atlantis

"There, you see? Stress. Stress is the fertilizer of creativity. Now let's play some darts."

— Jonas Hodges, 24 TV Series

Dedicated to the loving memory of NDEFRU BIMAMA HEDWIG.

ABSTRACT

In condensed matter physics, material science and quantum chemistry, recent experimental progress has laid the foundation to control and alter the properties of matter at will by coupling strongly to individual photons or even just the vacuum fluctuations of the electromagnetic field. This is usually realized by changing the photonic environment and with this the photon field, e.g., by using high-Q optical cavities or plasmonic nanostructures to which the matter system is then strongly coupled to. The ensuing strong coupling brings about novel states of matter with hybrid light-matter character known as polaritons. These hybridized systems allow to control material properties and chemistry in an unprecedented way such as altering chemical reactions, room-temperature polariton lasing, enhance charge and energy transfer, to name but a few. To better understand these intriguing effects, numerous theoretical studies have been performed, most of which are based on simple approximate models. These simplified models capture correctly the main features of the emerging novel physics but overlook important details pertaining to the coupled system. To overcome these restrictions, ab-initio methods such as quantum electrodynamical density-functional theory (QEDFT) that treat matter and photons on the same quantized footing have recently been developed. This method allow an in-depth modeling of the light-matter system from first principles. However, the application of these theoretical methods is so far still limited. This is, on the one hand, due to missing efficient numerical schemes to solve the resulting equations. On the other hand, it remains unclear in which cases a full ab-initio simulation would provide novel insights and uncovers new effects.

This work presents a first-principles linear-response formulation of QEDFT that captures the hallmark of strong light-matter coupling (Rabi splitting between polaritons) usually identified in linear spectroscopy. Crucial in the linear-response formulation is the stability of matter. While in the usual models this issue is irrelevant, we show how answering this question can shed light on the long-lasting debate about the existence of a Dicke superradiant phase. We extend three linear-response methods for matter-only systems to the linear-response framework of QEDFT that makes the problem computationally feasible. These methods are shown to be numerically equivalent and capture excited-states properties of strongly coupled light-matter systems which is identified by the emergence of polaritonic peaks not only in the matter spectrum but also the photonic spectrum. These strong coupling features are not captured by standard many-body methods that discard the photon degrees of freedom. This opens new possibilities to investigate different situations with complex systems coupled to many photon modes such as non-perturbative first-principles calculation of lifetimes of excited-states, beyond the single molecule limit and dissipation, and Lorentz to Fano transition of lineshapes in strong coupling. Making QEDFT practical now provides a route to analyze and propose experiments at the interface between quantum chemistry, nanoplasmonics and quantum optics and present novel observables that describes the strong coupling between light and matter. Beyond the linear response, this work also highlights new avenues of the down-conversion process that

become available in ab-initio simulations of coupled light-matter systems. By changing the photonic environment in an experimentally feasible way, we can engineer hybrid light-matter states that enhance at the same time the efficiency of the down-conversion process and the non-classicality of the generated photons. In addition, we show that this also causes the down-conversion to occur at earlier times with potential to overcome detrimental decoherence effects. By coupling the signal modes to virtual and polaritonic states we propose an inverse (high-) harmonic generation that acts as an N-photon gun (source). Such a cavity-controlled down-conversion process will not be captured using standard non-linear optics approach since the field is treated classically and only as an external perturbation and with a quantum optics approach, it becomes less accurate due to the simplification of the matter subsystem to a few "relevant" energy levels.

ZUSAMMENFASSUNG

Jüngste experimentelle Fortschritte in der Physik der kondensierten Materie, den Materialwissenschaften und der Quantenchemie haben den Grundstein gelegt, die Eigenschaften der Materie nach Belieben mittels starker Kopplung an einzelne (sogar oftmals nur virtuelle) Photonen zu steuern und zu verändern. Dies wird durch eine Änderung des photonischen Vakuums realisiert, z.B. durch Verwendung von optischen Hohlräumen oder plasmonischen Nanostrukturen. Die daraus resultierende starke Kopplung erzeugt neuartige Materienzustände mit hybridem Licht-Materie-Charakter. Die zugehörigen Quasiteilchen werden Polaritonen genannt. Diese hybridisierten Systeme ermöglichen die Steuerung von Material- und chemischen Eigenschaften. So können chemische Reaktionen verändert, Polaritonenlaser bei Raumtemperatur erzeugt, und eine Verbesserung der Ladungs- und Energie-Übertragung erreicht werden, um nur einige wenige Beispiele zu nennen. Um diese faszinierenden Effekte besser zu verstehen, wurden zahlreiche theoretische Studien durchgeführt, von denen die meisten auf einfachen Näherungsmodellen basieren. Diese vereinfachten Modelle beschreiben die Hauptmerkmale der neuartigen Effekte korrekt, übersehen jedoch wichtige Details. Um diese Einschränkungen zu überwinden, wurden kürzlich Ab-Initio-Methoden wie die quanten-elektrodynamische Dichtefunktionaltheorie (QEDFT) entwickelt, die Materie und Photonen auf gleicher Weise quantenmechanisch behandeln. Diese Methoden ermöglichen eine grundlegende Modellierung des gekoppelten Licht-Materie-Systems. Die Anwendbarkeit dieser theoretischen Methode ist jedoch bislang noch begrenzt. Dies ist einerseits auf fehlende effiziente numerische Lösungsmethoden zurückzuführen. Andererseits bleibt unklar, in welchen Fällen eine vollständige Ab-Initio-Simulation neue Erkenntnisse liefern und neue Effekte aufdecken würde.

In dieser Arbeit wird eine effiziente Lineare-Antwort-Formulierung der QEDFT eingeführt, die lineare spektroskopische Observablen der starken Licht-Materie-Kopplung exakt beschreiben kann. Entscheidend für diese Formulierung ist die Stabilität der Materie. Während dieses Problem in den üblichen Modellen irrelevant ist, zeigen wir, wie die Beantwortung dieser Frage neue Einsichten zur langanhaltenden Debatte über die Existenz einer Dicke-Superradianten-Phase bringt. Wir erweiterten drei Lineare-Antwort-Methoden der Quantenmechanik in das quantenelektrodynamische Setting, welche stark gekoppelte Licht-Materie-Systeme numerisch lösbar machen. Es wird gezeigt, dass diese Methoden numerisch äquivalent sind, und die Eigenschaften angeregter Zustände stark gekoppelter Licht-Materie-Systeme erfassen. Solche Situationen zeichnen sich durch das Auftreten eines Rabi-Splittings nicht nur im Materiespektrum, sondern auch im photonischen Spektrum aus. Diese Merkmale werden nicht durch Standard-Vielteilchenmethoden erfasst, bei denen die Photonenfreiheitsgrade nicht behandelt werden. Dies eröffnet neue Möglichkeiten zur Untersuchung komplexer Systeme, die an viele Photonenmoden gekoppelt sind. Zum Beispiel erhält man direkt Zugang zur Lebensdauer angeregter Zustände jenseits der Einzelmolekülgrenze, sowie die direkte Beschreibung von Dissipation und der Veränderung der Linienform bei starker Kopplung. Die praktische Umsetzung von QEDFT bietet

nun die Möglichkeit, Experimente an der Schnittstelle zwischen Quantenchemie, Nanoplasmonik und Quantenoptik zu analysieren und vorzuschlagen. Außerdem können neuartige Observablen, welche die Kopplung zwischen Licht und Materie beschreiben, berechnet werden. Über die Lineare-Antwort-Theorie hinaus werden in dieser Arbeit auch neue Wege zur Erzeugung parametrischer Fluoreszenz aufgezeigt, die in Ab-Initio-Simulationen nun zugänglich sind. Indem wir das elektromagnetische Vakuum auf experimentell realisierbare Weise verändern, können wir hybride Licht-Materie-Zustände erzeugen, die gleichzeitig die Effizienz des Prozesses und die Nichtklassizität der erzeugten Photonen erhöhen. Darüber hinaus zeigen wir, dass der Fluoreszenzprozess zu einem früheren Zeitpunkt erfolgt. Dies macht es möglich durch starke Kopplung gleichzeitig unerwünschte Dekohärenzprozesse zu unterbinden. Durch Kopplung der Signalmoden zu virtuellen und polaritonischen Zuständen schlagen wir eine inverse (hoch-)harmonische Erzeugung von Photonen vor. Dieser Prozess kann als N-Photonen Quelle fungieren. Solche hohlraumgesteuerten, parametrischen Flureszenzprozesse scheinen eine Ab-Initio-Behandlung zu benötigen, denn Standard-Ansätze aus der Nicht-Linearen-Optik sowie der Quantenoptik führen zu ungenauen oder falschen Vorhersagen, wenn man sie mit den Ab-Initio-Rechnungen vergleicht.

CONTENTS

Part I

INTRODUCTION

1 INTRODUCTION

In recent years, tremendous experimental advances have made it possible to study light-matter interactions in the strong and ultra-strong coupling regime. In such experiments, changing the photonic environment, e.g., by using a high-Q optical cavity or plasmonic device changes the photon field which leads to modification of matter properties as new hybrid light-matter states (polaritons) emerge. In such situations of strong light-matter interactions, novel physical effects can be observed such as modification of chemical landscapes [1], enhanced charge and energy transfer [2, 3], strong enhancement in the charge-carrier mobility for organic semiconductors [4], among others. These experimental observations highlight that discarding the photon degrees when studying chemical and physical properties of many-body systems is not always allowed and might miss important effects. Interestingly enough, the interplay between the basic constituents of matter (electrons and effective nuclei) can be accessible at room temperature and under ambient conditions. This makes strong light-matter interactions an interesting avenue for applications in quantum technologies.

So far, theoretical methods to account and predict these experimental observations were dominated by purpose-built phenomenological models (that often consider just a few energy levels of the matter subsystem). Although these simplified models usually applied to the study of strong coupling of atoms or molecules capture most of the relevant physical processes [5], there are still strong discrepancies when compared to experiments [6]. In such situations, a more general description that treats light and matter interaction on an equal footing from first-principles becomes preferable since it provides a detailed understanding of effects in the strong and ultra-strong coupling regime. Such first-principle descriptions can be based on the basic Hamiltonian of non-relativistic QED, i.e., the Pauli-Fierz Hamiltonian [7, 8]. In this setting, a solution of the Schrödinger equation becomes impossible to obtain due to in principle infinite (mode) degrees of freedom of the coupled light-matter system. A similar problem is already encountered in matter-only quantum mechanics, where the number of degrees of freedom can also become very large. The reason for this difficulty in obtaining a solution is best described by the exponential wall of many-body problems [9]. Many-body problem as used here refers to the problem of predicting the properties of a system of many quantum particles (such as electrons and nuclei) from first-principles. As an exact solution of the Schrödinger equation for large systems has proven almost impossible to obtain, physicists, chemists and other scientists in several disciplines have resorted to methods that circumvent the quest for an exact solution and redefine the problem in several different ways. One thing the approaches have in common is that they are often solved in an approximate way. A few prominent methods usually employed in the study of many-body problems are Hartree-Fock theory [10], configuration-interaction theory [10], coupled cluster [11] and density-functional theory (DFT) [9]. These methods however are not applicable to the problem of strong light-matter coupled systems. Therefore, they

need to be extended to include the photon degrees. Two possible ab-initio methods for describing strong light-matter interaction are quantum electrodynamical density-functional theory (QEDFT) [12–14] and quantum electrodynamics coupled cluster theory (QED-CC) [15, 16]. These recently introduced methods have both been applied to study ground-state and excited-state properties of strongly coupled light-matter systems, for example, in Refs. [17–20] for QEDFT and Refs. [15, 16, 21] for QED-CC. QED-CC is limited to small systems and only a few photon modes. QEDFT on the other hand, can in principle treat large complex matter systems coupled to arbitrarily many but finite number of modes and this general framework include in a particular case, features of QED-CC. So far, QEDFT misses efficient numerical approaches that make it easily applicable. For the functional development of quantum electrodynamical density-functional theory (QEDFT) that approximates the electron-photon correlations, only one functional has been proposed so far in Refs. [17, 22], which is a generalization of the optimized effective potential (OEP) approach to standard DFT. This functional needs further development since it does not perform well in the ultra-strong coupling regime. As with regard to the phenomenological models, it remains unclear where it becomes necessary to employ ab-initio methods and which new possibilities arise.

The goal of this thesis is to present a practical first-principle description and implementation of coupled light-matter systems that highlights the importance of a quantized treatment of both light and matter. Due to this level of theory, we highlight new possibilities that become accessible in strong light-matter coupling. First, we consider the linear-response since via linear spectroscopy the hallmark of strong coupling (Rabi splitting between polaritonic states) becomes accessible. We formulate a linear-response theory in non-relativistic QED and show new responses and response functions that arise in this setting. We make QEDFT practical by reformulating the linear-response theory of non-relativistic QED within the framework of QEDFT. We extend three linear-response methods of time-dependent density-functional theory (TDDFT) within the framework of QEDFT that allows for practical calculations of the responses and response functions. These methods are shown to be equivalent and capture changes in the excited-states properties of strongly coupled light-matter systems and also compute novel observables that become accessible at this level of theory. These strong coupling features are not captured by standard many-body methods that discard the photon degrees of freedom. Using the linear-response formulation of QEDFT, we highlight changes in the quantum Maxwell's equation due to the self-consistent interaction between light and matter. This opens new possibilities to investigate different situations with complex systems coupled to many photon modes such as first-principles computation of lifetimes of electronic and polaritonic states non-perturbatively, beyond single-molecule coupling and dissipation and transition from Lorentzian to Fano lineshapes. The methods developed here can solve many complex molecular systems coupled to photons [23]. Also, we consider beyond first-order (non-linear) processes of light-matter interactions. We also highlight new possibilities in non-linear processes that become accessible from an ab-initio perspective when light and matter are treated on an equal level of theory. This is done by considering the photon down-conversion process which is particularly of importance due to the ever growing range of applications, e.g., in quantum-information processing and science. We highlight how strong light-matter coupling allows to define novel polariton-

mediated photon sources. In this case, we propose how to achieve an N-photon gun (source) by coupling the signal modes to virtual (and polariton) states that serve as new down-conversion pathways. The efficiency of the N-photon down-conversions can be controlled by changing the photonic environment in an experimentally realizable way. For example, increasing the coupling strength increases the yield of the down-conversion process. We also show that by increasing the coupling strength the down-conversion can be pushed to occur at earlier times potentially overcoming decoherence effects due to the environment. Such a cavity-controlled down-conversion process will not be captured using standard non-linear optics approach since the field is treated only as an external perturbation and with a quantum optics approach, it becomes less accurate due to the simplification of the matter subsystem to a few "relevant" energy levels.

This thesis is divided into five chapters. In Chapter 2, we present the general theoretical frameworks applied in this thesis. It begins by discussing non-relativistic QED as defined by the minimal-coupling Pauli-Fierz Hamiltonian. Approximations to the Pauli-Fierz Hamiltonian that lead to the long-wavelength approximation and to the Maxwell-Schrödinger approximation and eventually the many-body problem of matter-only systems are presented. We also discuss the general framework of linear-response theory and present DFT, TDDFT, ground-state QEDFT and the time-dependent setting of QEDFT. The next chapters are the main results of the thesis. In chapter 3, the focus is on the general framework of linear response in non-relativistic QED. To set the stage, we first show that the dipole self-energy term, which is consistently disregarded in phenomenological models, is necessary for having a well defined (variationally accessible) ground-state. The stability of matter can shed light on the existence of the elusive superradiant phase transition of light-matter systems. The chapter proceeds to outline novel response functions in this setting and the changes in Maxwell's equations made evident by the framework of QEDFT. We then present three linear response methods formulated within QEDFT that allow for practical calculation of excited-states properties of strongly coupled light-matter systems. We then show what this framework now allows beyond what is possible with standard many-body methods or standard light-matter models. As examples, we show first-principles non-perturbative computation of lifetimes of electronic and polaritonic states, beyond the single molecule limit and dissipation and how to achieve a transition from Lorentzian to Fano lineshapes by strongly coupling to the continuum. In chapter 4, we present new possibilities in non-linear processes that become accessible from an ab-initio perspective when light and matter are treated on an equal level of theory. This is shown for a paradigmatic case of non-linear optics and quantum optics for photon down-conversion processes. We first present the non-degenerate parametric down-conversion and consider different possible ways of pumping the system and compare common approaches to study the down-conversion process. Next, we present the degenerate parametric down-conversion where we discuss various optimizations of the setup to boost the efficiency of the down-conversion as well as the non-classical properties. We later present a novel polariton-mediated down-conversion for realizing an N-photon gun (source). The summary of all findings of this thesis, a conclusion, and an outlook of future work are given in chapter 5.

Part II

THEORETICAL FOUNDATIONS

2

MATTER-PHOTON COUPLING IN NON-RELATIVISTIC QUANTUM ELECTRODYNAMICS

The complete account of how matter and light interacts is governed by QED. This theory describes in great detail all phenomena involving how electrically charged particles (such as electrons and positrons) interact via the exchange of photons [24]. In this description of the interaction, all the constituents of matter (e.g. electrons) and the electromagnetic field (photons) behave quantum mechanically. Therefore, QED provides a general framework that treats matter and electromagnetic degrees of freedom on an equal quantized footing. The success of QED lies in its extremely accurate predictions of observable quantities like the anomalous magnetic moment of the electron and the Lamb shift of the energy levels of hydrogen [25]. As this thesis mainly investigates changes in the optical and electronic properties of electron-photon coupled systems, the focus is on the low-energy regime of QED. Specifically, the focus is on non-relativistic QED which is applicable within the typical energy and time scales of atomic, molecular and solid-state systems [8]. This description does not take into account the quantum features of the nuclei, but rather treats them within the Born-Oppenheimer approximation [26]. Note that the quantum nature of the nuclei can also be treated in non-relativistic QED [27]. In this chapter we briefly recapitulate the basics of this general setting and discuss all the necessary results that become important in the later chapters of the thesis.

In the low-energy regime, the full QED Hamiltonian can be simplified to the Pauli Hamiltonian describing the evolution of charged particles in spinor representation, which are coupled via the total charge-current operator to the quantized photon field [8, 28, 29]. For a system (atom, molecule or solid) of N_e electrons with clamped nuclei, the Pauli-Fierz Hamiltonian [7] is

$$\hat{H}_{\mathrm{PF}}(t) = \sum_{i=1}^{N_e} \frac{1}{2m} \left[\hat{\boldsymbol{\sigma}}_i \cdot \left(\hat{\mathbf{p}}_i - e\hat{\mathbf{A}}_{\mathrm{tot}}(\mathbf{r}_i, t)\right)\right]^2 + \hat{W}_{ee} + \hat{V}_{eN} + \hat{H}_{pt}\,, \tag{1}$$

where the dependence of the Pauli-Fierz Hamiltonian on t indicates a possible explicit time dependence. Here, $\hat{\boldsymbol{\sigma}}_i$ is a vector of the usual Pauli matrices, reflecting the spin one-half character of the electrons. The positive parameter m is the bare mass and e is the charge of the electron. The kinetic energy, Coulomb potential and the external potential from the nuclei are respectively given as follows [1]

$$\hat{T}_e = \sum_{i=1}^{N_e} \frac{1}{2m} \hat{\mathbf{p}}_i^2\,, \tag{2}$$

$$\hat{W}_{ee} = \frac{1}{4\pi\epsilon_0} \sum_{i=1}^{N_e} \sum_{j>i}^{N_e} \frac{e^2}{|\mathbf{r}_i - \mathbf{r}_j|}\,, \tag{3}$$

$$\hat{V}_{eN} = -\frac{1}{4\pi\epsilon_0} \sum_{i=1}^{N_e} \sum_{j=1}^{N_n} \frac{Z_j e^2}{|\mathbf{r}_i - \mathbf{R}_j|}\,. \tag{4}$$

1 Throughout this thesis, the SI units are used, unless stated otherwise.

Here, Z_j is the atomic number of the N_n nuclei which carry a positive charge of $(Z_j e)$ and ϵ_0 is the permittivity of free space. The electrons are described by the electronic coordinates, $\mathbf{r}_j$, the nuclei by the coordinates, $\mathbf{R}_j$, and the momentum operator of the electrons is $\hat{\mathbf{p}}_i = -i\hbar\boldsymbol{\nabla}_i$ with $\boldsymbol{\nabla}$ and $\hbar$ being the gradient operator and the reduced Planck constant, respectively. Together with the electronic coordinates, the momentum operator satisfies the commutation relations given as $\left[\hat{\mathbf{r}}_i, \hat{\mathbf{p}}_j\right] = i\hbar\delta_{ij}$, $\left[\hat{\mathbf{r}}_i, \hat{\mathbf{r}}_j\right] = \left[\hat{\mathbf{p}}_i, \hat{\mathbf{p}}_j\right] = 0$. The Hamiltonian for the electromagnetic field is the integral of the energy density over a volume given by

$$\hat{H}_{pt} = \frac{\epsilon_0}{2} \int \mathrm{d}^3\mathbf{r} \left[\hat{\mathbf{E}}_\perp^2(\mathbf{r}) + c^2\hat{\mathbf{B}}^2(\mathbf{r})\right], \tag{5}$$

where $\hat{\mathbf{E}}_\perp(\mathbf{r})$ represents the quantized transverse electric field and $\hat{\mathbf{B}}(\mathbf{r})$ is the magnetic field. The quantized electromagnetic field can alternatively be described by individual quantum harmonic oscillators for each allowed mode and polarization. This form of representation of the quantized electromagnetic field will be derived below. The total transversal vector potential is the sum of the following two terms $\hat{\mathbf{A}}_{\text{tot}}(\mathbf{r}, t) = \hat{\mathbf{A}}(\mathbf{r}) + \hat{\mathbf{A}}_{\text{ext}}(\mathbf{r}, t)$ which are the quantized internal transversal photon degrees $\hat{\mathbf{A}}(\mathbf{r})$ as well as the possibility for a external vector potential $\hat{\mathbf{A}}_{\text{ext}}(\mathbf{r}, t)$. The minimal-coupling of Eq. (1) of the Pauli-Fierz Hamiltonian is given in Coulomb gauge, i.e., $\boldsymbol{\nabla} \cdot \hat{\mathbf{A}}_{\text{tot}}(\mathbf{r}, t) = 0$ where the vector potential is purely transverse. The form of the electric field, magnetic field and vector potential is presented in Sec. 2.1.

To describe the dynamics of electrons coupled to photons in the non-relativistic limit of QED described by Eq. (1), one has to solve the time-dependent Schrödinger equation [30] which is an evolution equation of the form

$$i\hbar\frac{\partial}{\partial t}|\Psi(t)\rangle = \hat{H}(t)|\Psi(t)\rangle\,, \tag{6}$$

for a given initial state $|\Psi(t=0)\rangle$. The time-dependent (normalized) wavefunction $|\Psi(t)\rangle$ contains all information about the properties of the system. Solving Eq. (6) gives explicitly access to the wavefunction from which all physical observables of the coupled system can be computed through the expectation value of an operator representing the desired observable. Unfortunately, solving the Schrödinger equation for realistic many-body systems exactly is very hard to accomplish.

Also, for static or equilibrium situations where the Hamiltonian is time-independent, i.e. $\hat{H}(t) = \hat{H}$, to obtain the ground-state and all excited states that corresponds to this static Hamiltonian, equation (6) can be cast into an eigenvalue problem. The resulting equation known as the time-independent Schrödinger equation is of the following form

$$\hat{H}|\Psi_n\rangle = E_n|\Psi_n\rangle\,. \tag{7}$$

Here, E_n are the eigenvalues and $|\Psi_n\rangle$ the eigenstates of the finite system coupled to the photon field. It is of particular importance that the time-independent Hamiltonian is bounded from below because this is needed to allow for the existence of a ground-state of the coupled system. Hamiltonians that are bounded from below satisfy a variational principle. The Rayleigh-Ritz minimal principle dictates that $\langle\Psi|\hat{H}|\Psi\rangle \geq \langle\Psi_0|\hat{H}|\Psi_0\rangle = E_0$ where E_0 is the ground-state energy and $|\Psi_0\rangle$ is the ground-state

wavefunction. Yet again, solving Eq. (7) is not realizable except for small systems. It should be noted that already solving Eq. (7) for an electron-only Hamiltonian beyond simple models has proven difficult. Therefore, the addition of the electromagnetic field as a dynamical part of the coupled electron-photon system makes the problem even more difficult. This led to the development of many different methods that circumvent solving the Schrödinger equation by employing different reformulations of the original Schrödinger problem [10]. Besides density-functional methods, which we will discuss in Sec. 2.5 in more detail, there are also Green's function [31] and reduced density-matrix reformulations [32] available.

Since the quantized electromagnetic field is treated in this thesis as a dynamical part of the coupled system that modifies its properties, it is relevant to outline the quantization procedure of the field and how it couples to the matter subsystem.

2.1 THE MICROSCOPIC FIELD EQUATIONS

In classical physics the microscopic Maxwell equations for the electromagnetic fields in a medium are expressed in differential form as

$$\boldsymbol{\nabla} \cdot \mathbf{E}(\mathbf{r}, t) = \frac{1}{\epsilon_0} \rho(\mathrm{r}, t) \,, \tag{8}$$

$$\boldsymbol{\nabla} \cdot \mathbf{B}(\mathbf{r}, t) = 0 \,, \tag{9}$$

$$\boldsymbol{\nabla} \times \mathbf{E}(\mathbf{r}, t) = -\frac{\partial}{\partial t} \mathbf{B}(\mathbf{r}, t) \,, \tag{10}$$

$$\boldsymbol{\nabla} \times \mathbf{B}(\mathbf{r}, t) = \mu_0 \mathbf{J}(\mathbf{r}, t) + \epsilon_0 \mu_0 \frac{\partial}{\partial t} \mathbf{E}(\mathbf{r}, t) \,, \tag{11}$$

where the sources are the electric charge density $\rho(\mathrm{r}, t)$ and the electric current density $\mathbf{J}(\mathbf{r}, t)$. The classical electric field $\mathbf{E}(\mathbf{r}, t)$ and magnetic field $\mathbf{B}(\mathbf{r}, t)$ including the source terms are functions of position $\mathbf{r}$ and time t. The vacuum permittivity ϵ_0 and magnetic permeability μ_0 are related to the speed of light c in vacuum by $c^2 = 1/\epsilon_0 \mu_0$. For the quantization procedure of the classical electromagnetic fields, it is convenient to cast the Maxwell equations in terms of a scalar potential $U(\mathbf{r}, t)$ and a vector potential $\mathbf{A}(\mathbf{r}, t)$. By using Eqs. (9) and (10), the electric and magnetic fields are expressed in terms of the scalar and vector potential as

$$\mathbf{E}(\mathbf{r}, t) = -\boldsymbol{\nabla} U(\mathbf{r}, t) - \frac{\partial}{\partial t} \mathbf{A}(\mathbf{r}, t) \,, \tag{12}$$

$$\mathbf{B}(\mathbf{r}, t) = \boldsymbol{\nabla} \times \mathbf{A}(\mathbf{r}, t) \,. \tag{13}$$

The $\mathbf{E}(\mathbf{r}, t)$ and $\mathbf{B}(\mathbf{r}, t)$ fields together with Eq. (8) and (11) lead to the following equations of motion for relating the potentials and sources

$$-\boldsymbol{\nabla}^2 U(\mathbf{r}, t) - \boldsymbol{\nabla} \cdot \left(\frac{\partial}{\partial t} \mathbf{A}(\mathbf{r}, t) \right) = \frac{1}{\epsilon_0} \rho(\mathrm{r}, t) \,, \tag{14}$$

$$\boldsymbol{\nabla} \left(\boldsymbol{\nabla} \cdot \mathbf{A}(\mathbf{r}, t) \right) - \boldsymbol{\nabla}^2 \mathbf{A}(\mathbf{r}, t) + \frac{1}{c^2} \frac{\partial}{\partial t} \boldsymbol{\nabla} U(\mathbf{r}, t) + \frac{1}{c^2} \frac{\partial^2}{\partial t^2} \mathbf{A}(\mathbf{r}, t) = \mu_0 \mathbf{J}(\mathbf{r}, t) \,. \tag{15}$$

2.1.1 GAUGE FREEDOM AND THE COULOMB GAUGE

The magnetic and the electric fields are invariant under the following gauge transformation on the vector and the scalar potentials

$$\mathbf{A}(\mathbf{r},t) \to \mathbf{A}'(\mathbf{r},t) = \mathbf{A}(\mathbf{r},t) + \boldsymbol{\nabla} F(\mathbf{r},t)\,, \tag{16}$$

$$U(\mathbf{r},t) \to U'(\mathbf{r},t) = U(\mathbf{r},t) - \frac{\partial}{\partial t} F(\mathbf{r},t)\,, \tag{17}$$

where $F(\mathbf{r},t)$ is an arbitrary gauge function that should be at least twice differentiable. In addition to the electric and magnetic fields, the Maxwell's equations are equally invariant under the gauge transformations of Eqs. (16) and (17). There is a redundancy in the vector and the scalar potentials, since the same physical fields $\mathbf{E}(\mathbf{r},t)$ and $\mathbf{B}(\mathbf{r},t)$ can be written with many different pairs of potentials $\mathbf{A}(\mathbf{r},t)$ and $U(\mathbf{r},t)$. This redundancy can be reduced by the choice of the gauge condition. In particular, in the Coulomb gauge [29, 33], the vector potential is chosen to be a transverse vector field

$$\boldsymbol{\nabla} \cdot \mathbf{A}(\mathbf{r},t) = 0\,. \tag{18}$$

The Helmholtz decomposition of a vector field allows to identify the transverse and longitudinal parts of a field. That is, any vector field $\mathbf{V}(\mathbf{r},t)$ can be decomposed into a "perpendicular" or transverse part $\mathbf{V}_\perp(\mathbf{r},t)$ and a "parallel" or longitudinal part $\mathbf{V}_\parallel(\mathbf{r},t)$ according to [29]

$$\mathbf{V}(\mathbf{r},t) = \mathbf{V}_\perp(\mathbf{r},t) + \mathbf{V}_\parallel(\mathbf{r},t)\,, \tag{19}$$

which can be defined using the transverse/longitudinal delta-functions $\mathbf{V}_{\perp/\parallel}(\mathbf{r},t) = \int d^3\mathbf{r}'\, \mathbf{V}(\mathbf{r},t)\delta_{\perp/\parallel}(\mathbf{r}-\mathbf{r}')$. The longitudinal tensor-valued delta-function is $\delta_\parallel(\mathbf{r}) = -\boldsymbol{\nabla}\otimes\boldsymbol{\nabla}(4\pi|\mathbf{r}|)^{-1}$ and the transverse part is $\delta_\perp(\mathbf{r}) = \delta(\mathbf{r}) - \delta_\parallel(\mathbf{r})$. Applying the vector decomposition to Eqs. (14) and (15) leads to the following simplifications:

$$\boldsymbol{\nabla}^2 U(\mathbf{r},t) = -\frac{1}{\epsilon_0}\rho(\mathbf{r},t)\,, \tag{20}$$

$$\left(\boldsymbol{\nabla}^2 - \frac{1}{c^2}\frac{\partial^2}{\partial t^2}\right)\mathbf{A}(\mathbf{r},t) = -\mu_0 \mathbf{J}_\perp(\mathbf{r},t)\,. \tag{21}$$

Due to the vector decomposition into a transverse and longitudinal part, in the Coulomb gauge the second term in Eq. (12) is the transverse part of the electric field and the first term the longitudinal part as follows

$$\mathbf{E}_\perp(\mathbf{r},t) = -\frac{\partial}{\partial t}\mathbf{A}(\mathbf{r},t)\,, \tag{22}$$

$$\mathbf{E}_\parallel(\mathbf{r},t) = -\boldsymbol{\nabla} U(\mathbf{r},t)\,. \tag{23}$$

The magnetic field is entirely transverse $\mathbf{B}(\mathbf{r},t) = \mathbf{B}_\perp(\mathbf{r},t)$ according to the Maxwell Eq. (9). The advantage of the Coulomb gauge for the electromagnetic field and its interaction with charges and currents lies in the separations of the field and Maxwell equations into longitudinal and transverse components.

2.1.2 ELECTROMAGNETIC FIELD IN FREE SPACE

If there are no sources of radiation, i.e. no currents $\mathbf{J}_\perp(\mathbf{r},t)$ and charges $\rho(\mathbf{r},t)$, the equation of motion for the vector and scalar potentials of Eqs. (20) and (21) reduce to

$$U(\mathbf{r},t) = 0\,, \tag{24}$$

$$\left(\boldsymbol{\nabla}^2 - \frac{1}{c^2}\frac{\partial^2}{\partial t^2}\right)\mathbf{A}(\mathbf{r},t) = 0\,. \tag{25}$$

Both source free equations (24) and (25) are the starting point for the quantization procedure of the electromagnetic field. The solution of the free-space fields can be obtained by solving Eq. (25) for the Coulomb-gauge vector potential subject to appropriate boundary conditions. Through a separation of variables approach the vector potential can be expanded as a product of a spatial and a temporal part as follows

$$\mathbf{A}(\mathbf{r},t) = \sum_{\mathbf{k}}\sum_{s=1,2}\left(A_{\mathbf{k}s}(t)\mathbf{u}_{\mathbf{k}s}(\mathbf{r}) + A^*_{\mathbf{k}s}(t)\mathbf{u}^*_{\mathbf{k}s}(\mathbf{r})\right). \tag{26}$$

The function $\mathbf{u}_{\mathbf{k}s}(\mathbf{r})$ is the mode function which contains all the spatial dependence of the field and s represents the two transversal polarization directions that are perpendicular to the direction of propagation $\mathbf{k}$. The mode function $\mathbf{u}_{\mathbf{k}s}(\mathbf{r})$ and temporal function $A_{\mathbf{k}s}(t)$ satisfy the following differential equations respectively

$$\left(\boldsymbol{\nabla}^2 + \frac{\omega_k^2}{c^2}\right)\mathbf{u}_{\mathbf{k}s}(\mathbf{r}) = 0\,, \tag{27}$$

$$\left(\frac{\partial^2}{\partial t^2} + \omega_k^2\right)A_{\mathbf{k}s}(t) = 0\,, \tag{28}$$

and the latter have the solution $A_{\mathbf{k}s}(t) = A_{\mathbf{k}s}e^{-i\omega_k t}$. The frequency ω_k and the wavevector $\mathbf{k}$ are related through the dispersion relation $\omega_k = c|\mathbf{k}|$. The mode functions are also required to satisfy the transversality condition and form a complete orthonormal set respectively as

$$\boldsymbol{\nabla}\cdot\mathbf{u}_{\mathbf{k}s}(\mathbf{r}) = 0, \quad \int_V d^3\mathbf{r}\;\mathbf{u}^*_{\mathbf{k}s}(\mathbf{r})\cdot\mathbf{u}_{\mathbf{k}'s'}(\mathbf{r}) = \delta_{\mathbf{k}\mathbf{k}'}\delta_{ss'}\,, \tag{29}$$

where V is the quantization volume. Using Eqs. (13) and (22), the electric and magnetic fields are expressed as

$$\mathbf{E}_\perp(\mathbf{r},t) = \sum_{\mathbf{k}}\sum_{s=1,2} i\omega_k\left(A_{\mathbf{k}s}e^{-i\omega_k t}\mathbf{u}_{\mathbf{k}s}(\mathbf{r}) - A^*_{\mathbf{k}s}e^{i\omega_k t}\mathbf{u}^*_{\mathbf{k}s}(\mathbf{r})\right), \tag{30}$$

$$\mathbf{B}(\mathbf{r},t) = \sum_{\mathbf{k}}\sum_{s=1,2}\left(A_{\mathbf{k}s}e^{-i\omega_k t}\boldsymbol{\nabla}\times\mathbf{u}_{\mathbf{k}s}(\mathbf{r}) + A^*_{\mathbf{k}s}e^{i\omega_k t}\boldsymbol{\nabla}\times\mathbf{u}^*_{\mathbf{k}s}(\mathbf{r})\right). \tag{31}$$

The mode functions depend on the boundary conditions of the physical volume under consideration, for example, periodic boundary conditions corresponding to traveling wave modes or conditions appropriate for a perfectly conducting rectangular box which leads to standing waves.

For the transition to the quantum theory of electromagnetic fields, the Schrödinger picture in which the operators become time-independent is employed. The electromagnetic field can be quantized by associating a quantum mechanical harmonic oscillator with each mode $\mathbf{k}s$ of the radiation field [34]. This proceeds by promoting the field variable amplitude to a quantum operator:

$$A_{\mathbf{k}s} \to \sqrt{\frac{\hbar}{2\epsilon_0\omega_k}}\,\hat{a}_{\mathbf{k}s}\,, \quad \text{and} \quad A^*_{\mathbf{k}s} \to \sqrt{\frac{\hbar}{2\epsilon_0\omega_k}}\,\hat{a}^\dagger_{\mathbf{k}s}\,.$$

Two cases are considered here for the quantization of the electromagnetic fields, the periodic and zero boundary conditions.

2.1.3 PERIODIC BOUNDARY CONDITION

The plane wave mode functions appropriate to a cubical volume of side L can be written as [35–37]

$$\mathbf{u}_{\mathbf{k}s}(\mathbf{r}) = \frac{1}{\sqrt{V}} e^{-i\mathbf{k}\cdot\mathbf{r}}\mathbf{e}_{\mathbf{k}s}\,, \tag{32}$$

where $\mathbf{e}_{\mathbf{k}s}$ is the unit polarization vector and the mode function of Eq. (32) satisfies the transversality and orthonormality conditions of Eq. (29). The three components of the propagation vector $\mathbf{k}$ each takes the values

$$k_x = \frac{2\pi n_x}{L}, \quad k_y = \frac{2\pi n_y}{L}, \quad k_z = \frac{2\pi n_z}{L}, \qquad n_x, n_y, n_z = 0, \pm1, \pm2, \pm3, \ldots\,. \tag{33}$$

With the mode function for periodic boundary condition the quantized vector potential, electric, and magnetic fields are expressed as

$$\hat{\mathbf{A}}(\mathbf{r}) = \sum_{\mathbf{k}}\sum_{s=1,2}\left(\frac{\hbar}{2\epsilon_0\omega_k V}\right)^{1/2}\mathbf{e}_{\mathbf{k}s}\left[\hat{a}_{\mathbf{k}s}e^{i\mathbf{k}\cdot\mathbf{r}} + \hat{a}^\dagger_{\mathbf{k}s}e^{-i\mathbf{k}\cdot\mathbf{r}}\right], \tag{34}$$

$$\hat{\mathbf{E}}_\perp(\mathbf{r}) = \sum_{\mathbf{k}}\sum_{s=1,2} i\left(\frac{\hbar\omega_k}{2\epsilon_0 V}\right)^{1/2}\mathbf{e}_{\mathbf{k}s}\left[\hat{a}_{\mathbf{k}s}e^{i\mathbf{k}\cdot\mathbf{r}} - \hat{a}^\dagger_{\mathbf{k}s}e^{-i\mathbf{k}\cdot\mathbf{r}}\right], \tag{35}$$

$$\hat{\mathbf{B}}(\mathbf{r}) = \sum_{\mathbf{k}}\sum_{s=1,2}\frac{i}{c}\left(\frac{\hbar\omega_k}{2\epsilon_0 V}\right)^{1/2}(\mathbf{k}\times\mathbf{e}_{\mathbf{k}s})\left[\hat{a}_{\mathbf{k}s}e^{i\mathbf{k}\cdot\mathbf{r}} - \hat{a}^\dagger_{\mathbf{k}s}e^{-i\mathbf{k}\cdot\mathbf{r}}\right], \tag{36}$$

where the volume is $V = L^3$ and the photon annihilation and creation operators are defined in terms of canonical photon coordinate and momentum as

$$\hat{a}_{\mathbf{k}s} = \frac{1}{\sqrt{2\hbar\omega_k}}\left(\omega_k\hat{q}_{\mathbf{k}s} + i\hat{p}_{\mathbf{k}s}\right), \qquad \hat{a}^\dagger_{\mathbf{k}s} = \frac{1}{\sqrt{2\hbar\omega_k}}\left(\omega_k\hat{q}_{\mathbf{k}s} - i\hat{p}_{\mathbf{k}s}\right), \tag{37}$$

with the photon creation and annihilation operators satisfying the commutation relations: $\left[\hat{a}_{\mathbf{k}s}, \hat{a}^\dagger_{\mathbf{k}'s'}\right] = \delta_{\mathbf{k}\mathbf{k}'}\delta_{ss'}$, $\left[\hat{a}_{\mathbf{k}s}, \hat{a}_{\mathbf{k}'s'}\right] = \left[\hat{a}^\dagger_{\mathbf{k}s}, \hat{a}^\dagger_{\mathbf{k}'s'}\right] = 0$. The field Hamiltonian of Eq. (5) can also be rewritten in terms of the photon creation and annihilation operators [33]

$$\hat{H}_{pt} = \sum_{\mathbf{k}}\sum_{s=1,2}\hbar\omega_k\left(\hat{a}^\dagger_{\mathbf{k}s}\hat{a}_{\mathbf{k}s} + \frac{1}{2}\right) = \frac{1}{2}\sum_{\mathbf{k}}\sum_{s=1,2}\left(\hat{p}^2_{\mathbf{k}s} + \omega_k^2\hat{q}^2_{\mathbf{k}s}\right). \tag{38}$$

The quantized electromagnetic field is described by individual quantum harmonic oscillators for each allowed mode and polarization. The canonical photon coordinate and momentum can also be defined in terms of the creation and annihilation operators as follows

$$\hat{q}_{\mathbf{k}s} = \sqrt{\frac{\hbar}{2\omega_k}}\left(\hat{a}_{\mathbf{k}s} + \hat{a}^\dagger_{\mathbf{k}s}\right), \tag{39}$$

$$\hat{p}_{\mathbf{k}s} = -i\sqrt{\frac{\hbar\omega_k}{2}}\left(\hat{a}_{\mathbf{k}s} - \hat{a}^\dagger_{\mathbf{k}s}\right). \tag{40}$$

From the commutation relations of the photon creation and annihilation operators it follows that the $\hat{q}_{\mathbf{k}s}$ and $\hat{p}_{\mathbf{k}s}$ satisfy the commutation relations $[\hat{q}_{\mathbf{k}s}, \hat{p}_{\mathbf{k}'s'}] = i\hbar\delta_{\mathbf{k}s,\mathbf{k}'s'}$, $[\hat{q}_{\mathbf{k}s}, \hat{q}_{\mathbf{k}'s'}] = 0 = [\hat{p}_{\mathbf{k}s}, \hat{p}_{\mathbf{k}'s'}]$.

2.1.4 ZERO BOUNDARY CONDITION

Next, consider a perfectly conducting rectangular metallic cavity of lengths L_x, L_y, L_z with one corner at the origin [34, 38–40]. The transverse components of the electric field must vanish at the boundaries, therefore, the mode functions that satisfies the boundary condition is

$$\begin{aligned}\mathbf{u}_{\mathbf{k}s}(\mathbf{r}) = \sqrt{\frac{8}{V}}\big[&\mathbf{e}_x\left(\mathbf{e}_{\mathbf{k}s}\cdot\mathbf{e}_x\right)\cos(k_x x)\sin(k_y y)\sin(k_z z)\\ &+\mathbf{e}_y\left(\mathbf{e}_{\mathbf{k}s}\cdot\mathbf{e}_y\right)\sin(k_x x)\cos(k_y y)\sin(k_z z)\\ &+\mathbf{e}_z\left(\mathbf{e}_{\mathbf{k}s}\cdot\mathbf{e}_z\right)\sin(k_x x)\sin(k_y y)\cos(k_z z)\big],\end{aligned} \tag{41}$$

where the volume of the rectangular cavity is $V = L_x L_y L_z$ and x, y, z are the coordinates of the position variable $\mathbf{r}$ with corresponding unit vectors $\mathbf{e}_x$, $\mathbf{e}_y$, $\mathbf{e}_z$. The components of the wavevector $\mathbf{k}$ are

$$k_x = \frac{\pi n_x}{L_x}, \quad k_y = \frac{\pi n_y}{L_y}, \quad k_z = \frac{\pi n_z}{L_z}, \qquad n_x, n_y, n_z = 0, 1, 2, 3, \ldots. \tag{42}$$

For the zero boundary condition, the vector potential, electric and magnetic fields confined in a perfectly conducting cavity are given by

$$\hat{\mathbf{A}}(\mathbf{r}) = \sum_{\mathbf{k}}\sum_{s=1,2}\left(\frac{\hbar}{2\epsilon_0\omega_k}\right)^{1/2}\left[\hat{a}_{\mathbf{k}s}\mathbf{u}_{\mathbf{k}s}(\mathbf{r}) + \hat{a}^\dagger_{\mathbf{k}s}\mathbf{u}^*_{\mathbf{k}s}(\mathbf{r})\right], \tag{43}$$

$$\hat{\mathbf{E}}_\perp(\mathbf{r}) = \sum_{\mathbf{k}}\sum_{s=1,2} i\left(\frac{\hbar\omega_k}{2\epsilon_0}\right)^{1/2}\left[\hat{a}_{\mathbf{k}s}\mathbf{u}_{\mathbf{k}s}(\mathbf{r}) - \hat{a}^\dagger_{\mathbf{k}s}\mathbf{u}^*_{\mathbf{k}s}(\mathbf{r})\right], \tag{44}$$

$$\hat{\mathbf{B}}(\mathbf{r}) = \sum_{\mathbf{k}}\sum_{s=1,2}\left(\frac{\hbar}{2\epsilon_0\omega_k}\right)^{1/2}\left[\hat{a}_{\mathbf{k}s}\boldsymbol{\nabla}\times\mathbf{u}_{\mathbf{k}s} + \hat{a}^\dagger_{\mathbf{k}s}\boldsymbol{\nabla}\times\mathbf{u}^*_{\mathbf{k}s}\right], \tag{45}$$

where the mode function is given as in Eq. (41). In order to satisfy the transversality condition of Eq. (29) and thus the Coulomb gauge condition $\boldsymbol{\nabla}\cdot\hat{\mathbf{A}}(\mathbf{r}) = 0$, the vector potential is required to satisfy

$$k_x\hat{A}_x + k_y\hat{A}_y + k_z\hat{A}_z = \frac{\pi n_x}{L_x}\hat{A}_x + \frac{\pi n_y}{L_y}\hat{A}_y + \frac{\pi n_z}{L_z}\hat{A}_z = 0. \tag{46}$$

Here, $\hat{A}_x$, $\hat{A}_y$, and $\hat{A}_z$ are the Cartesian components of the vector potential $\hat{\mathbf{A}}(\mathbf{r}) = \hat{A}_x(\mathbf{r})\mathbf{e}_x + \hat{A}_y(\mathbf{r})\mathbf{e}_y + \hat{A}_z(\mathbf{r})\mathbf{e}_z$. Equation (46) enforces that the number of independent polarizations of (n_x, n_y, n_z) is at most 2 and the allowed frequencies of Eq. (42) is defined as

$$\omega_{n_x,n_y,n_z} = c\, k_{n_x,n_y,n_z} = \pi c \sqrt{\frac{n_x^2}{L_x^2} + \frac{n_y^2}{L_y^2} + \frac{n_z^2}{L_z^2}}\,. \tag{47}$$

The boundary condition (zero or periodic) of the electromagnetic field is usually physically motivated by the situation under investigation. If the quantized field is coupled to the electrons usually it is only possible to use the periodic boundary conditions (since they need to agree with the ones of the electrons), and only in the dipole approximation can one switch to other boundary conditions such as the zero boundary conditions discussed in this section.

2.2 MINIMAL-COUPLING, VELOCITY AND THE LENGTH GAUGE HAMILTONIANS

In this section, the external part of the total vector potential in Eq. (1) is ignored and the minimal-coupling Hamiltonian in its time-independent form can be written in the following form

$$\hat{H}_{\mathrm{PF}} = \sum_{i=1}^{N_e} \frac{1}{2m}\left[\hat{\mathbf{p}}_i^2 - 2e\hat{\mathbf{A}}(\mathbf{r}_i)\cdot\hat{\mathbf{p}}_i + e^2\hat{\mathbf{A}}^2(\mathbf{r}_i) - e\hbar\hat{\sigma}_i\cdot\hat{\mathbf{B}}(\mathbf{r}_i)\right] + \hat{W}_{ee} + \hat{V}_{eN} + \hat{H}_{pt}\,. \tag{48}$$

The magnetic field that couples to the Pauli matrices was introduced in Eq. (48) using the Pauli vector identity: $(\sigma\cdot\mathbf{a})(\sigma\cdot\mathbf{b}) = \mathbf{a}\cdot\mathbf{b} + i\sigma\cdot(\mathbf{a}\times\mathbf{b})$ and $\hat{\mathbf{p}}\cdot\hat{\mathbf{A}}(\mathbf{r})$ was replaced by $\hat{\mathbf{A}}(\mathbf{r})\cdot\hat{\mathbf{p}}$ when simplifying the minimal-coupling term due to the Coulomb gauge condition of Eq. (18). Throughout this thesis, the contribution of the interaction of the spin with the magnetic field (Stern-Gerlach term) is dropped which leads to the spinless Pauli-Fierz Hamiltonian [41]. The Stern-Gerlach term is disregarded since the interest is mainly in bound systems where also the dipole approximation (as discussed afterwards) is applicable. Note that if one assumes a form factor for the electromagnetic fields of Eq. (48), i.e., a square integrable mask function that suppresses infinitely high photon energies, and allowing external fields of Kato type the Pauli-Fierz Hamiltonian is bounded from below and thus obeys a variational principle for ground-states [41].

2.2.1 THE VELOCITY GAUGE HAMILTONIAN AND FIELDS

The spinless Pauli-Fierz Hamiltonian can be simplified further by assuming that the spatial variation of the electromagnetic field can be neglected on the atomic or molecular length scale. This approximation replaces the vector potential $\hat{\mathbf{A}}(\mathbf{r})$ at the positions of the electrons by its value at the position $\mathbf{r}_0$ of the center of charge of the nuclei. This approximation is the so-called *long-wavelength approximation* [42]. Then the

minimal-coupling Hamiltonian reduces to the velocity gauge (or momentum gauge) Hamiltonian [28, 36, 42]:

$$\hat{H}_V = \sum_{i=1}^{N_e} \frac{1}{2m}\left[\hat{\mathbf{p}}_i^2 - 2e\hat{\mathbf{A}}(\mathbf{r}_0)\cdot\hat{\mathbf{p}}_i + e^2\hat{\mathbf{A}}^2(\mathbf{r}_0)\right] + \hat{W}_{ee} + \hat{V}_{eN} + \hat{H}_{pt}\,. \tag{49}$$

In Eq. (49), the diamagentic $\hat{\mathbf{A}}^2(\mathbf{r}_0)$ term can in this setting be absorbed through a Bogoliubov transformation that introduces a diamagnetic shift [43]. Such a transformation has several advantages [43]. However, here this term is kept explicitly for completeness. In the dipole approximation, the vector potential and the electric field in either periodic or zero boundary conditions reduce to

$$\hat{\mathbf{A}} = \sum_{\mathbf{k}}\sum_{s=1,2}\frac{1}{\sqrt{\epsilon_0}}\mathbf{u}_{\mathbf{k}s}\hat{q}_{\mathbf{k}s}\,, \tag{50}$$

$$\hat{\mathbf{E}}_\perp = -\sum_{\mathbf{k}}\sum_{s=1,2}\frac{1}{\sqrt{\epsilon_0}}\mathbf{u}_{\mathbf{k}s}\hat{p}_{\mathbf{k}s}\,, \tag{51}$$

where the center of charge is assumed to be at $\mathbf{r}_0 = 0$ and the canonical photon coordinate and momentum are given respectively in Eqs. (39) and (40).

The velocity gauge Hamiltonian of Eq. (49) contains explicitly the gauge-dependent vector potential $\hat{\mathbf{A}}$. However, it is convenient to work with gauge-independent transverse electromagnetic fields such as the electric field $\hat{\mathbf{E}}$. Therefore, in the next section a transformation from the velocity gauge Hamiltonian to the length gauge Hamiltonian is performed to work with gauge-independent fields.

2.2.2 THE LENGTH GAUGE HAMILTONIAN AND FIELDS

Due to the gauge-dependent field (vector potential) of the velocity gauge Hamiltonian of Eq. (49), it is worthwhile working in the length gauge which considers only gauge-independent fields. This is accomplished by performing a unitary transformation called the length-gauge transformation [28, 41, 42] defined as $\hat{H}'_L = \hat{U}^\dagger\hat{H}_V\hat{U}$ where the unitary operator is given by

$$\hat{U} = \exp\left\{-\frac{i}{\hbar}\hat{\mathbf{A}}\cdot\hat{\mathbf{R}}\right\}, \tag{52}$$

with the electronic dipole operator $\hat{\mathbf{R}} = \sum_{i=1}^{N_e}\mathbf{r}_i$ and the vector potential $\hat{\mathbf{A}}$ is given as in Eq. (50). Under the unitary transformation, the velocity gauge Hamiltonian transforms to

$$\hat{H}'_L = \hat{T}_e + \hat{W}_{ee} + \hat{V}_{eN} + \frac{1}{2}\sum_{\mathbf{k}}\sum_{s=1,2}\left[\hat{p}_{\mathbf{k}s}^2 + \omega_k^2\hat{q}_{\mathbf{k}s}^2 + \frac{2}{\sqrt{\epsilon_0}}\hat{p}_{\mathbf{k}s}\left(\mathbf{u}_{\mathbf{k}s}\cdot\hat{\mathbf{R}}\right) + \left(\frac{1}{\sqrt{\epsilon_0}}\mathbf{u}_{\mathbf{k}s}\cdot\hat{\mathbf{R}}\right)^2\right]. \tag{53}$$

Furthermore, a variable transformation can be performed that effectively swaps between conjugate momentum and photon coordinate as

$$\hat{p}_{\mathbf{k}s} \longrightarrow -\omega_{\mathbf{k}}\hat{q}_{\mathbf{k}s}\,, \quad \text{and} \quad \hat{q}_{\mathbf{k}s} \longrightarrow \frac{1}{\omega_k}\hat{p}_{\mathbf{k}s}\,. \tag{54}$$

The transformation above is merely a Fourier transformation of the mode $(\mathbf{k}s)$ of the full wavefunction

$$\Psi'(...,p_{\mathbf{k}s},...) \longrightarrow \Psi(...,q_{\mathbf{k}s},...) = \frac{1}{\sqrt{2\pi}}\int_{-\infty}^{\infty} e^{-iq_{\mathbf{k}s}p_{\mathbf{k}s}}\Psi'(...,p_{\mathbf{k}s},...)dp_{\mathbf{k}s}\,.$$

This variable transformation above leaves the commutation relations between the photon displacement coordinate and conjugate momentum unchanged and thus, the Hamiltonian in the length gauge becomes [13, 44]

$$\hat{H}_L = \hat{T}_e + \hat{W}_{ee} + \hat{V}_{eN} + \frac{1}{2}\sum_{\mathbf{k}}\sum_{s=1,2}\left[\hat{p}^2_{\mathbf{k}s} + \omega_k^2\left(\hat{q}_{\mathbf{k}s} - \frac{1}{\omega_k\sqrt{\epsilon_0}}\mathbf{u}_{\mathbf{k}s}\cdot\hat{\mathbf{R}}\right)^2\right]. \tag{55}$$

The individual terms that emerge from the last term of the Eq. (55) will be discussed in detail in Sec. 3.1 of Chap. 3. In the length gauge and after swapping the canonical photon coordinate and momentum using Eq. (54), the vector potential and the electric field are expressed as [44]:

$$\hat{\mathbf{A}} = \sum_{\mathbf{k}}\sum_{s=1,2}\frac{1}{\omega_k\sqrt{\epsilon_0}}\mathbf{u}_{\mathbf{k}s}\hat{p}_{\mathbf{k}s}\,, \tag{56}$$

$$\hat{\mathbf{E}}_\perp = \sum_{\mathbf{k}}\sum_{s=1,2}\frac{1}{\sqrt{\epsilon_0}}\mathbf{u}_{\mathbf{k}s}\,\omega_k\left(\hat{q}_{\mathbf{k}s} - \frac{1}{\omega_k\sqrt{\epsilon_0}}\mathbf{u}_{\mathbf{k}s}\cdot\hat{\mathbf{R}}\right). \tag{57}$$

The electric field in Eq. (57) was obtained in the Schrödinger picture using Eq. (22) and the Heisenberg equation of motion Eq. (68). An advantage of the length gauge is that light and matter get mixed which implies one does not work with the $\hat{\mathbf{E}}_\perp$ field but rather with the displacement field $\hat{\mathbf{D}}_\perp$. Making a comparison of the electric field $\hat{\mathbf{E}}_\perp$ and the transverse electric displacement field given by $\hat{\mathbf{D}} = \epsilon_0\hat{\mathbf{E}} + \hat{\mathbf{P}}$, the expression for the displacement field and polarization are given respectively by

$$\hat{\mathbf{D}} = \sum_{\mathbf{k}}\sum_{s=1,2}\sqrt{\epsilon_0}\,\mathbf{u}_{\mathbf{k}s}\,\omega_k\,\hat{q}_{\mathbf{k}s}\,, \tag{58}$$

$$\hat{\mathbf{P}} = \sum_{\mathbf{k}}\sum_{s=1,2}\sqrt{\epsilon_0}\,\mathbf{u}_{\mathbf{k}s}\left(\mathbf{u}_{\mathbf{k}s}\cdot\hat{\mathbf{R}}\right). \tag{59}$$

From here on, for arbitrarily many but a finite number M of photon modes, the collective index $\alpha \equiv (\mathbf{k}s)$ is used to denote both the propagation vector $\mathbf{k}$ and the two transversal polarization directions $s = 1, 2$. Taking into account this notation, the coupling term is defined as

$$\boldsymbol{\lambda}_\alpha = \frac{1}{\sqrt{\epsilon_0}}\,\mathbf{u}_\alpha\,. \tag{60}$$

Here, the mode function $\mathbf{u}_{\mathbf{k}s}(\mathbf{r}_0)$ can take expressions such as that for periodic and zero boundary conditions discussed respectively in Secs. 2.1.3 and 2.1.4 or that of half space or of a spherical cavity [38] amongst others.

It is important to note that both the velocity and length gauge Hamiltonians are physically equivalent. For a comprehensive comparison of these gauges, see Ref. [45] and references therein. Furthermore, it was demonstrated in [45] that both gauge choices have better convergence properties towards the exact solution for different observables.

2.3 APPROXIMATIONS COMMON TO NON-RELATIVISTIC QED

Usually, approximations are introduced to treat the interacting subsystems of the coupled matter-photon system as well as to model and interpret experimental results. The approximations that are usually considered strongly depend on the character of the matter-photon system that is being studied. The corresponding approximate equations might differ and provide access to different processes and interactions.

Consider for example one is interested in the solution of either Eq. (6) or (7) in which the Hamiltonian is the length or velocity gauge Hamiltonians of Eqs. (49) and (55), respectively or even the minimal coupling Hamiltonian of Eq. (48). The wavefunction which contains all information about the system in this case is labeled by the coordinates of N_e electrons with spin and M photon modes as

$$|\Psi\rangle = \Psi(\mathbf{r}_1\sigma_1, \mathbf{r}_2\sigma_2, ..., \mathbf{r}_{N_e}\sigma_{N_e}; q_1, q_2, ..., q_M)\,. \tag{61}$$

Due to the large degrees of freedom, it becomes increasingly difficult to solve the time-dependent and the static Schrödinger equations. The difficulty even increases beyond the dipole approximation also with the possibility of including a continuum of modes. For this reason, one resorts to approximations that reduces the complexity of the system. In the following, further different levels of approximations to the coupled matter-photon system in the dipole approximation that are considered in this thesis are discussed. From here on, the spin degrees of freedom of the wavefunction of Eq. (61) are not indicated for notational simplicity and without loss of generality.

2.3.1 THE MAXWELL-SCHRÖDINGER SEMI APPROXIMATION

For light-matter descriptions in which the electromagnetic field has a large number of photons, the quantum nature of light becomes less important and in this case a classical treatment of the electromagnetic field of the combined light-matter system becomes sufficient. Therefore, the non-relativistic QED description is approximated by including the coupling to a classical Maxwell field instead of the quantized photon field. By making a mean-field ansatz for the matter-photon coupling in non-relativistic QED, the correlated matter-photon wavefunction Ψ in Eq. (61) can be approximated as a factorizable product of the matter wavefunction ψ and photon wavefunction ϕ as

$$\Psi(\mathbf{r}_1, \mathbf{r}_2, ..., \mathbf{r}_{N_e}; q_1, q_2, ..., q_M) \simeq \psi(\mathbf{r}_1, \mathbf{r}_2, ..., \mathbf{r}_N) \otimes \phi(q_1, q_2, ..., q_M)\,.$$

Applying the Maxwell-Schrödinger approximation to the velocity gauge Hamiltonian of Eq. (49), the non-relativistic QED description in this gauge simplifies to the following two coupled equations [8]:

$$i\hbar\frac{\partial}{\partial t}|\psi(t)\rangle = \hat{H}_V^{(\mathrm{MS})}(t)|\psi(t)\rangle\,, \tag{62}$$

$$\left(\frac{\partial^2}{\partial t^2} + \omega_\alpha^2\right)\mathbf{A}_\alpha(t) = \frac{e}{m}\boldsymbol{\lambda}_\alpha\sum_{\alpha=1}^{M}\boldsymbol{\lambda}_\alpha\cdot\left(\sum_{i=1}^{N_e}\mathbf{p}_i(t) - eN_e\mathbf{A}_\alpha(t)\right), \tag{63}$$

where the approximated velocity gauge Hamiltonian $\hat{H}_V^{(\mathrm{MS})}(t)$ with a coupling to a classical field is given by

$$\hat{H}_V^{(\mathrm{MS})}(t) = \hat{T}_e + \hat{W}_{ee} + \hat{V}_{eN} - \frac{e}{m}\sum_{i=1}^{N_e}\sum_{\alpha=1}^{M}\mathbf{A}_\alpha(t)\cdot\hat{\mathbf{p}}_i\,, \tag{64}$$

and the time-dependent vector potential is $\mathbf{A}_\alpha(t) = \boldsymbol{\lambda}_\alpha q_\alpha(t)$ with the photon coordinate being $q_\alpha(t) = \langle\phi(t)|\hat{q}_\alpha|\phi(t)\rangle$. Note that Eq. (63) is the mode-resolved Maxwell's equation in dipole approximation of Eq. (21). Comparing terms of these two equations one finds that the right-hand side of Eq. (63) is the full transverse current in dipole approximation. It is relevant to note that in a similar way to Eqs. (62) and (64), one can obtain this form of equations for the photon part as in Ref. [13], i.e. an evolution equation of $|\phi(t)\rangle$. Since only the expectation value of the field is needed and not the wavefunction, the Maxwell's equation for $\mathbf{A}_\alpha(t)$ is rather considered here. Both formalisms are equivalent as will be discussed in Sec. 2.3.1.1. The same applies to the length gauge discussed below. The classical photon coordinate and electronic momentum account for the self-consistent back-reaction between both subsystems. However, in this approximation the back-reaction is between the matter subsystem treated quantum mechanically and the photonic subsystem treated classically. Also, the Maxwell-Schrödinger approximation can be applied in the length gauge. For the length gauge Hamiltonian of Eq. (55), the Maxwell-Schrödinger approximation results to the coupled equations

$$i\hbar\frac{\partial}{\partial t}|\psi(t)\rangle = \hat{H}_L^{(\mathrm{MS})}(t)|\psi(t)\rangle\,, \tag{65}$$

$$\left(\frac{\partial^2}{\partial t^2} + \omega_\alpha^2\right) q_\alpha(t) = \omega_\alpha\,\boldsymbol{\lambda}_\alpha\cdot\mathbf{R}(t)\,, \tag{66}$$

where the approximated length gauge Hamiltonian $\hat{H}_L^{(\mathrm{MS})}(t)$ with classical field coupling is given explicitly as

$$\hat{H}_L^{(\mathrm{MS})}(t) = \hat{T}_e + \hat{W}_{ee} + \hat{V}_{eN} - \sum_{\alpha=1}^{M}\omega_\alpha q_\alpha(t)\,\boldsymbol{\lambda}_\alpha\cdot\mathbf{R} + \frac{1}{2}\sum_{\alpha=1}^{M}(\boldsymbol{\lambda}_\alpha\cdot\mathbf{R})^2\,. \tag{67}$$

Equally in this gauge, the Maxwell-Schrödinger approximation takes into account the back-reaction between both subsystems. Analogous to Eq. (21), the right-hand side of the mode-resolved Maxwell equations of Eqs. (63) and (66) represent the current that couples self-consistently to the respective Hamiltonians. It is important to note that the Maxwell-Schrödinger equations for the length and velocity gauge will lead to different results since the unitary equivalence has been broken due to the mean-field ansatz.

To obtain the mode resolved equation of motion (EOM) for the photonic coordinate in Eqs. (63) and (66), the Heisenberg EOM was employed. The Heisenberg EOM provides a connection between the time derivative of an expectation value $O(t) = \langle\Psi(t)|\hat{O}(t)|\Psi(t)\rangle$ to the commutator of the corresponding operator $\hat{O}(t)$ with the Hamiltonian $\hat{H}(t)$ which is expressed in the Schrödinger picture as

$$\frac{d}{dt}O(t) = -\frac{i}{\hbar}\langle\Psi(t)|\left[\hat{O}(t),\hat{H}(t)\right]|\Psi(t)\rangle + \langle\Psi(t)|\frac{\partial}{\partial t}\hat{O}(t)|\Psi(t)\rangle. \tag{68}$$

For a time-independent operator, i.e. $\hat{O}(t) = \hat{O}$, which is usually the case in the Schrödinger picture as the wavefunctions carry the time-dependence, the k-th derivative of $\hat{O}$ is written as

$$\frac{d^k}{d^k t}O(t) = \left(-\frac{i}{\hbar}\right)^k \langle\Psi(t)|\left[\left[\left[\left[\left[\hat{O},\hat{H}(t)\right],\hat{H}(t)\right],\hat{H}(t)\right]...\right],\hat{H}(t)\right]|\Psi(t)\rangle, \tag{69}$$

where the minimum value of $k = 1$. An example application of the above formula is given in Eqs. (63) and (66) where the Heisenberg EOM was applied twice (i.e. for $k = 2$). These equations will be later used in this thesis.

2.3.1.1 *Photonic subspace: Driven quantum harmonic oscillator*

As discussed in the previous section, invoking the mean-field ansatz simplifies the problem to a matter-only description that couples self-consistently to a classical mode-resolved Maxwell equation. The analytic solution to the mode-resolved representation of the Maxwell equation is known [46]. The analytic solution becomes desirable for such coupled systems since it reduces the numerical complexity [47]. In order to present the analytic solution of the mode-resolved Maxwell equation, for example of Eq. (63), rather consider the situation of a driven quantum harmonic oscillator given by the Hamiltonian:

$$\hat{H}_{pt}(t) = \sum_{\alpha=1}^{M}\frac{1}{2}\left(\hat{p}_\alpha^2 + \omega_\alpha^2\hat{q}_\alpha^2\right) + \sum_{\alpha=1}^{M}\hat{\mathbf{A}}_\alpha\cdot\mathbf{j}_\alpha(t)\,. \tag{70}$$

Here, the harmonic oscillators describing M individual photon modes are driven by an external charge current $\mathbf{j}_\alpha(t)$ that couples via the vector potential $\hat{\mathbf{A}}_\alpha$. To obtain the mode-resolved Maxwell equation, one applies the Heisenberg EOM of Eq. (68) to the photon coordinate and momentum that yields the Ehrenfest theorem

$$\frac{\partial}{\partial t}q_\alpha(t) = p_\alpha(t), \quad \text{and} \quad \frac{\partial}{\partial t}p_\alpha(t) = -\omega_\alpha^2 q_\alpha(t) - \boldsymbol{\lambda}_\alpha\cdot\mathbf{j}_\alpha(t).$$

Combining the above equation yields the mode-resolved classical EOM of the photon coordinate $\hat{q}_\alpha$ given in the following form

$$\left(\frac{\partial^2}{\partial t^2} + \omega_\alpha^2\right)q_\alpha(t) = -\boldsymbol{\lambda}_\alpha\cdot\mathbf{j}_\alpha(t)\,. \tag{71}$$

The analytic solution can be obtained through the method of Laplace transforms. First, equation (71) can be expressed in the following form using the relation for Laplace transforms of second-order derivatives [48]

$$s^2 g(s) - s\,q_\alpha(t_0) - \dot{q}_\alpha(t_0) + \omega_\alpha^2 g(s) = h(s)\,,$$

where the Laplace transforms are $g(s) = \mathscr{L}\{q_\alpha(t)\}$ and $h(s) = \mathscr{L}\{F(t)\}$ with $F(t) = -\boldsymbol{\lambda}_\alpha\cdot\mathbf{j}_\alpha(t)$. Here the Laplace transform, for example, of $q_\alpha(t)$ is defined by $g(s) = \int_0^\infty q_\alpha(t)e^{-st}dt$ where s is assumed here to be real but in general is complex. From the above equation, one obtains $g(s)$ to be

$$g(s) = \frac{s\,q_\alpha(t_0) + \dot{q}_\alpha(t_0) + h(s)}{s^2 + \omega_\alpha^2}\,.$$

Taking the inverse Laplace transform [48] of the above equation defined by $q_\alpha(t) = \mathscr{L}^{-1}\{g(s)\}$ and $F(t) = \mathscr{L}^{-1}\{h(s)\}$ results to

$$\begin{aligned} q_\alpha(t) &= \mathscr{L}^{-1}\left\{\frac{s\, q_\alpha(t_0)}{s^2+\omega_\alpha^2}\right\} + \mathscr{L}^{-1}\left\{\frac{\dot{q}_\alpha(t_0)}{s^2+\omega_\alpha^2}\right\} + \mathscr{L}^{-1}\left\{\frac{h(s)}{s^2+\omega_\alpha^2}\right\} \\ &= q_\alpha(t_0)\cos(\omega_\alpha t) + \frac{\dot{q}_\alpha(t_0)}{\omega_\alpha}\sin(\omega_\alpha t) + \mathscr{L}^{-1}\left\{\frac{h(s)}{s^2+\omega_\alpha^2}\right\}, \end{aligned}$$

where $\cos(\omega_\alpha t) = \mathscr{L}^{-1}\left\{s/(s^2+\omega_\alpha^2)\right\}$ and $\sin(\omega_\alpha t) = \mathscr{L}^{-1}\left\{\omega_\alpha/(s^2+\omega_\alpha^2)\right\}$. Applying the convolution property of the Laplace transform [48] to the last term of the above equation yields the analytic solution of the mode-resolved Maxwell equation given by

$$q_\alpha(t) = q_\alpha(t_0)\cos(\omega_\alpha t) + \frac{\dot{q}_\alpha(t_0)}{\omega_\alpha}\sin(\omega_\alpha t) - \frac{1}{\omega_\alpha}\int_0^t dt' \sin\left(\omega_\alpha(t-t')\right)\boldsymbol{\lambda}_\alpha \cdot \mathbf{j}_\alpha(t'), \tag{72}$$

where $q_\alpha(t_0) = \langle\phi(t_0)|\hat{q}_\alpha|\phi(t_0)\rangle$ and $\dot{q}_\alpha(t_0) = \langle\phi(t_0)|\hat{p}_\alpha|\phi(t_0)\rangle$ are obtained from the choice of the initial state of the photon subsystem. From Eq. (72), the choice of the external charge current and initial state of the photon field determines the photon coordinate $q_\alpha(t)$ and thus the vector potential $\mathbf{A}_\alpha(t) = \boldsymbol{\lambda}_\alpha q_\alpha(t)$. By analogously comparing Eqs. (63) and (66) to Eq. (71) yields the solutions of these equations of the form of Eq. (72).

2.3.2 THE SEMI-CLASSICAL APPROXIMATION

A further simplification can be performed to the Maxwell-Schrödinger approximation in the velocity gauge described by Eqs. (63) and (64) and the length gauge described by Eqs. (66) and (67). This simplification known as the *semi-classical limit* or *semi-classical approximation* [36] does not account for the back-reaction of the photons on the matter subsystem but rather treats the photon field as an external perturbation that is not a part of the dynamical system. In this case, the velocity gauge prescription of the semi-classical limit is achieved by discarding the photon Hamiltonian in Eq. (55) and the quantized vector potential $\hat{\mathbf{A}}_\alpha$ will be in this case an external time-dependent field $\mathbf{A}_\alpha(t)$. Usually, the term $\mathbf{A}_\alpha^2(t)$ can be neglected since it is just a time-dependent constant and thus will not change any observables [49]. In this case the Hamiltonian for the semi-classical limit is solely described by Eq. (64) where $\mathbf{A}_\alpha(t)$ is merely an external perturbing field.

The semi-classical limit in the length gauge can have two forms depending on when the approximation is made: (i.) from the original velocity gauge Hamiltonian Eq. (49) or (ii.) after the length-gauge transformations leading to the Hamiltonian of Eq. (55). The former which is the standard semi-classical limit treats the vector potential in Eq. (49) as an external field that interacts with the electronic system (i.e. semi-classical limit in velocity gauge). Note that a static spatially independent vector potential has no physical effect (just adds a phase to the wavefunction) and hence $\mathbf{A}(t)$ is usually non-constant in time. Performing the length-gauge transformation Eq.(52), where a time-dependent classical vector potential is now used, eliminates

the $\mathbf{A}^2$ and $\mathbf{A}\cdot\hat{\mathbf{p}}$ terms as in the quantum case. However, the interaction term arising between classical field and matter now emerges with $\Psi_L(t) = \hat{U}^\dagger(t)\Psi_V(t)$ due to

$$i\hbar\frac{\partial}{\partial t}\Psi_L(t) = -e\mathbf{E}(t)\cdot\hat{\mathbf{R}}\,\Psi_L(t) + i\hbar\hat{U}^\dagger(t)\frac{\partial}{\partial t}\Psi_V(t),$$

not due to the transformation of the photon coordinates. The expression of the time-dependent $\hat{U}^\dagger(t)$ is obtained by replacing the quantized vector potential in Eq. (52) by a classical dipole field $\mathbf{A}(t)$. From the above equation, the standard semi-classical length-gauge Hamiltonian reads [49]:

$$\hat{H}_L^{(Sc)}(t) = \hat{T}_e + \hat{W}_{ee} + \hat{V}_{eN} - e\hat{\mathbf{R}}\cdot\mathbf{E}(t). \tag{73}$$

Next, when the semi-classical limit is performed *after* the length-gauge transformation, i.e., starting from the Hamiltonian Eq. (55) and proceed to the coupled Maxwell-Schrödinger approximation with Hamiltonian Eq. (67), the semi-classical limit now has the form [44]:

$$\hat{H}_L^{(aSc)}(t) = \hat{T}_e + \hat{W}_{ee} + \hat{V}_{eN} - \frac{1}{\epsilon_0}\mathbf{D}(t)\cdot\hat{\mathbf{R}} + \frac{1}{2}\sum_\alpha\left(\boldsymbol{\lambda}_\alpha\cdot\hat{\mathbf{R}}\right)^2, \tag{74}$$

where the displacement field is $\mathbf{D}(t) = \epsilon_0\sum_\alpha\boldsymbol{\lambda}_\alpha\omega_\alpha q_\alpha(t)$ and the photon coordinate $q_\alpha(t)$ can be a solution of the homogeneous part of a mode-resolved Maxwell equation (66).

An advantage the semi-classical limit of Eq. (74) has over that of Eq. (73) is that for static fields, Eq. (74) has eigenstates (see Chap. 3.1 for the boundedness from below of the length gauge Hamiltonian) due to the presence of the dipole self-energy term (last term) in contrast to the standard semi-classical limit [44]. Therefore, it allows to treat equilibrium effects such as the Stark effect non-perturbatively and can as well be applied to non-equilibrium situations, such as the ac-Stark shift.

2.4 GENERAL LINEAR RESPONSE IN NON-RELATIVISTIC QED

Most often, instead of solving the full time-dependent Schrödinger equation of Eq. (6), it is convenient to evaluate specific linear and non-linear responses of the coupled system using perturbation theory. The linear response is usually simpler to determine than the full dynamics of a system and hence is a good first step to investigate the properties of matter such as the absorption or emission spectrum. The linear-response discussion presented here becomes important in Chap. 3.2 where one considers from first-principles the change in the properties of the system due to strongly coupling light and matter.

In the following, a general linear response framework is presented. The derivation below follows that of Refs. [50] and [51]. Consider an external classical time-dependent probe characterized by the Hamiltonian $\hat{H}_{\text{ext}}(t)$ that is turned on at a time t_0. The perturbation $\hat{H}_{ext}(t)$ is assumed weak. The Hamiltonian describing the dynamics of the perturbed light-matter system becomes

$$\hat{H}(t) = \hat{H}_0 + \hat{H}_{\text{ext}}(t). \tag{75}$$

Here, the time-independent Hamiltonian $\hat{H}_0$ can be characterized by either of the Hamiltonians of Eqs. (48), (49), or (55). Now, by introducing the interaction picture[2], the wavefunction in the Schrödinger picture of the system is related to the wavefunction in the interaction picture as

$$|\Psi_I(t)\rangle = \hat{U}_0^\dagger(t)|\Psi(t)\rangle = e^{i\hat{H}_0 t/\hbar}|\Psi(t)\rangle,$$

where $|\Psi(t)\rangle$ is the wavefunction in the Schrödinger picture. Accordingly, an arbitrary operator $\hat{O}(\mathbf{r})$ not necessarily dependent on the position $\mathbf{r}$, can be transformed from the Schrödinger to the interaction picture by

$$\hat{O}_I(\mathbf{r},t) = \hat{U}_0^\dagger(t)\hat{O}(\mathbf{r})\hat{U}_0(t). \tag{76}$$

In the interaction picture, the evolution of the interacting coupled system from an initial state $|\Psi_0\rangle$ is described by the following time-dependent Schrödinger equation

$$i\hbar\frac{\partial}{\partial t}|\Psi_I(t)\rangle = \hat{H}_{\text{ext},I}(t)|\Psi_I(t)\rangle. \tag{77}$$

Through an integration, Eq. (77) can be formally solved to obtain the expression

$$|\Psi_I(t)\rangle = |\Psi_0\rangle - \frac{i}{\hbar}\int_{t_0}^{t} dt'\,\hat{H}_{\text{ext},I}(t')|\Psi_I(t')\rangle. \tag{78}$$

Where $|\Psi_0\rangle$ can be either the Schrödinger or interaction representation, since at $t = t_0$, the two are equivalent. Keeping only up to the first order, the closed solution in the Schrödinger picture reduces to

$$|\Psi(t)\rangle \simeq \hat{U}_0(t)|\Psi_0\rangle - \frac{i}{\hbar}\hat{U}_0(t)\int_{t_0}^{t} dt'\,\hat{H}_{\text{ext},I}(t')\hat{U}_0^\dagger(t')|\Psi_0\rangle. \tag{79}$$

The time evolution of the wavefunction is not of interest here, but rather the response of an observable $\hat{O}(\mathbf{r})$ to small external perturbations. The change in the expectation value of an arbitrary observable $\hat{O}(\mathbf{r})$ due to the external perturbation $\hat{H}_{\text{ext}}(t)$ is given by

$$\delta\langle\hat{O}(\mathbf{r},t)\rangle = \langle\Psi(t)|\hat{O}(\mathbf{r})|\Psi(t)\rangle - \langle\Psi_0|\hat{O}(\mathbf{r})|\Psi_0\rangle. \tag{80}$$

In linear response theory, it is assumed that the external perturbation in Eq. (75) is sufficiently small such that Eq. (79) is a good approximation to Eq. (77) and that $|\Psi_0\rangle$ equals the ground-state of $\hat{H}_0$. Thus, by making a substitution of Eq. (79) in Eq. (80) yields the response equation

$$\delta\langle\hat{O}(\mathbf{r},t)\rangle = -\frac{i}{\hbar}\int_{t_0}^{t} dt'\langle\Psi_0|\left[\hat{O}_I(\mathbf{r},t),\hat{H}_{\text{ext},I}(t')\right]|\Psi_0\rangle\,. \tag{81}$$

As a side remark, beyond linear response solutions can be obtained by including higher-order terms of Eq. (78). As external perturbation, consider the perturbation

2 The subscript "I" attached to the wavefunction, observable or external perturbation indicates that these quantities are given in the interaction picture.

Hamiltonian given as $\hat{H}_{\text{ext},I}(t) = \int d^3\mathbf{r}\, \hat{D}_I(\mathbf{r},t)v(\mathbf{r},t)$ where $v(\mathbf{r},t)$ is the external perturbing term that couple to some operator $\hat{D}_I(\mathbf{r},t)$ given in the interaction picture. The response of the observable $\hat{O}(\mathbf{r})$ at time t becomes

$$\delta\langle\hat{O}(\mathbf{r},t)\rangle = \int_{t_0}^{t} dt' \int d^3\mathbf{r}'\ \chi_D^O(\mathbf{r},t;\mathbf{r}',t')\delta v(\mathbf{r}',t')\,, \tag{82}$$

where the retarded response function in the above linear response equation is defined to be

$$\chi_D^O(\mathbf{r},t;\mathbf{r}',t') = -\frac{i}{\hbar}\Theta(t-t')\ \langle\Psi_0|\left[\hat{O}_I(\mathbf{r},t),\hat{D}_I(\mathbf{r}',t')\right]|\Psi_0\rangle. \tag{83}$$

Here, the use of the word "retarded" designates that the response at time t is as a result of a perturbation at an earlier time $t' \leq t$ and the Heaviside function $\Theta(t-t')$ guarantees the correct time ordering, that is, causality. The response function of Eq. (83) is an intrinsic property of the coupled system and it is independent of external influences. Assuming that the system is invariant under time translations, i.e., H_0 is time-independent, the response function becomes

$$\chi_D^O(\mathbf{r},t;\mathbf{r}',t') = \chi_D^O(\mathbf{r},\mathbf{r}';t-t'). \tag{84}$$

An alternate derivation of the response and response function of Eqs. (82) and (83) can be obtained using the functional dependence of the observables on the external perturbation $\delta v(\mathbf{r},t)$. Firstly, the wavefunction of the coupled system has a functional dependence $|\Psi([v];t)\rangle$ via the Hamiltonian Eq. (75), i.e., $\hat{H}(t) = \hat{H}([v];t)$ where $v(\mathbf{r},t)$ is the perturbation that couples to $\hat{D}_I(\mathbf{r},t)$. Therefore, through the expectation value as in Eq. (80), the observable has a functional dependence on the external perturbation $O([v];\mathbf{r},t)$. Performing a functional Taylor expansion of $O(\mathbf{r},t)$ around the static perturbation $v_0(\mathbf{r})$ to first-order yields

$$O([v];\mathbf{r},t) = O([v_0];\mathbf{r}) + \iint d^3\mathbf{r}'dt' \frac{\delta O([v_0];\mathbf{r},t)}{\delta v(\mathbf{r}',t')}\delta v(\mathbf{r}',t')\,. \tag{85}$$

To obtain the response $\delta O(\mathbf{r},t)$ from Eq. (85), one applies the Gateaux derivative which is a generalization of the directional derivative [52]. Applying the Gateaux derivative [52], the response $\delta O(\mathbf{r},t)$ is defined as

$$\begin{aligned}\delta O(\mathbf{r},t) &= \lim_{\varepsilon\to 0}\frac{O([v_0+\varepsilon\,\delta v];\mathbf{r},t) - O([v_0];\mathbf{r},t)}{\varepsilon} \\ &= \int_{t_0}^{t} dt' \int d^3\mathbf{r}'\ \underbrace{-\frac{i}{\hbar}\Theta(t-t')\ \langle\Psi_0|\left[\hat{O}_I(\mathbf{r},t),\hat{D}_I(\mathbf{r}',t')\right]|\Psi_0\rangle}_{\chi_D^O(\mathbf{r},t;\mathbf{r}',t')}\delta v(\mathbf{r}',t')\,,\end{aligned} \tag{86}$$

which can be expressed as [52]:

$$O([v_0+\varepsilon\,\delta v];\mathbf{r},t) = O([v_0];\mathbf{r},t) + \iint d^3\mathbf{r}'dt' \frac{\delta O([v_0];\mathbf{r},t)}{\delta v(\mathbf{r}',t')}\delta v(\mathbf{r}',t')\,, \tag{87}$$

where the quantity ε is an infinitesimal number. Using the definition of the linear-response in Eqs. (86) and (87), one deduces from Eq. (85) the response $\delta O(\mathbf{r},t)$ given by

$$\delta O(\mathbf{r},t) = \iint d^3\mathbf{r}'dt'\chi_D^O(\mathbf{r},t;\mathbf{r}',t')\delta v(\mathbf{r}',t')\,. \tag{88}$$

Here, the response function in Eq. (88) has the form

$$\chi_D^O(\mathbf{r},t;\mathbf{r}',t') = \left.\frac{\delta O([v];\mathbf{r},t)}{\delta v(\mathbf{r}',t')}\right|_{v_0(\mathbf{r})}. \tag{89}$$

The response functions defined in Eqs. (83) and (89) are formally equivalent. This becomes evident by comparing Eq. (86) and Eq. (88). In linear response theory, it is more convenient to deal with the Fourier transform of the response equation (82) given by [53]:

$$\delta\langle\hat{O}(\mathbf{r},\omega)\rangle = \int d^3\mathbf{r}'\ \chi_D^O(\mathbf{r},\mathbf{r}';\omega)\delta v(\mathbf{r},\omega), \tag{90}$$

where $\delta v(\mathbf{r},\omega)$ is the Fourier transform of the potential and $\chi_D^O(\mathbf{r},\mathbf{r}';\omega)$ is the Fourier transform of the time-dependent response function given by

$$\chi_D^O(\mathbf{r},\mathbf{r}';\omega) = \int_{-\infty}^{\infty} d\tau\ \chi_D^O(\mathbf{r},\mathbf{r}';\tau)e^{-i\omega\tau}, \tag{91}$$

where $\tau = t - t'$ represents the time difference. An important expression of the frequency-dependent response function $\chi_D^O(\mathbf{r},\mathbf{r}';\omega)$ is the Lehmann representation. The Lehmann representation [54] is a powerful tool that expresses the response function in terms of the system's energy eigenstates and allows for the interpretation of the response function in terms of excitation energies and corresponding transition amplitudes. A derivation of the Lehmann representation of the response function of Eq. (91) is detailed as follows. For a complete set of eigenstates $\{\Psi_0,\Psi_1,...,\Psi_n,...\}$ of the time-independent Hamiltonian $\hat{H}_0$, where Ψ_0 is the correlated ground-state, with corresponding energy E_0; Ψ_1 is the first excited state, with energy E_1; and so on. The nth excitation energy of the coupled system is defined as $\Omega_n = (E_n - E_0)/\hbar$. Making use of the completeness relation $\hat{\mathbb{1}} = \sum_{n=0}^{\infty}|\Psi_n\rangle\langle\Psi_n|$ in Eq. (91) results to

$$\begin{aligned}\chi_D^O(\mathbf{r},\mathbf{r}';\omega) = -\frac{i}{\hbar}\sum_{n=0}^{\infty}\int_{-\infty}^{\infty} d\tau\Theta(\tau)e^{-i\omega\tau}\Big\{&\langle\Psi_0|\hat{O}(\mathbf{r})|\Psi_n\rangle\langle\Psi_n|\hat{D}(\mathbf{r}')|\Psi_0\rangle e^{-i\Omega_n\tau}\\ &-\langle\Psi_0|\hat{D}(\mathbf{r}')|\Psi_n\rangle\langle\Psi_n|\hat{O}(\mathbf{r})|\Psi_0\rangle e^{i\Omega_n\tau}\Big\}.\end{aligned} \tag{92}$$

Next, making a substitution of the integral form of the Heaviside step function given as

$$\Theta(\tau) = \lim_{\eta\to 0^+}\frac{i}{2\pi}\int_{-\infty}^{\infty} d\tau\frac{e^{-i\omega\tau}}{\omega+i\eta}, \tag{93}$$

into Eq. (92) further simplifies the frequency-dependent response function to the form

$$\begin{aligned}\chi_D^O(\mathbf{r},\mathbf{r}';\omega) = \frac{1}{\hbar}\lim_{\eta\to 0^+}\sum_{n=0}^{\infty}\Bigg[&\frac{\langle\Psi_0|\hat{O}(\mathbf{r})|\Psi_n\rangle\langle\Psi_n|\hat{D}(\mathbf{r}')|\Psi_0\rangle}{\omega-\Omega_n+i\eta}\\ &-\frac{\langle\Psi_0|\hat{D}(\mathbf{r}')|\Psi_n\rangle\langle\Psi_n|\hat{O}(\mathbf{r})|\Psi_0\rangle}{\omega+\Omega_n+i\eta}\Bigg].\end{aligned} \tag{94}$$

Equation (94) is the Lehmann representation of the frequency-dependent response function. The term $\langle\Psi_0|\hat{O}(\mathbf{r})|\Psi_n\rangle\langle\Psi_n|\hat{D}(\mathbf{r}')|\Psi_0\rangle$ is the transition matrix elements and

describes the strength of the excitation peaks while the term $\Omega_n = (E_n - E_0)/\hbar$ of the finite interacting system are the poles of the response functions of the unperturbed system.

Solving for the response function $\chi_D^O(\mathbf{r}, \mathbf{r}'; \omega)$ is a challenging task since access to the eigenstates $\{\Psi_0, \Psi_1, ..., \Psi_n, ...\}$ and light-matter energies $\{E_0, E_1, ..., E_n, ...\}$ are computationally costly. However, there are many-body methods that solve this equation in an approximate way using different approaches as discussed in the next section.

2.5 DENSITY-FUNCTIONAL THEORIES

The previous sections so far presented the problem of the light-matter interaction in terms of wavefunctions. The wavefunctions resulting from such systems provide a natural path to obtain observables in and out of equilibrium by taking the expectation values of hermitian operators. In practice, solving for the wavefunction is often not feasible due to the large parameter space necessary to describe the wavefunction (see Eq. (61)). For an illustrative example, a system comprising of N_e electrons, the wavefunction depends on the spatial coordinates of each electron which gives $3N_e$ independent coordinates. These coordinates result to a total parameter space of 10^{3N_e}, given that each coordinate is just sampled on 10 points. If one now includes 10 photon Fock states for each photon mode, the parameter space now becomes $10^{3N_e} \times 10^M$. For larger systems with $N_e > 10$ coupled to more than one photon mode, even if the wavefunction was obtained, it would be impossible to store the total wavefunction on an ordinary hard disk. In the literature, this exponential scaling is often referred to as the exponential wall of quantum many-body problems [9]. Even though the wavefunction contains all information of the physical system in question, in most practical applications, the focus is not on the wavefunction, but instead on physical observables of such many-body systems.

Nevertheless, it is possible to approximate the many-body matter-photon problem in a different way. Instead of solving for the wavefunction, one can reformulate the full problem in terms of reduced quantities that avoid explicit calculations of the wavefunction. In light of this, one can follow well-known strategies routinely employed in quantum chemistry, in which the ground-state and time-dependent many-body Schrödinger problem is reformulated in terms of density-functional theory (DFT) [55] to make this problem affordable for numerical computations. In the literature, there exist several different flavors of density-functional theories. All the existing flavors of DFT are similar in that they are based on a specific one-to-one correspondence between conjugated variables. This thesis focuses only on those DFT formulations that are relevant to the work carried out in Chap. 3. However, to ease reading for people not familiar with density-functional methods in the context of ab-initio light-matter interactions, these formulations will be introduced in a two-step process. First, Sec. 2.5.1 introduces the basic idea of DFT [9] in the standard setting of electron-only quantum mechanics and then Sec. 2.5.2 presents its electron-only extension to time-dependent DFT [56]. Next, the introduced concepts of ground-state DFT and TDDFT are employed to discuss ground-state quantum electrodynamical density-functional theory (QEDFT) [14] in Sec. 2.5.4 and the time-dependent version of QEDFT in Sec. 2.5.5. In this way the main differences between QEDFT [12] and DFT methods will be highlighted.

2.5.1 GROUND-STATE DENSITY-FUNCTIONAL THEORY

Let us start with the most common form of density-functional methods, which is ground-state DFT. This section is clearly not exhaustive on the topic as massive literature exists on the subject [9, 55, 57–59]. However, DFT as presented here serves as a basis for the later formulation of the Pauli-Fierz problem in dipole approximation as a density-functional theory. Accordingly, important concepts are introduced here that are later expanded upon in ground-state QEDFT. Since the focus here is solely on the electron-only systems, the Hamiltonian of the system is given by

$$\hat{H}_{el} = \hat{T}_e + \hat{W}_{ee} + \hat{V}_{eN} \,. \tag{95}$$

Note that the photon field is taken into account only by the renormalized "physical mass" m_e (bare plus electromagnetic [41]) in $\hat{T}_e = \sum_{i=1}^{N_e} \frac{1}{2m_e} \hat{\mathbf{p}}_i^2$ and the (longitudinal) Coulomb interaction among the charged particles, as well as possible QED corrections. Usually, one would solve the equation $\hat{H}_{el}|\psi_n\rangle = E_n|\psi_n\rangle$ for the eigenstates $|\psi_n\rangle$ from which a particular observable of interest, say the ground-state electron density is computed

$$n(\mathbf{r}) = N_e \int d^3\mathbf{r}_2 \int d^3\mathbf{r}_3 \ldots \int d^3\mathbf{r}_{N_e} |\psi_0(\mathbf{r}, \mathbf{r}_2, \mathbf{r}_3, \ldots, \mathbf{r}_{N_e})|^2. \tag{96}$$

Also, provided the ground-state wavefunction $|\psi_0\rangle$ is available, the ground-state density can alternatively be computed using the electron density operator as

$$n(\mathbf{r}) = \langle\psi_0|\hat{n}(\mathbf{r})|\psi_0\rangle \quad \text{where} \quad \hat{n}(\mathbf{r}) = \sum_{i=1}^{N_e} \delta(\mathbf{r} - \mathbf{r}_i), \tag{97}$$

and the sum is over all electrons at positions $\mathbf{r}_i$. Of course, computing the ground-state wavefunction for large systems is practically infeasible.

In ground-state DFT, the fundamental *basic* quantity is the ground-state electron-density $n(\mathbf{r})$. The question of whether the infeasible computation of the wavefunction can be circumvented was answered by Hohenberg and Kohn [60]. They proved a one-to-one correspondence between the ground-state density $n(\mathbf{r})$ and an external potential $v(\mathbf{r})$, thus implying that the external potential uniquely determines the ground-state density and vice versa. The external potential here is written as a sum of single-particle potentials $\hat{V}_{eN} = \hat{V} = \sum_{i=1}^{N_e} v(\mathbf{r}_i)$. The Hohenberg and Kohn theorem and its proof is outlined below.

The Hohenberg-Kohn (HK) theorem for systems with non-degenerate ground-states reads as follows: *For a finite, interacting many-electron system there exists a one-to-one correspondence between the external potential $v(\boldsymbol{r})$ and the ground-state density $n(\boldsymbol{r})$ [60].* That is, the external potential is a unique functional of the ground-state density, $v([n], \mathbf{r})$, up to a trivial additive constant. The theorem can be proven in two steps: the first being that two different potentials V and V' that differ by more than a constant lead to different ground-state wavefunctions $|\psi_0\rangle$ and $|\psi_0'\rangle$. The time-independent Schrödinger equation for both potentials are:

$$\hat{H}_{el}|\psi_0\rangle = \left[\hat{T}_e + \hat{W}_{ee} + \hat{V}\right]|\psi_0\rangle = E_0|\psi_0\rangle, \tag{98}$$

$$\hat{H}'_{el}|\psi'_0\rangle = \left[\hat{T}_e + \hat{W}_{ee} + \hat{V}'\right]|\psi'_0\rangle = E'_0|\psi'_0\rangle, \tag{99}$$

where E_0 and E_0' are the respective ground-state energies for the two systems with potentials V and V'. Next, by assuming that $|\psi_0\rangle = |\psi_0'\rangle$ and subtracting Eqs. (98) and (99) leads to $\left(\hat{V} - \hat{V}'\right)|\psi_0\rangle = (E_0 - E_0')|\psi_0\rangle$ and simplifies to yield

$$\hat{V} - \hat{V}' = (E_0 - E_0'). \tag{100}$$

Since $(E_0 - E_0')$ is a constant, Eq. (100) contradicts the initial assumption that the potentials V and V' must differ by more than a constant, therefore, showing that for every ground-state wavefunction $|\psi_0\rangle$ the corresponds a unique potential $\hat{V}$ [60]. The proof is completed by showing that there exists only one $n(\mathbf{r})$ for each $\hat{V}$. This can be shown by assuming the contrary, that is, both $|\psi_0\rangle$ and $|\psi_0'\rangle$ produce the same density $n(\mathbf{r})$. For the external potential $\hat{V}'$, the ground-state energy is $E_0' = \langle\psi_0'|\hat{H}_{el}'|\psi_0'\rangle$. Employing the Rayleigh-Ritz variational principle and that two wavefunctions $|\psi_0\rangle$ and $|\psi_0'\rangle$ are different yields

$$E_0' = \langle\psi_0|\hat{H}_{el}'|\psi_0\rangle = \langle\psi_0|\left(\hat{H}_{el} + \hat{V}' - \hat{V}\right)|\psi_0\rangle < E_0 + \int d^3\mathbf{r}\left[v'(\mathbf{r}) - v(\mathbf{r})\right]n(\mathbf{r}). \tag{101}$$

Next, by interchanging the primed and unprimed quantities, one deduces that

$$E_0 = \langle\psi_0'|\hat{H}_{el}|\psi_0'\rangle = \langle\psi_0|\left(\hat{H}_{el}' + \hat{V} - \hat{V}'\right)|\psi_0\rangle < E_0' + \int d^3\mathbf{r}\left[v(\mathbf{r}) - v'(\mathbf{r})\right]n(\mathbf{r}). \tag{102}$$

Adding both inequalities of Eqs (101) and (102) leads to the contradiction

$$E_0 + E_0' < E_0 + E_0'\,. \tag{103}$$

This concludes the second part of the proof that assuming non-degeneracy, to every density there is one and only one ground-state wavefunction [60]. A generalization of this theorem to systems with degenerate ground-states has been demonstrated by Lieb [61]. An implication of the HK theorem is that the non-degenerate ground-state wavefunction is a unique functional of the ground-state density: $|\psi_0\rangle = |\psi_0[n]\rangle$ and as a consequence, the ground-state expectation value of any observable $\hat{O}(\mathbf{r})$ becomes a functional of the density $n(\mathbf{r})$ as

$$O([n],\mathbf{r}) = \langle\psi_0[n]|\hat{O}(\mathbf{r})|\psi_0[n]\rangle. \tag{104}$$

The HK theorem only guarantees that the mapping of the electron density $n(\mathbf{r})$ to the local external potential $v(\mathbf{r})$ is unique, but not that it exists. The question as to whether a given density $n(\mathbf{r})$, which can be constructed as in Eq. (96), is a ground-state density $n(\mathbf{r})$ of the external potential $v(\mathbf{r})$, is the v-representability problem [58, 62]. Although there are some examples for non-v-representable densities [63], there exist proofs for ensemble v-representability on lattice systems [58, 62]. As shown in Eq. (104), the HK theorem allows one to express every observable in terms of the ground-state density and hence define a universal HK functional

$$F[n] = \langle\psi_0[n]|\left(\hat{T}_e + \hat{W}_{ee}\right)|\psi_0[n]\rangle. \tag{105}$$

The functional $F[n]$ is known as the *universal* HK functional because it has no explicit dependence on the external potential $v(\mathbf{r})$. The term "universal" refers here to the fact

that for problems considered in electron-only DFT only the external potential changes while the kinetic and interaction energy is always the same. A consequence of this is that one can find for a given external potential $v(\mathbf{r})$ the exact density as the minimizer of the energy functional

$$E[v] = \min_n \left\{ F[n] + \int d^3\mathbf{r}\, v(\mathbf{r}) n(\mathbf{r}) \right\}. \tag{106}$$

The minimum can equivalently be found by functional variation with respect to the density as

$$\frac{\delta F[n]}{\delta n(\mathbf{r})} + v(\mathbf{r}) = \mu\,, \tag{107}$$

where μ is a Lagrange multiplier. The following section presents how one can make practical use of ground-state DFT.

2.5.1.1 *Kohn-Sham Density Functional Theory*

In 1965, Walter Kohn and Lu Sham, published a fundamental paper [64], where they presented a method that became the most practical implementation of ground-state DFT. The basic idea was to apply the HK theorem to a fictitious (auxiliary) system of non-interacting electrons exhibiting the same density as the fully interacting electronic system [64]. In other words, one can have an energy functional of the auxiliary non-interacting system as

$$E_s[v_s] = \min_n \left\{ T[n] + \int d^3\mathbf{r}\, v_s(\mathbf{r}) n(\mathbf{r}) \right\}, \tag{108}$$

where $v_s(\mathbf{r})$ is a single particle potential of the auxiliary non-interacting system[3] and $T[n]$ is the *universal* functional of the non-interacting system. The main difference is that instead of general many-electron states $|\psi_n\rangle$, the Kohn-Sham (KS) wavefunction consist of a single slater determinant

$$\Phi(\mathbf{r}_1, \mathbf{r}_2, ..., \mathbf{r}_{N_e}) = \frac{1}{\sqrt{N_e!}} \begin{vmatrix} \varphi_1(\mathbf{r}_1) & \varphi_2(\mathbf{r}_1) & \dots & \varphi_{N_e}(\mathbf{r}_1) \\ \varphi_1(\mathbf{r}_2) & \varphi_2(\mathbf{r}_2) & \dots & \varphi_{N_e}(\mathbf{r}_2) \\ \vdots & \vdots & \ddots & \vdots \\ \varphi_1(\mathbf{r}_{N_e}) & \varphi_2(\mathbf{r}_{N_e}) & \dots & \varphi_{N_e}(\mathbf{r}_{N_e}) \end{vmatrix}, \tag{109}$$

and the many-electron problem decouples into single-particle problems. Similarly, from the potential of the auxiliary system $v_s(\mathbf{r})$, one can obtain a given ground-state density via the derivative

$$\frac{\delta T[n]}{\delta n(\mathbf{r})} + v_s([n];\mathbf{r}) = \mu'. \tag{110}$$

The Hartree exchange-correlation (Hxc) energy is defined to be the difference between the universal functional of the interacting and that of the non-interacting system given by

$$E_{\text{Hxc}}[n] := F[n] - T[n]\,. \tag{111}$$

3 The subscript s is usually not explained in the density-functional literature but one can assume that it refers to 'single particle' as the potential often appears in effective single-particle equations [65].

With this definition, Eq. (106) can be written in the following equivalent form

$$E[v] = \min_{n} \left\{ T[n] + E_{\text{Hxc}}[n] + \int d^3\mathbf{r}\, v(\mathbf{r}) n(\mathbf{r}) \right\}. \tag{112}$$

To obtain the ground-state density of the interacting system due to $v(\mathbf{r})$ from the auxiliary non-interacting system, one solves the following equation

$$\frac{\delta T[n]}{\delta n(\mathbf{r})} + v(\mathbf{r}) + \underbrace{\frac{\delta}{\delta n(\mathbf{r})}\left[F[n] - T[n]\right]}_{v_s([n];\mathbf{r}) - v([n];\mathbf{r})} = \mu\,, \tag{113}$$

where the Hartree exchange-correlation (xc) potential is defined as

$$\begin{aligned} v_{\text{Hxc}}([n];\mathbf{r}) &:= \frac{\delta}{\delta n(\mathbf{r})} \overbrace{\left(F[n] - T[n]\right)}^{E_{\text{Hxc}}[n]} \\ &:= v_s([n];\mathbf{r}) - v([n];\mathbf{r})\,. \end{aligned} \tag{114}$$

In order to obtain the density of the interacting system from the non-interacting auxiliary system, requires that the following KS equations are solved self-consistently

$$\left(\frac{\hat{\mathbf{p}}^2}{2m_e} + \underbrace{v(\mathbf{r}) + v_{\text{H}}([n];\mathbf{r}) + v_{\text{xc}}([n];\mathbf{r})}_{v_{\text{KS}}([v,n];\mathbf{r})} \right) \varphi_i(\mathbf{r}) = \epsilon_i \varphi_i(\mathbf{r}), \tag{115}$$

where ϵ_i are the KS eigenvalues. The Hartree potential deduced from the explicit expression of the Hartree energy are given respectively as

$$v_{\text{H}}([n];\mathbf{r}) = \frac{e^2}{4\pi\epsilon_0} \int d^3\mathbf{r}' \frac{n(\mathbf{r}')}{|\mathbf{r} - \mathbf{r}'|}\,, \quad \text{and} \quad E_{\text{H}} = \frac{e^2}{8\pi\epsilon_0} \int d^3\mathbf{r} \int d^3\mathbf{r}' \frac{n(\mathbf{r}) n(\mathbf{r}')}{|\mathbf{r} - \mathbf{r}'|}\,, \tag{116}$$

and the xc potential and energy are given respectively by

$$v_{\text{xc}}([n];\mathbf{r}) = \frac{\delta E_{xc}[n]}{\delta n(\mathbf{r})}, \quad \text{and} \quad E_{xc} = F[n] - T[n] - E_H[n]. \tag{117}$$

The density to be obtained from the KS system is constructed from the single-particle orbitals of Eq. (109) and given explicitly as

$$n(\mathbf{r}) = \sum_{i=1}^{N_e} |\varphi_i(\mathbf{r})|^2. \tag{118}$$

The total electronic many-body ground-state energy is defined as

$$E_v[n] = T[n] + E_H[n] + E_{xc}[n] + \int d^3\mathbf{r}\, v(\mathbf{r}) n(\mathbf{r}). \tag{119}$$

2.5.1.2 *The local-density approximation (LDA)*

In practice, DFT calculations rely on approximations to the xc functional in Eq. (117), the quality of which determines the accuracy of the DFT results. Approximations to the functional can be found by a range of different strategies such as empirical fitting, mixing of exact and approximate exchange, and local scaling among others. For more on existing and commonly used approximate functionals, see Ref. [66] and references therein for an overview.

One of such approximations is the local-density approximation (LDA) [64]. The LDA is the most prominent approximation, which is widely used for different applications, ranging from solids, molecular clusters, atoms and molecules. As other approximate functionals, LDA seeks to provide an approximation to the xc functional. The xc energy functional of Eq. (119) can equally be expressed as follows

$$E_{xc}[n] = \int d^3\mathbf{r}\, \epsilon_{xc}([n];\mathbf{r})n(\mathbf{r}), \tag{120}$$

where the xc energy density is $\epsilon_{xc}([n];\mathbf{r})$. The idea behind the local-density approximation is to replace the functional of the density $\epsilon_{xc}([n_0];\mathbf{r})$ by the xc energy density of the homogeneous electron gas (HEG). Therefore, in the LDA, the xc energy is given by

$$E_{xc}^{\mathrm{LDA}}[n] = \int d^3\mathbf{r}\, \epsilon_{xc}^{\mathrm{HEG}}((n);\mathbf{r})n(\mathbf{r}). \tag{121}$$

Since the effective potential that enters in the self-consistent KS equations (i.e., the eigenvalue equation (115)) requires the knowledge of the xc potential, not of the xc energy, the functional derivative of Eq. (120) produces the xc potential of the form

$$\begin{aligned} v_{xc}([n];\mathbf{r}) &= \epsilon_{xc}([n];\mathbf{r}) + n(\mathbf{r})\frac{\delta\epsilon_{xc}([n];\mathbf{r})}{\delta n(\mathbf{r})}\bigg|_{n_0(\mathbf{r})}, \\ v_{xc}^{\mathrm{LDA}}([n];\mathbf{r}) &= \epsilon_{xc}^{\mathrm{HEG}}((n);\mathbf{r}) + n(\mathbf{r})\frac{\partial\epsilon_{xc}^{\mathrm{HEG}}((n);\mathbf{r})}{\partial n(\mathbf{r})}. \end{aligned} \tag{122}$$

For the HEG, the exchange contribution $\epsilon_x([n];\mathbf{r})$ can be determined analytically, while the correlation contribution $\epsilon_c([n];\mathbf{r})$ can be obtained by Monte-Carlo methods [67].

Other functionals have been proposed to overcome some shortcomings of the LDA. Among them, are the generalized-gradient approximations (GGA) [68–70], the optimized effective potential (OEP) [71] which can include the exact-exchange [72] or the hybrid functionals [73].

2.5.2 TIME-DEPENDENT DENSITY-FUNCTIONAL THEORY

The previous section considered the ground-state properties of electronic systems using DFT. However, for the description of dynamical properties of electronic systems an extension of the ground-state formalism of DFT is required. The framework of time-dependent density-functional theory (TDDFT) put forward by Erich Runge and Eberhard K.U. Gross [74], adds to the static external potential of DFT, a time-dependent potential. Some comprehensive review on the subject of TDDFT can be found in these Refs. [53, 56, 75, 76].

The dynamics of such time-dependent electronic systems is subject to the time-dependent Hamiltonian of Eq. (73) rewritten as $\hat{H}_{el}(t) = \hat{T}_e + \hat{W}_{ee} + \hat{V}(t)$. The external potential $\hat{V}(t)$ can also be written explicitly as a sum of time-dependent single-particle potentials $\hat{V}(t) = \sum_{i=1}^{N_e} v(\mathbf{r}_i, t)$ in which for an electronic system of N_n nuclei the potential is given as

$$v(\mathbf{r}, t) = -\frac{1}{4\pi\epsilon_0} \sum_{j=1}^{N_n} \frac{Z_j e^2}{|\mathbf{r} - \mathbf{R}_j|} + v_{\text{ext}}(\mathbf{r}, t). \tag{123}$$

The potentials are assumed to be Taylor expandable around the initial time t_0. The external time-dependent potential of Eq. (123) which drives the system out of its initial state often takes the form $v_{\text{ext}}(\mathbf{r}, t) = \mathbf{r} \cdot \mathbf{E}(t)$ where $\mathbf{E}(t)$ is a time-dependent electric field in dipole approximation. The time-dependent Schrödinger equation of Eq. (6) of the many-electron system with Hamiltonian $\hat{H}_{el}(t)$ can be used to describe the evolution of the system.

For a fixed initial state $|\psi_0\rangle$ and external potential $v(\mathbf{r}, t)$, one wants to solve Eq. (6) with the Hamiltonian $\hat{H}_{el}(t)$. The resulting wavefunction depends on the initial state and the external potential given as $|\psi([\psi_0, v]; t)\rangle$. Since the wavefunction has functional dependencies on the fixed initial state and external potential, the expectation value for an arbitrary operator $\hat{O}$ become a functional of $|\psi_0\rangle$ and $v(\mathbf{r}, t)$:

$$O([\psi_0, v]; t) = \langle \psi([\psi_0, v]; t) | \hat{O} | \psi([\psi_0, v]; t) \rangle.$$

For TDDFT to be a complete and exact theory, one needs to identify a fundamental variable which allows the labeling of the physical wavefunctions and their respective observables. For a functional-variable change starting from a fixed initial state, there is a need to have a one-to-one correspondence between the external variable $v(\mathbf{r}, t)$ and a chosen internal variable. In TDDFT, the conjugate variable to the external potential is the electron density $n(\mathbf{r}, t)$. Since every observable is labeled by $|\psi_0\rangle$ and $v(\mathbf{r}, t)$, the electron density is equally labeled by these variables as

$$n([\psi_0, v]; \mathbf{r}, t) = \langle \psi([\psi_0, v]; t) | \hat{n}(\mathbf{r}) | \Psi([\Psi_0, v]; t) \rangle . \tag{124}$$

Every density-functional theory is based on the uniqueness and existence of a mapping between a set of basic internal variables (here the electron density) and external variables (here the external potential). If this mapping is proven to exists and is unique, the functional dependence on the external variables in Eq. (124) can be replaced by a functional dependence on the basic internal variables. Therefore, to complete the theory of TDDFT, a proof of the one-to-one mapping for a fixed initial state $|\psi_0\rangle$, that is:

$$v(\mathbf{r}, t) \overset{1:1}{\underset{\psi_0}{\longleftrightarrow}} n(\mathbf{r}, t), \tag{125}$$

has to be established. This is achieved by formulating the time-dependent Schrödinger equation for the Hamiltonian $\hat{H}_{el}(t)$ equivalently by a non-linear fluid equation for the electron density [77, 78]. Therefore, the EOM for the electronic density is required and derived below.

From the evolved electronic wavefunction, one can compute the expectation value of the electron density as in Eq. (124). Using the Heisenberg EOM of Eq. 68 for the electron density, leads to the continuity equation

$$\frac{\partial}{\partial t} n(\mathbf{r},t) = -\boldsymbol{\nabla}\cdot\mathbf{j}(\mathbf{r},t), \tag{126}$$

where $\mathbf{j}(\mathbf{r},t)$ is the paramagnetic current density and is given in operator form as

$$\hat{\mathbf{j}}(\mathbf{r}) = \frac{\hbar}{2im_e}\sum_{l=1}^{N_e}\left[\delta(\mathbf{r}-\mathbf{r}_l)\overrightarrow{\nabla}_l - \overleftarrow{\nabla}_l\delta(\mathbf{r}-\mathbf{r}_l)\right]. \tag{127}$$

The first time-derivative of Eq. (127) employing Eq. (68) yields the EOM for the current density

$$\frac{\partial}{\partial t}\mathbf{j}(\mathbf{r},t) = -\mathbf{F}_{\text{str}}(\mathbf{r},t) + \frac{1}{m_e}n(\mathbf{r},t)\boldsymbol{\nabla}v(\mathbf{r},t), \tag{128}$$

where $\mathbf{F}_{\text{str}}(\mathbf{r},t)$ is the electronic stress force [53] resulting from the expectation value of the commutator $\mathbf{F}_{\text{str}}(\mathbf{r},t) = \langle\psi(t)|\left[\hat{\mathbf{j}}(\mathbf{r}), \hat{T}_e + \hat{W}_{ee}\right]|\psi(t)\rangle$. To obtain a relation between the external potential and electron density, one computes the second time-derivative of the density using Eq. (69) for $k=2$ which results to

$$\frac{\partial^2}{\partial t^2} n(\mathbf{r},t) = -\boldsymbol{\nabla}\cdot\mathbf{F}_{\text{str}}(\mathbf{r},t) + \frac{1}{m_e}\boldsymbol{\nabla}\cdot\left[n(\mathbf{r},t)\boldsymbol{\nabla}v(\mathbf{r},t)\right]. \tag{129}$$

Equation (129) can also be obtained through the relation of the second time-derivative of the density and the paramagnetic current $\frac{\partial^2}{\partial t^2}n(\mathbf{r},t) = -\boldsymbol{\nabla}\cdot\frac{\partial}{\partial t}\mathbf{j}(\mathbf{r},t)$.

2.5.2.1 *Runge-Gross Theorem*

The basic idea of TDDFT is to describe the time evolution of a many-electron quantum system solely in terms of the time-dependent particle density $n(\mathbf{r},t)$. In 1984, Erich Runge and Eberhard K.U. Gross proved [74] that for a given initial state $\psi(t_0)$, there exists a one-to-one mapping between the time-dependent density $n(\mathbf{r},t)$ and the time-dependent external potential $v(\mathbf{r},t)$. A summary of the Runge-Gross (RG) theorem is briefly sketched in the following.

Runge and Gross proved that, two solutions $\psi(t)$ and $\psi'(t)$ of the time-dependent Schrödinger equation for Hamiltonians $\hat{H}_{el}(t)$ and $\hat{H}'_{el}(t)$ which evolve from a fixed common initial state $\psi(t_0)$ under the influence of the respective potentials $v(\mathbf{r},t)$ and $v'(\mathbf{r},t)$, always lead to different electron densities $n(\mathbf{r},t)$ and $n'(\mathbf{r},t)$. This holds true provided the two potentials differ by more than a time-dependent constant function, $v(\mathbf{r},t) \neq v'(\mathbf{r},t) + c(t)$. Assuming that the potentials are analytic in time, the external potentials can be expanded in a Taylor series as

$$v(\mathbf{r},t) = \sum_{k=0}^{\infty}\frac{1}{k!}\left.\frac{\partial^k v_k(\mathbf{r},t)}{\partial t^k}\right|_{t_0}(t-t_0)^k, \quad \text{and} \quad v'(\mathbf{r},t) = \sum_{k=0}^{\infty}\frac{1}{k!}\left.\frac{\partial^k v'_k(\mathbf{r},t)}{\partial t^k}\right|_{t_0}(t-t_0)^k. \tag{130}$$

The condition that the two potentials differ by more than a constant function, $c(t)$, assures that there exists an integer $k \geq 0$, such that the Taylor coefficients of Eq. (130) differ by more than a constant as follows

$$\left.\frac{\partial^k v_k(\mathbf{r},t)}{\partial t^k}\right|_{t_0} - \left.\frac{\partial^k v_k'(\mathbf{r},t)}{\partial t^k}\right|_{t_0} \neq \text{const}\,. \tag{131}$$

The proof of the RG theorem employs the continuity equation (126) and the equation of motion for the paramagnetic current density, Eq. (128). The first step of the proof establishes the uniqueness of the current densities. For two wavefunctions $\psi(t)$ and $\psi'(t)$ that evolve from the same initial state $\psi(t_0)$, the difference in current densities is

$$\frac{\partial}{\partial t}\left[\mathbf{j}(\mathbf{r},t) - \mathbf{j}'(\mathbf{r},t)\right]\big|_{t_0} = -\frac{1}{m_e} n(\mathbf{r},t_0)\boldsymbol{\nabla}(v(\mathbf{r},t_0) - v'(\mathbf{r},t_0)). \tag{132}$$

Here the electronic stress forces in Eq. (128) for the unprimed and primed systems are identical at t_0 and cancel out since both systems start from the same initial state. From Eq. (132), it is evident that the current densities $\mathbf{j}(\mathbf{r},t)$ and $\mathbf{j}'(\mathbf{r},t)$ will differ infinitesimally later than t_0 if the two potentials $v(\mathbf{r},t_0)$ and $v'(\mathbf{r},t_0)$ are different [74]. Therefore, if the condition given in Eq. (131) is satisfied for $k = 0$, this implies the right-hand side of Eq. (132) is different from zero and the two current densities $\mathbf{j}(\mathbf{r},t)$ and $\mathbf{j}'(\mathbf{r},t)$ eventually become different infinitesimally later than t_0.

If the smallest integer k for which Eq. (131) is satisfied is greater than zero, the potentials are equal up to a constant at the initial time t_0 but differ at a later time $t > t_0$. Applying the Heisenberg EOM $k-$times by using Eq. (69), results to

$$\frac{\partial^{k+1}}{\partial t^{k+1}}\left[\mathbf{j}(\mathbf{r},t) - \mathbf{j}'(\mathbf{r},t)\right]\big|_{t_0} = -\frac{1}{m_e} n(\mathbf{r},t_0)\boldsymbol{\nabla}(v_k(\mathbf{r},t_0) - v_k'(\mathbf{r},t_0)), \tag{133}$$

where the potentials are assumed to be the same up to the $k-$th derivative. The right-hand side of Eq. (133) differs from zero in accordance to Eq. (132) for the smallest integer k, which then implies that $\mathbf{j}(\mathbf{r},t) \neq \mathbf{j}'(\mathbf{r},t)$ for $t > t_0$. Secondly, the next step demonstrates that

$$\begin{aligned}\frac{\partial^{k+2}}{\partial t^{k+2}}\left[n(\mathbf{r},t) - n'(\mathbf{r},t)\right]\big|_{t_0} &= -\boldsymbol{\nabla}\cdot\frac{\partial^{k+1}}{\partial t^{k+1}}\left[\mathbf{j}(\mathbf{r},t) - \mathbf{j}'(\mathbf{r},t)\right]\big|_{t_0} \\ &= -\boldsymbol{\nabla}\cdot\left(\frac{1}{m_e} n(\mathbf{r},t_0)\boldsymbol{\nabla}(v_k(\mathbf{r},t_0) - v_k'(\mathbf{r},t_0))\right).\end{aligned} \tag{134}$$

Assuming that the quantity $n(\mathbf{r},t)|\boldsymbol{\nabla}v^2(\mathbf{r},t)|$ decays faster than $1/\mathbf{r}^2$ for large $\mathbf{r}$ for both the primed and unprimed system it can be shown that the right hand side of Eq. (134) cannot vanish identically [74]. As a consequence, the densities $n(\mathbf{r},t)$ and $n'(\mathbf{r},t)$ become different infinitesimally later than t_0. Therefore, the electronic density $n(\mathbf{r},t)$ uniquely determines the time-dependent potential $v(\mathbf{r},t)$ up to a purely time-dependent function $c(t)$. A consequence of TDDFT is that all physical observables become functionals of the electron density and the initial state $O([n,\psi_0];t) = \langle\psi([n,\psi_0];t)|\hat{O}(t)|\psi([n,\psi_0];t)\rangle$.

2.5.2.2 *Kohn-Sham system of time-dependent density-functional theory*

As in the case of ground-state DFT introduced in Sec. 2.5.1, the central idea of Kohn-Sham DFT is to associate with an interacting system an effective non-interacting KS system, which has the same time-dependent electronic density as the interacting system. Since the KS system is a non-interacting system it is much easier to treat in numerical applications than the fully interacting system.

The time-dependent KS equations for single-particle wavefunctions $\varphi_i(\mathbf{r},t)$ are given by the following set of equations

$$i\hbar\frac{\partial}{\partial t}\varphi_i(\mathbf{r},t) = \left(\frac{\hat{\mathbf{p}}^2}{2m_e} + \underbrace{v(\mathbf{r},t) + v_{\mathrm{H}}([n];\mathbf{r},t) + v_{\mathrm{xc}}([n,\psi_0,\varphi_0];\mathbf{r},t)}_{v_{\mathrm{KS}}([v,n,\psi_0,\varphi_0];\mathbf{r},t)}\right)\varphi_i(\mathbf{r},t), \quad (135)$$

where $|\psi_0\rangle$ is the many-body electronic initial state, $\varphi_0(\mathbf{r},t_0)$ is the initial state of the non-interacting KS system and the KS potential $v_{\mathrm{KS}}([v,n,\psi_0,\varphi_0];\mathbf{r},t)$ is given in Eq. (135). The initial-state dependence of the KS potential $v_{\mathrm{KS}}([v,n,\psi_0,\varphi_0];\mathbf{r},t)$ can be avoided if one assumes that the ground-state is the starting point for the time-propagation [65, 79] of the system. The electronic density of the interacting system can be obtained from the time-dependent KS orbitals

$$n(\mathbf{r},t) = \sum_{i=1}^{N_e}|\varphi_i(\mathbf{r},t)|^2. \quad (136)$$

The time-dependent Hxc potential of the non-interacting KS system of Eq. (135) can be expressed as

$$\begin{aligned} v_{\mathrm{Hxc}}([n,\psi_0,\varphi_0];\mathbf{r},t) &= v_{\mathrm{H}}([n];\mathbf{r},t) + v_{\mathrm{xc}}([n,\psi_0,\varphi_0];\mathbf{r},t) \\ &= v_{\mathrm{s}}([n,\varphi_0];\mathbf{r},t) - v([n,\psi_0];\mathbf{r},t), \end{aligned} \quad (137)$$

where $v_{\mathrm{s}}(\mathbf{r},t)$ is the single-particle potential of the non-interacting system, the time-dependent Hartree potential $v_{\mathrm{H}}([n];\mathbf{r},t)$ that accounts for the classical electrostatic interaction between the electrons is given by

$$v_{\mathrm{H}}([n];\mathbf{r},t) = \frac{e^2}{4\pi\epsilon_0}\int d^3\mathbf{r}'\frac{n(\mathbf{r}',t)}{|\mathbf{r}-\mathbf{r}'|}. \quad (138)$$

The xc potential $v_{\mathrm{xc}}([n,\psi_0,\varphi_0];\mathbf{r},t)$ comprises of all the non-trivial many-body effects.

2.5.2.3 *Adiabatic approximation*

The price to pay for the simplification to a KS system is that the one-body KS potential is in general an unknown functional of the density. Despite this difficulty it turned out that practically useful approximations for this potential can be devised. The simplest and most widely used approximation to describe time-dependent systems is the adiabatic approximation.

In the adiabatic approximation, the density at time t is plugged into a ground-state functional of the xc potential as

$$v_{\mathrm{xc}}^{\mathrm{adiabatic}}([n,\psi_0,\varphi_0];\mathbf{r},t) = v_{\mathrm{xc}}([n];\mathbf{r})|_{n(\mathbf{r})\to n(\mathbf{r},t)}\,. \quad (139)$$

In Eq. (139), the same functional form is used but evaluated at each time with the density $n(\mathbf{r},t)$. The adiabatic approximation is justified for systems in which the time-dependent electron density does not change rapidly. Making a substitution of the LDA functional in Eq. (139) yields the so-called adiabatic local-density approximation (ALDA):

$$v_{\mathrm{xc}}^{\mathrm{ALDA}}([n,\psi_0,\varphi_0];\mathbf{r},t) = v_{\mathrm{xc}}^{\mathrm{HEG}}((n);\mathbf{r})\Big|_{n(\mathbf{r})\to n(\mathbf{r},t)}. \tag{140}$$

The ALDA assumes that the xc potential at the position $\mathbf{r}$ and time t is equal to the xc potential of a static homogeneous-electron gas of density $n(\mathbf{r},t)$.

2.5.3 LINEAR RESPONSE OF TDDFT

Despite the local nature of the effective single-particle KS potential, the full solution of the time-dependent KS equations can be quite demanding for large systems. However, the calculation of physical observables like excitation energies or polarizabilities of atomic and molecular systems requires only the knowledge of the linear density response of the system [4]. This is also true for coupled matter-photon systems. Therefore, a much simpler perturbative solution of the time-dependent KS equations is sufficient. In this case the linear-response theory become applicable. This section presents the basics of linear-response theory for matter-only system within the semi-classical limit and formulated within TDDFT. This will later highlight the main differences when compared to the linear-response theory in non-relativistic QED and its equivalent formulation within the framework of QEDFT that we derive in Chap. 3.2.

To begin a linear-response treatment in TDDFT, let us first describe the linear response in the semi-classical limit in which the Hamiltonian is given by Eq. (74) where the time-dependent potential is given explicitly by Eq. (123). In the linear-response regime, the time-dependent potential can now be written as $v(\mathbf{r},t) = v_0(\mathbf{r}) + \delta v(\mathbf{r},t)$. Here, $v_0(\mathbf{r})$ describes the attractive part of the external potential due to the nuclei and $\delta v(\mathbf{r},t)$ can have the form $\delta v(\mathbf{r},t) = \mathbf{r}\cdot\delta\mathbf{E}(t)$ where $\delta\mathbf{E}(t)$ is a weak classical external transversal probe field in dipole approximation that couples to the electronic subsystem. Formulated within linear response, the density response to an external perturbation (as presented in Sec. 2.4) using Eq. (83) is given as

$$\delta n(\mathbf{r},t) = \int_{t_0}^{t} dt' \int d^3\mathbf{r}' \chi_n^n(\mathbf{r},t;\mathbf{r}',t')\delta v(\mathbf{r}',t'). \tag{141}$$

Here, the density-density response function, $\chi_n^n(\mathbf{r},t;\mathbf{r}',t')$, of the interacting many-body electronic system is given in commutator and differential from as (see Sec. 2.4):

$$\begin{aligned}\chi_n^n(\mathbf{r},t;\mathbf{r}',t') &= -\frac{i}{\hbar}\Theta(t-t')\langle\psi_0|\left[\hat{n}_I(\mathbf{r},t),\hat{n}_I(\mathbf{r}',t')\right]|\psi_0\rangle \\ &= \frac{\delta n([v];\mathbf{r},t)}{\delta v(\mathbf{r}',t')}\bigg|_{v_0(\mathbf{r})},\end{aligned} \tag{142}$$

where the expectation value of the commutator of the electronic densities is with respect to the correlated electronic ground-state $|\psi_0\rangle$. The response function of Eq. (142)

4 In other cases the second, third and higher order responses and response functions can be computed depending on the spectroscopic observable one is interested in.

can be expressed in frequency space by using the Lehmann representation given in Eq. (94) which in this case is

$$\chi_n^n(\mathbf{r},\mathbf{r}';\omega) = \frac{1}{\hbar}\lim_{\eta\to 0^+}\sum_{n=0}^{\infty}\left[\frac{\langle\psi_0|\hat{n}(\mathbf{r})|\psi_n\rangle\langle\psi_n|\hat{n}(\mathbf{r}')|\psi_0\rangle}{\omega-\Omega_n+i\eta} - \frac{\langle\psi_0|\hat{n}(\mathbf{r}')|\psi_n\rangle\langle\psi_n|\hat{n}(\mathbf{r})|\psi_0\rangle}{\omega+\Omega_n+i\eta}\right], \tag{143}$$

where ψ_n are the eigenstates of the matter-only problem and Ω_n are the corresponding excitation frequencies. Practical calculations for the response of a many-electron system is a considerable challenge due to the large degrees of freedom. In practice, TDDFT is one of the most frequently applied theories to approach this problem. Formulated within TDDFT linear response, the density-density response function of the interacting system can be expressed in terms of the non-interacting density-density response function and a Hxc kernel that has a form of a Dyson-type equation [80]:

$$\begin{aligned}\chi_n^n(\mathbf{r},t;\mathbf{r}',t') = \chi_{n,\mathrm{s}}^n(\mathbf{r},t;\mathbf{r}',t') + \iint d^3\mathbf{x}\,\mathrm{d}\tau\;\chi_{n,\mathrm{s}}^n(\mathbf{r},t;\mathbf{x},\tau)\\ \times\iint d^3\mathbf{y}\,d\tau'\;f_{\mathrm{Hxc}}(\mathbf{x},\tau;\mathbf{y},\tau')\chi_n^n(\mathbf{y},\tau';\mathbf{r}',t')\,.\end{aligned} \tag{144}$$

The non-interacting density-density response function of the auxiliary KS system in the above equation can be expressed in the form of Eq. (83) and (89) given by

$$\begin{aligned}\chi_{n,\mathrm{s}}^n(\mathbf{r},t;\mathbf{r}',t') &= \langle\varphi_0|\left[\hat{n}_I(\mathbf{r},t),\hat{n}_I(\mathbf{r}',t')\right]|\varphi_0\rangle\\ &= \left.\frac{\delta n([v_s];\mathbf{r},t)}{\delta v_{\mathrm{s}}(\mathbf{r}',t')}\right|_{v_s([n];\mathbf{r})}.\end{aligned} \tag{145}$$

The so-called Hxc kernel in Eq. (144) can be obtained from Eq. (137) through a functional derivative with the density that yields

$$\begin{aligned}f_{\mathrm{Hxc}}([n];\mathbf{r},t;\mathbf{r}',t') &= \frac{\delta v_s([n];\mathbf{r},t)}{\delta n(\mathbf{r}',t')} - \frac{\delta v([n];\mathbf{r},t)}{\delta n(\mathbf{r}',t')}\\ &= \left[\chi_{n,\mathrm{s}}^n(\mathbf{r},t;\mathbf{r}',t')\right]^{-1} - \left[\chi_n^n(\mathbf{r},t;\mathbf{r}',t')\right]^{-1}.\end{aligned} \tag{146}$$

The Dyson-type equation (144) is the central result of the TDDFT linear-response formalism which relates the interacting and the non-interacting response functions. Substituting the density-density response function Eq. (144) into (142) leads to the time-dependent KS equation for the linear density response

$$\delta n(\mathbf{r},t) = \int_{t_0}^{t} dt' \int d^3\mathbf{r}'\chi_{n,\mathrm{s}}^n(\mathbf{r},t;\mathbf{r}',t')\delta v_{\mathrm{KS}}(\mathbf{r}',t'), \tag{147}$$

where the KS potential comprises of the external perturbation, the Hartree- and xc contributions as follows

$$\delta v_{\mathrm{KS}}(\mathbf{r},t) = \delta v(\mathbf{r},t) + \int d^3\mathbf{r}' \int dt'\;\left[f_{\mathrm{H}}(\mathbf{r},t;\mathbf{r}',t') + f_{\mathrm{xc}}(\mathbf{r},t;\mathbf{r}',t')\right]\delta n(\mathbf{r}',t'). \tag{148}$$

The Hartree- and xc kernels in Eq. (148) are respectively

$$f_{\mathrm{H}}(\mathbf{r},t;\mathbf{r}',t') = \frac{e^2}{4\pi\epsilon_0}\frac{\delta(t-t')}{|\mathbf{r}-\mathbf{r}'|}, \quad \text{and} \quad f_{\mathrm{xc}}([n];\mathbf{r},t;\mathbf{r}',t') = \frac{\delta v_{xc}([n];\mathbf{r},t)}{\delta n(\mathbf{r}',t')}. \tag{149}$$

When dealing with excitation energies and polarizabilities, it is useful to consider the KS equation (147) in frequency space. Inserting Eq. (148) into Eq. (147) and further performing a Fourier transform as in Eq. (91) due to the invariance under time translations, leads to the frequency-dependent linear density response of the electron density

$$\delta n(\mathbf{r},\omega) = \int d^3\mathbf{r}' \chi^n_{n,s}(\mathbf{r},\mathbf{r}';\omega)\delta v_{\mathrm{KS}}(\mathbf{r}',\omega), \tag{150}$$

where $\chi^n_{n,s}(\mathbf{r},\mathbf{r}';\omega)$ is the non-interacting response function in frequency space and $v_{\mathrm{KS}}(\mathbf{r}',\omega)$ is the KS potential given explicitly as

$$\delta v_{\mathrm{KS}}(\mathbf{r}',\omega) = \delta v(\mathbf{r}',\omega) + \int d^3\mathbf{x}\, f_{\mathrm{Hxc}}(\mathbf{r}',\mathbf{x},\omega)\delta n(\mathbf{x},\omega)\,. \tag{151}$$

The non-interacting KS response function of Eq. (150) is given in terms of the KS orbitals from Eq. (115) in the frequency space by [80]:

$$\chi^n_{n,s}(\mathbf{r},\mathbf{r}',\omega) = \frac{1}{\hbar}\sum_{j,k}(f_k - f_j)\frac{\varphi_j(\mathbf{r})\varphi_k(\mathbf{r}')\varphi^*_k(\mathbf{r})\varphi^*_j(\mathbf{r}')}{\omega - (\epsilon_l - \epsilon_k) + i\eta}\,, \tag{152}$$

where f_k, f_j are the Fermi-occupation factors that refers to the configuration of the KS ground-state (1 for occupied and 0 for unoccupied KS orbitals).

2.5.3.1 *The exchange-correlation kernel*

The linear response formulation of TDDFT introduces the quantity called the xc kernel f_{xc}. The f_{xc} is a very complex quantity that accounts for all non-trivial many-body effects. The simplest treatment of the xc kernel is the random-phase approximation (RPA) which sets the kernel to zero, i.e. $f^{\mathrm{RPA}}_{\mathrm{xc}} = 0$. This treatment of the kernel ignores all correlations in the linear response setting. On the other hand, many approximate xc kernels have been proposed and the most commonly used approximations for the f_{xc} include the ALDA and the so-called PGG (Petersilka, Gossmann, Gross) [80] kernel. The simplest is the ALDA kernel which is based on the functional form of the static LDA and given by

$$f^{\mathrm{ALDA}}_{\mathrm{xc}}([n];\mathbf{r},\mathbf{r}') = \delta(\mathbf{r}-\mathbf{r}')\frac{d^2}{dn^2}\epsilon^{\mathrm{HEG}}_{\mathrm{xc}}((n);\mathbf{r})\,. \tag{153}$$

The ALDA kernel is not only frequency-independent, it is also local in space. A consequence of a frequency-independent kernel is that it does not generate new poles and fails to describe the doubly excited states of the system [81].

2.5.3.2 *Computational Methods for Calculating linear response within TDDFT*

This section briefly outlines three different but equivalent methods to numerically solve linear responses within the framework of TDDFT. These methods will be reformulated within QEDFT in Chap. 3.5 which in the zero-coupling limit reduces back to the methods already established in TDDFT. The three standard methods in TDDFT linear response for calculating the density response of Eq. (147) are: time-propagation [82], frequency-dependent Sternheimer equations [83] and the Casida equation [84].

The time-propagation method propagates the time-dependent KS equations (135) from which the electron density of Eq. (136) can be obtained as well as the time-dependent dipole moments [82]. The Casida method rather obtains the excitation frequencies and oscillator strengths of the density-density response function of Eq. (143). This is done through an exact diagonalization of a pseudo-eigenvalue equation given in particle-hole basis [84] that employs the sum-over-states representation of Eq. (152). The frequency-dependent Sternheimer method solves for a specific order of the density response in terms of the first and higher order changes of the wavefunctions.

An extension of these methods within the framework of QEDFT and practical computations are presented in Chap. 3. A prerequisite to linear-response within QEDFT is to find the ground-state. Therefore, ground-state QEDFT and the time-dependent case are presented successively in the following two sections.

2.5.4 GROUND-STATE QUANTUM-ELECTRODYNAMICAL DENSITY-FUNCTIONAL THEORY

Sections 2.5.1 and 2.5.2 respectively focused on ground-state DFT and TDDFT which reformulated the matter-only problem in terms of reduced quantities that avoid unaffordable explicit calculations of the wavefunction. In the case of many-body matter-photon systems, similar approaches can be applied. To treat ground-state properties of coupled matter-photon systems, the ground-state quantum electrodynamical density-functional theory (QEDFT) was developed [14] which is a generalization of the HK theorem to matter-photon systems. Such a first-principles formulation is necessary for the same reason as ground-state DFT, i.e., explicit calculation of the wavefunction is impossible and even more difficult when the photons are included. The ground-state QEDFT presented here follows closely that of Ref. [14]. The proof for the full minimal coupling case is also given in Ref. [14]. The setting is the non-relativistic limit of QED in the length form for describing light-matter systems discussed in Sec. 2.2.2. The length gauge Hamiltonian introduced in Eq. (55) now includes a coupling to the external charge current given as

$$\hat{H}_L = \underbrace{\hat{T}_e + \hat{W}_{ee} + \frac{1}{2}\sum_{\alpha=1}^{M}\left[\hat{p}_\alpha^2 + \omega_\alpha^2\left(\hat{q}_\alpha - \frac{\boldsymbol{\lambda}_\alpha}{\omega_\alpha}\cdot\hat{\mathbf{R}}\right)^2\right]}_{\hat{H}_{L,0}} + \int d^3\mathbf{r}\,\hat{n}(\mathbf{r})v(\mathbf{r}) + \sum_{\alpha=1}^{M}\frac{j_\alpha}{\omega_\alpha}\hat{q}_\alpha\,. \tag{154}$$

Here, the static external charge current j_α merely polarizes the vacuum of the photon field and generates static electric fields and $\hat{H}_{L,0}$ is the *internal* Hamiltonian.

As in the case of ground-state DFT (see Sec. 2.5.1), a density-functional reformulation of the above ground-state problem seeks to avoid an explicit reference to the correlated hybrid electron-photon ground-state Ψ_0. This implies that, instead of expressing every observable in terms of the wavefunction one then expresses them via some reduced quantities. How to identify the pair of conjugate variables is discussed in Ref. [14], which are the internal pair $(n(\mathbf{r}), q_\alpha)$ and external external pair $(v(\mathbf{r}), j_\alpha)$ [5]. Here, the HK proof is used to show that for every such external pair $(v(\mathbf{r}), j_\alpha)$ there is

5 The photon coordinates q_α and static currents j_α refers to the sets $\{q_1, q_2, ..., q_M\}$ and $\{j_1, j_2, ..., j_M\}$, respectively.

a unique ground-state and that these external variables have a one-to-one mapping with the internal pair $(n(\mathbf{r}), q_\alpha)$, where $n(\mathbf{r})$ is the electron density expectation value and q_α is the expectation value of the photon displacement coordinates. The first step (as in Sec. 2.5.1) is to show that there is one and only one ground-state for a given external pair. To prove this, the opposite is assumed, i.e., that $\Psi_0 = \Psi_0'$ for different set of external pairs $(v(\mathbf{r}), j_\alpha)$ and $(v'(\mathbf{r}), j_\alpha')$ leads to a contradiction. Following similar steps as in Eqs. (98) and (99) using Eq. (154) leads to

$$\left[(v(\mathbf{r}) - v'(\mathbf{r})) + \sum_{\alpha=1}^{M} \frac{1}{\omega_\alpha}(j_\alpha - j_\alpha')\hat{q}_\alpha\right]\Psi_0 = (E_0 - E_0')\Psi_0\,. \tag{155}$$

If $j_\alpha = j_\alpha'$, Eq. (155) readily simplifies to the usual HK case of Eq. (100). For the case $j_\alpha \neq j_\alpha'$, Eq. (155) results to an eigenvalue equation which only allows the trivial solution [14]. Both cases lead to the condition that $v(\mathbf{r}) - v'(\mathbf{r}) = c$, which is a contradiction to the original assumption. The proof is completed by showing that two different ground-state wavefunctions produce different internal pair $(n(\mathbf{r}), q_\alpha)$. To prove this, one assumes the contrary, i.e., both Ψ_0 and Ψ_0' produce the same internal pair $(n(\mathbf{r}), q_\alpha)$. Again following similar steps as in Eqs. (101) and (102), the primed and unprimed inequalities are

$$E_0' = \langle\Psi_0|\hat{H}_{L,0}'|\Psi_0\rangle < E_0 + \int d^3\mathbf{r}\left[v'(\mathbf{r}) - v(\mathbf{r})\right]n(\mathbf{r}) + \sum_{\alpha=1}^{M}\frac{1}{\omega_\alpha}(j_\alpha' - j_\alpha)q_\alpha\,. \tag{156}$$

$$E_0 = \langle\Psi_0'|\hat{H}_{L,0}|\Psi_0'\rangle < E_0' + \int d^3\mathbf{r}\left[v(\mathbf{r}) - v'(\mathbf{r})\right]n(\mathbf{r}) + \sum_{\alpha=1}^{M}\frac{1}{\omega_\alpha}(j_\alpha - j_\alpha')q_\alpha\,. \tag{157}$$

Adding both inequalities of Eqs (156) and (157) leads to the contradiction $E_0 + E_0' < E_0 + E_0'$. This establishes the one-to-one mapping $(v(\mathbf{r}), j_\alpha) \overset{1:1}{\underset{\Psi_0}{\longleftrightarrow}} (n(\mathbf{r}), q_\alpha)$ and therefore, all ground-state wavefunctions can be uniquely labeled by their respective internal pair $\Psi_0[n, q_\alpha]$. As a consequence, the ground-state expectation value of any observable $\hat{O}(\mathbf{r})$ becomes a functional of the density $n(\mathbf{r})$ and photon displacement coordinates as

$$O([n, q_\alpha], \mathbf{r}) = \langle\psi_0[n, q_\alpha]|\hat{O}(\mathbf{r})|\psi_0[n, q_\alpha]\rangle. \tag{158}$$

Since the ground-state wavefunction is labeled by $\Psi_0[n, q_\alpha]$, one can define a universal functional in this setting to be

$$F[n, q_\alpha] := \langle\Psi[n, q_\alpha]|\hat{H}_{L,0}|\Psi[n, q_\alpha]\rangle\,. \tag{159}$$

The universal functional of Eq. (159) clearly differs from that of Eq. (106) as can be seen for the additional functional dependence on q_α. The ground-state energy of the coupled light-matter system can be found by a variational principle

$$E[v, j_\alpha] = \min_{(n,q_\alpha)}\left\{F[n, q_\alpha] + \int d^3\mathbf{r}\, v(\mathbf{r})n(\mathbf{r}) + \sum_{\alpha=1}^{M}\frac{j_\alpha}{\omega_\alpha}q_\alpha\right\}. \tag{160}$$

The minimum can equivalently be found by functional variation with respect to the density and photon coordinates as

$$\frac{\delta F[n, q_\alpha]}{\delta n(\mathbf{r})} + v(\mathbf{r}) = \mu \quad \text{and} \quad \frac{\delta F[n, q_\alpha]}{\delta q_\alpha} + \frac{j_\alpha}{\omega_\alpha} = \mu'\,, \tag{161}$$

where μ and μ' are Lagrange multipliers. The following section presents how one can make practical use of ground-state QEDFT.

2.5.4.1 *Maxwell-Kohn-Sham Ground-state QEDFT*

To make ground-state QEDFT practical, one defines a numerically tractable auxiliary non-interacting system. All the above proofs work in the same manner when applied to the non-interacting system describe by the Hamiltonian

$$\hat{H}_L^{(s)} = \underbrace{\hat{T}_e + \frac{1}{2}\sum_{\alpha=1}^{M}\left(\hat{p}_\alpha^2 + \omega_\alpha^2\hat{q}_\alpha^2\right)}_{\hat{H}_{L,0}^{(s)}} + \int d^3\mathbf{r}\,\hat{n}(\mathbf{r})v_s(\mathbf{r}) + \sum_{\alpha=1}^{M}\frac{j_{\alpha,s}}{\omega_\alpha}\hat{q}_\alpha\,, \tag{162}$$

where $j_{\alpha,s}$ is the current of the non-interacting system. The mean-field exchange-correlation (Mxc) energy functional can be defined as the difference between the universal functional of the interacting and that of the non-interacting auxiliary systems

$$E_{\mathrm{Mxc}}[n,q_\alpha] := F[n,q_\alpha] - F_s[n,q_\alpha]\,. \tag{163}$$

Here the universal functional of the non-interacting system has the explicit form $F_s[n,q_\alpha] := \langle\Psi_s[n,q_\alpha]|\hat{H}_{L,0}^{(s)}|\Psi_s[n,q_\alpha]\rangle$ where $|\Psi_s[n,q_\alpha]\rangle = |\psi[n]\rangle\otimes|\phi[q_\alpha]\rangle$ is here a factorizable product state between the electronic and photonic subsystems. Using Eq. (163) the minimization of Eq. (160) can be rewritten as

$$E[v,j_\alpha] = \min_{(n,q_\alpha)}\left\{F_s[n,q_\alpha] + E_{\mathrm{Mxc}}[n,q_\alpha] + \int d^3\mathbf{r}\,v(\mathbf{r})n(\mathbf{r}) + \sum_{\alpha=1}^{M}\frac{j_\alpha}{\omega_\alpha}q_\alpha\right\}. \tag{164}$$

Next, to find the internal pair $(n(\mathbf{r}),q_\alpha)$ of the interacting system due to the external pair $(v(\mathbf{r}),j_\alpha)$ from the auxiliary non-interacting system, one solves the following equation

$$\begin{aligned}
&\frac{\delta F_s[n,q_\alpha]}{\delta n(\mathbf{r})} + \underbrace{\frac{\delta}{\delta n(\mathbf{r})}\left(F[n,q_\alpha] - F_s[n,q_\alpha]\right)}_{v_s([n];\mathbf{r})-v([n,q_\alpha];\mathbf{r})} + v(\mathbf{r}) = \mu\,,\\
&\frac{\delta F_s[n,q_\alpha]}{\delta q_\alpha} + \underbrace{\frac{\delta}{\delta q_\alpha}\left(F[n,q_\alpha] - F_s[n,q_\alpha]\right)}_{j_{\alpha,s}([q_\alpha])-j_\alpha([n,q_\alpha])} + \frac{j_\alpha}{\omega_\alpha} = \mu'\,.
\end{aligned} \tag{165}$$

Here the Mxc potential and current from the above equation are defined to be

$$v_{\mathrm{Mxc}}([n,q_\alpha];\mathbf{r}) = \frac{\delta E_{\mathrm{Mxc}}[n,q_\alpha]}{\delta n(\mathbf{r})}\,, \quad \text{and} \quad j_{\alpha,\mathrm{Mxc}}([n,q_\alpha]) = \frac{\delta E_{\mathrm{Mxc}}[n,q_\alpha]}{\delta q_\alpha}. \tag{166}$$

With these definitions, the KS equations to be solved are the following coupled equations [14]:

$$\hat{h}\left([v,n,q_\alpha]\right)\varphi_k(\mathbf{r}) = \left[\frac{\hat{\mathbf{p}}^2}{2m} + \underbrace{v(\mathbf{r}) + v_{\mathrm{Mxc}}\left([n,q_\alpha];\mathbf{r}\right)}_{v_{\mathrm{KS}}([v,n,q_\alpha];\mathbf{r})}\right]\varphi_k(\mathbf{r}) = \epsilon_k\varphi_k(\mathbf{r})\,, \tag{167}$$

$$\omega_\alpha^2 q_\alpha = -\frac{1}{\omega_\alpha}j_{\alpha,\mathrm{KS}}\left([j_\alpha,n,q_\alpha]\right). \tag{168}$$

The above equations reproduces the ground-state electron density $n(\mathbf{r}) = \sum_k |\varphi_k(\mathbf{r})|^2$ and the photon coordinates obtained from Eq. (168). Here, the KS current has the form $j_{\alpha,\mathrm{KS}}([j_\alpha, n, q_\alpha]) = j_\alpha + j_{\alpha,\mathrm{Mxc}}([n, q_\alpha])$. Considering the mean-field contributions of the explicit electron-photon interaction term of Eq. (154) given as $\sum_\alpha^M \omega_\alpha q_\alpha \boldsymbol{\lambda}_\alpha \cdot \mathbf{R}$, one can deduce from the EOM for $q_\alpha(t)$ (see Eq. (178)) that the Mxc current components are $j_{\alpha,\mathrm{Mxc}} = j_{\alpha,\mathrm{M}} = -\omega_\alpha^2 \int d^3\mathbf{r}\, \boldsymbol{\lambda}_\alpha \cdot \mathbf{r}\, n(\mathbf{r})$ are given in terms of mean-field expressions.

The Mxc potential of Eq. (166) can be divided into the usual Hxc potential that is known from electronic DFT and an additional term called photon-exchange-correlation potential (Pxc) [18] as

$$v_{\mathrm{Mxc}}([n, q_\alpha]; \mathbf{r}) = v_{\mathrm{Hxc}}([n]; \mathbf{r}) + v_{\mathrm{Pxc}}([n, q_\alpha]; \mathbf{r}). \tag{169}$$

Clearly, the term v_{Pxc} will vanish if the coupling $|\boldsymbol{\lambda}_\alpha|$ goes to zero and recover the purely electronic ground-state DFT. The LDA discussed in Sec. 2.5.1.2 can be applied to the xc part of v_{Hxc} and provided reasonable approximations for xc part of v_{Pxc} exist, the self-consistent solution of the coupled non-linear KS equations provides a numerically feasible way to determine the ground-state properties of an interacting multi-particle system coupled to photons.

2.5.5 QUANTUM-ELECTRODYNAMICAL DENSITY-FUNCTIONAL THEORY

The previous section focused on the reformulation of the equilibrium matter-photon problem in terms of the electronic density and displacement coordinates of the photon modes. For dynamical properties of matter-photon systems, QEDFT was developed as in Refs. [12, 46, 85]. Ref. [12] formulates QEDFT on various level of approximations starting from the relativistic Dirac equation to non-relativistic QED all the way down to the dipole approximation of non-relativistic limit as in Ref. [46] while Ref. [85] starts from the Pauli-Fierz field theory down to the dipole limit. Earlier work on this topic have been carried out in Refs. [86, 87].

QEDFT outlined here is formulated in the non-relativistic limit and in the length gauge as described in Ref. [12]. The time-independent length gauge Hamiltonian was already introduced in Eq. (154). Now, the time-dependent Hamiltonian in the length gauge with time-dependent external perturbations coming either from an external potential or current is given by

$$\hat{H}_L(t) = \hat{T}_e + \hat{W}_{ee} + \hat{V}(t) + \frac{1}{2}\sum_{\alpha=1}^{M}\left[\hat{p}_\alpha^2 + \omega_\alpha^2\left(\hat{q}_\alpha - \frac{\boldsymbol{\lambda}_\alpha}{\omega_\alpha}\cdot\hat{\mathbf{R}}\right)^2\right] + \sum_{\alpha=1}^{M}\frac{j_\alpha(t)}{\omega_\alpha}\hat{q}_\alpha\,. \tag{170}$$

Here, $\hat{V}(t) = \sum_{i=1}^{N_e} v(\mathbf{r}_i, t)$ is the time-dependent potential where $v(\mathbf{r}, t)$ is given in Eq. (123). The external current $j_\alpha(t)$ acts directly on the mode α of the photon subsystem by coupling to the photon coordinates.

As QEDFT is an extension of TDDFT, concepts already discussed in Sec. 2.5.2 can be applied here directly. Thus, for a fixed initial state Ψ_0 and external pair $(v(\mathbf{r}, t), j_\alpha(t))$ [6], one desires to solve Eq. (6) with the Hamiltonian given by Eq. (170). The resulting

6 As in the ground-state case, the time-dependent photon coordinates $q_\alpha(t)$ and currents $j_\alpha(t)$ refers to the sets $\{q_1(t), q_2(t), ..., q_M(t)\}$ and $\{j_1(t), j_2(t), ..., j_M(t)\}$, respectively.

wavefunction depends on the initial state and the external pair as $|\Psi([\Psi_0, v, j_\alpha]; t)\rangle$. Since the wavefunction have functional dependencies on the fixed initial state and external pair, the expectation value, for example, of the electron density and photon coordinates also become a functional of Ψ_0 and $(v(\mathbf{r}, t), j_\alpha(t))$ as

$$n([\Psi_0, v, j_\alpha]; \mathbf{r}, t) = \langle \Psi([\Psi_0, v, j_\alpha]; t)|\hat{n}(\mathbf{r})|\Psi([\Psi_0, v, j_\alpha]; t)\rangle,$$
$$q_\alpha([\Psi_0, v, j_\alpha]; t) = \langle \Psi([\Psi_0, v, j_\alpha]; t)|\hat{q}_\alpha|\Psi([\Psi_0, v, j_\alpha]; t)\rangle.$$

The formulation of QEDFT is complete when a one-to-one correspondence (bijective mapping) between the set of external pair $(v(\mathbf{r}, t), j_\alpha(t))$ and a chosen internal pair is established. Here, the choice of internal pair of conjugate variables is the electron density $n(\mathbf{r}, t)$ and photon coordinates $q_\alpha(t)$ as in ground-state QEDFT (see Sec. 2.5.4). In the spirit of TDDFT, a closed set of equations relating $(n(\mathbf{r}, t), q_\alpha(t))$ and $(v(\mathbf{r}, t), j_\alpha(t))$ is required and can be obtained via their respective equations of motion. Before deriving the proof, one starts by computing the EOM for the photon coordinates using Eq. (68) which yields the first and second derivatives

$$\frac{\partial}{\partial t} q_\alpha(t) = p_\alpha(t), \tag{171}$$
$$\frac{\partial^2}{\partial t^2} q_\alpha(t) = -\omega_\alpha^2 q_\alpha(t) + \omega_\alpha \boldsymbol{\lambda}_\alpha \cdot \mathbf{R}(t) - \frac{j_\alpha(t)}{\omega_\alpha}. \tag{172}$$

Equation (172) is the mode-resolved Maxwell's equation given in Eq. (66) but here with the possibility of driving the α mode with an external current. Equally, using Eq. (68) in conjunction with Eq. (170) yields the continuity equation (126) and the second derivative of the electron density

$$\frac{\partial^2}{\partial t^2} n(\mathbf{r}, t) = -\boldsymbol{\nabla} \cdot \mathbf{F}_{\text{str}}(\mathbf{r}, t) + \frac{1}{m} \boldsymbol{\nabla} \cdot [n(\mathbf{r}, t) \boldsymbol{\nabla} v(\mathbf{r}, t)] + \frac{1}{m} \sum_\alpha \boldsymbol{\nabla} \cdot \underbrace{\boldsymbol{\lambda}_\alpha \langle \Psi(t)|\hat{n}(\mathbf{r}) \left(\boldsymbol{\lambda}_\alpha \cdot \hat{\mathbf{R}} - \omega_\alpha \hat{q}_\alpha\right) |\Psi(t)\rangle}_{\mathbf{F}_\alpha(\mathbf{r}, t)}. \tag{173}$$

As compared to the EOM of Eq. (129) for TDDFT, here the EOM of the density in Eq. (173) has an extra term $\mathbf{F}_\alpha(\mathbf{r}, t)$ that accounts for the coupling of the transversal part of the photon field to the mode-resolved Maxwell's equation of Eq. (172). The term $\mathbf{F}_\alpha(\mathbf{r}, t)$ is the internal force densities of the matter-photon system due to the explicit electron-photon interaction and transversal dipole-dipole interaction effects. It is important to note that the stress force term in Eq. (173) differs from that of Eq. (129) since the expectation value is evaluated with the correlated electron-photon wavefunction $\mathbf{F}_{\text{str}}(\mathbf{r}, t) = \langle \Psi(t)| \left[\hat{\mathbf{j}}(\mathbf{r}), \hat{T}_e + \hat{W}_{ee}\right] |\Psi(t)\rangle$.

The next step is to demonstrate that starting from a fixed initial state Ψ_0, there is a one-to-one correspondence between the internal pair $(n(\mathbf{r}, t), q_\alpha(t))$ and the external pair $(v(\mathbf{r}, t), j_\alpha(t))$ given by the mapping

$$(v(\mathbf{r}, t), j_\alpha(t)) \overset{1:1}{\underset{\Psi_0}{\longleftrightarrow}} (n(\mathbf{r}, t), q_\alpha(t)). \tag{174}$$

To prove the one-to-one correspondence between the sets of conjugated variables as formulated in Eq. (174), the original Runge-Gross proof in Sec. 2.5.2.1 can be applied here. In this case it is required that two different sets of external potentials and

currents $(v(\mathbf{r},t), j_\alpha(t))$ and $(v'(\mathbf{r},t), j'_\alpha(t))$ always lead to two different sets of internal variables $(n(\mathbf{r},t), q_\alpha(t))$ and $(n'(\mathbf{r},t), q'_\alpha(t))$ under the condition that the system evolves from a common initial state Ψ_0. From Eq. (172), a direct connection between the external current $j_\alpha(t)$ and the set of internal variables $(n(\mathbf{r},t), q_\alpha(t))$ is given by

$$j_\alpha(t) = \left(\frac{\partial^2}{\partial t^2} + \omega_\alpha^2\right)\omega_\alpha q_\alpha(t) - \omega_\alpha^2 \int d^3\mathbf{r}\, \boldsymbol{\lambda}_\alpha \cdot \mathbf{r}\, n(\mathbf{r},t)\,. \tag{175}$$

Thus, if the internal pair $(n(\mathbf{r},t), q_\alpha(t))$ are given, the current $j_\alpha(t)$ can be constructed using Eq. (175) and is unique. Therefore, all that is left to prove is whether Eq. (173) uniquely determines $v(\mathbf{r},t)$. This is done by assuming the conditions on the potential as in Eqs. (130) and (131). The next step establishes the uniqueness of the densities. That is, for two wavefunctions $\Psi(t)$ and $\Psi'(t)$ that evolve from the same initial state Ψ_0, the difference in the electron densities is

$$\frac{\partial^2}{\partial t^2}\left[n(\mathbf{r},t) - n'(\mathbf{r},t)\right]\big|_{t_0} = -\frac{1}{m}\boldsymbol{\nabla}\cdot\left(n(\mathbf{r},t_0)\boldsymbol{\nabla}(v(\mathbf{r},t_0) - v'(\mathbf{r},t_0))\right)\,. \tag{176}$$

As in Eq. (128) the electronic stress forces in Eq. (173) for the unprimed and primed systems are identical at t_0 and cancel out since both systems start from the same initial state. The same is true for the force $\mathbf{F}_\alpha(\mathbf{r},t)$. Therefore, the arguments that follow after Eq. (128) holds here, that is, the densities $n(\mathbf{r},t)$ and $n'(\mathbf{r},t)$ will differ infinitesimally later than t_0 if the two potentials $v(\mathbf{r},t_0)$ and $v'(\mathbf{r},t_0)$ are different. Then, assuming that up to k they are the same, one finds exactly the same Eqs. (131) - (134). This leads to the conclusion that the time-dependent density $n(\mathbf{r},t)$ uniquely determines the time-dependent potential $v(\mathbf{r},t)$ up to a purely time-dependent function $c(t)$ [12]. This concludes the proof that the mapping given in Eq. (174) is bijective. Therefore, solving the non-linear coupled equations (172) and (173) for a given initial state and external pair $(v(\mathbf{r},t), j_\alpha(t))$ determines the density $n(\mathbf{r},t)$ and photon coordinates $q_\alpha(t)$ of the coupled matter-photon system from which all observables could be computed.

2.5.5.1 *Maxwell-Kohn-Sham Quantum-Electrodynamical Density-Functional Theory*

The formulation of QEDFT as outlined above allows one to solve instead of the time-dependent Schrödinger equation equivalently a non-linear fluid equation for the electron density $n(\mathbf{r},t)$ coupled non-linearly to the mode-resolved inhomogeneous Maxwell's equation [12, 14, 46, 88] given by equations (172) and (173). While these equations are in principle easy to handle numerically, the forms of all the different terms explicitly in terms of the basic variables of QEDFT, i.e. $(n(\mathbf{r},t), q_\alpha(t))$ are not known. To find accurate approximations one then employs the KS scheme, where the unknown terms are modeled by a numerically easier to handle auxiliary system in terms of wavefunctions.

The approach is to use non-interacting subsystems of fermions and bosons which lead to a similar set of equations, which are however uncoupled. Enforcing that both give the same density and displacement field dynamics (see Sec. 2.2.2 on how $q_\alpha(t)$ corresponds to the displacement field) gives rise to mean-field exchange-correlation (Mxc) potentials and currents [13, 18, 65]. In this way, one can recast the coupled

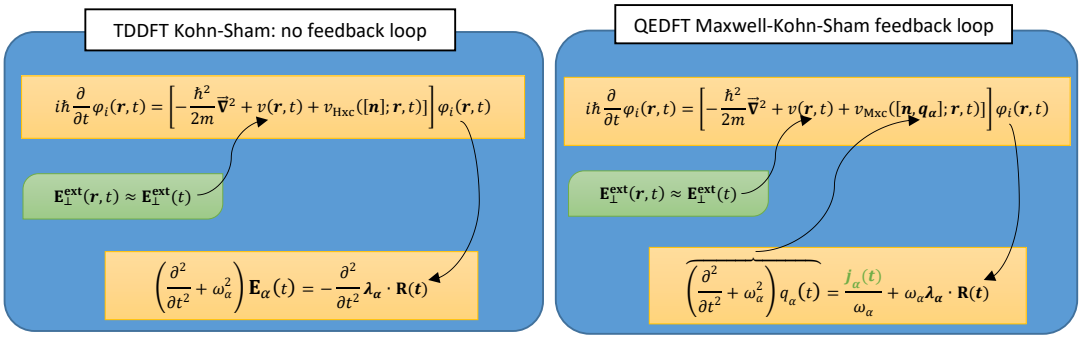

Figure 1: Schematics showing the Maxwell-KS approach contrasted with the usual semi-classical KS theory. While in the semi-classical approach the KS orbitals are used as fixed input into the mode-resolved inhomogeneous Maxwell's equation in vacuum through the total dipole $\mathbf{R}(t)=\int d^3\mathbf{r}\,\mathbf{r}\sum_i|\varphi_i(\mathbf{r},t)|^2$, in the Maxwell-KS framework the induced field acts back on the orbitals, which leads to an extra self-consistency cycle.

Maxwell-quantum-fluid equations in terms of coupled non-linear Maxwell-KS equations for auxiliary electronic orbitals, which sum to the total density $\sum_i|\varphi_i(\mathbf{r},t)|^2=n(\mathbf{r},t)$, and the displacement fields $q_\alpha(t)$ given by

$$i\hbar\frac{\partial}{\partial t}\varphi_i(\mathbf{r},t)=\left(\frac{\hat{\mathbf{p}}^2}{2m}+\underbrace{v(\mathbf{r},t)+v_{\mathrm{Mxc}}([n,q_\alpha];\mathbf{r},t)}_{v_{\mathrm{KS}}([v,n,q_\alpha];\mathbf{r},t)}\right)\varphi_i(\mathbf{r},t), \tag{177}$$

$$\left(\frac{\partial^2}{\partial t^2}+\omega_\alpha^2\right)q_\alpha(t)=-\frac{j_\alpha(t)}{\omega_\alpha}+\omega_\alpha\boldsymbol{\lambda}_\alpha\cdot\mathbf{R}(t). \tag{178}$$

Here, the so-called initial-state dependence has been ignored because one assumes (for notational simplicity and without loss of generality) in the following that the ground state is the starting point for the time-propagation [65, 79] of the matter-photon coupled system. The mode-resolved equation of motion for the photon coordinates of Eq. (178) can be solved analytically in the same way as in Sec. 2.3.1.1 and leads to the following expression

$$q_\alpha(t)=q_\alpha(t_0)\cos(\omega_\alpha t)+\frac{\dot{q}_\alpha(t_0)}{\omega_\alpha}\sin(\omega_\alpha t)-\frac{1}{\omega_\alpha^2}\int_{t_0}^{t}dt'\sin(\omega_\alpha(t-t'))j_{\alpha,\mathrm{KS}}(t')\,. \tag{179}$$

Here, $q_\alpha(t_0)=q_\alpha(0)$ and $\dot{q}_\alpha(t_0)=p_\alpha(0)$ are the photon coordinates and its first-order derivative at time $t=0$, respectively. The photon coordinates $q_\alpha(t_0)$ corresponds to the static case of ground-state QEDFT in Sec. 2.5.4. The KS current in Eq. (179) deduced from Eq. (178) can be written explicitly as

$$j_{\alpha,\mathrm{KS}}(t)=j_\alpha(t)\underbrace{-\omega_\alpha^2\int d^3\mathbf{r}\,\boldsymbol{\lambda}_\alpha\cdot\mathbf{r}\,n(\mathbf{r},t)}_{j_{\alpha,\mathrm{M}}([n];t)}\,. \tag{180}$$

As discussed in Sec. 2.5.4, the last term of Eq. (180) has only a mean-field contribution and no xc contribution. This is inferred by defining the mean-field contribution of the

explicit electron-photon interaction term of Eq. (170). As mentioned above, assuming that the ground-state (see Sec. 2.5.4) is the starting point for the time-propagation, the Mxc potential and current defined equivalently in Eqs. (165) and (166) now evolve in time as in Eqs. (177) and (179). Thus, these time-dependent Mxc potential and current are defined as

$$v_{\mathrm{Mxc}}([n,q_\alpha];\mathbf{r},t) = v_{\mathrm{s}}([n];\mathbf{r},t) - v([n,q_\alpha];\mathbf{r},t)\,, \tag{181}$$
$$j_{\alpha,\mathrm{Mxc}}([n,q_\alpha];t) = j_{\alpha,\mathrm{s}}([q_\alpha],t) - j_\alpha([n,q_\alpha],t)\,. \tag{182}$$

As in ground-state QEDFT, the Mxc current $j_{\alpha,\mathrm{Mxc}}(t)$ has only a mean-field contribution, i.e., $j_{\alpha,\mathrm{Mxc}}(t) = j_{\alpha,\mathrm{M}}(t)$. The Mxc potential can be divided into the usual Hartree xc potential that is known from electronic TDDFT and an additional photon-exchange-correlation potential [18] as

$$v_{\mathrm{Mxc}}([n,q_\alpha];\mathbf{r},t) = v_{\mathrm{Hxc}}([n];\mathbf{r},t) + v_{\mathrm{Pxc}}([n,q_\alpha];\mathbf{r},t)\,. \tag{183}$$

Clearly, the term v_{Pxc} will vanish if the coupling $|\boldsymbol{\lambda}_\alpha|$ goes to zero and recover the purely electronic case of TDDFT. The explicit form of the mean-field contribution of the potential of Eq. (183) is given by

$$\begin{aligned} v_{\mathrm{M}}([n,q_\alpha];\mathbf{r},t) &= v_{\mathrm{H}}([n];\mathbf{r},t) + v_{\mathrm{P}}([n,q_\alpha];\mathbf{r},t)\,, \\ v_{\mathrm{H}}([n];\mathbf{r},t) &= \frac{e^2}{4\pi\epsilon_0}\int d^3\mathbf{r}'\frac{n(\mathbf{r}',t)}{|\mathbf{r}-\mathbf{r}'|}\,, \\ v_{\mathrm{P}}([n,q_\alpha];\mathbf{r},t) &= \sum_{\alpha=1}^{M}\left(\int d^3\mathbf{r}'\boldsymbol{\lambda}_\alpha\cdot\mathbf{r}'n(\mathbf{r}',t) - \omega_\alpha q_\alpha(t)\right)\boldsymbol{\lambda}_\alpha\cdot\mathbf{r}\,. \end{aligned} \tag{184}$$

The ground-state QEDFT and in particular the time-dependent formulation will be employed in Chap. 3 for practical calculations of atomic and molecular systems coupled to photons.

2.6 SUMMARY

This chapter discussed the state-of-the-art theoretical description of light-matter interaction and presented different methods of solving the problem in an efficient and less computationally costly way, for example ground-state QEDFT and the time dependent case. We will expand upon this in the next chapter by formulating non-relativistic QED linear-response theory within the framework of QEDFT and deriving ab-initio methods that can compute excited-state properties of coupled light-matter systems. We will show novel perspectives that can be realized using our ab-initio linear-response theory within the framework of QEDFT. In Chap. 4 we go beyond the linear-response theory and investigate from an ab-initio perspective down-conversion processes and how strong light-matter coupling opens new possibilities.

Part III

LINEAR-RESPONSE IN NON-RELATIVISTIC QED

3

LINEAR RESPONSE IN NON-RELATIVISTIC QUANTUM ELECTRODYNAMICS

Nowadays, the influence of strong light-matter coupling allows for the emergence of interesting physical and chemical effects [1, 89, 90] that will not be captured if light is treated only as an external perturbing field. Ab-initio methods such as QEDFT has been developed to provide detailed understanding of strong light-matter interactions as well as predict new effects that can be observed in such coupled systems. So far, the application of QEDFT was mainly restricted to static situations [17] or very simple time-dependent problems [12, 13, 22, 91] because the time-dependent problem is much more complicated. To make QEDFT workable also for large time-dependent systems, in this chapter we therefore develop a linear-response formulation which is sufficient for many interesting observables such as the linear polarizability, absorption and emission spectrum, among others. The linear-response setting is adequate to describe such matter-photon coupled systems since strong light-matter coupling is usually identified by linear spectroscopy. That is, it captures the hallmark of strong coupling which is the Rabi splitting usually observed in, for example, an absorption measurement [90]. This formulation allows to make this ab-initio method for strongly-coupled matter-photon systems practical.

First, we will address strong coupling between light and matter from first-principles within the linear-response regime of non-relativistic QED. In light of this, we show novel responses and response functions that arise in the linear response setting of non-relativistic QED. We then reformulate these response equations within the framework of QEDFT and show how the self-consistent feedback between light and matter changes the quantum Maxwell's equation in matter. Next, we will show different ways of implementing the corresponding response equations of QEDFT and highlight that these different implementations provide the same results. Since the implementations are non-trivial, the comparison of the different methods is an important check of validity. With these new ab-initio methods, we then show physical effects that becomes accessible when light and matter strongly couple and new avenues that can be investigated using our ab-initio theory. For example, non-perturbative first-principles calculation of electronic and polaritonic lifetimes by sampling the photon bath, transition from Lorentz to Fano lineshapes in strong coupling. In addition, we show novel observables that can be computed in this setting. For example, we show the spectrum of the response of the photon displacement field due to an external potential as well as an external current. These results highlight that the limiting case of non-relativistic QED, i.e., the *semi-classical approximation* (see Chap. 2.5.3) miss out a lot on new interesting physics.

Before we start the derivation of the linear-response formulation of non-relativistic QED and then subsequently QEDFT, we first have to guarantee the existence of a ground-state to start from. This question, which in the usual model approaches to strong light-matter coupling do not appear, is of fundamental importance for any ab-initio framework. This question is not as trivial as it sounds, since the question

under which conditions a Hamiltonian has a ground-state is still lacking a general answer even in quantum mechanics [61]. Only for the special yet important case of Coulombic potentials could the stability of matter be shown [92]. For the Pauli-Fierz Hamiltonian a similar result exists [41]. However, in the long-wavelength limit various approximate forms of the Pauli-Fierz Hamiltonian are in use. Most importantly, in many situations the dipole self-energy term is discarded [93]. It remains, however, unclear whether the length-gauge Pauli-Fierz Hamiltonian without the dipole self-energy is a viable alternative. In principle, we could also use this adapted Hamiltonian for our investigations. But in the following we will show that this approach is fundamentally flawed and that the full Pauli-Fierz Hamiltonian including the dipole self-energy is needed for the stability of matter [1].

3.1 NO GROUND-STATE WITHOUT THE DIPOLE SELF-ENERGY

Since the entirety of this chapter is focused on the description of matter-photon coupling within the length gauge, we show the relevance of the dipole-self energy term that is often ignored in the length gauge Hamiltonian. Before proceeding to the importance of the dipole self-energy term, we first present the individual terms of the length gauge Hamiltonian discussed in Chap. 2.2.2 and here written as

$$\hat{H}_L = \hat{T}_e + \hat{W}_{ee} + \hat{V}_{eN} + \hat{H}_{pt} + \hat{H}_{\text{int}} + \hat{H}_{\text{dip}}\,. \tag{185}$$

In equation (185), the terms $\hat{T}_e$, $\hat{W}_{ee}$, $\hat{V}_{eN}$, $\hat{H}_{pt}$ are given respectively in Eqs. (2), (3), (4), (38) and the explicit electron-photon interaction term $\hat{H}_{\text{int}}$ is given by

$$\hat{H}_{\text{int}} = -\sum_{\alpha=1}^{M} \omega_\alpha \hat{q}_\alpha \boldsymbol{\lambda}_\alpha \cdot \mathbf{R} = -\sum_{\alpha=1}^{M} \omega_\alpha \hat{q}_\alpha \int d^3\mathbf{r}\; \boldsymbol{\lambda}_\alpha \cdot \mathbf{r}\; \hat{n}(\mathbf{r}). \tag{186}$$

In this bilinear coupling term, the interaction of the photon field with the matter subsystem is via the electronic dipole operator. The last term of Eq. (185) is the electronic dipole self-energy interaction given as

$$\hat{H}_{\text{dip}} = \frac{1}{2}\sum_{\alpha=1}^{M} (\boldsymbol{\lambda}_\alpha \cdot \mathbf{R})^2 = \frac{1}{2}\sum_{\alpha=1}^{M}\sum_{i,j=1}^{N_e} (\boldsymbol{\lambda}_\alpha \cdot \mathbf{r}_i)\,(\boldsymbol{\lambda}_\alpha \cdot \mathbf{r}_j)\,. \tag{187}$$

This quadratic term describes electron-electron interaction via the transversal photon field.

Now, we are interested in the question of whether the velocity and length gauge Hamiltonians can support a ground-state. The existence of a ground-state is pertinent provided we want to have a variational principle [94] and employ ground-state QEDFT (see Chap. 2.5.4 or [14]) within the dipole approximation in non-relativistic QED. A ground-state as used here implies that there exist no other state that has less energy, i.e., for all $|\Psi\rangle$ in the self-adjoint domain of the Hamiltonian it holds that $\langle\Psi|\hat{H}|\Psi\rangle \geq E_0$, where E_0 is the ground-state energy. Remarkably, for a broad class of potentials such as $v(\mathbf{r}) \in L^2(\mathbb{R}^3) + L^\infty(\mathbb{R}^3)$ [41, 95–97], it holds that both Hamiltonians are bounded from below by a minimum energy E_0. Although, for such a broad class of potentials, a ground-state does not necessarily exist, e.g., for $v(\mathbf{r}) = 0$ there are only

1 Some of the results presented in this Chapter have been published in these articles [18, 44].

scattering states with a lower bound energy which is zero. Therefore, one needs to vary over all possible wavefunctions in the domains of the respective Hamiltonians and show that they are bounded from below. In the dipole approximation, the velocity gauge Hamiltonian of Eq. (49) is bounded from below which is a basic requirement for a ground-state. Since the length gauge Hamiltonian of Eq. (185) results from a unitary transform, then the Hamiltonian $\hat{H}_L$ is bounded from below as well.

Quite often, the dipole self-energy term $\hat{H}_{\text{dip}}$ in the length gauge Hamiltonian is ignored. One of the reasons is that $\hat{H}_{\text{dip}}$ depends on the normalization volume of the field and for interactions of photons with an individual electron, atom or molecule, taking the limit $V \to \infty$ seems to imply that $\hat{H}_{\text{dip}} \to 0$ [42]. This simple argument has two severe flaws. Firstly, irrespective how small the prefactor of an unbounded operator becomes, there are wavefunctions for which it becomes arbitrarily strong and hence there is no well-defined limiting procedure as erroneously indicated above. Secondly, while it makes some sense to discard for certain states the influence of just one arbitrarily weak mode, in the case of $V \to \infty$ there are infinitely many modes that contribute within an arbitrarily small energy window and hence countering this simplified picture even for individual wavefunctions. A further reason why the dipole self-energy is often ignored is due to simplified models of matter-photon systems such as the Rabi model [98, 99], Jaynes-Cummings model [36, 100] and Dicke model [101] presented in Sec. 3.6.1.1. In these models, the simplified dipole self-energy term in the two-dimensional electronic subspace is just the identity operator which gives a constant energy offset [44].

In order to investigate how the dipole self-energy term impacts the spectral properties of the length gauge Hamiltonian, we rather consider what happens when the dipole self-energy is ignored. The general case of the proof is discussed in Ref. [44] but here for simplicity we restrict the length gauge Hamiltonian to the case of one electron coupled to a single photon mode, i.e., $N_e = M = 1$. This restriction simplifies Eq. (185) to

$$\begin{aligned}\hat{H}_{L,1} &= \hat{T}_{e,1} + \hat{W}_{ee,1} + \hat{V}_{eN,1} + \frac{1}{2}\left[\hat{p}^2 + \omega^2\left(\hat{q} - \frac{\boldsymbol{\lambda}}{\omega}\cdot\hat{\mathbf{R}}\right)^2\right] \\ &= \hat{T}_{e,1} + \hat{W}_{ee,1} + \hat{V}_{eN,1} + \hat{H}_{pt,1} + \hat{H}_{\text{int},1} + \hat{H}_{\text{dip},1}\,. \end{aligned} \tag{188}$$

We make an assumption that the single electron confined within a cavity has the possibility of escaping the cavity through the mirrors. Note that we could also use boundary conditions for the mirrors which will not change the outcome. This is evident since the mode is polarized perpendicular to the mirrors and the direction to which the electron will escape is also perpendicular to the mirrors. Therefore, we consider the full space $\mathbb{R}^3$ in accordance to the minimal-coupling and the uncoupled problem (i.e. without coupling to photons). The length gauge Hamiltonian without the dipole self-energy is given by

$$\hat{H}'_{L,1} = \hat{T}_{e,1} + \hat{V}_{eN,1} + \hat{H}_{pt,1} + \hat{H}_{\text{int},1}. \tag{189}$$

The question now arises, is the Hamiltonian $\hat{H}'_{L,1}$ bounded from below, which is a necessary prerequisite for a ground-state to exist? In order to answer this question, we consider a trial wavefunction and calculate the energy of $\hat{H}'_{L,1}$ with respect to

the trial wavefunction. The photonic part of the trial wavefunction is given by the function

$$\Phi(q) = \frac{1}{\sqrt{2}}\left[\phi_1(q) + \phi_2(q)\right], \tag{190}$$

where the functions $\phi_1(q)$ and $\phi_2(q)$ are the normalized ground and first excited states of the quantized harmonic oscillator [97]. We treat the electronic part of the trial wavefunction by considering the function

$$F_a(\mathbf{r}) = \begin{cases} \mathscr{N}\exp[-\frac{1}{1-|\mathbf{r}-\mathbf{a}|^2}], & \text{if} \quad |\mathbf{r}-\mathbf{a}| < 1 \\ 0, & \text{if} \quad |\mathbf{r}-\mathbf{a}| \geq 1 \\ \text{where} \qquad \mathbf{a} = a\boldsymbol{\kappa}, & a \in \mathbb{R} \end{cases}, \tag{191}$$

where $\boldsymbol{\kappa}$ is an arbitrary vector, a an arbitrary parameter and $\mathscr{N}$ is the normalization constant of the function. The function $F_a(\mathbf{r})$ is a mollifier which has properties of being infinitely many times differentiable, is non-zero only within the unit ball $|\mathbf{r}-\mathbf{a}| < 1$ where the vector $\mathbf{a}$ is the center of the unit ball. Physically, the mollifier corresponds to a single component of a Slater determinant [44]. The complete trial wavefunction is a factorizable tensor product of the form

$$|\Psi\rangle = F_a(\mathbf{r}) \otimes \Phi(q). \tag{192}$$

The wavefunction $|\Psi\rangle$ belongs to the domain of $\hat{H}_{L,1}$ since $\langle\Psi|\hat{H}_{L,1}|\Psi\rangle < \infty$ and also of $\hat{H}'_{L,1}$. The energy of $\hat{H}'_{L,1}$ with respect to $|\Psi\rangle$ has the following terms

$$\langle\Psi|\hat{H}'_{L,1}|\Psi\rangle = \langle\Psi|\hat{T}_{e,1}|\Psi\rangle + \langle\Psi|\hat{V}_{eN,1}|\Psi\rangle + \langle\Psi|\hat{H}_{pt,1}|\Psi\rangle + \langle\Psi|\hat{H}_{\text{int},1}|\Psi\rangle. \tag{193}$$

The expectation value of the kinetic energy of the electron is given explicitly by

$$\begin{aligned} \langle\Psi|\hat{T}_{e,1}|\Psi\rangle &= -\frac{\hbar^2}{2m}\langle F_a(\mathbf{r})|\boldsymbol{\nabla}^2|F_a(\mathbf{r})\rangle \\ &= -|\mathscr{N}|^2\frac{\hbar^2}{2m}\int\limits_{|\mathbf{r}-\mathbf{a}|<1} d^3\mathbf{r}\, e^{-\frac{1}{1-|\mathbf{r}-\mathbf{a}|^2}}\boldsymbol{\nabla}^2\left(e^{-\frac{1}{1-|\mathbf{r}-\mathbf{a}|^2}}\right). \end{aligned} \tag{194}$$

Since the kinetic energy operator is translationally invariant, we perform the transformation $\mathbf{r} \to \mathbf{r} + \mathbf{a}$ which does not change the value. Applying this transformation to Eq. (194) results to

$$\begin{aligned} \langle\Psi|\hat{T}_{e,1}|\Psi\rangle &= -\frac{\hbar^2}{2m}\langle F_0(\mathbf{r})|\boldsymbol{\nabla}^2|F_0(\mathbf{r})\rangle \\ &= -|\mathscr{N}|^2\frac{\hbar^2}{2m}\int\limits_{|\mathbf{r}|<1} d^3\mathbf{r}\, e^{-\frac{1}{1-|\mathbf{r}|^2}}\boldsymbol{\nabla}^2\left(e^{-\frac{1}{1-|\mathbf{r}|^2}}\right) \\ &= t < \infty\,. \end{aligned} \tag{195}$$

The expectation value of the second term gives the potential energy of the electron. The external potential is chosen with respect to atomic and molecular systems such

that it is an attractive potential. Thus, the expectation value of the binding potential is

$$\langle\Psi|\hat{V}_{eN,1}|\Psi\rangle = \langle F_a(\mathbf{r})|\hat{V}_{eN,1}|F_a(\mathbf{r})\rangle = -v_a\,, \quad \text{where} \qquad v_a \geq 0\,. \tag{196}$$

The third term on the right hand side of Eq. (193) yields the photon energy given by

$$\langle\Psi|\hat{H}_{pt,1}|\Psi\rangle = \frac{1}{2}(E_1+E_2), \quad \text{where} \quad E_n = \hbar\omega\left(n+\frac{1}{2}\right), \tag{197}$$

with n being the photon occupation and $n \in \mathbb{N}$. The last term of Eq. (193) is the energy from the bilinear electron-photon coupling term that simplifies to

$$\begin{aligned}\langle\Psi|\hat{H}_{\text{int},1}|\Psi\rangle &= -\omega\langle\Phi|\hat{q}|\Phi\rangle\langle F_a(\mathbf{r})|\boldsymbol{\lambda}\cdot\mathbf{r}|F_a(\mathbf{r})\rangle \\ &= -\sqrt{\frac{\hbar\omega}{2}}\boldsymbol{\lambda}\cdot\langle F_a(\mathbf{r})|\mathbf{r}|F_a(\mathbf{r})\rangle \\ &= -\sqrt{\frac{\hbar\omega}{2}}|\mathscr{N}|^2 \int\limits_{|\mathbf{r}-\mathbf{a}|<1} d^3\mathbf{r}\;\boldsymbol{\lambda}\cdot\mathbf{r}\;e^{-\frac{2}{1-|\mathbf{r}-\mathbf{a}|^2}}.\end{aligned} \tag{198}$$

Now, performing the translation $\mathbf{r} \to \mathbf{r}+\mathbf{a}$ in Eq. (198) results to

$$\begin{aligned}\langle\Psi|\hat{H}_{\text{int},1}|\Psi\rangle &= -\sqrt{\frac{\hbar\omega}{2}}\left[|\mathscr{N}|^2\int\limits_{|\mathbf{r}|<1} d^3\mathbf{r}\;\boldsymbol{\lambda}\cdot\mathbf{r}\;e^{-\frac{2}{1-|\mathbf{r}|^2}} - \boldsymbol{\lambda}\cdot\mathbf{a}\langle F_0(\mathbf{r})|F_0(\mathbf{r})\rangle\right] \\ &= -\sqrt{\frac{\hbar\omega}{2}}\boldsymbol{\lambda}\cdot\mathbf{a} = -a\,,\end{aligned} \tag{199}$$

where the integral of the first term of Eq. (199) is zero and the energy of the bilinear term is proportional to $-a$ with $\boldsymbol{\kappa}$ chosen to be $\boldsymbol{\kappa} = (\hbar\omega/2)^{-1/2}\boldsymbol{\lambda}/|\boldsymbol{\lambda}|^2$. Now, summing all the terms that contributes to the total energy of $\hat{H}'_{L,1}$ yields

$$\begin{aligned}\langle\Psi|\hat{H}'_{L,1}|\Psi\rangle &= t - v_a + \frac{1}{2}(E_1+E_2) - a \\ &\leq t + \frac{1}{2}(E_1+E_2) - a \sim -a\,.\end{aligned} \tag{200}$$

From the total energy expression it becomes clear that the Hamiltonian is unbounded from below, since the parameter a can be chosen arbitrarily. Formulated differently, F_a can be moved further and further away from the origin thereby lowering the energy of $\hat{H}'_{L,1}$ as much as we want. Therefore, we conclude that there exists no ground-state without the dipole self-energy term in the length gauge. A further point to note is that $\hat{H}'_{L,1}$ will in general not have any eigenstates but rather have a purely continuous spectrum with only scattering states. Thus, $\hat{H}'_{L,1}$ makes physical sense only in a time-dependent setting. The general case of the proof for arbitrary many electrons and photon modes can be treated in a similar approach as presented above and is outlined in Ref. [44]. Furthermore, a consequence of ignoring this term leads to a violation of Maxwell equations in matter as demonstrated in Ref. [44].

Numerical investigations that question omitting the dipole self-energy term has been studied in Ref. [102]. Using a real-space model system coupled to a photon

mode, it was shown that omitting this term of the length gauge Hamiltonian leads to the breaking of gauge invariance, emergence of a dependence on the coordinate system (or basis set), radiating ground states, unphysical dependence on the total dipole moment, and in the limit of finite basis set leads to disintegration of the complete system as discussed above. Due to the unphysical results that arise when the dipole-self energy term is ignored [44, 102], it becomes necessary to always include this term in order to obtain the correct spectral features of the length gauge Hamiltonian.

The result of this discussion is that if we want to define equilibrium properties and a ground state, from which we perturb our system to investigate its response, we need to include the dipole self-energy. This is what we will do in the following.

3.2 LINEAR RESPONSE IN THE LENGTH GAUGE

The previous section showed the necessity of the dipole-self energy term of the length gauge Hamiltonian. This is important to make sure that the Hamiltonian is bounded from below (stable) such that we can employ ground-state QEDFT and its extension to the time-dependent case. We now present the linear response formulation for electron-photon coupled systems in the dipole approximation of non-relativistic QED. This first-principles formulation is important to capture and compliment recent experimental observations in the strong-coupling regime where hybrid light-matter particles (polaritons) emerge that are capable of modifying the properties of the coupled system significantly [2, 3] when compared to the separate subsystems. Thus, the linear response formulation here obtains modified response functions as well as introduces novel response functions that can describe and predict features of the strong-coupling regime as well as propose novel spectroscopic observables.

The setting for such a description of light and matter is that of the length gauge Hamiltonian. With the Hamiltonian of Eq. (170) we can then in principle solve the corresponding time-dependent Schrödinger equation (6) for a given initial state $|\Psi_0\rangle$ of the coupled matter-photon system. Here, we do not solve for the full time-dependent many-body wavefunction. We restrict ourselves to weak perturbations from the external potential $\delta v(\mathbf{r}, t)$ and current $\delta j_\alpha(t)$ and assume that our system is in the ground state of the coupled matter-photon system at time $t = 0$. This new perturbation $\delta j_\alpha(t)$ is not accessible in the linear-response setting of the semi-classical limit discussed in Chap. 2.5.3. As can be expected, this new way of perturbing the coupled system highlights new possibilities that become available as will be shown below. In this case, first-order time-dependent perturbation theory can be used (see Chap. 2.4 for details) to approximate the dynamics of the coupled matter-photon system. This framework gives access to linear spectroscopy, e.g., the absorption spectrum of an atom or molecule.

The formulation of the linear response can be done in two different ways which are formally equivalent. One formalism defines the response function as an expectation value of the commutator of an observable of interest at different times with respect to the ground-state wavefuction while the other formalism defines the response function as a functional derivative of an observable with respect to the external perturbation. The latter is beneficial for deriving the basic equations of linear-response QEDFT in various forms as will be discussed in Sec. 3.3. In the following, we present the two formalisms as applied in the length gauge description of the matter-photon system.

3.2.1 LINEAR RESPONSE: A WAVEFUNCTION BASED FORMALISM

In this subsection, we present the wavefunction based formalism of the linear response. Basically, this formalism defines the response function to be a ground-state expectation value of the commutator of an observable (or different observables) of interest at different times. Following the linear-response derivation in Chap. 2.4, we define the external perturbation in the length gauge to be

$$\hat{H}_{\text{ext}}(t) = \sum_{i=1}^{N_e} v(\mathbf{r}_i, t) + \sum_{\alpha=1}^{M} \frac{j_\alpha(t)}{\omega_\alpha} \hat{q}_\alpha. \tag{201}$$

The term $\hat{H}_{\text{ext}}(t)$ is included in the length gauge Hamiltonian of Eq. (170). Here, we are interested in the dipole response as well as the response of the photon field due to an external perturbation $\hat{H}_{\text{ext}}(t)$. To investigate these responses we consider the electron density (which is related to $\mathbf{R} = \int d^3\mathbf{r}\, \mathbf{r}\, \hat{n}(\mathbf{r})$) and photon coordinate as in Chap. 2.5.5. The linear response of the electron density is obtained by substituting $\hat{n}(\mathbf{r})$ for $\hat{O}(\mathbf{r})$ in Eq. (81) together with the external perturbation of Eq. (201) which results to

$$\delta n(\mathbf{r}, t) = \int dt' \int d^3\mathbf{r}' \chi_n^n(\mathbf{r}, t; \mathbf{r}', t') \delta v(\mathbf{r}', t') + \sum_{\alpha=1}^{M} \int dt' \chi_{q_\alpha}^n(\mathbf{r}, t; t') \delta j_\alpha(t'). \tag{202}$$

Here the response function $\chi_n^n(\mathbf{r}, t; \mathbf{r}', t')$ corresponds to the density-density response function for a coupled light-matter system and $\chi_{q_\alpha}^n(\mathbf{r}, t; t')$ corresponds to the density response induced by exciting the photon field. The response functions of Eq. (202) are given by

$$\chi_n^n(\mathbf{r}, t; \mathbf{r}', t') = -\frac{i}{\hbar} \Theta(t - t') \langle \Psi_0 | \left[\hat{n}_I(\mathbf{r}, t), \hat{n}_I(\mathbf{r}', t') \right] | \Psi_0 \rangle, \tag{203}$$

$$\chi_{q_\alpha}^n(\mathbf{r}, t; t') = -\frac{i}{\hbar} \Theta(t - t') \frac{1}{\omega_\alpha} \langle \Psi_0 | \left[\hat{n}_I(\mathbf{r}, t), \hat{q}_{\alpha,I}(t') \right] | \Psi_0 \rangle. \tag{204}$$

It is important to note that the density-density response function of Eq. (203) is computed with respect to the coupled light-matter ground state $|\Psi_0\rangle$ which differs from Eq. (142) which is computed with respect to the electron-only ground state $|\psi_0\rangle$. Also, the Hamiltonian in the interaction picture of Eq. (203) is the length gauge Hamiltonian of Eq. (154) while that of Eq. (142) is the Hamiltonian of Eq. (95). Therefore, the density-density response function of Eq. (203) includes contributions of the photon field as opposed to the semi-classical counterpart.

In the standard (i.e. semi-classical limit) linear response formulation, since the photon field is not included as a dynamical part of the system, changes in the transversal photon field would not induce any changes in the electronic subsystem. However, our treatment of the full matter-photon system in the length gauge allows for a cross-talk between light and matter which accordingly leads to a linear response of the quantized light field

$$\delta q_\alpha(t) = \int dt' \int d^3\mathbf{r}' \chi_n^{q_\alpha}(t; \mathbf{r}', t') \delta v(\mathbf{r}', t') + \sum_{\alpha'=1}^{M} \int dt' \chi_{q_{\alpha'}}^{q_\alpha}(t, t') \delta j_{\alpha'}(t'), \tag{205}$$

where $\chi_n^{q_\alpha}(t;\mathbf{r}',t')$ is the full response function of the photons due to perturbing the electronic degrees, and $\chi_{q'_\alpha}^{q_\alpha}(t,t')$ is the response function of the photons by perturbing the photonic degrees. Equation (205) corresponds to the linear response of the displacement field $\delta\mathbf{D}_\alpha(t) = \epsilon_0\omega_\alpha\boldsymbol{\lambda}_\alpha\,\delta q_\alpha(t)$ (see Chap. 2.2.2). The response function $\chi_n^{q_\alpha}(t;\mathbf{r}',t')$ is in general not trivially connected to $\chi_{q_\alpha}^{n}(\mathbf{r},t;t')$, due to the different time-ordering of t and t'. The response functions of Eq. (205) are defined as

$$\chi_n^{q_\alpha}(t;\mathbf{r}',t') = -\frac{i}{\hbar}\Theta(t-t')\langle\Psi_0|\left[\hat{q}_{\alpha,I}(t),\hat{n}_I(\mathbf{r}',t')\right]|\Psi_0\rangle, \tag{206}$$

$$\chi_{q_{\alpha'}}^{q_\alpha}(t,t') = -\frac{i}{\hbar}\Theta(t-t')\frac{1}{\omega_{\alpha'}}\langle\Psi_0|\left[\hat{q}_{\alpha,I}(t),\hat{q}_{\alpha',I}(t')\right]|\Psi_0\rangle. \tag{207}$$

The response function $\chi_{q_{\alpha'}}^{q_\alpha}(t,t')$ is particularly interesting since it describes photon-photon interaction mediated by the matter subsystem as can be observed by the expectation value with the correlated matter-photon ground-state and the length gauge Hamiltonian in the interaction picture.

3.2.2 LINEAR RESPONSE: A FUNCTIONAL BASED FORMALISM

Alternatively, the response and response functions of the electron density and photon coordinate of Eqs. (202)-(207) can be obtained using the functional dependence of the observables on the external pair $(v(\mathbf{r},t), j_\alpha(t))$ as discussed in Chap. 2.4. For the setting considered here, the wavefunction of the coupled matter-photon system has a functional dependence $|\Psi([v,j_\alpha];t)\rangle$ via the Hamiltonian Eq. (170), i.e., $\hat{H}_L(t) = \hat{H}_L([v,j_\alpha];t)$. Therefore, through the expectation value of electron density and photon displacement coordinate, both have a functional dependence on the external pair as $n([v,j_\alpha];\mathbf{r},t)$ and $q_\alpha([v,j_\alpha];t)$, respectively. We can perform a functional Taylor expansion of the density $n(\mathbf{r},t)$ and photon coordinate $q_\alpha(t)$ to first-order around the static external potential and current $(v_0(\mathbf{r}), j_{\alpha,0})$ that yields

$$\begin{aligned} n([v,j_\alpha];\mathbf{r},t) = n([v_0,j_{\alpha,0}];\mathbf{r}) &+ \iint d^3\mathbf{r}'dt'\frac{\delta n([v_0,j_{\alpha,0}];\mathbf{r},t)}{\delta v(\mathbf{r}',t')}\delta v(\mathbf{r}',t') \\ &+ \sum_\alpha\int dt'\frac{\delta n([v_0,j_{\alpha,0}];\mathbf{r},t)}{\delta j_\alpha(t')}\delta j_\alpha(t'), \\ q_\alpha([v,j_\alpha];t) = q_\alpha([v_0,j_{\alpha,0}]) &+ \iint d^3\mathbf{r}'dt'\frac{\delta q_\alpha([v_0,j_{\alpha,0}];t)}{\delta v(\mathbf{r}',t')}\delta v(\mathbf{r}',t') \\ &+ \sum_{\alpha'}\int dt'\frac{\delta q_\alpha([v_0,j_{\alpha,0}];t)}{\delta j_{\alpha'}(t')}\delta j_{\alpha'}(t'). \end{aligned}$$

This reduces to the response of the electron density and photon coordinate given as

$$\delta n([v,j_\alpha];\mathbf{r},t) = \iint d^3\mathbf{r}'dt'\chi_v^n(\mathbf{r},t;\mathbf{r}',t')\delta v(\mathbf{r}',t') + \sum_\alpha\int dt'\chi_{j_\alpha}^n(\mathbf{r},t;t')\delta j_\alpha(t'), \tag{208}$$

$$\delta q_\alpha([v,j_\alpha];t) = \iint d^3\mathbf{r}'dt'\chi_v^{q_\alpha}(t;\mathbf{r}',t')\delta v(\mathbf{r}',t') + \sum_{\alpha'}\int dt'\chi_{j_{\alpha'}}^{q_\alpha}(t,t')\delta j_{\alpha'}(t'), \tag{209}$$

where we define the response functions of the above relation as

$$\chi_v^n(\mathbf{r},t;\mathbf{r}',t') = \left.\frac{\delta n([v,j_\alpha];\mathbf{r},t)}{\delta v(\mathbf{r}',t')}\right|_{v_0(\mathbf{r}),j_{\alpha,0}}, \tag{210}$$

$$\chi_{j_\alpha}^n(\mathbf{r},t;t') = \left.\frac{\delta n([v,j_\alpha];\mathbf{r},t)}{\delta j_\alpha(t')}\right|_{v_0(\mathbf{r}),j_{\alpha,0}}, \tag{211}$$

$$\chi_v^{q_\alpha}(t;\mathbf{r}',t') = \left.\frac{\delta q_\alpha([v,j_\alpha];t)}{\delta v(\mathbf{r}',t')}\right|_{v_0(\mathbf{r}),j_{\alpha,0}}, \tag{212}$$

$$\chi_{j_{\alpha'}}^{q_\alpha}(t,t') = \left.\frac{\delta q_\alpha([v,j_\alpha];t)}{\delta j_{\alpha'}(t')}\right|_{v_0(\mathbf{r}),j_{\alpha,0}}. \tag{213}$$

Here, the density-density response function written in the notation $\chi_v^n(\mathbf{r},t;\mathbf{r}',t')$ signifies the functional variation of the time-dependent density $n(\mathbf{r},t)$ with respect to a time-dependent potential $v(\mathbf{r},t)$. The notation for the other response functions follow a similar reasoning. The response functions defined in Eqs. (210)-(213) and Eqs. (203)-(207) are formally equivalent. This can be inferred from Eqs. (210)-(213) as they can be expressed as the response equations in (202) and (205) (see Chap. 2.4 for details). Both formalisms will be employed later in the thesis to derive the response equations and response functions within the framework of QEDFT.

These novel response functions that include the photon field together with χ_n^n highlight the following possibilities already for the usual weak-coupling situation in which the semi-classical theory is commonly applied:

- the finite radiative lifetimes of excited states which is inferred from the de-excitations of the photon field can be obtained naturally since the photon bath is included.
- the excited-state properties can be viewed as arising from quantum modifications of the Maxwell's equations in matter due to the self-consistent feedback loop.
- the emerging resonances for a real system are mainly photonic in nature, as they describe either the emission or absorption of photons.
- the onset of Rabi splitting which indicates the hybridization of the light-matter system and emergence of new states (polaritonic states).

All these features and more will be discussed below.

3.2.3 THE COUPLED LINEAR RESPONSE EQUATIONS

The linear response equations (202) and (205) in non-relativistic QED for the electron density and photon coordinate can be grouped in a matrix form which shows how the

individual photon modes couple to the matter subsystem and how different modes interact with each other given as

$$\begin{pmatrix} \delta n \\ \delta q_1 \\ \delta q_2 \\ \vdots \\ \delta q_M \end{pmatrix} = \begin{pmatrix} \chi_n^n & \chi_{q_1}^n & \chi_{q_2}^n & \cdots & \chi_{q_M}^n \\ \chi_n^{q_1} & \chi_{q_1}^{q_1} & \chi_{q_2}^{q_1} & \cdots & \chi_{q_M}^{q_1} \\ \chi_n^{q_2} & \chi_{q_1}^{q_2} & \chi_{q_2}^{q_2} & \cdots & \chi_{q_M}^{q_2} \\ \vdots & \vdots & \vdots & \ddots & \vdots \\ \chi_n^{q_M} & \chi_{q_1}^{q_M} & \chi_{q_2}^{q_M} & \cdots & \chi_{q_M}^{q_M} \end{pmatrix} \begin{pmatrix} \delta v \\ \delta j_1 \\ \delta j_2 \\ \vdots \\ \delta j_M \end{pmatrix}, \tag{214}$$

where integration over time and space is implied as defined in Eqs. (202) and (205). In this form we observe that the electron density response of the coupled electron-photon system depends on whether we use a classical field from the potential $\delta v(\mathbf{r}, t)$ or classical external charge current $\delta j_\alpha(t)$, or combinations thereof for the perturbation. Furthermore, we can also decide to not consider the response of the coupled matter-photon system due to $\delta n(\mathbf{r}, t)$, but rather directly monitor the quantized modes of the photon field $\delta q_\alpha(t)$. This response yet again depends on whether we choose to use a classical field $\delta v(\mathbf{r}, t)$ that induces photons in mode α or whether we directly generate those photons by an external current $\delta j_\alpha(t)$. In addition, we also see that the different modes are coupled, i.e., that photons interact. Similarly as charged particles interact via coupling to photons, also photons interact via coupling to the charged particles. Keeping the coupling to the photon field explicitly, on the one hand, changes the standard spectroscopic observables, and on the other hand also allows for many more spectroscopic observables than in the standard matter-only theory.

To obtain the responses in Eq. (214), we can simultaneously perturb the coupled system with both the external potential $\delta v(\mathbf{r}, t)$ and current $\delta j_\alpha(t)$. However, in this thesis we consider only the situation in which we perturb the couple system with either the external potential or the current but not both at the same time. Considering an external perturbation of the coupled system with the external potential $\delta v(\mathbf{r}, t)$ (while $\delta j_\alpha(t) = 0$) reduces Eq. (214) to the coupled set of responses

$$\begin{cases} \delta n_v(\mathbf{r}, t) = \iint dt' d^3\mathbf{r}' \chi_n^n(\mathbf{r}, t; \mathbf{r}', t') \delta v(\mathbf{r}', t'), \\ \delta q_{\alpha,v}(t) = \iint dt' d^3\mathbf{r}' \chi_n^{q_\alpha}(t; \mathbf{r}', t') \delta v(\mathbf{r}', t'). \end{cases} \tag{215}$$

Here, the cross-correlation response function $\chi_n^{q_\alpha}(t; \mathbf{r}', t')$ accounts for the action of the matter subsystem on the photon field which gives rise to a response of the photon field as a result of perturbing the matter subsystem. In the semi-classical approach on which TDDFT is based on, the cross-correlation response function does not show up and thus the cross-talk between light and matter is not included. Similarly, a perturbation of the coupled system with the external charge current $\delta j_\alpha(t)$ (while $\delta v(\mathbf{r}, t) = 0$) reduces Eq. (214) to the coupled equations

$$\begin{cases} \delta n_v(\mathbf{r}, t) = \sum_{\alpha=1}^M \int dt' \chi_{q_\alpha}^n(\mathbf{r}, t; t') \delta j_\alpha(t'), \\ \delta q_{\alpha,j}(t) = \sum_{\alpha'=1}^M \int dt' \chi_{q_{\alpha'}}^{q_\alpha}(t, t') \delta j_{\alpha'}(t'). \end{cases} \tag{216}$$

The cross-correlation response function $\chi_{q_\alpha}^n(\mathbf{r}, t; t')$ accounts for the action of the photon field on the matter thus specifying the response of the density by perturbing the

photon field and $\chi^{q_\alpha}_{q_{\alpha'}}(t,t')$ describes how photons interact via matter thus specifying changes in response of the photon field. In Eqs. (215) and (216) the subscript v (j) on $\delta n_v(\mathbf{r},t)$ ($\delta n_j(\mathbf{r},t)$) represents the electron density response due to an external potential $\delta v(\mathbf{r},t)$ (current $\delta j_\alpha(t)$). Similarly, the subscript v (j) on $\delta q_{\alpha,v}(t)$ ($\delta q_{\alpha,j}(t)$) represents the response of the photon coordinate due to an external potential $\delta v(\mathbf{r},t)$ (current $\delta j_\alpha(t)$).

We note that when we take the decoupling limit between light and matter in our description, i.e. setting $|\boldsymbol{\lambda}_\alpha| = 0$, the response functions $\chi^{q_\alpha}_n$ and $\chi^n_{q_\alpha}$ become zero as there is no cross-talk between the subsystems. The response function $\chi^{q_\alpha}_{q_{\alpha'}}$ reduces to the solution of Eq. (72) while the density-density response function χ^n_n is now given by Eq. (142). Since the semi-classical limit (see Chap. 2.5.3) is the limiting case of our electron-photon linear-response formulation, this highlights that the semi-classical limit misses important effects that are captured in our light-matter setting and new physical possibilities that become accessible as shown later.

The response functions for the electron density and photon coordinate of Eqs. (203) and (204) and Eqs. (206) and (207) can be expressed in the frequency space following the Lehmann representation of Chap. 2.4 given as

$$\chi^n_n(\mathbf{r},\mathbf{r}',\omega) = \frac{1}{\hbar}\lim_{\eta\to 0^+}\sum_{k=0}^{\infty}\left[\frac{f_k(\mathbf{r})f_k^*(\mathbf{r}')}{\omega-\Omega_k+i\eta} - \frac{f_k(\mathbf{r}')f_k^*(\mathbf{r})}{\omega+\Omega_k+i\eta}\right], \tag{217}$$

$$\chi^n_{q_\alpha}(\mathbf{r},\omega) = \frac{1}{\hbar}\lim_{\eta\to 0^+}\sum_{k=0}^{\infty}\left[\frac{f_k(\mathbf{r})g^*_{\alpha,k}}{\omega-\Omega_k+i\eta} - \frac{g_{\alpha,k}f_k(\mathbf{r})}{\omega+\Omega_k+i\eta}\right], \tag{218}$$

$$\chi^{q_\alpha}_n(\mathbf{r}',\omega) = \frac{1}{\hbar}\lim_{\eta\to 0^+}\sum_{k=0}^{\infty}\left[\frac{\omega_\alpha g_{\alpha,k}f_k^*(\mathbf{r}')}{\omega-\Omega_k+i\eta} - \frac{\omega_\alpha f_k(\mathbf{r}')g^*_{\alpha,k}}{\omega+\Omega_k+i\eta}\right], \tag{219}$$

$$\chi^{q_\alpha}_{q_{\alpha'}}(\omega) = \frac{1}{\hbar}\lim_{\eta\to 0^+}\sum_{k=0}^{\infty}\left[\frac{\omega_\alpha g_{\alpha,k}g^*_{\alpha',k}}{\omega-\Omega_k+i\eta} - \frac{\omega_\alpha g_{\alpha',k}g^*_{\alpha,k}}{\omega+\Omega_k+i\eta}\right], \tag{220}$$

where $f_k(\mathbf{r}) = \langle\Psi_0|\hat{n}(\mathbf{r})|\Psi_k\rangle$ and $g_{\alpha,k} = \langle\Psi_0|\hat{q}_\alpha|\Psi_k\rangle/\omega_\alpha$ are the transition matrix elements between the ground-state and all excited states and $|\Psi_0\rangle$ is the correlated electron-photon ground-state wavefunction. The excitation energies $\Omega_k = (E_k - E_0)/\hbar$ of the interacting system are the poles of the response functions of the unperturbed system.

3.3 LINEAR RESPONSE FORMULATION OF QEDFT

As previously discussed in the case of a matter-only system, it is computationally costly to compute the density-density response function which led to the formulation of linear response within the TDDFT framework. Therefore, for a matter-photon system the computational cost increases with respect to the matter-only problem due to the added dimensionality of M-photon modes. In order to compute the responses or response functions of matter-photon systems, we employ the Maxwell-KS scheme of QEDFT presented in Chap. 2.5.5. This approach utilizes the bijective mapping between the interacting and non-interacting system that yields the exact electron density and displacement field of the interacting system given by

$$(v(\mathbf{r},t), j_\alpha(t)) \overset{1:1}{\underset{\Psi_0}{\longleftrightarrow}} (n(\mathbf{r},t), q_\alpha(t)) \overset{1:1}{\underset{\Phi_0}{\longleftrightarrow}} (v_s(\mathbf{r},t), j_{\alpha,s}(t)), \tag{221}$$

which implies $(v_s([v,j_\alpha];\mathbf{r},t), j_{\alpha,s}([v,j_\alpha];t))$. This allows to recover the exact linear response of the interacting coupled system.

The linear response formulation for a coupled matter-photon system within the framework of QEDFT expresses the interacting response functions in terms of non-interacting response functions of the decoupled subsystems while employing Mxc kernels. To show this, we now derive expressions of the response functions within the QEDFT framework. Making use of the functional chain rule, the interacting density-density response function $\chi^n_n(\mathbf{r},t;\mathbf{r}',t')$ can also be written as

$$\chi^n_n(\mathbf{r},t;\mathbf{r}',t') = \iint d^3\mathbf{x}d\tau \underbrace{\frac{\delta n\left([v_s];\mathbf{r},t\right)}{\delta v_s(\mathbf{x},\tau)}}_{\chi^n_{n,s}(\mathbf{r};t;\mathbf{x},\tau)} \frac{\delta v_s\left([v,j_\alpha];\mathbf{x},\tau\right)}{\delta v(\mathbf{r}',t')}, \tag{222}$$

where the non-interacting response function $\chi^n_{n,s}(\mathbf{r},t;\mathbf{x},\tau')$ is defined in Eq. (145). From Eq. (221), we have $v_s\left([n];\mathbf{r},t\right)$ which allows Eq. (222) to be expressed as

$$\chi^n_n(\mathbf{r},t;\mathbf{r}',t') = \iint d^3\mathbf{x}d\tau\chi^n_{n,s}(\mathbf{r},t;\mathbf{x},\tau)\iint d^3\mathbf{y}d\tau'\frac{\delta v_s\left([n];\mathbf{x},\tau\right)}{\delta n(\mathbf{y}',\tau')}\frac{\delta n\left([v,j_\alpha];\mathbf{y},\tau'\right)}{\delta v(\mathbf{r}',t')}.$$

At this point we introduce the definitions of the Mxc kernels that account for the electron-electron and electron-photon interactions within the framework of QEDFT. The Mxc kernels are defined as

$$f^n_{\mathrm{Mxc}}([n,q_\alpha];\mathbf{r},t;\mathbf{r}',t') = \frac{\delta v_s([n];\mathbf{r},t)}{\delta n(\mathbf{r}',t')} - \frac{\delta v([n,q_\alpha];\mathbf{r},t)}{\delta n(\mathbf{r}',t')}, \tag{223}$$

$$f^{q_\alpha}_{\mathrm{Mxc}}([n,q_\alpha];\mathbf{r},t;t') = -\frac{\delta v([n,q_\alpha];\mathbf{r},t)}{\delta q_\alpha(t')}, \tag{224}$$

$$g^n_{\mathrm{Mxc}}([n,q_\alpha];t;\mathbf{r}',t') = -\frac{\delta j_\alpha([n,q_\alpha];t)}{\delta n(\mathbf{r}',t')}, \tag{225}$$

$$g^{q_{\alpha'}}_{\mathrm{Mxc}}([n,q_\alpha];t,t') = \frac{\delta j_{\alpha,s}([q_\alpha];t)}{\delta q_{\alpha'}(t')} - \frac{\delta j_\alpha([n,q_\alpha];t)}{\delta q_{\alpha'}(t')}, \tag{226}$$

where $\frac{\delta v_s([n];\mathbf{r},t)}{\delta q_\alpha(t')} = 0 = \frac{\delta j_{\alpha,s}([q_\alpha];t)}{\delta n(\mathbf{r}',t')}$ and the above kernels are obtained from Eq. (181) and Eq. (182) via a functional derivative with respect to the electron density and photon coordinate. These Mxc kernels are inverses of the interacting and non-interacting response functions. The physical interpretation of the above Mxc kernels will be explained below. For the density-density response function given above, the Mxc kernels are introduced in the expression by writing the response function as

$$\begin{aligned}\chi^n_n(\mathbf{r},t;\mathbf{r}',t') = &\iint d^3\mathbf{x}d\tau\chi^n_{n,s}(\mathbf{r},t;\mathbf{x},\tau)\iint d^3\mathbf{y}d\tau' f^n_{\mathrm{Mxc}}(\mathbf{x},\tau;\mathbf{y},\tau')\frac{\delta n\left([v,j_\alpha];\mathbf{y},\tau'\right)}{\delta v(\mathbf{r}',t')}\\ &+\iint d^3\mathbf{x}d\tau\chi^n_{n,s}(\mathbf{r},t;\mathbf{x},\tau)\iint d^3\mathbf{y}d\tau'\frac{\delta v([n,q_\alpha];\mathbf{x},\tau)}{\delta n(\mathbf{y},\tau')}\frac{\delta n\left([v,j_\alpha];\mathbf{y},\tau'\right)}{\delta v(\mathbf{r}',t')}.\end{aligned}$$

Making a substitution of the following expression in the above equation

$$\begin{aligned}&\iint d^3\mathbf{y}d\tau'\frac{\delta v([n,q_\alpha];\mathbf{x},\tau)}{\delta n(\mathbf{y},\tau')}\frac{\delta n\left([v,j_\alpha];\mathbf{y},\tau'\right)}{\delta v(\mathbf{r}',t')}\\ &\quad= \delta(\mathbf{x}-\mathbf{r}')\delta(\tau-t') - \sum_\alpha\int d\tau'\frac{\delta v_{\mathrm{Mxc}}\left([n,q_\alpha];\mathbf{x},\tau\right)}{\delta q_\alpha(\tau')}\frac{\delta q_\alpha\left([v,j_\alpha];\tau'\right)}{\delta v(\mathbf{r}',t')}\\ &\quad= \delta(\mathbf{x}-\mathbf{r}')\delta(\tau-t') + \sum_\alpha\int d\tau' f^{q_\alpha}_{\mathrm{Mxc}}(\mathbf{x},\tau;\tau')\frac{\delta q_\alpha\left([v,j_\alpha];\tau'\right)}{\delta v(\mathbf{r}',t')},\end{aligned}$$

where $\delta v([n,q_\alpha];\mathbf{x},\tau)/\delta v(\mathbf{r}',t') = \delta(\mathbf{x}-\mathbf{r}')\delta(\tau-t')$ we arrive at the expression of the density-density response function in terms of non-interacting response functions and Mxc kernels

$$\begin{aligned}\chi^n_n(\mathbf{r},t;\mathbf{r}',t') = \chi^n_{n,s}(\mathbf{r},t;\mathbf{r}',t') \\ + \iint d^3\mathbf{x}d\tau\chi^n_{n,s}(\mathbf{r},t;\mathbf{x},\tau)\iint d^3\mathbf{y}d\tau' f^n_{\mathrm{Mxc}}(\mathbf{x},\tau;\mathbf{y},\tau')\,\chi^n_n(\mathbf{y},\tau';\mathbf{r}',t') \\ + \iint d^3\mathbf{x}d\tau\chi^n_{n,s}(\mathbf{r},t;\mathbf{x},\tau)\int d\tau'\sum_\alpha f^{q_\alpha}_{\mathrm{Mxc}}(\mathbf{x},\tau;\mathbf{y},\tau')\,\chi^{q_\alpha}_n(\mathbf{y},\tau';\mathbf{r}',t')\,.\end{aligned} \tag{227}$$

Following the same approach as above, the response function $\chi^n_{q_\alpha}(\mathbf{r},t;t')$ can be expressed as

$$\chi^n_{q_\alpha}(\mathbf{r},t;t') = \iint d^3\mathbf{x}d\tau\underbrace{\frac{\delta n([v_s];\mathbf{r},t)}{\delta v_s(\mathbf{x},\tau)}}_{\chi^n_{n,s}(\mathbf{r},t;\mathbf{x},\tau)}\iint d^3\mathbf{y}d\tau'\frac{\delta v_s([n];\mathbf{x},\tau)}{\delta n(\mathbf{y},\tau')}\frac{\delta n([v,j_\alpha];\mathbf{y},\tau')}{\delta j_\alpha(t')}. \tag{228}$$

Introducing the Mxc kernels into the above response equation results to

$$\begin{aligned}\chi^n_{q_\alpha}(\mathbf{r},t;t') &= \iint d\tau d\mathbf{x}\chi^n_{n,s}(\mathbf{r},t;\mathbf{x},\tau)\iint d\tau' d\mathbf{y} f^n_{\mathrm{Mxc}}(\mathbf{x},\tau;\mathbf{y},\tau')\frac{\delta n([v,j_\alpha];\mathbf{y},\tau')}{\delta j_\alpha(t')} \\ &+ \iint d\tau d\mathbf{x}\chi^n_{n,s}(\mathbf{r},t;\mathbf{x},\tau)\iint d\tau' d\mathbf{y}\frac{\delta v([n,q_\alpha];\mathbf{x},\tau)}{\delta n(\mathbf{y},\tau')}\frac{\delta n([v,j_\alpha];\mathbf{y},\tau')}{\delta j_\alpha(t')}.\end{aligned}$$

In the next step, using the expression given below obtained from the functional derivative of $\delta v([n,q_\alpha];\mathbf{x},\tau)/\delta j_\alpha(t')$ given by

$$\begin{aligned}\iint d\mathbf{y}d\tau'\frac{\delta v([n,q_\alpha];\mathbf{x},\tau)}{\delta n(\mathbf{y},\tau')}\frac{\delta n([v,j_\alpha];\mathbf{y},\tau')}{\delta j_\alpha(t')} &= -\sum_{\alpha'}\int d\tau'\frac{\delta v([n,q_\alpha];\mathbf{x},\tau)}{\delta q_{\alpha'}(\tau')}\frac{\delta q_{\alpha'}([v,j_\alpha];\tau')}{\delta j_\alpha(t')} \\ &= \sum_{\alpha'}\int d\tau' f^{q_{\alpha'}}_{\mathrm{Mxc}}([n,q_\alpha];\mathbf{x},\tau;\tau')\chi^{q_{\alpha'}}_{q_\alpha}(\tau',t')\end{aligned}$$

into Eq. (228), we arrive at the expression of $\chi^n_{q_\alpha}(\mathbf{r},t;t')$ in linear response QEDFT

$$\begin{aligned}\chi^n_{q_\alpha}(\mathbf{r},t;t') = \iint d^3\mathbf{x}d\tau\chi^n_{n,s}(\mathbf{r},t;\mathbf{x},\tau)\iint d^3\mathbf{y}d\tau' f^n_{\mathrm{Mxc}}(\mathbf{x},\tau;\mathbf{y},\tau')\,\chi^n_{q_\alpha}(\mathbf{y},\tau';\mathbf{r}',t') \\ + \iint d^3\mathbf{x}d\tau\chi^n_{n,s}(\mathbf{r},t;\mathbf{x},\tau)\int d\tau'\sum_{\alpha'} f^{q_{\alpha'}}_{\mathrm{Mxc}}(\mathbf{x},\tau;\mathbf{y},\tau')\,\chi^{q_{\alpha'}}_{q_\alpha}(\mathbf{y},\tau';\mathbf{r}',t')\,.\end{aligned} \tag{229}$$

Equally, the response functions of Eqs. (206) and (207) can be expressed in a similar form as above. First, the response function $\chi^{q_\alpha}_{q_{\alpha'}}(t,t')$ can be expressed as

$$\chi^{q_\alpha}_{q_{\alpha'}}(t,t') = \int d\tau\sum_\beta\underbrace{\frac{\delta q_\alpha([j_{\alpha,s}];t)}{\delta j_{\beta,s}(\tau)}}_{\chi^{q_\alpha}_{q_{\beta,s}}(t,\tau)}\frac{\delta j_{\beta,s}([v,j_\alpha]\tau)}{\delta j_{\alpha'}(t')}, \tag{230}$$

where $\chi^{q_\alpha}_{q_{\beta,s}}(t,\tau)$ is the non-interacting response function of the photonic subsystem given in the expectation value notation as

$$\chi^{q_\alpha}_{q_{\beta,s}}(t,\tau) = -\frac{i}{\hbar}\Theta(t-\tau)\langle\phi_0|\left[q_{\alpha,I}(t), q_{\beta,I}(\tau)\right]|\phi_0\rangle\,. \tag{231}$$

From Eq. (182), we have that $j_{\alpha,s}([q_\alpha]\tau)$. Using this in the above interacting photon-photon response function we obtain

$$\chi^{q_\alpha}_{q_{\alpha'}}(t,t') = \int d\tau \sum_\beta \chi^{q_\alpha}_{q_{\beta,s}}(t,\tau)\int d\tau' \sum_{\beta'} \frac{\delta j_{\beta,s}([q_\alpha]\tau)}{\delta q_{\beta'}(\tau')}\frac{\delta q_{\beta'}([v,j_\alpha]\tau')}{\delta j_{\alpha'}(t')}.$$

Introducing the Mxc kernels in the above equation we obtain

$$\begin{aligned}\chi^{q_\alpha}_{q_{\alpha'}}(t,t') = &\sum_\beta \int d\tau \chi^{q_\alpha}_{q_{\beta,s}}(t,\tau)\sum_{\beta'}\int d\tau' g^{q_{\beta'}}_{\mathrm{Mxc}}(\tau,\tau')\chi^{q_{\beta'}}_{q_{\alpha'}}(\tau',t') \\ &+\sum_\beta \int d\tau \chi^{q_\alpha}_{q_{\beta,s}}(t,\tau)\sum_{\beta'}\int d\tau' \frac{\delta j_\beta([n,q_\alpha];\tau)}{\delta q_{\beta'}(\tau')}\frac{\delta q_{\beta'}([n,q_\alpha];\tau')}{\delta j_{\alpha'}(t')}\,.\end{aligned}$$

Making a substitution of the following expression in the above equation (where $j_\beta([n,q_\alpha];\tau)/j_{\alpha'}(t') = \delta(\tau-t')\delta_{\beta,\alpha'}$)

$$\begin{aligned}&\sum_{\beta'}\int d\tau' \frac{\delta j_\beta([n,q_\alpha];\tau)}{\delta q_{\beta'}(\tau')}\frac{\delta q_{\beta'}([v,j_\alpha];\tau')}{\delta j_{\alpha'}(t')} \\ &\quad= \delta(\tau-t')\delta_{\beta,\alpha'} - \iint d\tau' d\mathbf{x}\frac{\delta j_\beta([n,q_\alpha];\tau)}{\delta n(\mathbf{x},\tau')}\frac{\delta n([v,j_\alpha];\mathbf{x},\tau')}{\delta j_{\alpha'}(t')} \\ &\quad= \delta(\tau-t')\delta_{\beta,\alpha'} + \iint d\tau' d\mathbf{x} g^{n_\beta}_{\mathrm{Mxc}}(\tau;\mathbf{x},\tau')\chi^n_{q_{\alpha'}}(\mathbf{x},\tau';t')\,,\end{aligned}$$

we obtain the expression of the photon-photon response function within the framework of QEDFT given by

$$\begin{aligned}\chi^{q_\alpha}_{q_{\alpha'}}(t,t') = &\chi^{q_\alpha}_{q_{\alpha,s}}(t,t') + \iint d\tau d\tau' \sum_\beta\sum_{\beta'}\chi^{q_\alpha}_{q_{\beta,s}}(t,\tau)g^{q_{\beta'}}_{\mathrm{Mxc}}(\tau,\tau')\chi^{q_{\beta'}}_{q_\alpha}(\tau',t') \\ &+\iiint d\tau d\tau' d^3\mathbf{x}\sum_\beta \chi^{q_\alpha}_{q_{\beta,s}}(t,\tau)g^{n_\beta}_{\mathrm{Mxc}}(\tau;\mathbf{x},\tau')\chi^n_{q_{\alpha'}}(\mathbf{x},\tau',t').\end{aligned} \tag{232}$$

Finally, the response function $\chi^{q_\alpha}_n(t;\mathbf{r},t')$ can be expressed in the following form

$$\chi^{q_\alpha}_n(t;\mathbf{r}',t') = \int d\tau \sum_\beta \underbrace{\frac{\delta q_\alpha([j_{\alpha,s}];t)}{\delta j_{\beta,s}(\tau)}}_{\chi^{q_\alpha}_{q_{\beta,s}}(t,\tau)}\int d\tau' \sum_{\beta'}\frac{\delta j_{\beta,s}([q_\alpha]\tau)}{\delta q_{\beta'}(\tau')}\frac{\delta q_{\beta'}([v,j_\alpha]\tau)}{\delta v(\mathbf{r}',t')}. \tag{233}$$

In a similar way, introducing the Mxc kernels in the above equation results to

$$\begin{aligned}\chi^{q_\alpha}_n(t;\mathbf{r}',t') = &\sum_\beta\int d\tau\chi^{q_\alpha}_{q_{\beta,s}}(t,\tau)\sum_{\beta'}\int d\tau' g^{q_{\beta'}}_{\mathrm{Mxc}}(\tau,\tau')\chi^{q_{\beta'}}_n(\tau';\mathbf{r}',t') \\ &+\sum_\beta\int d\tau\chi^{q_\alpha}_{q_{\beta,s}}(t,\tau)\sum_{\beta'}\int d\tau'\frac{\delta j_\beta([n,q_\alpha];\tau)}{\delta q_{\beta'}(\tau')}\frac{\delta q_{\beta'}([v,j_\alpha];\tau')}{\delta v(\mathbf{r}',t')}.\end{aligned}$$

Next, substituting the expression below obtained from $\delta j_\beta([n,q_\alpha];\tau)/\delta v(\mathbf{r}',t')$

$$\sum_{\beta'}\int d\tau' \frac{\delta j_\beta([n,q_\alpha];\tau)}{\delta q_{\beta'}(\tau')}\frac{\delta q_{\beta'}([v,j_\alpha];\tau')}{\delta v(\mathbf{r}',t')} = -\iint d\tau' d\mathbf{y}\frac{\delta j_\beta([n,q_\alpha];\tau)}{\delta n(\mathbf{y},\tau')}\frac{\delta n([v,j_\alpha];\mathbf{y},\tau')}{\delta v(\mathbf{r}',t')}$$
$$= \iint d\tau' d\mathbf{y} g^{n_\beta}_{\mathrm{Mxc}}(\tau;\mathbf{y},\tau')\chi^n_n(\mathbf{y},\tau';\mathbf{r}',t')$$

into Eq. (233) leads to the following form of the response function

$$\chi^{q_\alpha}_n(t;\mathbf{r}',t') = \iint d\tau d\tau' \sum_\beta\sum_{\beta'}\chi^{q_\alpha}_{q_{\beta,s}}(t,\tau)g^{q_{\beta'}}_{\mathrm{Mxc}}(\tau,\tau')\,\chi^{q_{\beta'}}_n(\tau';\mathbf{r}',t')$$
$$+\iiint d\tau d\tau' d^3\mathbf{x}\sum_\beta \chi^{q_\alpha}_{q_{\beta,s}}(t,\tau)g^{n_\beta}_{\mathrm{Mxc}}(\tau;\mathbf{x}\tau')\chi^n_n(\mathbf{x},\tau';\mathbf{r}',t'). \tag{234}$$

In equations (232) and (234), we note that the Mxc kernel $g^{q_{\beta'}}_{\mathrm{Mxc}}$ of the photons is zero. This becomes apparent when we consider the expression of the Mxc current $j_{\alpha,\mathrm{Mxc}}(t) = j_{\alpha,\mathrm{M}}(t) = -\omega_\alpha^2\int d^3\mathbf{r}\,\boldsymbol{\lambda}_\alpha\cdot\mathbf{r}\,n(\mathbf{r},t)$ which has only a mean-field contribution (see Chap. 2.5.5). Through a functional derivative with respect to q_α, we find that $g^{q_{\alpha'}}_{\mathrm{Mxc}} = \delta j_{\alpha,\mathrm{Mxc}}/\delta q_{\alpha'} = 0$. The equations (227), (229), (232) and (234) are the formulation of the interacting response functions of the matter-photon system within the framework of QEDFT. We note that substituting the expressions for the Mxc kernels in Eqs. (223)-(226) into the expressions of the response functions (227), (229), (232) and (234) gives back the response functions of the interacting system (see App. A.1 for details).

The linear responses of Eqs. (215) and (216) can now be expressed within the QEDFT framework as a variation of the KS potentials and currents:

$$v_{\mathrm{KS}}([v,n,q_\alpha];\mathbf{r},t) = v(\mathbf{r},t) + \underbrace{v_s([n];\mathbf{r},t) - v([n,q_\alpha];\mathbf{r},t)}_{v_{\mathrm{Mxc}}([n,q_\alpha];\mathbf{r},t)},$$
$$j_{\alpha,\mathrm{KS}}([j_\alpha,n,q_\alpha];t) = j_\alpha(t) + \underbrace{j_{\alpha,s}([q_\alpha];t) - j_\alpha([n,q_\alpha];t)}_{j_{\alpha,\mathrm{Mxc}}([n,q_\alpha];t)}.$$

This is accomplished by substituting Eqs. (227), (229), (232) and (234) into the respective responses of Eqs. (215) and (216) that leads to

$$\delta n_v(\mathbf{r},t) = \iint d^3\,\mathbf{r}' dt' \chi^n_{n,s}(\mathbf{r},t;\mathbf{r}',t')\delta v_{\mathrm{KS},v}(\mathbf{r}',t'), \tag{235}$$
$$\delta n_j(\mathbf{r},t) = \iint d^3\mathbf{r}'\; dt' \chi^n_{n,s}(\mathbf{r},t;\mathbf{r}',t')\delta v_{\mathrm{KS},j}(\mathbf{r}',t'), \tag{236}$$
$$\delta q_{\alpha,v}(t) = \int dt' \chi^{q_\alpha}_{q_\alpha,s}(t,t')\delta j_{\alpha,\mathrm{KS},v}(t'), \tag{237}$$
$$\delta q_{\alpha,j}(t) = \int dt' \chi^{q_\alpha}_{q_\alpha,s}(t,t')\delta j_{\alpha,\mathrm{KS},j}(t'). \tag{238}$$

Here, we emphasize again that the subscripts v and j on the electron density response and photon coordinate response represent the responses due to an external potential

$\delta v(\mathbf{r},t)$ and current $\delta j_\alpha(t)$. Equally, the notation applies to the KS potentials and currents of Eqs. (235)-(238) which are given explicitly as

$$\begin{aligned}
\delta v_{\mathrm{KS},v}(\mathbf{r}',t') &= \delta v(\mathbf{r}',t') + \iint d^3\mathbf{y}\, d\tau' f^n_{\mathrm{Mxc}}(\mathbf{r}',t';\mathbf{y},\tau')\delta n(\mathbf{y},\tau') \\
&\quad + \sum_\alpha \int d\tau' f^{q_\alpha}_{\mathrm{Mxc}}(\mathbf{r}',t';\tau')\delta q_\alpha(\tau'), \qquad (239)\\
\delta v_{\mathrm{KS},j}(\mathbf{r}',t') &= \iint d^3\mathbf{y}\, d\tau' f^n_{\mathrm{Mxc}}(\mathbf{r}',t';\mathbf{y},\tau')\delta n(\mathbf{y},\tau') \\
&\quad + \sum_\alpha \int d\tau' f^{q_\alpha}_{\mathrm{Mxc}}(\mathbf{r}',t';\tau')\delta q_\alpha(\tau'), \qquad (240)\\
\delta j_{\alpha,\mathrm{KS},v}(t') &= \iint d^3\mathbf{y}\, d\tau' g^{n_\alpha}_{\mathrm{M}}(t',\mathbf{y}\tau')\delta n(\mathbf{y},\tau'), \qquad (241)\\
\delta j_{\alpha,\mathrm{KS},j}(t') &= \delta j_\alpha(t') + \iint d^3\mathbf{x}\, d\tau' g^{n_\alpha}_{\mathrm{M}}(t';\mathbf{x},\tau')\delta n(\mathbf{x},\tau'). \qquad (242)
\end{aligned}$$

We now comment further on the Mxc kernels in Eqs. (223)-(226). Since $g^{q_{\beta'}}_{\mathrm{Mxc}} = 0$, we focus on the other Mxc kernels which can be expressed in the equivalent form

$$\begin{aligned}
f^n_{\mathrm{Mxc}}(\mathbf{r},t;\mathbf{r}',t') &= f^n_{\mathrm{Hxc}}(\mathbf{r},t;\mathbf{r}',t') + f^n_{\mathrm{Pxc}}(\mathbf{r},t;\mathbf{r}',t'),\\
f^{q_\alpha}_{\mathrm{Mxc}}(\mathbf{r},t;t') &= f^{q_\alpha}_{\mathrm{Pxc}}(\mathbf{r},t;t'),\\
g^n_{\mathrm{Mxc}}(t;\mathbf{r}',t') &= g^n_{\mathrm{M}}(t;\mathbf{r}',t').
\end{aligned} \qquad (243)$$

Since the Mxc current given above has only a mean-field contribution, so too is the kernel $g^n_{\mathrm{Mxc}} = g^n_{\mathrm{M}}$ which is given in Eq. (244). Our linear-response formulation within QEDFT in addition to the f^n_{Hxc}, introduces the following three new Mxc kernels: f^n_{Pxc}, $f^{q_\alpha}_{\mathrm{Mxc}}$, g^n_{Mxc} that accounts for the self-consistent interaction (cross-talk) between the light-matter coupled system. These kernels basically represent the interaction terms of Eqs. (186) and (187) of the length gauge Hamiltonian. The kernel f^n_{Hxc} is known in TDDFT which accounts for the longitudinal electron-electron interactions, f^n_{Pxc} accounts for electron-electron interaction via the transverse field (dipole self-energy term) while $f^{q_\alpha}_{\mathrm{Pxc}}$ and g^n_{M} represent the contributions from the electron-photon coupling (i.e. the bilinear interaction term). In principle these Mxc kernels can be constructed as inverses of their respective interacting and non-interacting response functions (see Eqs. (223)-(226)) but in practice they need to be approximated. The approximations applied to the kernels of Eq. (243) as used in this thesis are described as follows. The interaction of the photon field with the matter subsystem is treated on a mean-field level by not including their xc kernels while the electron-electron interaction is treated with ALDA (see Chap. 2.5.3.1 for details):

$$\begin{aligned}
f^n_{\mathrm{Hxc}}(\mathbf{r},t;\mathbf{r}',t') &= f^n_{\mathrm{H}}(\mathbf{r},t;\mathbf{r}',t') + f^n_{\mathrm{xc}}(\mathbf{r},t;\mathbf{r}',t')\\
&\simeq \frac{e^2}{4\pi\epsilon_0}\frac{\delta(t-t')}{|\mathbf{r}-\mathbf{r}'|} + f^n_{\mathrm{xc,ALDA}}(\mathbf{r},t;\mathbf{r}',t')\,,\\
f^n_{\mathrm{Pxc}}(\mathbf{r},t;\mathbf{r}',t') &\approx f^n_{\mathrm{P}}(\mathbf{r},t;t') = \delta(t-t')e^2\sum_\alpha (\boldsymbol{\lambda}_\alpha\cdot\mathbf{r})\,\boldsymbol{\lambda}_\alpha\cdot\mathbf{r}'\,,\\
f^{q_\alpha}_{\mathrm{Pxc}}(\mathbf{r},t;t') &\approx f^{q_\alpha}_{\mathrm{P}}(\mathbf{r},t;t') = -\delta(t-t')\,\omega_\alpha\,\boldsymbol{\lambda}_\alpha\cdot e\mathbf{r}\,,\\
g^n_{\mathrm{M}}(t;\mathbf{r}',t') &= -\delta(t-t')\,\omega_\alpha^2\,\boldsymbol{\lambda}_\alpha\cdot e\mathbf{r}'\,.
\end{aligned} \qquad (244)$$

We note that in the decoupling limit of light and matter, i.e. $|\boldsymbol{\lambda}_\alpha| = 0$, the three new kernels in Eq. (243) are zero and our linear-response QEDFT framework reduces to that of TDDFT presented in Chap. 2.5.3.

3.4 MODIFICATION OF THE MAXWELL'S EQUATION

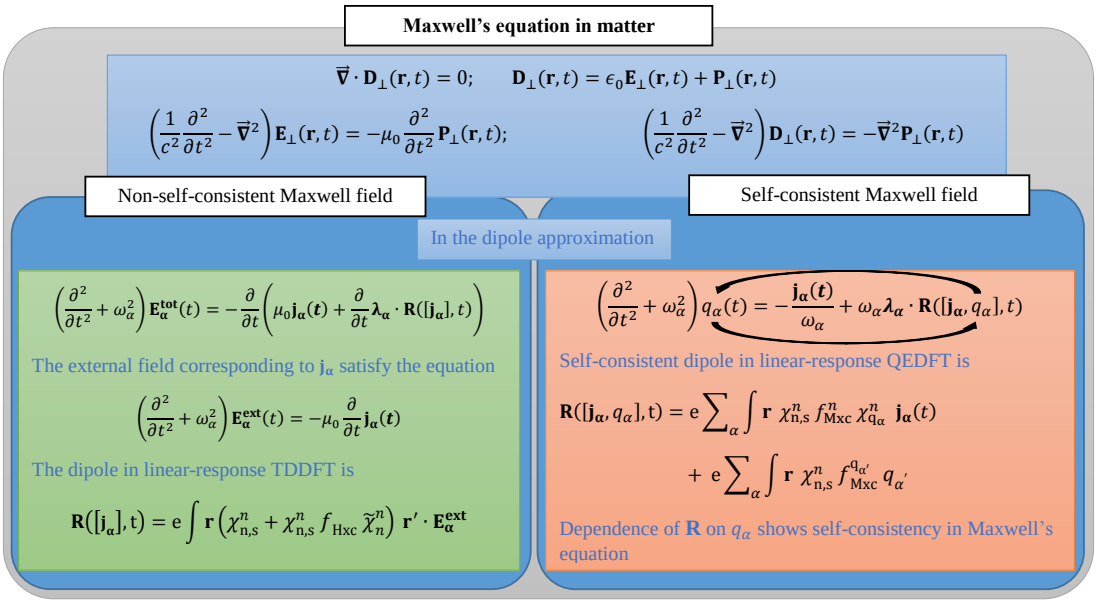

Figure 2: Schematics contrasting the standard Maxwell's equation (left) with the fully self-consistent Maxwell's equation (right). Top: The induced transverse electric field $\mathbf{E}_\perp$ due to the induced polarization $\mathbf{P}_\perp$, which in an equivalent way can be expressed in terms of the auxiliary displacement field $\mathbf{D}_\perp$. Left: mode-resolved Maxwell's equation without self-consistent back-reaction. The external charge current $\mathbf{j}_\alpha$ can be used to induce the external electric field in $\mathbf{E}_\alpha^{\mathrm{tot}} = \mathbf{E}_\alpha + \mathbf{E}_\alpha^{\mathrm{ext}}$ which acts as an external perturbation via the dipole. The induced field does not couple back to the Maxwell field since the constituents of $\tilde{\chi}_n^n$ expressed in TDDFT are purely electronic. Right: a self-consistent Maxwell's equation where $\mathbf{j}_\alpha$ induces the internal field $q_\alpha(t)$ via the electronic dipole which has an explicit dependence on q_α as seen in the QEDFT form of $\chi_{q_\alpha}^n$. The self-consistency of the induced field via the dipole response introduces nonlinearities in the coupled system and thus, changes the Maxwell field at the level of linear response.

In the last two sections, we presented the linear-response of non-relativistic QED and its formulation within the framework of QEDFT and showed that our results are a generalization to the linear-response in the semi-classical limit and its formulation within TDDFT presented in Chap. 2.5.3. This highlights that including the quantized field as a dynamical part of the system changes not only the matter subsystem but also the photon field as well. In this section we employ the above results to show the modifications of the Maxwell's equations due to a self-consistent treatment of the matter-photon system. This will highlight the limitations of the semi-classical description of light-matter interaction as it treats the transverse field only as an external perturbation, thereby, ignoring the feedback loop between light and matter that leads to changes in the Maxwell's equation.

In order to make these changes apparent in the Maxwell's equation, we start from the classical description and focus on the induced fields due to an external perturbation. When the fields and sources are purely classical there is no difference whether

we perturb by an external transversal field $\mathbf{a}_\perp$ or an external classical current $\mathbf{j}_\perp$ [2] due to the inhomogeneous Maxwell's equation in vacuum

$$\left(\frac{1}{c^2}\frac{\partial^2}{\partial t^2} - \boldsymbol{\nabla}^2\right)\mathbf{a}_\perp(\mathbf{r},t) = \mu_0 \mathbf{j}_\perp(\mathbf{r},t). \tag{245}$$

Provided we have some theory to relate this external perturbation to the induced current $\mathbf{J}_\perp[\mathbf{a}_\perp]$, then the induced field reads

$$\left(\frac{1}{c^2}\frac{\partial^2}{\partial t^2} - \boldsymbol{\nabla}^2\right)\mathbf{A}_\perp(\mathbf{r},t) = \mu_0 \mathbf{J}_\perp([\mathbf{a}_\perp],\mathbf{r},t), \tag{246}$$

from which induced physical fields can be calculated, for example, the transversal electric field in Coulomb gauge can be obtained from Eq. (22). Furthermore, these two results can be combined to obtain the total field $\mathbf{A}_\perp^{\mathrm{tot}} = \mathbf{A}_\perp + \mathbf{a}_\perp$, which obeys

$$\left(\frac{1}{c^2}\frac{\partial^2}{\partial t^2} - \boldsymbol{\nabla}^2\right)\mathbf{A}_\perp^{\mathrm{tot}}(\mathbf{r},t) = \mu_0 \left(\mathbf{j}_\perp(\mathbf{r},t) + \mathbf{J}_\perp([\mathbf{j}_\perp],\mathbf{r},t)\right). \tag{247}$$

Making use of the Maxwell relations once again, we can equivalently find for example the induced electric field from the equation

$$\left(\frac{1}{c^2}\frac{\partial^2}{\partial t^2} - \boldsymbol{\nabla}^2\right)\mathbf{E}_\perp(\mathbf{r},t) = -\mu_0 \frac{\partial}{\partial t}\mathbf{J}_\perp([\mathbf{a}_\perp],\mathbf{r},t). \tag{248}$$

Now, a connection to the Maxwell's equation in matter can be established, where the $\mathbf{j}_\perp$ is called the free current and $\mathbf{J}_\perp$ the bound current. Assuming that the transversal induced current can be expressed locally around the center of charge as $\mathbf{J}_\perp(\mathbf{r},t) \approx \frac{\partial}{\partial t}\mathbf{P}_\perp(\mathbf{r},t)$, where the polarization is given by

$$\mathbf{P}_\perp(\mathbf{r},t) = \epsilon_0 e \sum_{\alpha=1}^{M} \boldsymbol{\lambda}_\alpha(\mathbf{r}) \int d^3\mathbf{r}'\, \boldsymbol{\lambda}_\alpha(\mathbf{r}') \cdot \mathbf{r}' n([\mathbf{a}_\perp];\mathbf{r}',t),$$

the electric field can be expanded in the modes $\boldsymbol{\lambda}_\alpha(\mathbf{r})$ as

$$\mathbf{E}_\perp(\mathbf{r},t) = \sum_{\alpha=1}^{M} \boldsymbol{\lambda}_\alpha(\mathbf{r}) \mathrm{E}_\alpha(t). \tag{249}$$

The above equation can be expressed at the center of charge, i.e., $\boldsymbol{\lambda}_\alpha(\mathbf{r}) \to \boldsymbol{\lambda}_\alpha$, as

$$\left(\frac{\partial^2}{\partial t^2} + \omega_\alpha^2\right)\mathrm{E}_\alpha(t) = -\frac{\partial^2}{\partial t^2}\boldsymbol{\lambda}_\alpha \cdot \mathbf{R}([\mathbf{a}_\perp],t). \tag{250}$$

Using the approach illustrated above, we can connect the density response $\delta n(\mathrm{r},t)$ to the induced electric field $\delta\mathbf{E}_\perp(\mathbf{r},t)$, where a spatially homogeneous vector potential $\mathbf{a}_\perp(t)$ is employed that gives rise to the external electric field $\mathbf{E}_\perp^{\mathrm{ext}}(t) = -\frac{\partial}{\partial t}\mathbf{a}_\perp(t)$. In a final step, to avoid solving the above mode-resolved Maxwell's equations, one often ignores the spatial dependence of the induced field and merely uses $\mathrm{E}_\alpha(t) = -\boldsymbol{\lambda}_\alpha \cdot \mathbf{R}([\mathbf{a}_\perp],t)$.

2 Here, the lowercase notation of the vector potential and current represents external fields that are not dynamical variables of the system.

In a next step, computing the linear response $\mathbf{R}([\mathbf{a}_\perp], t)$ we immediately see that when $\chi_n^n(\mathbf{r}, t; \mathbf{r}', t')$ is changed due to the light-matter coupling the induced field also changes. In addition, the reformulation of the linear response kernel in Eq. (227) shows that a feedback loop is present from the induced photon field onto the matter. However, the reformulation of the same linear response kernel in the semi-classical limit given in Eq. (144) does not account for the feedback loop, thus neglecting important features of the light-matter system (see Fig. (2)). For example, the intrinsic back-reaction (screening) effects are very important for large systems such as those in solid-state physics, where it is well known that the bare (vacuum) electric field as obtained from Eq. (250) does not agree with the measured spectrum. Thus the self-consistent polarization of the system that counter-acts the external perturbing field has to be included to obtain the correct spectrum. This can be achieved in an approximate way in the linear response regime by self-consistently solving the Maxwell's equation with the matter response as input [103–106]. Classical electrodynamics approaches the problem by using the Maxwell's equations in matter. To connect to the length gauge which mixes the matter and photon degrees (see Chap. 2.2.2), this implies that we use displacement field $\mathbf{D}_\perp = \epsilon_0 \mathbf{E}_\perp + \mathbf{P}_\perp$ where the polarization term $\mathbf{P}_\perp$ encodes all the information about how the system reacts to an external perturbation. The Maxwell's equation in terms of the displacement field is

$$\left(\frac{1}{c^2}\frac{\partial^2}{\partial t^2} - \boldsymbol{\nabla}^2\right)\mathbf{D}_\perp(\mathbf{r}, t) = -\nabla^2 \mathbf{P}_\perp([\mathbf{a}_\perp]; \mathbf{r}, t). \tag{251}$$

To obtain the displacement field in a mode-resolved form and in the long wavelength limit, we expand $\mathbf{D}_\perp(\mathbf{r}, t) = \epsilon_0 \sum_\alpha \omega_\alpha \boldsymbol{\lambda}_\alpha(\mathbf{r}) q_\alpha(t)$ and then invoking the dipole approximation results to

$$\left(\frac{\partial^2}{\partial t^2} + \omega_\alpha^2\right) q_\alpha(t) = \omega_\alpha \boldsymbol{\lambda}_\alpha \cdot \mathbf{R}([\mathbf{a}_\perp], t), \tag{252}$$

which is the classical analogue of Eq. (178) for $j_\alpha(t) = 0$. In the semi-classical description that does not include the self-consistency, the quantity $\mathbf{R}([\mathbf{a}_\perp], t)$ is simply determined from the electric permittivity and the feedback that describes how the matter system affects (screens) the field is ignored. The self-consistency can be found in an approximate way if the induced field $\mathbf{E}_\perp$ is taken into account to screen the perturbing field $\mathbf{E}_\perp^{\text{ext}}$. However, we will go beyond this simple approximate self-consistency which breaks down when the coupling between light and matter is strong. Note that the electric field in the macroscopic Maxwell's equation now becomes $E_\alpha(t) = \omega_\alpha q_\alpha(t) - \boldsymbol{\lambda}_\alpha \cdot \mathbf{R}([\mathbf{a}_\perp], t)$, and ignoring the spatial dependence when determining $\mathbf{E}_\perp$ results to the assumption that $\mathbf{D}_\perp = \mathbf{E}_\perp$.

In our description of light-matter systems, the photon field is accounted for as a dynamical variable of the system such that the Maxwell field couples to the electronic subsystem, which leads to a fully self-consistent description of the light-matter response. Similar to the changes in $\chi_n^n(\mathbf{r}, t; \mathbf{r}', t')$, which upon substituting as an input into Eqs. (248) or (252), accounts for the self-consistent response of the light-matter system, we also have direct access to the induced electric field by considering the response of the displacement field due to $\chi_{q_\alpha}^n(\mathbf{r}, t; t')$. The physical implication of this highlights that the excited states of the coupled light-matter system can be viewed as changes in the quantized Maxwell field in accordance to the usual experimental

situation as will be shown below. On the other hand, we have the possibility of investigating what the quantum description of the coupled light-matter system does to the Maxwell's equations.

In order to highlight these changes, consider the case where the current $\delta j_\alpha(t)$ is non-zero while the external classical field is zero, i.e., $\delta v(\mathbf{r},t) = 0$. In this case, we find the variation of the electron density to the external current in Eq. (178) to be

$$\begin{aligned}\left(\frac{\partial^2}{\partial t^2}+\omega_\alpha^2\right)\delta q_\alpha(t) &= -\frac{\delta j_\alpha(t)}{\omega_\alpha}+\omega_\alpha\boldsymbol{\lambda}_\alpha\cdot\iint dt'd^3\mathbf{r}\,\mathbf{r}\frac{\delta n(\mathbf{r},t)}{\delta j_\alpha(t')}\delta j_\alpha(t')\\ &= -\frac{\delta j_\alpha(t)}{\omega_\alpha}+\omega_\alpha\boldsymbol{\lambda}_\alpha\cdot\iint dt'd^3\mathbf{r}\,\mathbf{r}\,\chi^n_{q_\alpha}(\mathbf{r},t;t')\delta j_\alpha(t').\end{aligned} \tag{253}$$

Substituting Eq. (229) into Eq. (253) we obtain the following equation

$$\begin{aligned}\left(\frac{\partial^2}{\partial t^2}+\omega_\alpha^2\right)\delta q_\alpha(t) =& -\frac{\delta j_\alpha(t)}{\omega_\alpha}+\omega_\alpha\boldsymbol{\lambda}_\alpha\cdot\int e\mathbf{r}\,\chi^n_{n,s}f^n_{\mathrm{Mxc}}\chi^n_{q_\alpha}\delta j_\alpha\\ &+\omega_\alpha\boldsymbol{\lambda}_\alpha\cdot\sum\int e\mathbf{r}\,\chi^n_{n,s}f^{q_{\alpha'}}_{\mathrm{Mxc}}\delta q_{\alpha'}.\end{aligned} \tag{254}$$

When we contrast the above equation to the classical Maxwell's equation in matter

$$\left(\frac{\partial^2}{\partial t^2}+\omega_\alpha^2\right)\delta q_\alpha(t) = -\frac{\delta j_\alpha(t)}{\omega_\alpha}+\omega_\alpha\boldsymbol{\lambda}_\alpha\cdot\delta\mathbf{R}([\mathbf{j}_\perp],t), \tag{255}$$

where the dipole $\mathbf{R}([\mathbf{j}_\perp],t)$ can be obtained from the response of the matter system due to the corresponding external field $\mathbf{a}_\perp$, we observe that in addition to the self-consistent response of the matter system (second term on the right hand side), there is also a genuine new (matter-mediated) photon-photon interaction term (third term on the right hand side) that appears. Making the mean-field explicit by employing Eq. (244) leads to

$$\begin{aligned}\left(\frac{\partial^2}{\partial t^2}+\omega_\alpha^2\right)\delta q_\alpha(t) =& -\frac{\delta j_\alpha(t)}{\omega_\alpha}-\omega_\alpha\boldsymbol{\lambda}_\alpha\cdot\sum\int e\mathbf{r}\,\chi^n_{n,s}\left(\omega_{\alpha'}\boldsymbol{\lambda}_{\alpha'}\cdot e\mathbf{r}'\right)\delta q_{\alpha'}\\ &+\omega_\alpha\boldsymbol{\lambda}_\alpha\cdot\int e\mathbf{r}\,\chi^n_{n,s}\left[\frac{e^2}{4\pi\epsilon_0|\mathbf{r}'-\mathbf{r}''|}\right.\\ &\qquad\left.+\sum_{\alpha'}e^2\left(\boldsymbol{\lambda}_{\alpha'}\cdot\mathbf{r}''\right)\boldsymbol{\lambda}_{\alpha'}\cdot\mathbf{r}'\right]\chi^n_{q_\alpha}\delta j_\alpha\\ &+\omega_\alpha\boldsymbol{\lambda}_\alpha\cdot\int e\mathbf{r}\,\chi^n_{n,s}f^n_{\mathrm{xc}}\chi^n_{q_\alpha}\delta j_\alpha+\omega_\alpha\boldsymbol{\lambda}_\alpha\cdot\sum\int e\mathbf{r}\,\chi^n_{n,s}f^{q_{\alpha'}}_{\mathrm{xc}}\delta q_{\alpha'}.\end{aligned}$$

Ignoring the xc contributions to the photon-photon and matter-photon response results to the pRPA of the Maxwell's equation in matter. In the above pRPA form of the Maxwell equation, we clearly see how the equation becomes non-linear because of the feedback between light and matter (see Fig. (2)). This kind of non-linearities of the Maxwell's equations are investigated in great detail in high-energy physics in the context of strong-field QED [107] in which the strong fields lead to particle creation and thus a matter-mediated photon-photon interaction. However, in our setting such high energies are not needed because we consider the photon-photon interaction due to condensed matter in the form of atoms, molecules or solids and use, e.g., a cavity or plasmonic nanostructures to enhance the coupling. We note that the changes

in the Maxwell's equations presented here are not purely theoretical concepts but lead to observable effects that can be seen in many physical situations. The example mentioned about the polarization effects in solid-state systems [106] is the most well-known effect, but more strikingly are effects due to the quantum-matter-mediated photon-photon interactions, see e.g. Ref. [108]. In this context, the presented linear-response method allows to theoretically investigate the photon-photon interactions and possibly predict systems with very strong photon-photon correlations. We therefore highlight that the quantized Maxwell's equation in matter, if we allow for both, an external current and an external field, can indeed discriminate between these two sorts of perturbations. In a purely classical theory such as the Maxwell equation of Eq. (245), there can be no difference. Our linear-response formulation in non-relativistic QED and formulated within QEDFT provides an interesting playground to investigate the difference between classical and quantum physics.

3.5 LINEAR RESPONSE METHODS WITHIN THE FRAMEWORK OF QEDFT

So far, we have presented the linear response equations in non-relativistic QED and showed within the QEDFT framework the changes in Maxwell's equation due to the self-consistent coupling between light and matter. To investigate the changes that arise in the coupled matter-photon system, the response equations or response functions of Eqs. (215) and (216) have to be computed. However, obtaining these responses for large systems is not computational feasible, therefore, we resort to the KS setting of QEDFT of the response equations given by Eqs. (235)-(238). In this setting, practical calculations are feasible when we apply approximations to the Mxc kernels. This section presents linear-response methods derived within the framework of QEDFT that compute either the responses or response functions of Eqs. (215) and (216). The methods derived in this section were already briefly introduced in Chap. 2.5.3.2 within the context of linear response of TDDFT. In the following, we present extensions of these methods for obtaining the response properties of matter-photon systems. The response methods that are presented here are the Casida equations, frequency-dependent Sternheimer equations and the time-propagation scheme. In these methods, we focus on singlet excitations in closed-shell systems, therefore, restricting ourselves to the spin-independent formalism. However, we note that generalizations to spin-dependent formulations are straightforward.

3.5.1 THE CASIDA METHOD OF QEDFT

In matter-only formulation of TDDFT, the Casida [84] approach has become almost the standard method for computing the linear response of a system. The method is built on expanding the many-electron excitations in a particle-hole basis. The problem is then cast into to a pseudo-eigenvalue equation in which excitation energies and oscillator strengths are obtained from the eigenvalues and eigenvectors of a response matrix. In this section, we present a matrix formulation of non-relativistic QEDFT response equations which in the no-coupling limit (i.e. switching off the coupling of the electrons to the photons) reduces to the well-known electron-only Casida equation. As mentioned in Chap. 2.5.3.2, this method does not directly determine

the electron density response but rather the density-density response function. Similarly, this method as derived within the framework of QEDFT computes the response functions of Eqs. (217) - (220) in the frequency space.

We now derive the Casida pseudo-eigenvalue equation for coupled electron-photon systems within the framework of QEDFT [18]. The time-dependent responses given in Eqs. (235)-(238) can be expressed in frequency space as

$$\delta n_v(\mathbf{r},\omega) = \int d^3\mathbf{r}'\chi^n_{n,s}(\mathbf{r},\mathbf{r}',\omega)\delta v_{\mathrm{KS},v}(\mathbf{r}',\omega), \tag{256}$$

$$\delta n_j(\mathbf{r},\omega) = \int d^3\mathbf{r}'\chi^n_{n,s}(\mathbf{r},\mathbf{r}',\omega)\delta v_{\mathrm{KS},j}(\mathbf{r}',\omega), \tag{257}$$

$$\delta q_{\alpha,v}(\omega) = \chi^{q_\alpha}_{q_{\alpha,s}}(\omega)\delta j_{\alpha,\mathrm{KS},v}(\omega), \tag{258}$$

$$\delta q_{\alpha,j}(\omega) = \chi^{q_\alpha}_{q_{\alpha,s}}(\omega)\delta j_{\alpha,\mathrm{KS},j}(\omega), \tag{259}$$

where the KS potentials and currents in the above equation are Fourier transforms of Eqs. (256)-(238) given by

$$\delta v_{\mathrm{KS},v}(\mathbf{r}',\omega) = \delta v(\mathbf{r}',\omega) + \int d^3\mathbf{x}\, f^n_{\mathrm{Mxc}}(\mathbf{r}',\mathbf{x},\omega)\delta n_v(\mathbf{x},\omega) + \sum_\alpha f^{q_\alpha}_{\mathrm{Mxc}}(\mathbf{r}',\omega)\delta q_{\alpha,v}(\omega), \tag{260}$$

$$\delta v_{\mathrm{KS},j}(\mathbf{r}',\omega) = \int d^3\mathbf{x}\, f^n_{\mathrm{Mxc}}(\mathbf{r}',\mathbf{x},\omega)\delta n_j(\mathbf{x},\omega) + \sum_\alpha f^{q_\alpha}_{\mathrm{Mxc}}(\mathbf{r}',\omega)\delta q_{\alpha,j}(\omega), \tag{261}$$

$$\delta j_{\alpha,\mathrm{KS},v}(\omega) = \int d^3\mathbf{x}\, g^{n_\alpha}_{\mathrm{M}}(\mathbf{x})\delta n_v(\mathbf{x},\omega), \tag{262}$$

$$\delta j_{\alpha,\mathrm{KS},j}(\omega) = \delta j_\alpha(\omega) + \int d^3\mathbf{x}\, g^{n_\alpha}_{\mathrm{M}}(\mathbf{x})\delta n_j(\mathbf{x},\omega). \tag{263}$$

The non-interacting response function of the electronic subsystem in frequency space in Eqs. (256) and (257) is given in Eq. (152). An equivalent form of this non-interacting response function as used in this section is given explicitly as

$$\chi^n_{n,s}(\mathbf{r},\mathbf{r}',\omega) = \frac{1}{\hbar}\sum_{k=1}^{N_e}\sum_{l=1}^{\infty}\left[\frac{\varphi_l(\mathbf{r})\varphi_k(\mathbf{r}')\varphi^*_k(\mathbf{r})\varphi^*_l(\mathbf{r}')}{\omega-(\epsilon_l-\epsilon_k)+i\eta} - \frac{\varphi_k(\mathbf{r})\varphi_l(\mathbf{r}')\varphi^*_l(\mathbf{r})\varphi^*_k(\mathbf{r}')}{\omega+(\epsilon_l-\epsilon_k)+i\eta}\right] \tag{264}$$

$$= \frac{1}{\hbar}\sum_{i=1}^{N_e}\sum_{a=N_e+1}^{\infty}\left[\frac{\varphi_a(\mathbf{r})\varphi_i(\mathbf{r}')\varphi^*_i(\mathbf{r})\varphi^*_a(\mathbf{r}')}{\omega-(\epsilon_a-\epsilon_i)+i\eta} - \frac{\varphi_i(\mathbf{r})\varphi_a(\mathbf{r}')\varphi^*_a(\mathbf{r})\varphi^*_i(\mathbf{r}')}{\omega+(\epsilon_a-\epsilon_i)+i\eta}\right]. \tag{265}$$

Also, the non-interacting response function of the photonic subsystem in frequency space in Eqs. (258) and (259) is given explicitly as

$$\begin{aligned}\chi^{q_\alpha}_{q_{\alpha,s}}(\omega) &= \frac{1}{\hbar}\frac{1}{\omega_\alpha}\left(\frac{\langle 0_\alpha|\hat{q}_\alpha|1_\alpha\rangle\langle 1_\alpha|\hat{q}_\alpha|0_\alpha\rangle}{\omega-\omega_\alpha+i\eta'} - \frac{\langle 0_\alpha|\hat{q}_\alpha|1_\alpha\rangle\langle 1_\alpha|\hat{q}_\alpha|0_\alpha\rangle}{\omega+\omega_\alpha+i\eta'}\right)\\ &= \frac{1}{2\omega^2_\alpha}\left(\frac{1}{\omega-\omega_\alpha+i\eta'} - \frac{1}{\omega+\omega_\alpha+i\eta'}\right).\end{aligned} \tag{266}$$

Here, the Fock number $n_\alpha = 1_\alpha$ is valid for the linear response regime while noting that the transition elements from the vacuum state with higher Fock number states have zero contribution. It is important to note that the η and η' parameters that shifts

the poles of Eqs. (265) and (266) to the lower half of the complex plane need not be equal in both uncoupled systems. In the following we set $\eta, \eta' \to 0$ and $\hbar = 1$ for notational simplicity.

In a next step, we combined Eqs. (256)-(259) according to their external perturbations as in Eqs. (215) and (216) to arrive at the equations

$$\delta n_v(\mathbf{r},\omega) = \sum_{i,a} \left[\varphi_a(\mathbf{r})\varphi_i^*(\mathbf{r})\mathbf{P}^{(+)}_{ai,v}(\omega) + \varphi_i(\mathbf{r})\varphi_a^*(\mathbf{r})\mathbf{P}^{(-)}_{ia,v}(\omega) \right], \tag{267}$$

$$\delta q_{\alpha,v}(\omega) = \mathbf{L}^{(+)}_{\alpha,v}(\omega) + \mathbf{L}^{(-)}_{\alpha,v,+}(\omega), \tag{268}$$

and

$$\delta n_j(\mathbf{r},\omega) = \sum_{i,a} \left[\varphi_a(\mathbf{r})\varphi_i^*(\mathbf{r})\mathbf{P}^{(+)}_{ai,j}(\omega) + \varphi_i(\mathbf{r})\varphi_a^*(\mathbf{r})\mathbf{P}^{(-)}_{ia,j}(\omega) \right], \tag{269}$$

$$\delta q_{\alpha,j}(\omega) = \mathbf{L}^{(+)}_{\alpha,j}(\omega) + \mathbf{L}^{(-)}_{\alpha,j}(\omega). \tag{270}$$

The first-order responses $\mathbf{P}^{(+)}_{ai,v}(\omega)$, $\mathbf{P}^{(-)}_{ia,v}(\omega)$, $\mathbf{L}^{(+)}_{\alpha,v}(\omega)$ and $\mathbf{L}^{(-)}_{\alpha,v}(\omega)$ are given by

$$[\omega - \omega_{ai}]\, \mathbf{P}^{(+)}_{ai,v}(\omega) = \int d^3\mathbf{r}\; \varphi_i(\mathbf{r})\varphi_a^*(\mathbf{r})\delta v_{\mathrm{KS},v}(\mathbf{r},\omega), \tag{271}$$

$$[\omega + \omega_{ai}]\, \mathbf{P}^{(-)}_{ia,v}(\omega) = -\int d^3\mathbf{r}\; \varphi_a(\mathbf{r})\varphi_i^*(\mathbf{r})\delta v_{\mathrm{KS},v}(\mathbf{r},\omega), \tag{272}$$

$$[\omega - \omega_{\alpha}]\, \mathbf{L}^{(+)}_{\alpha,v}(\omega) = \frac{1}{2\omega_\alpha^2}\delta j_{\alpha,\mathrm{KS},v}(\omega), \tag{273}$$

$$[\omega + \omega_{\alpha}]\, \mathbf{L}^{(-)}_{\alpha,v}(\omega) = -\frac{1}{2\omega_\alpha^2}\delta j_{\alpha,\mathrm{KS},v}(\omega), \tag{274}$$

and responses $\mathbf{P}^{(+)}_{ai,j}(\omega)$, $\mathbf{P}^{(-)}_{ia,j}(\omega)$, $\mathbf{L}^{(+)}_{\alpha,v}(\omega)$ and $\mathbf{L}^{(-)}_{\alpha,j}(\omega)$ are given by

$$[\omega - \omega_{ai}]\, \mathbf{P}^{(+)}_{ai,j}(\omega) = \int d^3\mathbf{r}\; \varphi_i(\mathbf{r})\varphi_a^*(\mathbf{r})\delta v_{\mathrm{KS},j}(\mathbf{r},\omega), \tag{275}$$

$$[\omega + \omega_{ai}]\, \mathbf{P}^{(-)}_{ia,j}(\omega) = -\int d^3\mathbf{r}\; \varphi_a(\mathbf{r})\varphi_i^*(\mathbf{r})\delta v_{\mathrm{KS},j}(\mathbf{r},\omega), \tag{276}$$

$$[\omega - \omega_{\alpha}]\, \mathbf{L}^{(+)}_{\alpha,j}(\omega) = \frac{1}{2\omega_\alpha^2}\delta j_{\alpha,\mathrm{KS},j}(\omega), \tag{277}$$

$$[\omega + \omega_{\alpha}]\, \mathbf{L}^{(-)}_{\alpha,j}(\omega) = -\frac{1}{2\omega_\alpha^2}\delta j_{\alpha,\mathrm{KS},j}(\omega), \tag{278}$$

where the transition frequencies are $\omega_{ai} = (\epsilon_a - \epsilon_i)$. Making a substitution of Eqs. (260) and (262) into Eqs. (271)-(274) and after some simplifications, we arrive at

$$\sum_{j,b} \left[\delta_{ab}\delta_{ij}\left(\omega_{ai} - \omega\right) + K_{ai,jb}(\omega)\right] \mathbf{P}^{(+)}_{bj,v}(\omega) + K_{ai,bj}(\omega)\mathbf{P}^{(-)}_{jb,v}(\omega)$$
$$+ \sum_{\alpha} \delta_{ab}\delta_{ij} M_{\alpha,bj}(\omega) \left(\mathbf{L}^{(+)}_{\alpha,v}(\omega) + \mathbf{L}^{(-)}_{\alpha,v}(\omega)\right) = -v_{ai}(\omega), \tag{279}$$

$$\sum_{j,b} \left[\delta_{ab}\delta_{ij}\left(\omega_{ai} + \omega\right) + K_{ia,bj}(\omega)\right] \mathbf{P}^{(-)}_{jb,v}(\omega) + K_{ia,jb}(\omega)\mathbf{P}^{(+)}_{bj,v}(\omega)$$
$$+ \sum_{\alpha} \delta_{ab}\delta_{ij} M_{\alpha,jb}(\omega) \left(\mathbf{L}^{(+)}_{\alpha,v}(\omega) + \mathbf{L}^{(-)}_{\alpha,v}(\omega)\right) = -v_{ia}(\omega), \tag{280}$$

$$\left[\omega_\alpha - \omega\right] \mathbf{L}^{(+)}_{\alpha,v}(\omega) + \sum_{jb} \left[N_{\alpha,jb}\mathbf{P}^{(+)}_{bj,v}(\omega) + N_{\alpha,bj}\mathbf{P}^{(-)}_{jb,v}(\omega)\right] = 0, \tag{281}$$

$$\left[\omega_\alpha + \omega\right] \mathbf{L}^{(-)}_{\alpha,v}(\omega) + \sum_{jb} \left[N_{\alpha,jb}\mathbf{P}^{(+)}_{bj,v}(\omega) + N_{\alpha,bj}\mathbf{P}^{(-)}_{jb,v}(\omega)\right] = 0. \tag{282}$$

Also, substituting Eqs. (261) and (263) into Eqs. (275)-(278) and after some algebra, we obtain

$$\sum_{j,b} \delta_{ab}\delta_{ij} \Big[\left(\left(\omega_{ai} - \omega\right) + K_{ai,jb}(\omega)\right) \mathbf{P}^{(+)}_{bj,j}(\omega) + K_{ai,bj}(\omega)\mathbf{P}^{(-)}_{jb,j}(\omega)$$
$$+ \sum_{\alpha} M_{\alpha,bj}(\omega) \left[\mathbf{L}^{(+)}_{\alpha,j}(\omega) + \mathbf{L}^{(-)}_{\alpha,j}(\omega)\right]\Big] = 0, \tag{283}$$

$$\sum_{j,b} \delta_{ab}\delta_{ij} \Big[\left(\left(\omega_{ai} + \omega\right) + K_{ia,bj}(\omega)\right)\mathbf{P}^{(1)}_{jb,j}(\omega) + K_{ia,jb}(\omega)\mathbf{P}^{(1)}_{bj,j}(\omega)$$
$$+ \sum_{\alpha} M_{\alpha,jb}(\omega) \left[\mathbf{L}^{(1)}_{\alpha,j,-}(\omega) + \mathbf{L}^{(1)}_{\alpha,j,+}(\omega)\right]\Big] = 0, \tag{284}$$

$$\left[\omega_\alpha - \omega\right] \mathbf{L}^{(+)}_{\alpha,j}(\omega) + \sum_{jb} \left[N_{\alpha,jb}\mathbf{P}^{(+)}_{bj,j}(\omega) + N_{\alpha,bj}\mathbf{P}^{(-)}_{jb,j}(\omega)\right] = -\frac{1}{2\omega^2_\alpha}\delta j_\alpha(\omega), \tag{285}$$

$$\left[\omega + \omega_\alpha\right] \mathbf{L}^{(+)}_{\alpha,j}(\omega) + \sum_{jb} \left[N_{\alpha,jb}\mathbf{P}^{(+)}_{bj,j}(\omega) + N_{\alpha,bj}\mathbf{P}^{(-)}_{jb,j}(\omega)\right] = -\frac{1}{2\omega^2_\alpha}\delta j_\alpha(\omega). \tag{286}$$

The coupling matrices and external potential introduced in Eqs. (279)-(286) are defined explicitly to be

$$K_{ai,jb}(\omega) = \iint d^3\mathbf{r}\, d^3\mathbf{y}\; \varphi_i(\mathbf{r})\varphi^*_a(\mathbf{r}) f^n_{\mathrm{Mxc}}(\mathbf{r},\mathbf{y},\omega)\varphi_b(\mathbf{y})\varphi^*_j(\mathbf{y}), \tag{287}$$

$$M_{\alpha,ai}(\omega) = \int d^3\mathbf{r}\; \varphi_i(\mathbf{r})\varphi^*_a(\mathbf{r}) f^{q_\alpha}_{\mathrm{Mxc}}(\mathbf{r},\omega), \tag{288}$$

$$N_{\alpha,ia} = \frac{1}{2\omega^2_\alpha} \int d^3\mathbf{r}\; \varphi^*_i(\mathbf{r})\varphi_a(\mathbf{r}) g^{n_\alpha}_{\mathrm{M}}(\mathbf{r}), \tag{289}$$

$$v_{ia}(\omega) = \int d^3\mathbf{r}\; \varphi^*_i(\mathbf{r})\delta v(\mathbf{r},\omega)\varphi_a(\mathbf{r}). \tag{290}$$

The coupling matrix $N_{\alpha,ia}$ has no frequency dependence since it stems from the mean-field kernel of the photon modes. We now introduce the following notations

$$\begin{cases} L(\omega) = \delta_{ij}\delta_{ab}\omega_{ai} + K_{ia,jb}(\omega), \\ K(\omega) = K_{ia,jb}(\omega), \\ M(\omega) = M_{\alpha,bj}(\omega), \\ N = \frac{1}{2\omega_\alpha^2} N_{\alpha,bj}, \end{cases} \quad \begin{cases} \mathbf{X}_v(\omega) = \mathbf{P}^{(+)}_{bj,v}(\omega), \\ \mathbf{Y}_v(\omega) = \mathbf{P}^{(-)}_{jb,v}(\omega), \\ \mathbf{X}_j(\omega) = \mathbf{P}^{(+)}_{bj,j}(\omega), \\ \mathbf{Y}_j(\omega) = \mathbf{P}^{(-)}_{jb,j}(\omega), \end{cases} \quad \begin{cases} \mathbf{A}_v(\omega) = \mathbf{L}^{(+)}_{\alpha,v}(\omega), \\ \mathbf{B}_v(\omega) = \mathbf{L}^{(-)}_{\alpha,v}(\omega), \\ \mathbf{A}_j(\omega) = \mathbf{L}^{(+)}_{\alpha,j}(\omega), \\ \mathbf{B}_j(\omega) = \mathbf{L}^{(-)}_{\alpha,j}(\omega), \end{cases}$$

and the potential and currents have the notations $V(\omega) = -v_{ai}(\omega)$ and $J(\omega) = -\frac{\delta j_\alpha(\omega)}{2\omega_\alpha}$. Using these notations, we cast Eqs. (279)-(282) and Eqs. (283)-(286) into two matrix equations given by

$$\left[\begin{pmatrix} L(\omega) & K(\omega) & M(\omega) & M(\omega) \\ K^*(\omega) & L(\omega) & M^*(\omega) & M^*(\omega) \\ N & N^* & \omega_\alpha & 0 \\ N & N^* & 0 & \omega_\alpha \end{pmatrix} + \omega \begin{pmatrix} -1 & 0 & 0 & 0 \\ 0 & 1 & 0 & 0 \\ 0 & 0 & -1 & 0 \\ 0 & 0 & 0 & 1 \end{pmatrix}\right] \begin{pmatrix} \mathbf{X}_v(\omega) \\ \mathbf{Y}_v(\omega) \\ \mathbf{A}_v(\omega) \\ \mathbf{B}_v(\omega) \end{pmatrix} = \begin{pmatrix} V(\omega) \\ V^*(\omega) \\ 0 \\ 0 \end{pmatrix}, \tag{291}$$

$$\left[\begin{pmatrix} L(\omega) & K(\omega) & M(\omega) & M(\omega) \\ K^*(\omega) & L(\omega) & M^*(\omega) & M^*(\omega) \\ N & N^* & \omega_\alpha & 0 \\ N & N^* & 0 & \omega_\alpha \end{pmatrix} + \omega \begin{pmatrix} -1 & 0 & 0 & 0 \\ 0 & 1 & 0 & 0 \\ 0 & 0 & -1 & 0 \\ 0 & 0 & 0 & 1 \end{pmatrix}\right] \begin{pmatrix} \mathbf{X}_j(\omega) \\ \mathbf{Y}_j(\omega) \\ \mathbf{A}_j(\omega) \\ \mathbf{B}_j(\omega) \end{pmatrix} = \begin{pmatrix} 0 \\ 0 \\ J(\omega) \\ J(\omega) \end{pmatrix}. \tag{292}$$

Next, the right hand side of the above matrices remains finite as the frequency ω approaches the exact excitation frequencies $\omega \to \Omega_q$ of the interacting system while the density and displacement field responses on the left hand side has poles at the true excitation frequencies Ω_q. This allows us to cast Eq. (291) and Eq. (292) into an eigenvalue problem

$$\begin{pmatrix} L(\Omega_q) & K(\Omega_q) & M(\Omega_q) & M(\Omega_q) \\ K^*(\Omega_q) & L(\Omega_q) & M^*(\Omega_q) & M^*(\Omega_q) \\ N & N^* & \omega_\alpha & 0 \\ N & N^* & 0 & \omega_\alpha \end{pmatrix} \begin{pmatrix} \mathbf{X}_v(\Omega_q) \\ \mathbf{Y}_v(\Omega_q) \\ \mathbf{A}_v(\Omega_q) \\ \mathbf{B}_v(\Omega_q) \end{pmatrix} = \Omega_q \begin{pmatrix} 1 & 0 & 0 & 0 \\ 0 & -1 & 0 & 0 \\ 0 & 0 & 1 & 0 \\ 0 & 0 & 0 & -1 \end{pmatrix} \begin{pmatrix} \mathbf{X}_v(\Omega_q) \\ \mathbf{Y}_v(\Omega_q) \\ \mathbf{A}_v(\Omega_q) \\ \mathbf{B}_v(\Omega_q) \end{pmatrix}, \tag{293}$$

$$\begin{pmatrix} (\Omega_q) & K(\Omega_q) & M(\Omega_q) & M(\Omega_q) \\ K^*(\Omega_q) & L(\Omega_q) & M^*(\Omega_q) & M^*(\Omega_q) \\ N & N^* & \omega_\alpha & 0 \\ N & N^* & 0 & \omega_\alpha \end{pmatrix} \begin{pmatrix} \mathbf{X}_j(\Omega_q) \\ \mathbf{Y}_j(\Omega_q) \\ \mathbf{A}_j(\Omega_q) \\ \mathbf{B}_j(\Omega_q) \end{pmatrix} = \Omega_q \begin{pmatrix} 1 & 0 & 0 & 0 \\ 0 & -1 & 0 & 0 \\ 0 & 0 & 1 & 0 \\ 0 & 0 & 0 & -1 \end{pmatrix} \begin{pmatrix} \mathbf{X}_j(\Omega_q) \\ \mathbf{Y}_j(\Omega_q) \\ \mathbf{A}_j(\Omega_q) \\ \mathbf{B}_j(\Omega_q) \end{pmatrix}. \tag{294}$$

It is convenient to cast Eqs. (293) and (294) into a Hermitian eigenvalue problem which is given by

$$\begin{pmatrix} U & V \\ V^\dagger & \omega_\alpha^2 \end{pmatrix} \begin{pmatrix} \mathbf{E}_v \\ \mathbf{P}_v \end{pmatrix} = \Omega_q^2 \begin{pmatrix} \mathbf{E}_v \\ \mathbf{P}_v \end{pmatrix}, \tag{295}$$

$$\begin{pmatrix} U & V \\ V^\dagger & \omega_\alpha^2 \end{pmatrix} \begin{pmatrix} \mathbf{E}_j \\ \mathbf{P}_j \end{pmatrix} = \Omega_q^2 \begin{pmatrix} \mathbf{E}_j \\ \mathbf{P}_j \end{pmatrix}, \tag{296}$$

where we assumed without loss of generality real-valued orbitals, i.e., $K = K^*$, $M = M^*$ and $N = N^*$, and the matrices are $U = (L-K)^{1/2}(L+K)(L-K)^{1/2}$, $V = 2(L-K)^{1/2}M^{1/2}N^{1/2}\omega_\alpha^{1/2}$, $V^\dagger = 2\omega_\alpha^{1/2}N^{1/2}M^{1/2}(L-K)^{1/2}$, and the eigenvectors are $\mathbf{E}_v = N^{1/2}(L-K)^{-1/2}(\mathbf{X}_v + \mathbf{Y}_v)$ and $\mathbf{P}_v = M^{1/2}\omega_\alpha^{-1/2}(\mathbf{A}_v + \mathbf{B}_v)$. A similar definition holds for $\mathbf{P}_j$ and $\mathbf{E}_j$.

From the eigenvectors, $\mathbf{P}_v$ and $\mathbf{E}_v$ due to $\delta v(\mathbf{r},\omega)$ and $\mathbf{P}_j$ and $\mathbf{E}_j$ due to $\delta j_\alpha(\omega)$, we can assign to each of the absorption peaks of the coupled response functions, the amount of photonic and electronic contribution of the excitation by using

$$\sigma_{el} = \sum_{i=1}^{N_{\text{pairs}}} \mathbf{E}_{v,j}^{(i)} \quad \text{and} \quad \sigma_{pt} = \sum_{\alpha=1}^{M} \mathbf{P}_{v,j}^{(\alpha)}, \tag{297}$$

where N_{pairs} corresponds to the number of occupied-unoccupied pairs of KS orbitals. The sum of the vectors σ_{el} and σ_{pt} is normalized to one as, $\sigma_{el} + \sigma_{pt} = 1$. From this equation we can determine the photonic contribution as $\sigma_{pt} = 1 - \sigma_{el}$ and vice versa.

The generalized pseudo-eigenvalue problem of Eqs. (295) and (296) is the final form of QEDFT matrix equation for obtaining exact excitation frequencies and oscillator strengths. The derivation of the oscillator strengths resulting from the eigenvectors of the pseudo-eigenvalue problem of Eqs. (295) and (296) is presented in App. A.3. Since the Casida equations are formulated in the frequency domain, we present the approximations to the kernels of the electron-photon coupled system of Eq. (244) in the frequency space as

$$\begin{aligned} f_{\text{Hxc}}^n(\mathbf{r},\mathbf{r}',\omega) &= f_{\text{H}}^n(\mathbf{r},\mathbf{r}') + f_{\text{xc}}^n(\mathbf{r},\mathbf{r}',\omega) \\ &\simeq \frac{e^2}{4\pi\epsilon_0}\frac{1}{|\mathbf{r}-\mathbf{r}'|} + f_{\text{xc,ALDA}}^n(\mathbf{r};\mathbf{r}'), \\ f_{\text{Pxc}}^n(\mathbf{r},\mathbf{r}',\omega) &\approx f_{\text{P}}^n(\mathbf{r}) = e^2\sum_\alpha (\boldsymbol{\lambda}_\alpha\cdot\mathbf{r})\,\boldsymbol{\lambda}_\alpha\cdot\mathbf{r}', \\ f_{\text{Pxc}}^{q_\alpha}(\mathbf{r},\omega) &\approx f_{\text{P}}^{q_\alpha}(\mathbf{r}) = -\omega_\alpha\,\boldsymbol{\lambda}_\alpha\cdot e\mathbf{r}, \\ g_{\text{M}}^n(\mathbf{r}) &= -\omega_\alpha^2\,\boldsymbol{\lambda}_\alpha\cdot e\mathbf{r}. \end{aligned} \tag{298}$$

In the limit of no coupling to photons (i.e. $|\boldsymbol{\lambda}_\alpha| = 0$), the pseudo-eigenvalue problem of Eq. (295) simplifies to the Casida equation known in TDDFT [53, 84] given by

$$U\,\mathbf{E}_v = \Omega_q^2\,\mathbf{E}_v, \tag{299}$$

where the explicit form of the matrix elements in the above equation is given as

$$\begin{aligned} U_{qq'} &= \delta_{qq'}\omega_q^2 + 2\sqrt{\omega_q\omega_{q'}}K_{qq'}(\Omega_q), \\ K_{ai,jb}(\Omega_q) &= \iint d^3\mathbf{r}\,d^3\mathbf{r}'\,\varphi_i(\mathbf{r})\varphi_a^*(\mathbf{r})f_{\text{Hxc}}(\mathbf{r},\mathbf{r}',\Omega_q)\varphi_b(\mathbf{r}')\varphi_j^*(\mathbf{r}'). \end{aligned}$$

Here, the matrix $K_{ai,jb}(\Omega_q)$ is shown to depend only on the electronic Hxc kernel f_{Hxc}. Also, in this limit Eq. (296) reduces to a solution of the vacuum Maxwell equation given by Eq. (72) is Chap. 2.3.1.1 as the electronic subsystem does not couple.

3.5.2 THE FREQUENCY-DEPENDENT STERNHEIMER METHOD OF QEDFT

The Sternheimer method [109, 110] is a perturbative approach in the KS orbitals that solves for a specific order of the response and relies only on occupied orbitals. This approach has been used for a long time for static DFT in the context of density functional perturbation theory for calculating phonon spectra [111] and in many other electronic structure methods such as calculation of screening functions, many-body self-energies, among others. Recently, the Sternheimer method has been used to compute the frequency-dependent electronic response of electron-only systems [112–114]. In the framework of TDDFT so far, there have been only a few applications of the Sternheimer approach for calculating dynamic responses of atoms and molecules [83, 115–117]. In Refs. [83, 117], the Sternheimer equation was derived starting from the TDDFT Kohn-Sham equation (i.e. Eq. (135)), however, here we present a derivation solely in the frequency space as in Ref. [53].

While the Casida method computes the response functions by finding the poles and residues (i.e. transitions and oscillator strengths), the Sternheimer method rather computes the first-order response of the density and in the case of the electron-photon coupled system, the photon coordinate. We want to solve for the coupled responses due to a perturbation from the external potential $\delta v(\mathbf{r},\omega)$ and from the external current $\delta j_\alpha(\omega)$.

First, we consider the density response due to an external potential $\delta v(\mathbf{r},\omega)$ while $\delta j_\alpha(\omega) = 0$ which implies solving Eqs. (256) and (258) self-consistently. In order to derive the frequency-dependent Sternheimer equation for electron-photon systems within QEDFT, we follow the derivation of Ref. [53]. By substituting Eq. (264) into Eq. (256), the density response $\delta n_v(\mathbf{r},\omega)$ can be written as

$$\delta n_v(\mathbf{r},\omega) = \sum_{k=1}^{N_e} \left[\varphi_k^*(\mathbf{r}) \varphi_{k,v}^{(+)}(\mathbf{r},\omega) + \varphi_k(\mathbf{r}) \left[\varphi_{k,v}^{(-)}(\mathbf{r},\omega) \right]^* \right], \tag{300}$$

where the first-order responses of the KS states in Eq. (300) are given explicitly by

$$\varphi_{k,v}^{(+)}(\mathbf{r},\omega) = \int d^3\mathbf{r}' \sum_{l=1}^{\infty} \frac{\varphi_l(\mathbf{r})\varphi_l^*(\mathbf{r}')\varphi_k(\mathbf{r}')}{\omega - (\epsilon_l - \epsilon_k) + i\eta} \delta v_{\text{KS},v}(\mathbf{r}',\omega), \tag{301}$$

$$\varphi_{k,v}^{(-)}(\mathbf{r},\omega) = -\int d^3\mathbf{r}' \sum_{l=1}^{\infty} \frac{\varphi_l(\mathbf{r})\varphi_l^*(\mathbf{r}')\varphi_k^*(\mathbf{r}')}{\omega + (\epsilon_l - \epsilon_k) + i\eta} \delta v_{\text{KS},v}(\mathbf{r}',\omega). \tag{302}$$

Obtaining the KS orbital responses $\varphi_{k,v}^{(\pm)}(\mathbf{r},\omega)$ becomes tedious since one needs to first determine infinitely many KS orbitals and evaluate an infinite sum over all occu-

pied and unoccupied KS orbitals. However, this can be circumvented by acting with $\left(\omega - \hat{h} + \epsilon_k + i\eta\right)$ and $\left(\omega + \hat{h} - \epsilon_k + i\eta\right)$ on Eqs. (301) and (302), respectively

$$\left(\omega - \hat{h} + \epsilon_k + i\eta\right) \varphi^{(+)}_{k,v}(\mathbf{r},\omega) = \int d^3\mathbf{r}' \sum_{l=1}^{\infty} \left(\omega - \hat{h} + \epsilon_k + i\eta\right) \times \frac{\varphi_l(\mathbf{r})\varphi^*_l(\mathbf{r}')\varphi_k(\mathbf{r}')}{\omega - (\epsilon_l - \epsilon_k) + i\eta} \delta v_{\mathrm{KS},v}(\mathbf{r}',\omega)\,,$$

$$\left(\omega + \hat{h} - \epsilon_k + i\eta\right) \varphi^{(-)}_{k,v}(\mathbf{r},\omega) = -\int d^3\mathbf{r}' \sum_{l=1}^{\infty} \left(\omega + \hat{h} - \epsilon_k + i\eta\right) \times \frac{\varphi_l(\mathbf{r}')\varphi^*_l(\mathbf{r})\varphi^*_k(\mathbf{r}')}{\omega + (\epsilon_l - \epsilon_k) + i\eta} \delta v_{\mathrm{KS},v}(\mathbf{r}',\omega)\,.$$

Here, we recall that $\hat{h} = \hat{h}([v,n,q_\alpha])$ is the ground-state QEDFT KS Hamiltonian and ϵ_k are the KS eigenvalues resulting from solving the equilibrium electron-photon problem of Eq. (167). Using the static KS equation of Eq. (167) in the above two equations, the right-hand sides now simplifies to the following forms

$$\left(\omega - \hat{h} + \epsilon_k + i\eta\right) \varphi^{(+)}_{k,v}(\mathbf{r},\omega) = \int d^3\mathbf{r}' \sum_{l=1}^{\infty} \varphi_l(\mathbf{r})\varphi^*_l(\mathbf{r}')\varphi_k(\mathbf{r}')\delta v_{\mathrm{KS},v}(\mathbf{r}',\omega)\,, \tag{303}$$

$$\left(\omega + \hat{h} - \epsilon_k + i\eta\right) \varphi^{(-)}_{k,v}(\mathbf{r},\omega) = -\int d^3\mathbf{r}' \sum_{l=1}^{\infty} \varphi_l(\mathbf{r}')\varphi^*_l(\mathbf{r})\varphi^*_k(\mathbf{r}')\delta v_{\mathrm{KS},v}(\mathbf{r}',\omega)\,. \tag{304}$$

Taking advantage of the completeness of the infinite set of ground-state KS states, i.e., $\sum_{l=1}^{\infty} \varphi_l(\mathbf{r})\varphi^*_l(\mathbf{r}') = \delta(\mathbf{r}-\mathbf{r}')$ in Eqs. (303) and (304), we arrive and the frequency-dependent Sternheimer equation given by

$$\left(\omega - \hat{h} + \epsilon_k + i\eta\right) \varphi^{(+)}_{k,v}(\mathbf{r},\omega) = \delta v_{\mathrm{KS},v}(\mathbf{r},\omega)\varphi_k(\mathbf{r})\,, \tag{305}$$

$$\left(\omega + \hat{h} - \epsilon_k + i\eta\right) \varphi^{(-)}_{k,v}(\mathbf{r},\omega) = -\delta v_{\mathrm{KS},v}(\mathbf{r},\omega)\varphi^*_k(\mathbf{r})\,, \tag{306}$$

where the KS potential $\delta v_{\mathrm{KS},v}(\mathbf{r},\omega)$ is given in Eq. (260). For the response of the photon coordinate to the external potential $\delta v(\mathbf{r},\omega)$, by substituting Eq. (266) into Eq. (258) we obtain

$$\delta q_{\alpha,v}(\omega) = \delta q^{(+)}_{\alpha,v}(\omega) + \delta q^{(-)}_{\alpha,v}(\omega)\,, \tag{307}$$

where the first-order responses of $\delta q^{(+)}_{\alpha,v}(\omega)$ and $\delta q^{(-)}_{\alpha,v}(\omega)$ are given by

$$\delta q^{(+)}_{\alpha,v}(\omega) = \frac{1}{2\omega_\alpha^2}\left(\frac{1}{\omega - \omega_\alpha + i\eta'}\right) \int d^3\mathbf{r}' g^{n_\alpha}_M(\mathbf{r}')\delta n_v(\mathbf{r}',\omega)\,, \tag{308}$$

$$\delta q^{(-)}_{\alpha,v}(\omega) = -\frac{1}{2\omega_\alpha^2}\left(\frac{1}{\omega + \omega_\alpha + i\eta'}\right) \int d^3\mathbf{r}' g^{n_\alpha}_M(\mathbf{r}')\delta n_v(\mathbf{r}',\omega)\,. \tag{309}$$

Here, determining the photon coordinate $\delta q_{\alpha,v}(\omega)$ entails solving the analytic expressions of $\delta q^{(\pm)}_{\alpha,v}(\omega)$ given in Eqs. (308) and (309). Eqs. (305)-(306) together with Eq. (260) and Eqs. (308)-(309) are the frequency-dependent Sternheimer equations for coupled matter-photon systems that have to be solved self-consistently to obtain the responses $\delta n_v(\mathbf{r},\omega)$ and $\delta q_{\alpha,v}(\omega)$ of Eqs. (300) and (307). The Sternheimer equations (305)-(306)

appear to be a system of linear equations but indeed are nonlinear since the right-hand side depends on the solution through $\delta v_{\mathrm{KS},v}(\mathbf{r},\omega)$ which depends on $\delta n_v(\mathbf{r},\omega)$ and $\delta q_{\alpha,v}(\omega)$ and eventually on the first-order perturbed orbitals $\varphi_{k,v}^{(\pm)}(\mathbf{r},\omega)$.

Next, we obtain the frequency-dependent Sternheimer equations that determine the responses $\delta n_j(\mathbf{r},\omega)$ and $\delta q_{\alpha,j}(\omega)$ of Eqs. (257) and (259), respectively. This corresponds to the case when the system is perturbed by an external charge current $\delta j_\alpha(\omega)$ while $\delta v(\mathbf{r},\omega) = 0$. Through similar steps as for $\delta n_v(\mathbf{r},\omega)$, the density response $\delta n_j(\mathbf{r},\omega)$ can be written as

$$\delta n_j(\mathbf{r},\omega) = \sum_{k=1}^{N_e} \left[\varphi_k^*(\mathbf{r}) \varphi_{k,j}^{(+)}(\mathbf{r},\omega) + \varphi_k(\mathbf{r}) \left[\varphi_{k,j}^{(-)}(\mathbf{r},\omega) \right]^* \right], \tag{310}$$

where the first-order responses of the KS states are given by

$$\varphi_{k,j}^{(+)}(\mathbf{r},\omega) = \int d^3\mathbf{r}' \sum_{l=1}^{\infty} \frac{\varphi_l(\mathbf{r})\varphi_l^*(\mathbf{r}')\varphi_k(\mathbf{r}')}{\omega - (\epsilon_l - \epsilon_k) + i\eta} \delta v_{\mathrm{KS},j}(\mathbf{r}',\omega),$$
$$\varphi_{k,j}^{(-)}(\mathbf{r},\omega) = -\int d^3\mathbf{r}' \sum_{l=1}^{\infty} \frac{\varphi_l(\mathbf{r})\varphi_l^*(\mathbf{r}')\varphi_k^*(\mathbf{r}')}{\omega + (\epsilon_l - \epsilon_k) + i\eta} \delta v_{\mathrm{KS},j}(\mathbf{r}',\omega).$$

Following similar steps as for the case were the external perturbation comes from the classical potential, the first-order KS orbital responses can be cast into a frequency-dependent Sternheimer equation of the form

$$\left(\omega - \hat{h} + \epsilon_k + i\eta\right) \varphi_{k,j}^{(+)}(\mathbf{r},\omega) = \delta v_{\mathrm{KS},j}(\mathbf{r},\omega)\varphi_k(\mathbf{r}), \tag{311}$$
$$\left(\omega + \hat{h} - \epsilon_k + i\eta\right) \varphi_{k,j}^{(-)}(\mathbf{r},\omega) = -\delta v_{\mathrm{KS},j}(\mathbf{r},\omega)\varphi_k^*(\mathbf{r}). \tag{312}$$

Here, the KS potential $\delta v_{\mathrm{KS},j}(\mathbf{r},\omega)$ is given in Eq. (261). The response of the photon coordinate to the external charge current $\delta j_\alpha(\omega)$ can be written in a similar form as Eq. (307) by substituting Eq. (266) into Eq. (259) to obtain

$$\delta q_{\alpha,j}(\omega) = \delta q_{\alpha,j}^{(+)}(\omega) + \delta q_{\alpha,j}^{(-)}(\omega), \tag{313}$$

where the first-order response of $\delta q_{\alpha,j}^{(\pm)}(\omega)$ is given explicitly by

$$\delta q_{\alpha,j}^{(+)}(\omega) = \frac{1}{2\omega_\alpha^2} \left(\frac{1}{\omega - \omega_\alpha + i\eta'} \right) \left[\delta j_\alpha(\omega) + \int d^3\mathbf{r}' g_M^{n_\alpha}(\mathbf{r}') \delta n_j(\mathbf{r}',\omega) \right], \tag{314}$$
$$\delta q_{\alpha,j}^{(-)}(\omega) = -\frac{1}{2\omega_\alpha^2} \left(\frac{1}{\omega - \omega_\alpha + i\eta'} \right) \left[\delta j_\alpha(\omega) + \int d^3\mathbf{r}' g_M^{n_\alpha}(\mathbf{r}') \delta n_j(\mathbf{r}',\omega) \right]. \tag{315}$$

In order to obtain the responses $\delta n_j(\mathbf{r},\omega)$ and $\delta q_{\alpha,j}(\omega)$ of Eqs. (310) and (313), the frequency-dependent Sternheimer equations of Eqs. (311) and (312) together with Eq. (261) and Eqs. (313)-(315) have to be solved self-consistently. The first-order KS orbitals in response to perturbations from either the external potential $v(\mathbf{r},\omega)$ or external current $j_\alpha(\omega)$ must satisfy the orthogonality condition with the ground-state KS orbitals:

$$\int d^3\mathbf{r}\ \varphi_k^*(\mathbf{r})\varphi_{k,v}^{(\pm)}(\mathbf{r},\omega) = 0, \qquad \int d^3\mathbf{r}\ \varphi_k^*(\mathbf{r})\varphi_{k,j}^{(\pm)}(\mathbf{r},\omega) = 0.$$

A similar derivation of the frequency-dependent Sternheimer equation for coupled electron-photon system that includes a projector to the subspace of the unoccupied states manifold is given in App. A.2. The projector ensures that the components of the perturbed KS orbitals $\varphi^{(\pm)}_{k,v}(\mathbf{r},\omega)$ are zero in the subspace of the occupied ground state orbitals $\varphi_k(\mathbf{r})$. In the linear response regime, these components have been shown to not contribute to the first-order perturbed density, therefore, the projector can be ignored [83].

In the decoupling limit of light and matter when $|\boldsymbol{\lambda}_\alpha| = 0$, the Sternheimer equations (305) and (306) obtained by perturbing the system with $\delta v(\mathbf{r},\omega)$ have the same form, however, the potential $\delta v_{\mathrm{KS},v}(\mathbf{r}',\omega)$ now has the form of Eq. (151), i.e. $f^{q_\alpha}_{\mathrm{Mxc}} = 0$. Also, the potential v_{Mxc} in the KS Hamiltonian $\hat{h}$ of Eq. (167) becomes $v_{\mathrm{Mxc}} \to v_{\mathrm{Hxc}}$ and we recover the TDDFT electron-only frequency-dependent Sternheimer equations [83, 117]. Equally in this limiting case were the perturbation comes from an external current $\delta j_\alpha(\omega)$, the Sternheimer equations (311) and (312) vanish since we have no access to the unperturbed and perturbed KS orbitals. However, only the response of the photon coordinate of Eq. (313) can be computed which is a solution of the Maxwell equation in vacuum (see Eq. (179) of Chap. 2.3.1.1) since $g^{n_\alpha}_M = 0$ in the responses $\delta q^{(\pm)}_{\alpha,j}(\omega)$ of Eqs. (314) and (315).

3.5.3 THE TIME-PROPAGATION METHOD OF QEDFT

The derivation of this method is the construction of the Maxwell-KS system of QEDFT discussed in Chap. 2.5.5.1. Therefore, we no not derive it here again but rather explain how this method can be used to solve the linear response equations. This method simply propagates a system under a given external perturbing field. In this approach, the time-dependent nonlinear coupled Maxwell-KS equations of Eqs. (177) and (178) are propagated in real-time. In the following, we present the case in which the external current is switched off (i.e. $\delta j_\alpha(t) = 0$) and the external classical perturbation is non-zero $\delta v(\mathbf{r},t) \neq 0$. The KS orbitals of Eqs. (177) are then propagated as [82, 118, 119]:

$$\varphi_i(\mathbf{r},t+\Delta t) = \exp\left(-\frac{i}{\hbar}\int_t^{t+\Delta t} d\tau \left(\frac{\hat{\mathbf{p}}^2}{2m} + v_{\mathrm{KS}}([v,n,q_\alpha];\mathbf{r},t)\right)\right)\varphi_i(\mathbf{r},t),$$

along with analytic expression for the photon coordinate of Eq. (179) given here as

$$q_{\alpha,v}(t) = q_\alpha(t_0)\cos(\omega_\alpha t) + \frac{\dot{q}_\alpha(t_0)}{\omega_\alpha}\sin(\omega_\alpha t) - \frac{1}{\omega_\alpha^2}\int_{t_0}^{t} dt' \sin(\omega_\alpha(t-t'))j_{\alpha,\mathrm{KS},v}(t')\,. \tag{316}$$

The KS current $j_{\alpha,\mathrm{KS},v}(t)$ has a similar form to the linear response form of Eq. (241) given by $j_{\alpha,\mathrm{KS},v}(t) = -\omega_\alpha^2\boldsymbol{\lambda}_\alpha\cdot\int d^3\mathbf{r}\ \mathbf{r}\ n(\mathbf{r},t)$. From Eq. (316), the choice of the initial conditions for $q_\alpha(t_0)$ and $\dot{q}_\alpha(t_0)$ is determined from ground-state QEDFT presented in Chap. 2.5.4. The analytic formula of Eq. (316) combined with numerical integration of the last term reduces the numerical cost at each time step as opposed to solving Eq. (178) at every time step [47]. Since the time-propagation method is non-perturbative, all orders of responses are present in the computation, therefore, specific orders have to be numerically extracted. In order to propagate the coupled system

in the linear response regime, we follow the scheme proposed in Refs. [82, 118, 119], and excite all frequencies of the system by giving some small momentum k to the electrons. This is achieved by transforming the ground-state orbitals according to: $\varphi_i(\mathbf{r}, \delta t) = e^{ik\mathbf{r}}\varphi_i(\mathbf{r}, 0)$ and then propagating these KS orbitals for some (finite) time from which desired observables (dipole and photon coordinate response) can be computed.

With the three methods given above, we can now compute linear response properties of strongly coupled light-matter systems from first principles which allows us to complement experimental observations as well as predict new physical effects. We have implemented the above three linear response methods in the real-space code OCTOPUS [83, 120, 121] (see App. D.2 for details).

3.5.4 COMPARISON OF THE DIFFERENT LINEAR RESPONSE METHODS OF QEDFT

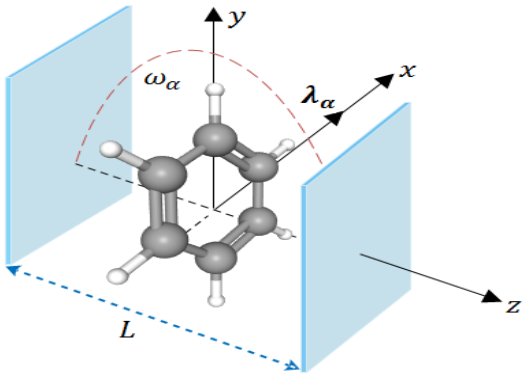

Figure 3: Schematic of a single Benzene (C_6H_6) molecule confined in a high-Q optical cavity. The polarization together with the coupling λ_α is along the x-direction. The photon frequency is ω_α and L represents the distance (length) between the cavity mirrors.

In the previous section, we extended three linear response methods of TDDFT to the framework of QEDFT. These methods are capable of determining excited-state properties of coupled matter-photon systems from first-principles. In this section, we compare these numerical methods we implemented as a validation of our linear response formulation of coupled electron-photon systems. Such a comparison is important because it serves as a consistency check not only for our rather involved analytic derivations but also for the non-trivial numerical implementations of the different methods in the simulation software Octopus. If all the different methods with their different derivations and implementations agree, we can rest be assured that we have a working theory that is applicable to many new and interesting situations. We do this comparison for the case of a single benzene ring described below.

For the molecular system, we are interested in situations in which a cavity or plasmonic nanostructures can be used to enhance the coupling of a photon mode to a single benzene (C_6H_6) ring as depicted in Fig. (3). The coupling λ_α can be increased by reducing for example the cavity volume via the cavity length L. TDDFT calculations in the linear-response regime have been very successful in studying the absorption spectrum of the benzene molecule [82, 120]. Small organic molecules and even large polycyclic aromatic hydrocarbons are rewarding systems to be studied

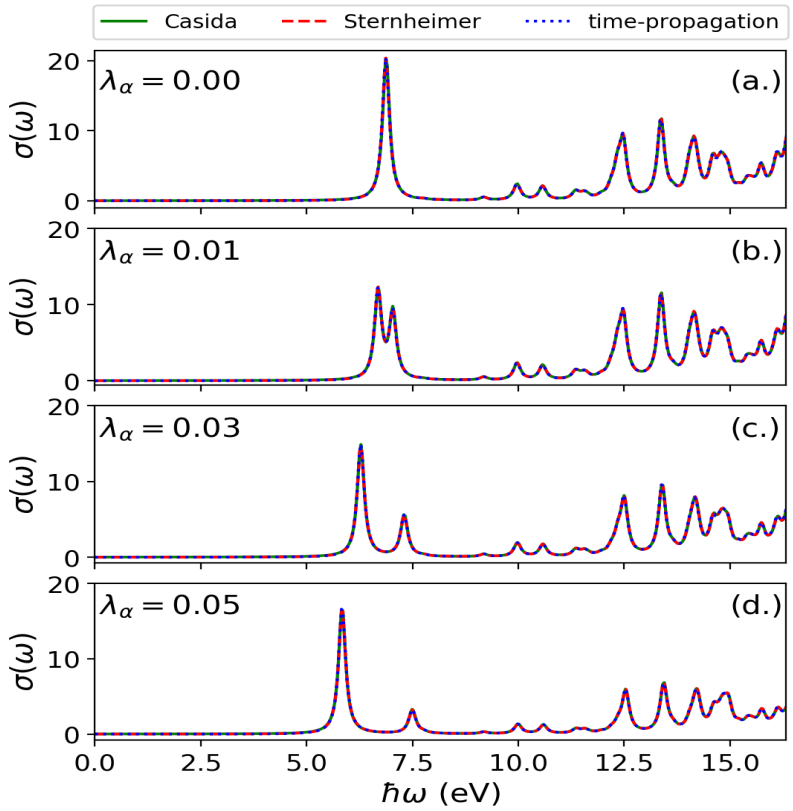

Figure 4: Comparison of electron-photon linear-response methods of QEDFT. Panel (a.) shows the free space case where the $\Pi - \Pi^*$ transition occurs around 7 eV. Panels (b.)-(d.) shows the spectrum of the benzene molecule inside the cavity from the weak to strong coupling regime when the cavity mode is resonant to the $\Pi - \Pi^*$ transition. For increasing coupling strength, a Rabi splitting of the Π-Π^* peak into two polaritonic branches is captured. All the three response methods are shown to agree for increasing coupling strengths $\lambda_\alpha = 0.00, 0.01, 0.03, 0.05$.

with TDDFT [122], since the adiabatic approximation in concert with the LDA [64, 67] captures the occurring Π-Π^* transition exceptionally well. This transition is a characteristic of carbon conjugate compounds [120] which occurs around 7 eV in the case of a benzene molecule.

To compare the above linear-response methods (Casida, Sternheimer and time-propagation), we here compute the photo-absorption cross-section given by

$$\bar{\sigma}(\omega) = \frac{4\pi\omega}{c}\mathrm{Im}\,\bar{\alpha}(\omega)\,, \quad \text{where} \quad \bar{\alpha}(\omega) = \frac{1}{3}\mathrm{Tr}\,\bar{\alpha}_{\mu\mu}(\omega)\,. \tag{317}$$

The photo-absorption cross-section is related to the dipole *strength function* $\mathrm{S}(\omega)$ [118] as

$$\mathrm{S}(\omega) = \frac{m_e c}{2\pi^2 e^2 \hbar^2}\bar{\sigma}(\omega). \tag{318}$$

To obtain the photo-absorption cross-section of the benzene molecule, we first calculate the electronic structure as described in App. B.1.1. Next, we include a single cavity mode in resonance to the Π-Π^* transition of the benzene molecule [82, 120], i.e., $\hbar\omega_\alpha = 6.88$ eV. For the light-matter coupling strength $\lambda_\alpha = |\boldsymbol{\lambda}_\alpha|$, we choose four

different values, i.e. $\lambda_\alpha = (0, 0.01, 0.03, 0.05)$ that correspond to a transition from the weak to the strong-coupling regime and the cavity mode is assumed to be polarized along the x-direction. To employ linear response methods, we use the approximations in Eq. (244) for the Casida and Sternheimer methods and the approximations in Eq. (184) for the time-propagation method. The results of Eq. (244) and (184) are the same since Eq. (184) is the Fourier transform of Eq. (244). For the comparison of the different methods, we use the same real-space basis set and identical calculation parameters as discussed above and in App. B.1.1.

In Fig. (4), we show the photo-absorption cross-section for the four different values of λ_α given above. The case $\lambda_\alpha = 0$ corresponds to the absorption spectra in free space. That is, the spectrum one will obtain in the TDDFT framework by solving, for example, the electron-only Casida equation given in Eq. (299). Here, we capture the Π-Π^* peak at 6.88 eV with the ALDA [120]. Since the photon field is treated classically and only acts as an external perturbation, the excited state properties are not modified. However, by including the photon field in our non-relativistic QED setting, we now have the possibility to change the excited state properties by enhancing the coupling of the molecule to the photon mode. Thus, by tuning the electron-photon coupling strength λ_α as in Fig. (4.b,c,d.) we find for increasing coupling strength a Rabi splitting of the Π-Π^* peak into lower and upper polaritonic branches. The Rabi splitting Ω_R is the difference in energy between the lower and upper polariton peaks and is used to quantify the strength of the electron photon coupling. Values of up to $\Omega_R/\omega_\alpha \simeq 0.25$ have been measured in molecular experiments [123, 124]. The lower polaritonic branch in Fig. (4) has a higher intensity, compared to the upper polaritonic peak. In Sec. 3.6.1, we will scrutinize the pRPA by comparing its results to different approximations in a model system.

From the comparison of the methods, we observe that the three approaches are numerically equivalent as one would expect. This shows that the electron-photon Casida, frequency-dependent Sternheimer and time-propagation methods are valid alternatives for studying excited state properties of matter-photon systems from the weak- to the strong-coupling regime. Using either of these methods will be physically motivated and will also depend on the numerical complexity of the system to be studied. Thus predictive theoretical first-principle calculations for excited states properties of real systems (e.g. atoms, molecules) strongly coupled to the quantized electromagnetic field are now available. This now sets the stage for unprecedented insights into coupled light-matter systems, since we have access to many observables that are not (or not well [27]) captured by quantum-optical models. It is important to note here that the broadening of the peaks in Fig. (4) is only done artificially with the parameter $\hbar\eta = 0.1$ eV since the photon bath is not included in the calculation. However, as we will show in Sec. 3.6.3 that sampling the photon bath, we obtain the Lorentzian broadening and thus the finite lifetime in a direct manner. In the following sections, we show what we can now obtain and what new possibilities become in reach of ab-initio methods.

3.6 DRESSED LINEAR SPECTROSCOPY IN ELECTRON-PHOTON SYSTEMS

In the previous section, we presented practical calculations for a molecular system strongly coupled to photons using three different linear-response methods of QEDFT

that were shown numerically to obtain the same results. While validating the linear-response methods, we showed the emergence of polaritonic peaks which are apparent modifications of the absorption spectrum when a photon mode is strongly coupled to the matter subsystem. In this section, we further explore strong light-matter coupling and also show novel observables that are now accessible in ab-initio theory as well as show new perspectives that can be accessed using our response formalism. First, we will present a simple model system and show the new effects that arises and novel observables that become accessible due to treating both light and matter on a quantized footing. Next, we will show how to compute lifetimes non-perturbatively by sampling the photon bath with thousands of photon modes. This method will be further explored to show how one can determine not only lifetimes of electronic excited states but also lifetimes of polaritonic states. We will further investigate situations where perturbative free-space methods become less accurate when we have more than a single molecule and show how our ab-initio theory performs in these situations. Finally, we show how strong coupling of a continuum of modes can change lineshapes.

3.6.1 AN ILLUSTRATIVE EXAMPLE WITH A MODEL SYSTEM

In this section, we will first verify that the pRPA can describe the couped system accurately for different coupling regimes. To do this, we consider a simple and illustrative model system known as the extended Rabi model. We compute the absorption spectra using the pRPA and compare to that of the rotating-wave approximation (RWA) and the numerically exact case. Next, using this simple model we highlight new possibilities that can be investigated. We do this by *defining* novel linear spectroscopic observables that are connected to the novel response functions $\chi_q^{\sigma_x}$, $\chi_{\sigma_x}^q$ and χ_q^q and give their physical interpretations. Before showing these results, we first present the model system and approximations applied to the model.

3.6.1.1 *The extended Rabi model*

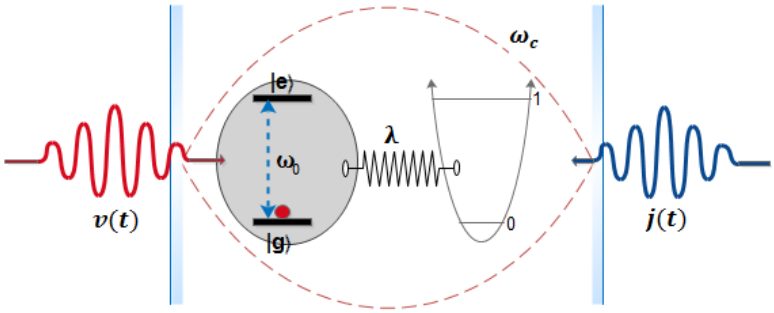

Figure 5: Two-level system coupled to one mode of the electromagnetic field. The electron subsystem is driven by an external classical field $v(t)$ and the field of the photon mode is driven by an external classical current $j(t)$.

The Rabi model is the simplest model that describes the interaction between a two-level atom and a single mode of a quantized electromagnetic field. It was introduced over 80 years ago [98] and has applications in different fields ranging from quantum optics [49] to cavity and circuit QED [101, 125] and even molecular physics [126]. The Rabi Hamiltonian and its simplifications (see below) have been applied for phenomena such as Rabi oscillations, oscillation collapses and revivals, coherences, entanglement, and the dynamics of dissipative systems [100]. The model features two electronic energy levels of an atom (or molecule) coupled to a single quantized mode of the electromagnetic field. The Hamiltonian for the extended Rabi model is given by (atomic units are used for this model)

$$\hat{H}_R(t) = \underbrace{\frac{\omega_0}{2}\hat{\sigma}_z + \omega_c \hat{a}^\dagger \hat{a} + \lambda \hat{\sigma}_x \hat{q}}_{\hat{H}_R} + j(t)\hat{q} + v(t)\hat{\sigma}_x\,, \tag{319}$$

where ω_0 is the transition frequency between the ground state $|g\rangle$ and excited state $|e\rangle$, $\hat{\sigma}_x$ as well as $\hat{\sigma}_z$ are the usual Pauli matrices and the frequency of the mode considered is ω_c. The coupling between matter and light is described by a coupling strength λ and the displacement coordinate $\hat{q} = \frac{1}{\sqrt{2\omega_c}}\left(\hat{a} + \hat{a}^\dagger\right)$. Finally, the matter subsystem is coupled to a classical external perturbation $v(t)$ and the photon system to a classical external current $j(t)$. A pictorial representation of the coupled system is given in Fig. (5). Equation (319) is called the extended Rabi model due to the additional time-dependent classical potential and current that couples to the respective electronic and photonic subsystems. Despite the simplicity of the model, an analytic solution for the spectrum of the time-independent Rabi model Hamiltonian $\hat{H}_R$ was not known until derived in Ref. [99]. We note here for consistency with respect to other works [12, 22, 127] that employed the above Rabi model, a unitary transformation can be performed $\hat{H}_R^{(\text{site})}(t) = \hat{U}^\dagger \hat{H}_R(t)\hat{U}$ that in principle swaps $\hat{\sigma}_x \leftrightarrow \hat{\sigma}_z$ which yields the site basis representation of the problem where the unitary operator has the form $\hat{U} = \frac{1}{\sqrt{2}}(\hat{\sigma}_x + \hat{\sigma}_z)$. A further point to note is that with respect to the full non-relativistic QED problem in the long wavelength approximation of Eq. (170) the Rabi model does not include the dipole self-energy term proportional to $(\boldsymbol{\lambda}_\alpha \cdot \mathbf{R})^2$. This is because the analogous term in this model is just a constant energy shift, i.e., it is proportional to $\hat{\sigma}_x^2 = \hat{\mathbb{1}}$ [44]. Since the dipole-self energy term is ignored in this model, we note that the kernel related to the dipole-self energy is $f^n_{\text{Pxc}} = 0$, when we employ the linear-response QEDFT framework.

By performing the RWA [36, 100], the electron-photon interaction term of the Rabi Hamiltonian of Eq. (319) simplifies to $\hat{\sigma}_x(\hat{a} + \hat{a}^\dagger) \to \hat{\sigma}_+\hat{a} + \hat{\sigma}_-\hat{a}^\dagger$, where $\hat{\sigma}_x = \hat{\sigma}_+ + \hat{\sigma}_-$ and $\hat{\sigma}_\pm = (\hat{\sigma}_x \pm i\hat{\sigma}_y)/2$. The resulting form is known as the Jaynes-Cummings model [36, 100] and the Hamiltonian is given as

$$\hat{H}_{\text{JC}}(t) = \underbrace{\frac{\omega_0}{2}\hat{\sigma}_z + \omega_c \hat{a}^\dagger \hat{a} + \frac{\lambda}{\sqrt{2\omega_c}}\left(\hat{\sigma}_+\hat{a} + \hat{\sigma}_-\hat{a}^\dagger\right)}_{\hat{H}_{\text{JC}}} + j(t)\hat{q} + v(t)\hat{\sigma}_x\,. \tag{320}$$

The ground-state of the system is a factorizable tensor product of the ground-state of the two-level system and the vacuum state of the photon number state, i.e., $|g\rangle|0\rangle$.

The spectrum of the time-independent Jaynes-Cummings Hamiltonian $\hat{H}_{\mathrm{JC}}$ is known analytically and the energies are [128]

$$E_{\pm}(n) = \frac{1}{2}\left(\omega_c + \omega_0 \pm \Omega_n\right), \tag{321}$$

where $\Omega_n = \sqrt{\delta^2 + 4\lambda'^2(n+1)}$ with $\delta = \omega_0 - \omega_c$ being the detuning from resonance, n is the number of photons in the mode and $\lambda' = \frac{\lambda}{\sqrt{2\omega_c}}$. The corresponding energy eigenvectors also known as dressed states or polariton states are expressed analytically as

$$\begin{aligned} |-,n\rangle &= -\sin\theta_n|g\rangle|n+1\rangle + \cos\theta_n|e\rangle|n\rangle\,, \\ |+,n\rangle &= \cos\theta_n|g\rangle|n+1\rangle + \sin\theta_n|e\rangle|n\rangle\,. \end{aligned} \tag{322}$$

Here, $\sin\theta_n$ and $\cos\theta_n$ are the amplitudes [128].

Next, another simplification of the Rabi Hamiltonian (319) is the mean-field approximation [12, 22] or photon random-phase approximation (pRPA) which approximate the bilinear electron-photon term to $\hat{\sigma}_x\hat{q} = \langle\hat{\sigma}_x\rangle\hat{q} + \hat{\sigma}_x\langle\hat{q}\rangle - \langle\hat{\sigma}_x\rangle\langle\hat{q}\rangle$. This approximation stems from the decoupling of the correlated electron-photon wavefunction into a factorizable product between wavefunctions of the individual subsystems [8], i.e. $|\Psi\rangle = |\psi\rangle \otimes |\phi\rangle$. Making a direct substitution of the approximation into Eq. (319) results to the mean-field approximation of the Rabi model. An equivalent form is to cast the resulting mean-field Hamiltonian into a form of two coupled equations (as in Chap. 2.3.1) given by

$$\begin{aligned} i\frac{\partial}{\partial t}|\psi(t)\rangle &= \left[\frac{\omega_0}{2}\hat{\sigma}_z + \left(v(t) + \lambda q(t)\right)\hat{\sigma}_x\right]|\psi(t)\rangle, \\ \left(\frac{\partial^2}{\partial t^2} + \omega_c^2\right) q(t) &= -j(t) - \lambda\sigma_x(t), \end{aligned} \tag{323}$$

where $q(t) = \langle\phi(t)|\hat{q}|\phi(t)\rangle$ and $\sigma_x(t) = \langle\psi(t)|\hat{\sigma}_x|\psi(t)\rangle$ and the constant energy shift resulting from the term $\langle\hat{\sigma}_x\rangle\langle\hat{q}\rangle$ was dropped. The mode-resolved inhomogeneous Maxwell equation of Eq. (323) can be solved as in Chap. 2.3.1.1. The pRPA differs from RWA in that it includes the fast frequency terms while the RWA excludes these terms.

In the following section, we will employ the pRPA to compute different spectra of the Rabi model and see how it compares to that of the RWA and the exact results (i.e. obtained by numerical diagonalization of $\hat{H}_R$). Within the framework of QEDFT for the model system, the electron density is here the Pauli matrix $\hat{\sigma}_x$ which represents the dipole of the electronic subsystem and the photon coordinate remains the same. Using the Casida equation (295) of QEDFT with the pRPA, the components of the matrix equation simplify to $K = f^{\sigma_x}_{\mathrm{Mxc}} = 0$, $M = f^{q}_{\mathrm{P}} = \lambda$ and $N = \frac{1}{2\omega_c}g^{\sigma_x}_{\mathrm{M}} = \frac{\lambda}{2\omega_c}$. Consequently we have $U = \omega_0^2$, $V = W = 2\lambda\sqrt{\omega_0/2}$, $\omega_\alpha^2 = \omega_c^2$. The resulting eigenvalue equation yields the excitation frequencies

$$\Omega^2(\pm) = \frac{1}{2}\left(\omega_0^2 + \omega_c^2\right) \pm \frac{1}{2}\sqrt{\left(\omega_0^2 - \omega_c^2\right)^2 + 8\lambda^2\omega_0}\,, \tag{324}$$

and the corresponding normalized eigenvectors can be given in closed form as

$$\mathbf{E}_v = \begin{pmatrix} -\sin\theta \\ \cos\theta \end{pmatrix}, \quad \text{and} \quad \mathbf{P}_v = \begin{pmatrix} \cos\theta \\ \sin\theta \end{pmatrix}.$$

To compare these two approximations (i.e. pRPA and RWA) to the exact case, we compute the photo-absorption cross-section for the model system. Using Eq. (317), we can determine the photo-absorption cross-section of the Rabi model

$$\sigma(\omega) = \frac{4\pi\omega}{c}\,\mathrm{Im}\,\chi^{\sigma_x}_{\sigma_x}(\omega), \quad \text{with} \quad \chi^{\sigma_x}_{\sigma_x}(\omega) = \lim_{\eta\to 0^+}\sum_{k=0}\left[\frac{|\langle\Psi_0|\hat{\sigma}_x|\Psi_k\rangle|^2}{\omega-\Omega_k+i\eta} - \frac{|\langle\Psi_0|\hat{\sigma}_x|\Psi_k\rangle|^2}{\omega+\Omega_k+i\eta}\right]. \tag{325}$$

Here, $\alpha(\omega) = \chi^{\sigma_x}_{\sigma_x}(\omega)$ and the mean of the polarizability was not considered since the Rabi model is a one-dimensional system. The Lehmann representation of the response $\chi^{\sigma_x}_{\sigma_x}(\omega)$ in Eq. (325) was deduced from Eq. (217). Since we include the quantized field in our light-matter description, we therefore have access to photonic observables. Analogous to the polarizability, we define a linear "field polarizability" $\beta(\omega)$ due to polarizing the photon mode by an external current. This quantity is given as

$$\tilde{\sigma}(\omega) := \frac{4\pi\omega}{c}\,\mathrm{Im}\,\chi^{q}_{q}(\omega), \quad \text{with} \quad \chi^{q}_{q}(\omega) = \lim_{\eta\to 0^+}\sum_{k=0}\left[\frac{|\langle\Psi_0|\hat{q}|\Psi_k\rangle|^2}{\omega-\Omega_k+i\eta} - \frac{|\langle\Psi_0|\hat{q}|\Psi_k\rangle|^2}{\omega+\Omega_k+i\eta}\right], \tag{326}$$

where $\chi^{q}_{q}(\omega)$ in Eq. (326) was deduced from Eq. (220). Finally, we consider mixed spectroscopic observables where we perturb one subsystem and then consider the response in the other. The versatility of our light-matter descriptions allows us to determine "mixed polarizability" spectra. We define the *mixed polarizability* to be given as

$$\tilde{\sigma}_{\mathrm{mix}}(\omega) := \frac{4\pi\omega}{c}\,\mathrm{Im}\,\chi^{\sigma_x}_{q}(\omega), \quad \text{where} \quad \chi^{q}_{\sigma_x}(\omega) = \chi^{\sigma_x}_{q}(\omega)\,. \tag{327}$$

The response functions in the above equation was deduced from Eqs. (218) and (219) and are given explicitly by

$$\chi^{q}_{\sigma_x}(\omega) = \chi^{\sigma_x}_{q}(\omega) = \lim_{\eta\to 0^+}\sum_{k=0}\left[\frac{\langle\Psi_0|\hat{\sigma}_x|\Psi_k\rangle\langle\Psi_k|\hat{q}|\Psi_0\rangle}{\omega-\Omega_k+i\eta} - \frac{\langle\Psi_0|\hat{q}|\Psi_k\rangle\langle\Psi_k|\hat{\sigma}_x|\Psi_k\rangle}{\omega+\Omega_k+i\eta}\right].$$

We note that the equality of the response functions $\chi^{q}_{\sigma_x}(\omega) = \chi^{\sigma_x}_{q}(\omega)$ is not necessarily true in the general case given in Eqs. (218) and (219).

3.6.1.2 *Modified and novel linear spectroscopy in a model system*

We now make a comparison between the spectra given by Eqs. (325)-(327) of the *numerical exact* Rabi model and the two approximations: pRPA and RWA discussed in Sec. 3.6.1.1. Since the spectrum of the RWA is given analytically, we can compute Eqs. (325)-(327) directly. In Fig. (6.a-c.), we show a comparison of the spectra resulting from the pRPA (dashed-blue), the RWA (full-orange) and the numerical exact (dotted-red) cases. In this figure the photon frequency resonantly couples to the two-level system (i.e. $\delta = \omega_0 - \omega_c = 0$, where $\omega_0 = \omega_c = 1$) and the spectrum changes for an increasing electron-photon coupling strength λ. For the coupling $\lambda = 0.07$, the splitting of the electronic excited state into an upper and lower polariton becomes

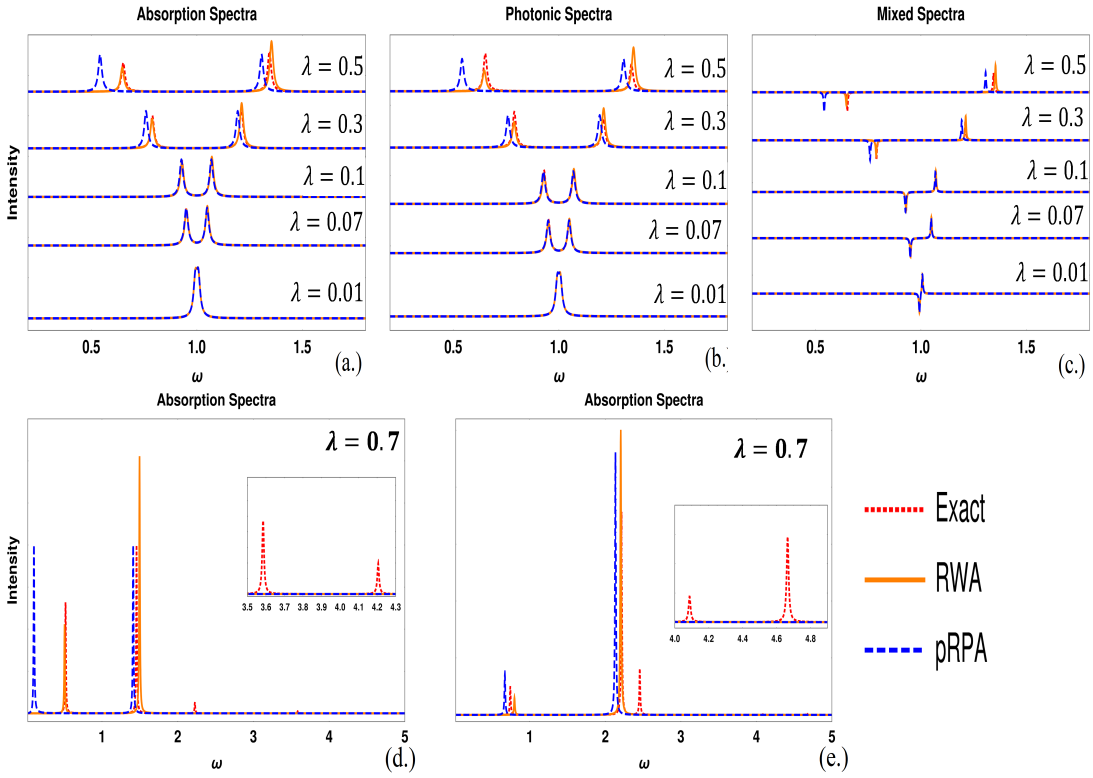

Figure 6: Linear response spectra for the extended Rabi model (dotted-red) compared to the pRPA (dashed-blue) and RWA (full-orange) approximations and for different coupling strengths λ. (a.) Photo-absorption cross-section due to dipole-dipole response, (b.) spectra due to photon-photon response, (c.) spectra due to dipole-photon or photon-dipole response. (d.) The case for $\lambda = 0.7$ shows all excitations that arise in strong coupling. (a.) through (d.) describes resonant coupling. In (e.) the field is half-way detuned from atomic resonance, i.e., $\omega_0 = 2$ and $\omega_c = 1$ with strength and energies shifted to frequencies favoring 2-photon processes. The insets in (d.) and (e.) zoom into the frequency axis showing many-photon process.

apparent. We observe that up to $\lambda = 0.1$ the different spectra for the exact, the pRPA as well as the RWA are in close agreement before they start to differ. This signifies that the mean-field treatment is sufficient to capture the quantized electron-photon response properties and thus, is a reasonable approximation for linear response spectra even for relatively strong coupling situations. When the coupling strength is increased further going into the ultra-strong coupling regime, the discrepancies becomes large. We observe for ultra-strong coupling (i.e., for $\lambda \geq 0.3$) the approximations do not only disagree in transition frequencies (pole positions) but also the weights of the transitions become increasingly different.

In addition, we investigate how the pRPA of our QEDFT linear response compare to the RWA and the exact case for multi-photon processes. We show this specifically for the photo-absorption spectrum of Eq. (325) in the ultra-strong coupling regime, i.e., $\lambda = 0.7$. First, we show in Fig. (6.d.) still for the resonant coupling that three new peaks arise for the exact case which accounts for high-lying excited states with non-vanishing dipole moments in the ultra-strong coupling regime. These new absorption peaks (also shown in the inset) in the exact case are not captured with the RWA and pRPA since processes beyond one-photon are involved. With these results

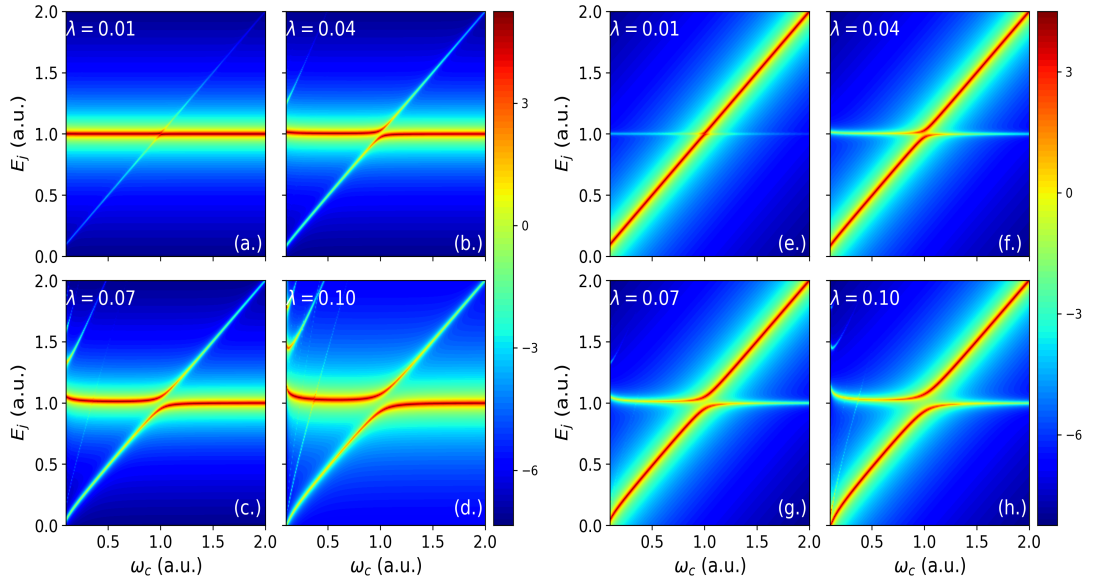

Figure 7: Rabi spectrum as a function of the mode frequency ω_c for four different coupling strength λ. Panels (a.)-(d.) is from the perspective of the electronic subsystem from weak to strong coupling as the electronic degrees hybridize with that of the photon to form lower and upper polariton branches resulting in Rabi splitting which increases with increasing λ. Panels (e.)-(h.) is from the perspective of the photonic subsystem from weak to strong coupling as the linear dispersing photon branch is split into lower and upper polariton branches with similar features of increasing splitting when the coupling λ is increased.

in mind, we now investigate multi-photon processes with the Rabi model. For such a process, the field is half-detuned from the electronic resonance indicating a two-photon process (i.e. $\omega_0 = 2$ and $\omega_c = 1$) via virtual states. In Fig. (6.e), as expected the absorption peaks are shifted close to the bare frequencies of the respective subsystems, but remain dressed by the photon field as new peaks arise in the ultra-strong coupling regime. The pRPA and RWA are shown to capture the two peaks around the bare frequencies of the individual subsystems but fail to capture higher lying non-vanishing contributions to the spectra. These higher-lying peaks (shown in the inset of Fig. (6.e)) correspond to multi-photon processes. If more accurate approximations for the xc potential are used, the results in Fig. (6) will get closer to the exact case.

Next, we investigate the novel response functions $\chi_q^{\sigma_x}$, $\chi_{\sigma_x}^q$, χ_q^q and hence the novel linear spectroscopic observables in Eqs. (326) and (327). The *mixed spectroscopic observables* of Eq. (327) describe a situation where we perturb one subsystem and then consider the response in the other. These observables are shown in Fig. (6.c.) for the numerically exact case and for the pRPA and the RWA. We find positive and negative peaks which highlights that excitations due to external perturbations can be exchanged between subsystems, i.e., energy absorbed in the electronic subsystem can excite the photonic subsystem and vice versa. In addition, we show in Fig. (6.b.) the linear-response spectra of the displacement field (and with this also the electric

field) obtained from Eq. (326) due to an external classical charge current. Clearly, if $\lambda = 0$ we do not have access to these observables. This highlights that by including the quantized photon field, new possibilities in linear spectroscopy arise when light and matter strongly couple.

An alternative way to access features of strong light-matter couplings is by computing the polariton dispersion spectrum. To visualize the polariton dispersion, the linear response theory can be applied to compute the electron and photon components given by Eqs. (325) and (326). We will show only the polariton dispersion for the numerical exact case while noting that the approximations (pRPA and RWA) can obtain similar results. Figure (7.a) shows the formation of the polaritonic branches for different λ values and the dispersion was computed using Eq. (325). The formation of the polaritons is accompanied by the characteristic appearance of avoided crossing in the energy dispersion due to the hybridization between the linear dispersing photon branch and the non-dispersive electron branch. For a given cavity frequency (i.e. resonant coupling $\omega_c = \omega_0 = 1$) within the hybridization region, the lower and upper branches emerge as a splitting of the electronic peak (or transitions) into two separate peaks. Increasing the coupling λ as in Fig. (7.b-d), increases the avoided crossing around $\omega_0 = \omega_c = 1$. We also see that higher photonic excitations start to get populated for $\lambda \geq 0.04$. Such a dispersion spectrum can be measured in an experiment [90] for strong light-matter interactions. Using Eq. (326), we also show that such a spectrum can be obtained for the response of the displacement field due to an external classical charge current. This is shown in Fig. (7.e-h) where the linear dispersing photon splits into upper and lower polariton branches and the avoided crossing also increases with increasing λ. The main difference between Figs. (7.a-d) and (7.e-h) is that the weights are more intense on the non-dispersive electron branch for Fig. (7.a-d) and on the linear dispersing photon branch for Fig. (7.e-h).

3.6.2 PHOTONIC SPECTRA OF A MOLECULAR SYSTEM

The previous section presented new possibilities that become accessible when we treat light and matter on an equal quantized footing. Using the Rabi model, we investigated the photo-absorption spectra that get modified when light and matter strongly interact. We also proposed novel photonic and mixed spectra that can be computed for such strong light-matter coupling situations. In this section, we compute the *mixed spectra* for a real molecular system.

The molecular system considered here is a naphthalene ($C_{10}H_8$) molecule which is the simplest polycyclic aromatic hydrocarbon. The electronic structure of the naphthalene molecule as used here is described in App. B.1.2. We are interested in situations of strong light-matter interaction which can be achieved by confining the naphthalene molecule in a photonic environment (such as an optical cavity) depicted in Fig. (8.a). To show how the spectrum of the naphthalene molecule gets modified when the system strongly couples to a photon mode, we first show in Fig. (8.b) a reference computation of the photo-absorption cross-section of the naphthalene molecule in free space using the linear-response time-propagation method of TDDFT which captures the $\Pi \rightarrow \Pi^*$ transition occurring at around 5.66 eV [122, 129]. In the next step, we couple the naphthalene molecule to a single photon mode and resonantly couple

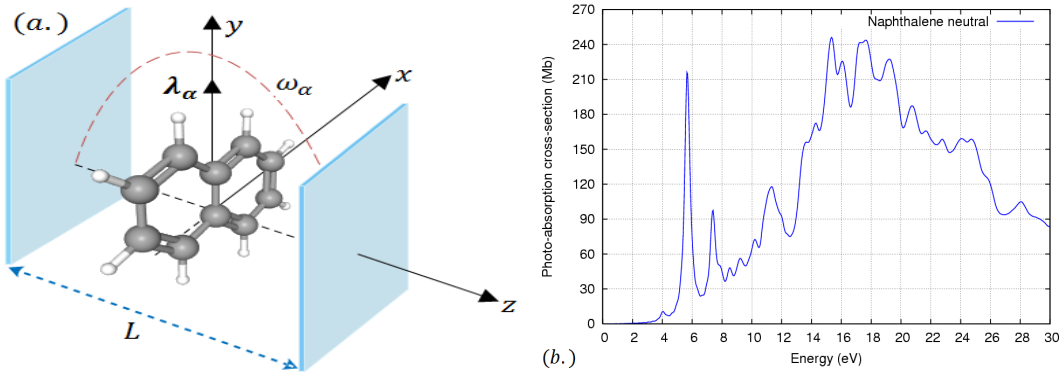

Figure 8: (a.) Schematic setup of a naphthalene molecule confined within an optical cavity. The cavity field is polarized along the y-axis with a coupling strength $\boldsymbol{\lambda}_\alpha$ and the photon propagation vector is along the cavity length L. (b.) Reference photo-absorption cross-section spectrum of a naphthalene molecule in free space computed with TDDFT linear-response method [122, 129] showing the $\Pi - \Pi^*$ transition at roughly 5.66 eV. The absorption cross-sections in this figure is expressed in megabarns ($1\text{Mb} = 10^{-18}\text{cm}^2$)

the cavity frequency to the $\Pi - \Pi^*$ transition, that is $\hbar\omega_\alpha = 5.66$ eV. While in the free space case (see Fig. (8.b)) the mean polarizability $\bar{\alpha}(\omega)$ (see Eq. (317)) was computed, here we compute just the y-component of the polarizability tensor, i.e., $\alpha_{yy}(\omega)$ since the y-component of the dipole contributes strongly to the $\Pi - \Pi^*$ transition. Using the linear-response time-propagation method of QEDFT (see Sec. 3.5.3 for details) we obtain the spectrum in Fig. (9) for different values of λ_α. First for the free-space case (when $\lambda_\alpha = 0$) we obtain the $\Pi - \Pi^*$ transition at around 5.66 eV. When the coupling of the molecule to the cavity mode is switched on and for a coupling strength of $\lambda_\alpha = 0.01$, we see the onset of features of electron-photon coupled systems which are the lower and upper polariton branches as shown in Fig. (9.b.). Upon increasing the coupling strength λ_α as in Fig. (9.c,d), the Rabi splitting between the lower and upper polariton branches increase. This result in conjunction with the results in Sec. 3.5.4 highlights how the photo-absorption spectrum gets modified by strongly coupling the matter subsystem to photons in an ab-initio description.

Now, we also show photonic observables that become accessible in our ab-initio theory. The absorption spectrum presented above described the case in Sec. 3.5.4, i.e., the response of the matter subsystem due to a perturbation from the external potential $\delta v(\mathbf{r}, t)$ while $\delta j_\alpha(t) = 0$. Since the photon field is included in our theory as a dynamical part of the coupled system, we have access to the displacement field of Eq. (238). In the time-propagation method of QEDFT, we obtain the time-evolution of the displacement field $q_\alpha(t)$ from Eq. (316). In Fig. (10) we show the real-time photon coordinate $q_\alpha(t)$ and the imaginary part of its Fourier transform in frequency space $q_\alpha(\omega)$ obtained from

$$q_\alpha(\omega) = \frac{1}{k}\int_0^\infty dt\ \left(q_\alpha(t) - q_\alpha(t_0)\right) e^{i(\omega + i\eta)t}. \tag{328}$$

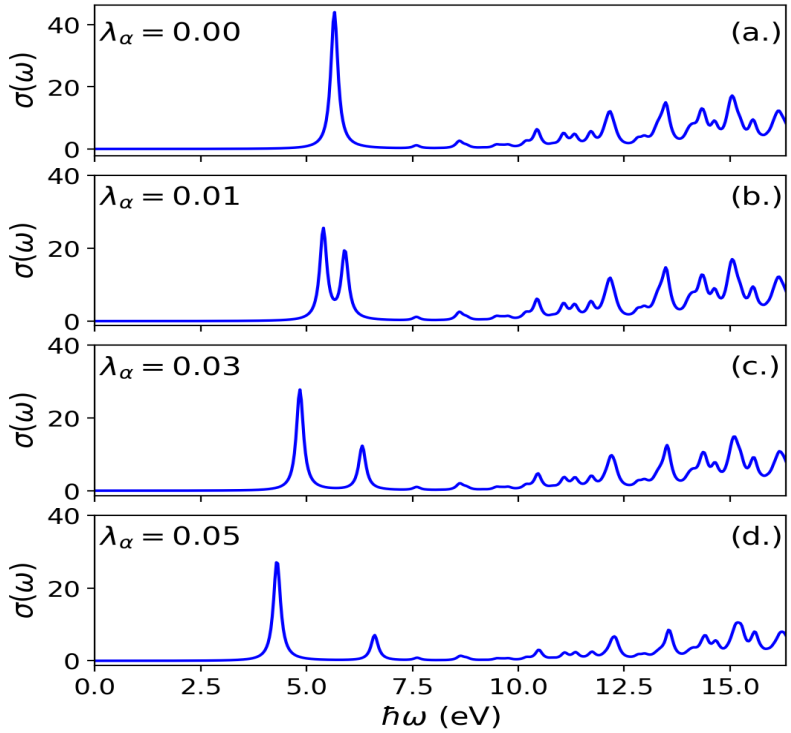

Figure 9: Photo-absorption cross-section of a naphthalene molecule confined in an optical cavity. Panel (a.) shows the spectrum of the naphthalene molecule in free space (i.e. $\lambda_\alpha = 0$) with the $\Pi - \Pi^*$ transition at around 5.66 eV. Coupling the cavity mode resonantly to this transition and increasing the coupling strength as in (b.), (c.) and (d.) results to a splitting of the peak into lower and upper polariton branches with a Rabi splitting that increases with increasing λ_α.

The form of this equation is analogous to the frequency-dependent polarizability tensor [118, 130, 131]:

$$\alpha_{\mu\nu}(\omega) = \frac{e^2}{k_\nu} \int_0^\infty dt \ \left(\mathbf{r}_\mu(t) - \mathbf{r}_\mu(t_0)\right) e^{i(\omega + i\eta)t}, \tag{329}$$

used to obtain Fig. (9) where k_ν has to be small to ensure being in the linear response regime [131]. In Fig. (10.a) we observe Rabi-like oscillations for the coupling strength of $\lambda_\alpha = 0.01$ as in Ref. [47] and increasing the coupling strength $\lambda_\alpha = 0.03, 0.05$ (see Fig. (10.b,c)) the Rabi-like oscillatory pattern cannot be easily identified due to strong light-matter coupling. In Fig. (10.d,e,f), we show the spectrum obtained using Eq. (328) which is a Fourier transform of the corresponding Fig. (10.a,b,c). We observe features of strong light-matter coupling as lower and upper polaritonic branches emerge with increasing Rabi splitting as the coupling strength is increased. Similar to the spectrum in Sec. 3.6.1.2, we have positive and negative peaks which in this case indicate that perturbing the electronic subsystem with an external potential, induces changes in the photonic spectra. This result also signifies the feedback between light and matter as both become modified since they show features of strong light-matter coupling. We once again mention that the above results can be computed with any of the linear-response methods of QEDFT in Sec. 3.5. As a further example, in App. B.2

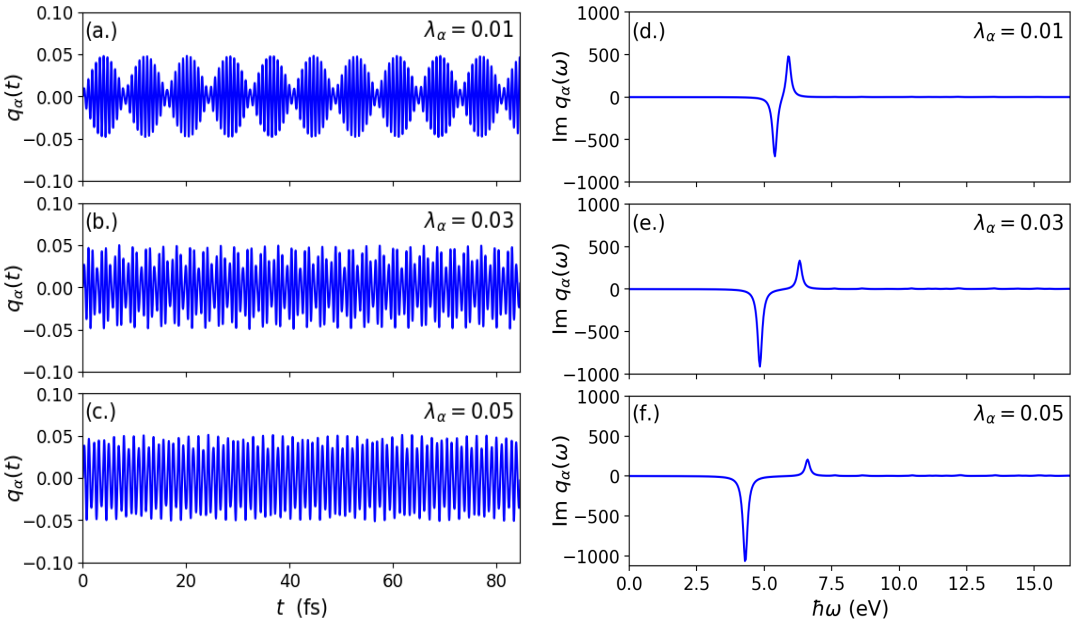

Figure 10: Real-time photon coordinate $q_\alpha(t)$ (left panels) and corresponding imaginary part of $q_\alpha(\omega)$ (right panels) of a naphthalene molecule coupled to a single photon mode. Increasing the coupling strength $\lambda = 0.01, 0.03, 0.05$ as in panels (a.)-(c.) changes the Rabi-like oscillations as a result of traversing into the strong coupling regime. Panels (d.)-(f.) show spectrum obtained by Fourier transform of $q_\alpha(t)$ depicting polaritonic features with increasing Rabi split with an increasing coupling strength.

we compute the photonic spectra of an azulene molecule coupled to photons using the Sternheimer method.

3.6.3 LIFETIMES OF EXCITATIONS FROM FIRST PRINCIPLES

The computation of linear response spectra in the previous sections employed an artificial broadening of the absorption peaks to mimic the finite lifetimes of excited states. Such artificial broadening of the transition peaks was done to overcome problems in the semi-classical limit that fails to account for the finite lifetimes of excited states in a direct way since the electromagnetic field is treated classically and only as an external perturbation. However, our ab-initio treatment of the quantized field interacting with matter captures the finite lifetimes of the excited states in a direct way without the need of any artificial broadening. In this section, we show how this can be done non-perturbatively within the framework of linear-response QEDFT.

Before we show how to compute lifetimes of excitations from first principles, we note that since our ab-initio QEDFT linear-response formalism is a reformulation of the non-relativistic QED case which includes M-photon modes, the QEDFT linear-response formulation also includes these M-photon modes. Therefore, we can sample the photon bath with thousands of photon modes. In the example below, we employ the electron-photon Casida equation (295) while noting that the other methods can obtain the same results as shown in Sec. 3.5.4. As matter system, we consider the benzene molecule studied in Sec. 3.5.4 and explicitly couple it to 80,000 photon modes. The energies of the photon modes that are considered range from 0.19 meV, for the

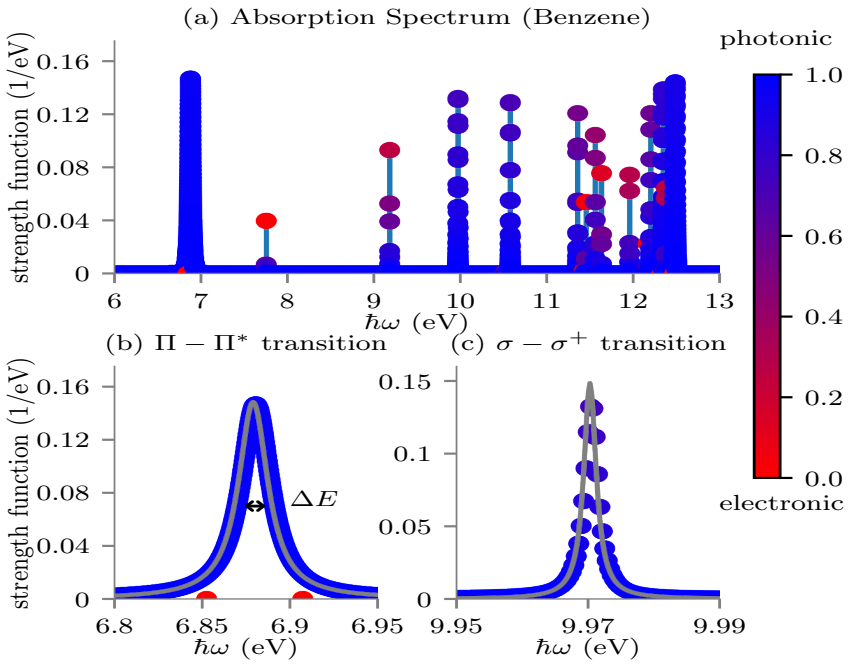

Figure 11: First principles lifetime calculation of the electronic excitation spectrum of the benzene molecule in an quasi one-dimensional cavity: (a) Full spectrum of the benzene molecule, (b) zoom to the $\Pi - \Pi^*$ transition, where the black arrow indicates the full width at half maximum (FWHM) ΔE, (c) zoom to a peak contributing to the $\sigma - \sigma^+$ transition. The gray spectrum is obtained by Wigner-Weisskopf theory [132]. The dotted spectral data points correspond to many coupled electron-photon excitation energies which together comprise the natural lineshape of the excitation. Blue color refers to a more photonic nature of the excitations, vs. red color to a more electronic nature.

smallest energy up to 30.51 eV for the largest one with a spacing of $\hbar\Delta\omega = 0.38$ meV which indicates a dense sampling of the modes. In this example we do not sample the full three-dimensional mode space together with the two polarization possibilities per mode but rather consider a one-dimensional slice in mode space. Sampling the one-dimensional mode frequencies will change the actual three-dimensional lifetimes but for the purpose of demonstrating the possibilities of obtaining lifetimes from first-principles this is sufficient[3]. We sample the photon modes to corresponds to that of a quasi-one dimensional optical cavity, thus, we choose a cavity of length L_x [91] in the x-direction with a finite width in the other two directions that are much more confined. In this case, the frequencies are obtained from $\omega_\alpha = \alpha c\pi/L_x$ and $\boldsymbol{\lambda}_\alpha = \sqrt{\frac{2}{\hbar\epsilon_0 L_x L_y L_z}}\sin(\omega_\alpha/c\, x_0)\mathbf{e}_x$, where $x_0 = L_x/2$ is the position of the molecule in the x-direction. While we have a sine mode function in the x-direction, we assume a constant mode function in the other directions. For this example, we choose a cavity of length $L_x = 3250\mu$m in the x-direction, $L_y = 10.58$ in the y-direction and $L_z = 2.65$ in the z-direction. In Sec. 3.6.5, we show how the spectrum changes by varying the quantization volume of the photon field.

3 A detailed analysis of real lifetimes would include a three-dimensional sampling of the mode space and also considerations with respect to the bare mass of the particles.

In Fig. (11.a), we show the full spectrum of this calculation computed using Eq. (318). Since we sampled the photon part densely with 80,000 modes, the peaks do not need to be artificially broaden anymore. Formulated differently, we can directly plot the oscillator strength and the excitation energies of our resulting eigenvalue equation (295) without the need to employ any Lorentzian broadening. In Fig. (11), from blue (more photonic, i.e., $\sigma_{pt} = 1 - \sigma_{el}$) to red (more electronic, i.e., $\sigma_{el} = 1 - \sigma_{pt}$) for the electron-photon absorption spectrum we plot the different contributions of each pole in the response function. These results validates our intuition that resonances are mainly photonic in nature (since excitations are dominantly blue) and that a Maxwell's perspective of excited states (see Sec. 3.4 for more details) is quite natural. We zoom to the Π-Π^* transition in Fig. (11.b) and find a broadening of the peak that is larger than it is for the case of a three-dimensional cavity due to the sampling of the electromagnetic vacuum using a quasi one-dimensional nature of the quantization volume. This is analogous to changing the vacuum of the electromagnetic field and in this way the lifetimes of the electronic states are shorter if the electromagnetic field is confined to one dimension.

Before showing how to compute lifetimes, e.g., of the Π-Π^* transition in Fig. (11.b), we comment on perturbative methods that are commonly used. When the coupling between light and matter is very weak such that neither subsystem gets appreciably modified due to the other, the radiative lifetimes of atoms and molecules can be calculated using the perturbative Wigner-Weisskopf theory [132] in single excitation approximation in concert with the Markov approximation. These approximations are justified in the standard free-space case where the Wigner-Weisskopf results reproduce the prior results of Einstein based on the ad-hoc A and B coefficients. However, it does not include the treatment of ensembles of molecules that effectively enhance the matter-photon coupling strength as shown in the following section. The Wigner-Weisskopf theory obtains the radiative decay rate given by

$$\Gamma_{3D} = \frac{\omega_0^3 |\mathbf{d}|^2}{3\pi\epsilon_0\hbar c^3}. \tag{330}$$

For a one-dimensional cavity in the x-direction the results simplify to [133]

$$\Gamma_{1D} = \frac{\omega_0 |\mathbf{d}|^2}{L_y L_z \epsilon_0 \hbar c}. \tag{331}$$

Comparing the result obtained with the Wigner-Weisskopf theory (using Eq. (331)) to our ab-initio non-perturbative results (sampling densely the photon bath), we find for both peaks shown in Fig. (11.b) to be in good agreement (grey peak for Wigner-Weisskopf). Thus, taking the continuum limit for the photon modes, we recover in our framework the lifetimes predicted by Wigner-Weisskopf theory including the diverging energy shifts [134], i.e. the Lamb shift. Due to the Lamb shift, our resulting peaks are slightly shifted due to the divergences that arise which can be handled by renormalization theory. We obtain the lifetimes in the following way: first, we measure the full width at half maximum (FWHM), indicated by the black arrow in Fig. (11.b). We find $\Delta E_{\mathrm{FWHM}} = 0.0204$ eV and the corresponding lifetime $\tau_{\Pi-\Pi^*}$ follows by $\tau_{\Pi-\Pi^*} = \hbar/\Delta E_{\mathrm{FWHM}} = 32.27$ fs. Using the Wigner-Weisskopf result of Eq. (331), and the dipole moments and energies from the LDA calculation without a photon field, we find a lifetime of 32.21 fs. As a side remark, the same transition now

using Eq. (330) has a free-space lifetime of 0.89 ns, roughly in the range of the 2p-1s lifetime of the Hydrogen atom of 1.6 ns. In Fig. (11.c.), we also show the ab-initio peak of the $\sigma - \sigma^+$ transition where we find a narrow ab-initio peak that is not as well sampled as the $\Pi - \Pi^*$. Here, it is important to note that we find an ionization energy of 9.30 eV using Δ-SCF in the benzene molecule with the LDA exchange-correlation functional. In our simulation, coupling to peaks higher than the ionization energy are broadened by continuum (box) states.

3.6.4 SPECTRAL DEPENDENCE ON ENERGY CUTOFF

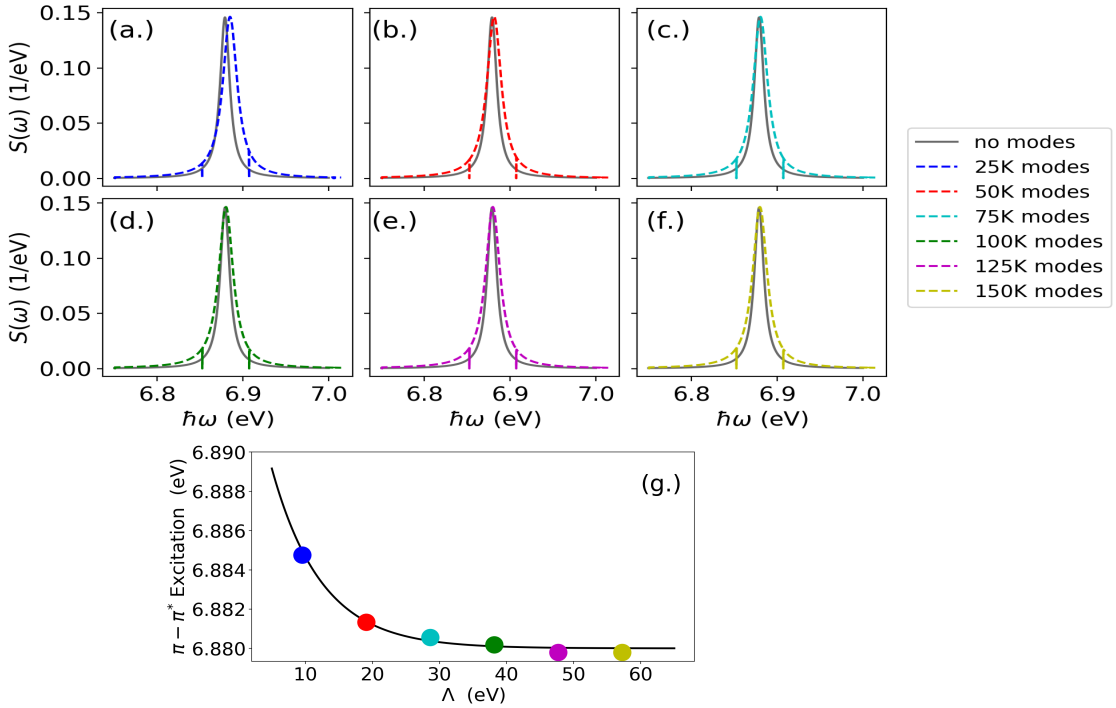

Figure 12: Continuous slight shift in the peak position of the $\Pi - \Pi^*$ transition of benzene by increasing the number of modes. The gray peak in (a.)-(f.) is the case of the benzene molecule in free space. Increasing the number of photon modes in steps of 25,000 from (a.) to (f.) shifts the peak position close to the free space case. In (g.), the peak position follows an exponential decay for increasing cut-off. In the legend K= 1000.

The previous section introduced a non-perturbative first-principles approach to obtaining lifetimes of excited states by sampling the photon bath. By so doing, we observed shifts in peak positions that can be attributed to the Lamb shift. In this section, we want to investigate this further by increasing the energy cutoff of the photon bath which entails sampling more photon modes using the quasi one-dimensional cavity. This will give us a feeling on how to treat these shifts either by renormalization theory. Also, this will be beneficial to situations where one samples densely the photon bath with a high energy cut-off because we will need to take into account the "electromagnetic masses" [41] to obtain the correct results.

To investigate how these shifts in peak position arise, we include more photon modes that couple weakly to the benzene molecule as in Sec. 3.6.3. For this we vary

the number of photon modes as $M = [25,000,\ 150,000]$ in steps of $25,000$. Using the sine mode function described above, the energy cut-off for varying the photon modes is given in Tab. (1). We note that the sampling of the minimum number of photon

Number of modes	Cutoff Λ (eV)	$\Pi - \Pi^*$ (eV)
$25,000$	9.535	6.88476094
$50,000$	19.070	6.88132799
$75,000$	28.605	6.88056404
$100,000$	38.140	6.88018232
$125,000$	47.676	6.87980256
$150,000$	57.211	6.87980069

Table 1: Shift of the $\Pi - \Pi^*$ transition of a benzene molecule for increasing photon modes M and increasing energy cut-off Λ. The value of the $\Pi - \Pi^*$ without coupling to photons in 6.87900000 eV.

modes considered (i.e. $25,000$) has an energy cut-off $\Lambda = 9.535$ eV well above the $\Pi - \Pi^*$ excitation energy $E_{\Pi-\Pi^*} = 6.87900000$ eV in free space, therefore, it is a good starting point for mode sampling. It is known from QED, that when electrons are coupled to the continuum of the electromagnetic field their *bare masses* needs to be renormalized [135]. Since we sample thousands of modes densely with increasing energy cut-off, we expect to see effects that require a renormalization of the bare masses. In Fig. (12), we show the $\Pi \to \Pi^*$ absorption peak for the case of coupling to thousands of photon modes and the free space situation. Fig. (12.a.) shows clearly the shift in peak position when comparing the case of the molecule coupled to $25,000$ modes and the free space case. Increasing the number of photon modes (and hence the cut-off) as in Fig. (12.b-f), the case coupled to many modes is shown to shift slightly towards the free space result. A clear depiction of the shift is shown in Fig. (12.g) where the shifts in peak positions have an exponential decay pattern with increasing energy cut-off (see Tab. (1) for detail values). The exponential decay fit in Fig. (12.g.) is obtained using the function

$$E_{\Pi-\Pi^*}(\Lambda) \simeq 6.880 + (6.898 - 6.880)e^{-\alpha\Lambda}\,\text{eV}\,,$$

where $\alpha = 0.135\,(1/\text{eV})$ is the approximated shift of the $\Pi \to \Pi^*$ absorption peak. The Lamb shift as observed for the case of the Hydrogen atom was due to the interaction between the electromagnetic vacuum and the electron in the 2s and 2p orbitals [25]. Since we couple the benzene molecule to thousands of modes that sample the electromagnetic vacuum field, we can attribute the energy shifts to be the Lamb shift of the $\Pi \to \Pi^*$ transition. By so doing, results to the situation where both agree since the Schrödinger Hamiltonian (see Sec. 2.5.1) accounts for the photons in its "physical mass" m_e since it is the sum of bare mass and electromagnetic masses. We note from QED that for increasing energy cut-off, we will need to renormalize the bare mass to make the results of the case where the electron is coupled to a continuum of modes match the free space case [135]. However, here we find that increasing the cut-off the peak position approaches that of the free space case. There are several reasons that

can be attributed to this behavior. First, since the Lamb shift is a quantum mechanical effect, the pRPA which excludes the xc contributions of the electron-photon interactions is not adequate to capture this effect correctly. If one would use an xc functional beyond mean-field we expect to see deviations from the results in Fig. (12). Secondly, while the effective field theory of non-relativistic QED (with three-dimensional fields) shows a logarithmic divergence in the effective coupling [41, 43], this is however not the case when we have a one-dimensional sampling of the modes. It can be shown using the arguments in Ref. [43] that for a one-dimensional sampling of the modes, the effective coupling is not divergent. Also, it could be that the ultraviolet cut-offs are not large enough compared to a sensible energy cut-off, for example, an ultraviolet cutoff at the rest mass energy of the electrons. All these reasons call for further investigations which we will explore in a different work.

3.6.5 BEYOND SINGLE MOLECULE AND LORENTZ TO FANO TRANSITION

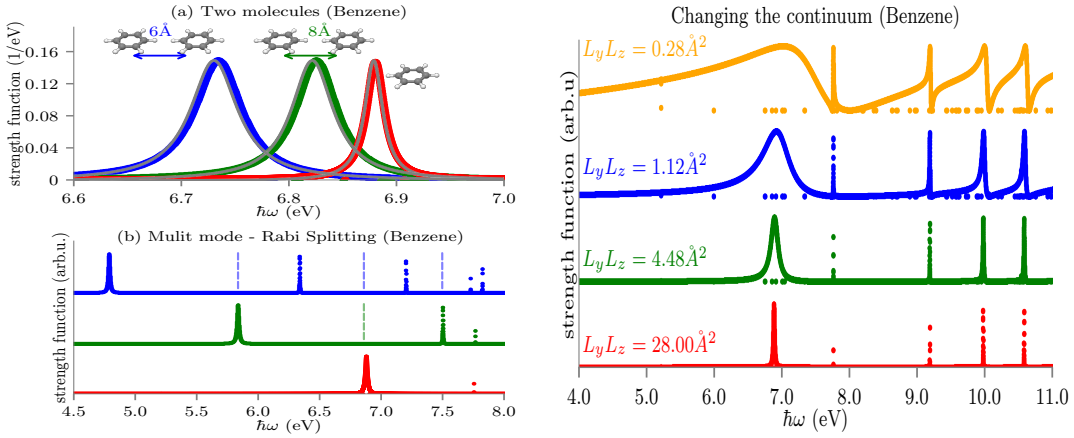

Figure 13: (a) Two molecules of benzene strongly coupled to 80,000 cavity modes of an one-dimensional cavity. The further apart the molecules are, the closer the peak gets to the single molecule peak. Also we notice the doubled peak broadening (shorter lifetime). The gray spectrum is obtained by Wigner-Weisskopf theory [132]. (b) We show the Rabi splitting in a situation of a single strongly coupled mode with 80,000 cavity modes (green), and three strongly coupled modes with 80,000 cavity modes (blue). The red lines correspond to the same setup as in (a). The dashed lines refer to the frequency of the cavity modes. The peaks become broadened due to the interaction with the continuum.

In the last two sections, we studied the case where we sampled thousands of photon modes that coupled weakly to the a single benzene molecule. We showed how to determine the lifetimes non-perturbatively from the ab-initio theory and how this compared to the Wigner-Weisskopf theory. While both were shown to be in good agreement, in this section we consider a situation where the Wigner-Weisskopf theory is less accurate compared to the ab-initio theory. We further show new perspectives that can be addressed within the linear-response QEDFT framework.

We first consider the case where the perturbative Wigner-Weisskopf theory for obtaining the lifetimes becomes less accurate. The usual perturbative theories are known to perform well in free-space where weak coupling together with the as-

sumption of a dilute gas of molecules are implied. However, in the case of single-molecule strong coupling [136] or when nearby molecules or an ensemble of interacting molecules modify the vacuum, the usual perturbative theories are expected to break down. This is because changes in the electronic and the photonic subsystem become self-consistent (see Sec. 3.6.2) and the usual distinction of light and matter becomes less clear. In such situations, the linear response formulation within the framework of QEDFT as well as the Maxwell's perspective of excited-state properties (see Sec. 3.4) becomes most powerful. To show this, consider for example two benzene molecules weakly coupled to a one-dimensional continuum of photon modes (80, 000). In Fig. (13.a) we show three different results of the $\Pi - \Pi^*$ absorption peak: (i.) the case of a single benzene molecule (which is equivalent to assume a large distance with another molecule), (ii.) when the two molecules are 8Å apart and (iii.) when the two molecules are 6Å apart. If the molecules are far apart (i.e. case (i.)) we just find the usual Wigner-Weisskopf result. However, if we bring the molecules closer and closer, we observe that the combined resonance shifts and the combined linewidth becomes broader, implying a shortened lifetime. The perturbative Wigner-Weisskopf theory (free space grey) starts to deviate further. One will expect that if the molecules are brought closer together the Wigner-Weisskopf theory becomes less accurate since changes in the electronic and the photonic subsystem become fully self-consistent and such perturbative approaches cannot capture such intricate details. Such a feature were the Wigner-Weisskopf theory is less accurate when compared to the ab-initio results has also been shown even for the case of a single molecule coupled to photons [20]. These results shows one situation where non-self-consistent approaches become less accurate when compared to the ab-initio theory.

Next, we consider new perspectives that can be determined in the linear-response formulation of QEDFT. The first case is single-molecule strong coupling with continuum of modes. Consider the case where a few out of the 80, 000 modes that couple to a single benzene molecule have an enhanced coupling strength. In Fig. (13.b.), we show the spectrum where the molecule is coupled to the continuum (red plot), the same is shown in Fig. (11). We then introduce a single strongly coupled mode at the $\Pi - \Pi^*$ transition peak and the resulting spectra is shown in green. The dashed lines in the figure are the introduced cavity frequencies. The single mode introduces the expected Rabi splitting into the lower and upper polaritons and these polaritonic peaks become broadened due to the interaction with the continuum. Interestingly, we find a different broadening for the lower and the upper polaritonic peaks, since only the sum of both has to be conserved. The smaller broadening for these two lower polaritonic states implies that the radiative lifetime of the lower and upper polaritonic state is longer than the lifetime of the excitation in weakly-coupled free-space. In blue, we show another spectra where we have now introduced three strongly coupled modes in addition to the cavity 80, 000 modes of the continuum. The two additional cavity modes are tuned in resonance to the lower and upper polariton peak of the green plot. We find additional peak splitting, but also a shifting of peak positions at 7.8 eV. These results show that we can compute the lifetimes of polaritonic peaks from first-principles using the QEDFT framework since together with a few enhanced modes, we can sample the photon bath. Perturbative approaches such as the Wigner-Weisskopf theory will not be accurate in such situations since the self-consistent interaction be-

tween the electronic and the photonic subsystems are not accounted for properly even for the weak coupling case above.

In this last example, we investigate the strong coupling to the continuum for the case of a single benzene molecule. In this case we effectively enhance the light-matter coupling strength by reducing the volume of the cavity along the y and z direction. In Fig. (13.c), we show the absorption spectrum for 4 different volumes of the cavity. For comparison, the first case (in red) is the spectrum that is also shown in Fig. (11), where the excitations have Lorentzian lineshape consistent with Wigner-Weisskopf theory as discussed in Sec. 3.6.3. By gradually reducing the dimensions along the y and z direction and with this the volume of the cavity, we find drastic changes in the lineshape of the excitations. These changes lead to the transition of the lineshape from a Lorentzian to a Fano lineshape, as becomes clearly visible for $L_x L_z = 0.28$Å (orange plot). Asymmetric Fano absorption line shapes are known to occur when discrete excited states are coupled to a continuum of excitations [137]. A transition of a Lorentzian to a Fano lineshape was observed after excitation of autoionizing states in a Helium atom by attosecond extreme ultraviolet pulse [138]. However, here we see that we can achieve such a transition not with intense fields but via strong light-matter coupling to the continuum. The perturbative Weigner-Weisskopf theory will not be accurate in this non-standard situation. This presents another perspective that becomes accessible from the linear-response formulation of QEDFT.

The physical settings considered in this section need a self-consistent treatment of matter and photons alike and cannot be captured by any available electronic-structure or quantum-optical method. This puts the ab-initio linear-response of QEDFT at the forefront for accurate description of light-matter interactions.

3.7 SUMMARY

In this chapter, we first discussed the fundamental contribution of the dipole self-energy term of the length gauge Hamiltonian as it is a necessary part to have a Hamiltonian which is bounded from below. This was important since we want to employ ground-state QEDFT to determine initial states for linear-response computations in the QEDFT framework. Next, we introduced the linear-response of non-relativistic QED in the length gauge where novel responses and response functions emerge. This linear-response problem was then reformulated within the framework of QEDFT. Within this framework, we extended three linear response methods of TDDFT to the framework of QEDFT which presented a viable way of computing the novel responses and response functions. Using these responses and response functions we showed changes in the quantum Maxwell's equation due to the self-consistent feedback between light and matter. Applying these linear-response QEDFT methods, we showed how the response spectra get modified due to strong coupling as well as introduced new linear spectroscopic observables that become accessible in our ab-initio theory. We presented different new perspective that can be computed within our linear response QEDFT framework such as first-principles computation of lifetimes of electronic and polaritonic states non-perturbatively, single-molecule strong coupling in the continuum, the need for a mass-renormalization and transition from Lorentzian to Fano lineshapes. In this chapter we investigated different interesting situations in the linear-response regime. In the next chapter, we now go beyond the linear-response setting of non-

relativistic QED. We turn our focus now to the photonic subsystem and for this case we investigate the photon down-conversion process from an ab-initio perspective and propose new avenues that become possible when we treat light and matter on an equal quantized footing.

Part IV

PHOTON DOWN-CONVERSION IN NON-RELATIVISTIC QED

4

PHOTON DOWN-CONVERSION IN NON-RELATIVISTIC QED

In the previous chapter, we showed how treating light-matter interactions on an equal quantized footing not only changes the usual linear spectroscopy but also introduces novel spectroscopic observables and opens new possibilities to investigate other effects that arise in the strong coupling regime. These results were obtained in the linear-response setting where strong light-matter coupling is usually identified by linear spectroscopy. In this chapter, we consider beyond first-order (non-linear) processes of light-matter interactions. We highlight new possibilities in non-linear processes that become accessible from an ab-initio perspective when light and matter are treated on an equal level of theory. This is shown for a paradigmatic case of non-linear optics and quantum optics for photon down-conversion processes. Photon down-conversion is particularly of importance due to the ever growing range of applications such as building quantum-information processing protocols [139, 140], cryptography [141], or teleportation [142]. Such applications make it increasingly important to diversify the available quantum sources. We will highlight how strong light-matter coupling allows to realize an N-photon gun which generates a bundle of photons with non-classical properties. But first, we consider the usual spontaneous parametric down-conversion or parametric down-conversion (PDC) and show new possibilities that can be realized.

Photon down-conversion as described here is the coherent generation of photons with lower frequency (signal photons) by injecting a higher-frequency photonic field (pump photon) into a nonlinear medium [143]. One of such cases is PDC which is the generation of two signal photons with lower frequency from a pump photon with higher-frequency via a nonlinear medium. The necessity for on-demand deterministic two-photon sources expanded PDC from using nonlinear crystals with picoseconds pulsed lasers [144, 145] to photon-pair generation using the biexciton-exciton cascade in quantum dots [146–149] and even the nascent fields of polaritonic chemistry [150] and circuit quantum electrodynamics [151, 152]. As we showed in the linear-response regime that treating light classically and only as an external perturbation does not capture all changes in the matter system and even more so, properties of the field are not accessible in a direct way (see Chap. 3.6). Yet, such a semi-classical treatment is also considered beyond the linear regime as in the case of the down-conversion. So far, in order to study down-conversion processes theoretically one usually assumes that light and matter can be separated and treated differently. For example, the nonlinear optics approach uses nonlinear response functions and susceptibilities of matter-only quantum mechanics to characterize such a process and connects them with a classical description of the light field [144, 145, 153] (see Chap. 2.3.1). On the other hand, the quantum-optics approach, treats the light field quantized and couples the photons to a simplified few-level description of the matter [154–156] (see Rabi model in Chap. 3.6.1.1). The latter approach often gets rid of the matter part altogether by defining effective photon-only Hamiltonians which model the photon-photon interaction due to the matter system [153, 157, 158]. In both approaches the efficiency and

properties of the down-conversion process in question are usually determined by dipole-transition elements which depends on the symmetry of the matter subsystem. For example, since PDC is a three-wave mixing process, the second-order non-linear susceptibility is the dominant contribution to this process. For systems that possess a single symmetry (like the quantum ring (QR) considered in this chapter) this quantity is negligible [159], thus resulting in an inefficient or even impossible PDC process. In such situations, one would conventionally break the symmetry of the QR by some external classical field to engineer appropriate dipole-allowed transitions [160, 161] or use double-ring structures [162]. However, besides these conventional approaches, we here highlight the possibilities that arise if one does not make the initial assumption to treat light and matter separately similar to the linear-response setting (see Chap. 3.6). We do not employ QEDFT here, but rather perform numerically exact simulations of non-relativistic QED, where light and matter are treated on equal quantized footing. Since numerically exact simulations are only possible for simple systems, this part can be viewed as an exploratory investigation into possible applications of time-dependent ab-initio light-matter simulations beyond linear-response.

Our first-principles non-perturbative real-time simulations of the down-conversion employs as matter subsystem, a semiconductor GaAs QR (shown below) coupled to photons and highlights that strong coupling leads to a faster down-conversion and potentially avoiding detrimental decoherence effects. Also, we show how strong fields and strong coupling leads to efficient photon generation with non-classical properties. We further show how hybrid light-matter states (polaritons) (see Chap. 3.5.4) can act as pathways for a photon down-conversion process and thus propose an inverse harmonic generation scheme for generating N-photons. Due to the full quantized treatment of the down-conversion process, we highlight new observables that become accessible. In addition, we show cases where the standard approaches for describing the down-conversion process (few-level and Maxwell-Schrödinger approximations) do not recover all the necessary observables of the full ab-initio simulation.

The numerical results presented below were obtained with a purpose-built code (see App. D.1 for details) which we developed to explore ab-initio light-matter interactions for simple systems numerically exactly [1].

4.1 NON-DEGENERATE TWO-PHOTON DOWN-CONVERSION

Our numerical investigation of the down-conversion process is rather general and we only make the assumption that our bound matter system is small compared to the wavelength of the relevant photon modes. This specific case of the Pauli-Fierz Hamiltonian in dipole approximation is described by the velocity gauge Hamiltonian of Eq. (49). The numerical approach that is employed in the following can solve the general form of the Hamiltonian of Eq. (49), however, for our investigation of the down-conversion process we make a specific choice for the matter system to be a single 2D GaAs semiconductor QR described below. To better understand the down-conversion process using the GaAs QR as medium and to also highlight the new possibilities that become available when we treat light and matter on the same level

1 Some of the results presented in this Chapter have been published in this article [163].

of theory, we describe some interesting features of the model system in the following section.

4.1.1 THE TWO-DIMENSIONAL SEMICONDUCTOR QUANTUM RING

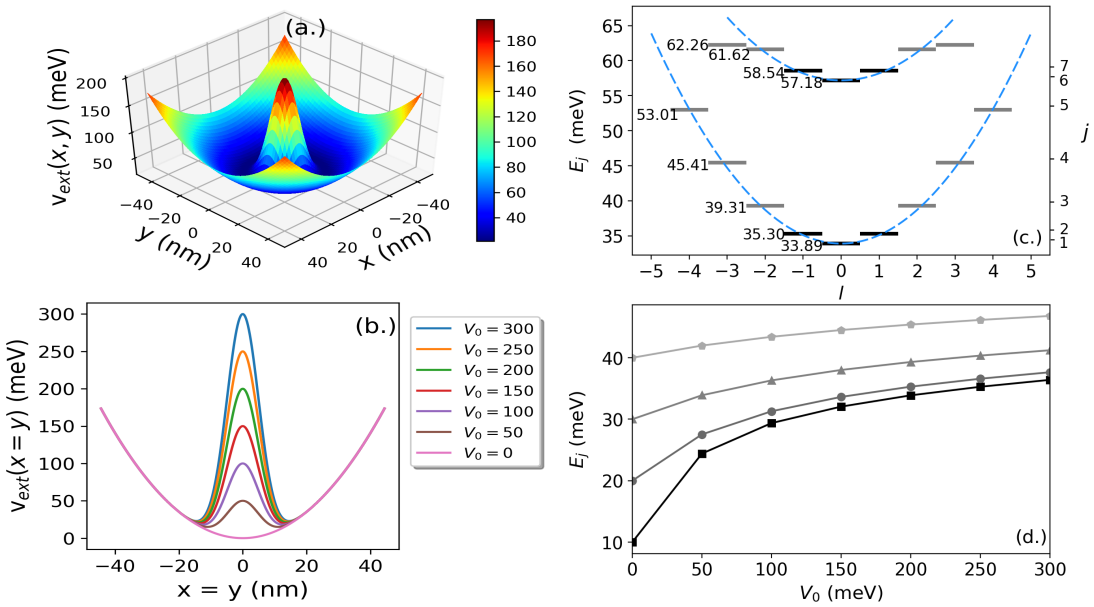

Figure 14: (a.) Real-space 2D potential of the quantum ring with a Gaussian peak at the center. The potential strength parameter $V_0 = 200$ meV. (b.) Diagonal cut ($x = y$) of 2D potential showing increasing Gaussian peak for increasing V_0. (c.) Energy spectrum of the 2D quantum ring showing the two lowest radial bands with degenerate and non-degenerate excited states and a non-degenerate ground-state for $V_0 = 200$ meV against angular momentum l. (d.) Changes in the low-lying energies by varying the potential strength parameter V_0. The lowest energy line is for the ground-state while the rest are for the degenerate excited states.

The 2D semiconductor QR of finite width features a single effective electron confined in two-dimensions in real-space ($\mathbf{r} = x\mathbf{e}_x + y\mathbf{e}_y$). The effective electron is confined to move in a parabolic Mexican-hat like potential. The Hamiltonian describing this model is given by

$$\hat{H}_{2D} = -\frac{\hbar^2}{2m}\left(\frac{\partial^2}{\partial x^2} + \frac{\partial^2}{\partial y^2}\right) + \underbrace{\frac{1}{2}m\omega_0^2\mathbf{r}^2 + V_0 e^{-\mathbf{r}^2/d^2}}_{v_{\text{ext}}(\mathbf{r})}, \tag{332}$$

where the potential $v_{\text{ext}}(\mathbf{r})$ introduces a parabolic confinement and a Gaussian peak located at the center as depicted in Fig. (14.a). In a semiconductor QR, the charge carriers are confined in the radial direction and since the ring is circular, it has a continuous rotational symmetry [161, 164]. The parameters of the binding potential are chosen to reflect the energy and length scales used in experiments with semiconductor GaAs QRs [165, 166] which are $\hbar\omega_0 = 10$ meV, $d = 10$ nm, $m = 0.067m_e$, and

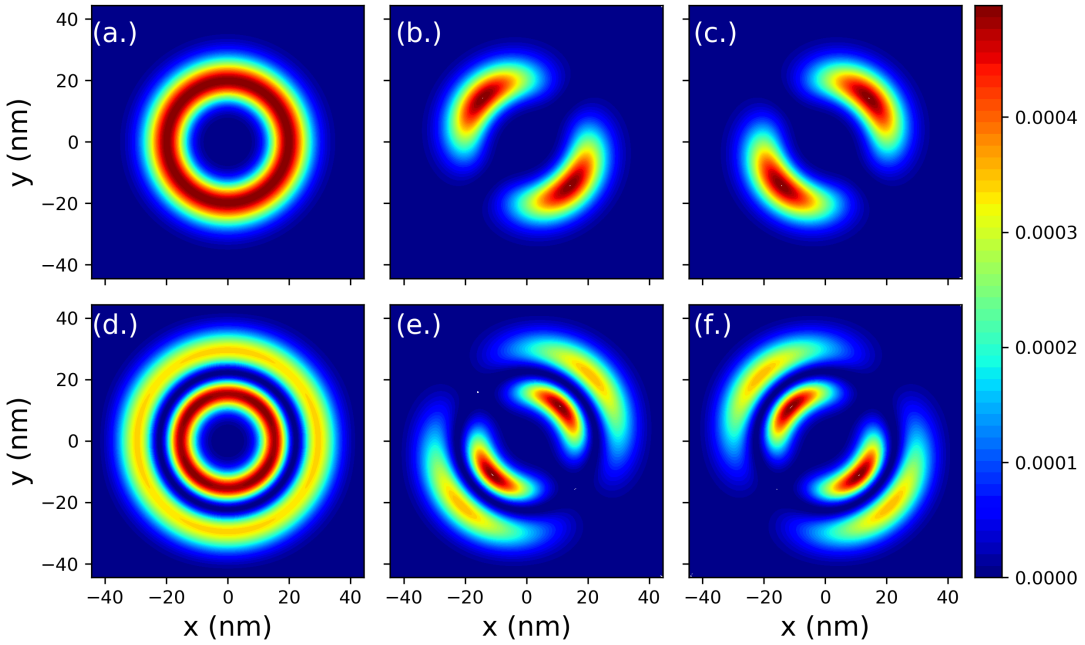

Figure 15: The electron density of some selected relevant states of the GaAs QR (a.) ground-state ψ_1^0, (b.) and (c.) degenerate first excited states $\psi_2^{1,-1}$, (d.) tenth excited state ψ_6^0, (e.) and (f.) degenerate eleventh- and twelfth-excited states $\psi_7^{1,-1}$. Here the potential strength parameter is $V_0 = 200$ meV

$V_0 = 200$ meV. The units of the semiconductor QR are defined using the dielectric constant of GaAs $\epsilon = 12.7\epsilon_0$ which scales the atomic units as in Ref. [160] to the following effective atomic units $\text{Ha}^* = (m/\epsilon^2)\text{Ha} \approx 11.30$ meV, $a_B^* = (m/\epsilon)a_0 \approx 10.03$ nm, and $u_t^* = \hbar/\text{Ha}^* \approx 58.23$ fs.

The spectrum of the QR can be changed depending on the chosen amplitude (strength) of V_0. For example, when $V_0 = 0$ meV, Eq. (332) reduces to a 2D isotropic harmonic oscillator with energies $E_n = \hbar\omega_0(2n+1)$ where $n = 0, 1, 2, 3, ...$ and the degeneracy in energy is $(n+1)$. When $V_0 > 0$ meV (and $V_0 = 200$ meV is chosen unless otherwise stated) the eigenstates ψ_j^l are labeled by the angular momentum $l = 0, \pm1, \pm2, \pm3, ...$ and the index $j = |l| + 1$ enumerates over the energy levels as shown in Fig. (14.c). The ground-state and excited state with $l = 0$ are singlets, while the excited states with finite angular momentum differing from $l = 0$ are doubly degenerate. Therefore, changing V_0 changes the spectral properties of the semiconductor QR. This feature of the QR is of particular interest here since increasing V_0 increases the height of the Gaussian peak thereby making the electronic system more anharmonic as shown in Fig. (14.b). Also, increasing V_0 increases the transition dipole moments between dipole-allowed transitions (see Tab. (2.b)). This is particularly of interest in an electron-photon coupled system since the coupling parameter is proportional to the transition dipoles as given in Eq. (384). Thus if the transition dipoles are increased, this leads to an increase in the electron-photon coupling. Changing the spectral features of the QR is possible to realize experimentally [161]. This is achieved here by varying the potential parameter strength V_0 which changes the geometric properties by reducing the ring width which in turn increases the Gaussian peak at the center (see Fig. (14.b)) thereby changing the electronic spectra as in Fig. (14.d).

The selection rules of this model allow for dipole transitions only between states with consecutive angular momenta, i.e., between states with angular momentum $|l|$ differing by one [13, 160]. For example, in the first radial band the allowed transitions are $\psi_1^0 \leftrightarrow \psi_2^{1,-1} \leftrightarrow \psi_3^{2,-2} \leftrightarrow \psi_4^{3,-3} \leftrightarrow \psi_5^{4,-4}$ and for the two lowest radial bands, some of the allowed transitions are $\psi_1^0 \leftrightarrow \psi_2^{1,-1} \leftrightarrow \psi_6^0 \leftrightarrow \psi_7^{1,-1}$. For the down-conversion considered in this chapter, the following electronic states $|\psi_1^0\rangle$, $|\psi_2^{-1,1}\rangle$, $|\psi_6^0\rangle$ and $|\psi_7^{-1,1}\rangle$ are coupled resonantly to selected cavity modes. For this reason, we give as example the x-component of the transition dipole in effective atomic units for the relevant transitions in Tab. (2.a). The bound electron in the 2D parabolic potential

Transitions	Amplitudes
$\langle\psi_1^0\|\hat{x}\|\psi_7^1\rangle$	0.2077
$\langle\psi_6^0\|\hat{x}\|\psi_7^1\rangle$	1.2786
$\langle\psi_2^1\|\hat{x}\|\psi_6^0\rangle$	0.2685
$\langle\psi_1^0\|\hat{x}\|\psi_2^1\rangle$	1.0867
$\langle\psi_1^0\|\hat{x}\|\psi_6^0\rangle$	4.0090×10^{-13}

(a) Transition dipoles for $V_0 = 200$ meV between different states.

V_0 (meV)	$\langle\psi_1^0\|\hat{x}\|\psi_2^1\rangle$
0	0.53159199
50	0.84520553
100	0.97645376
150	1.04263107
200	1.08705932
250	1.11987106
300	1.14420501

(b) Transition dipoles for varying V_0.

Table 2: (a.) The x-component of the transition dipole matrix elements for selected transitions shown in Fig. (14.c) (dark-shaded). (b.) Increasing $x-$component of the dipole transition amplitudes between the ground-state and first degenerate excited states for increasing potential strength parameter V_0.

still retains some features of 3D atomic systems such as the s, p, d, f orbital structures. This can be visualized by plotting the electron density $n(x, y)$ of these selected states $|\psi_1^0\rangle$, $|\psi_2^{1,-1}\rangle$, $|\psi_6^0\rangle$, $|\psi_7^{1,-1}\rangle$ as depicted in Fig. (15), respectively. First, Fig. (15.a and d.) depicts the ground-state and tenth excited (lowest energy state of second radial band) states densities with $1s$- and $2s$-type orbital symmetry, respectively. Secondly, Fig. (15.b and c.) corresponds to the densities of the first degenerate excited states of the first radial band showing $2p_x$- and $2p_y$-type orbital symmetry, respectively. Similarly, Fig. (15.e and f) shows the densities of the eleventh- and twelfth- degenerate excited states which are the first degenerate excited states of the second radial band showing $3p_x$- and $3p_y$-type orbital symmetry, respectively. With the properties and orbital structure of the 2D semiconductor QR discussed above, the QR can be thought of as a variable atom-like system and extending to a three-dimensional atomic system is expected to not change much of the properties of the down-conversion discussed in this chapter.

4.1.2 SETUP OF THE PHOTON DOWN-CONVERSION SCHEME

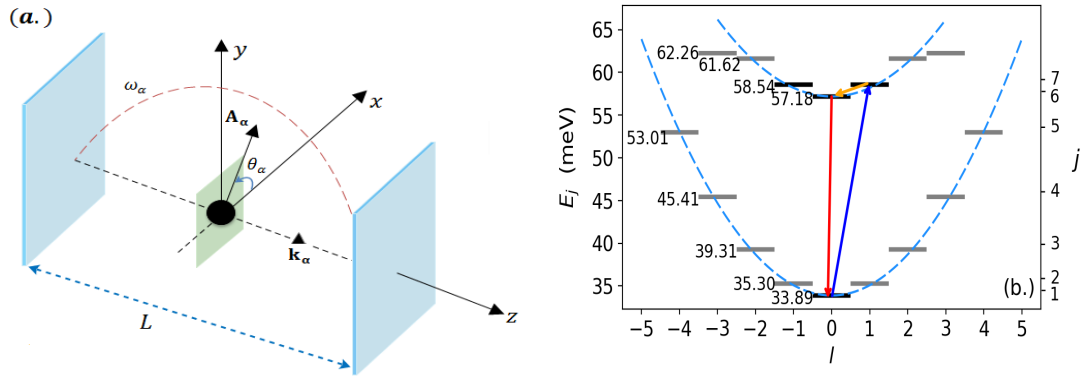

Figure 16: (a.) Schematic setup for investigating down-conversion processes featuring a 2D GaAs semiconductor QR at the center of a multi-mode photonic environment. The fields are linearly polarized in the x,y-plane and the propagation vectors $\mathbf{k}_\alpha$ is along the z-axis. (b.) Resonant coupling to specific energy-levels (dark-shaded) for non-degenerate PDC.

One of the reasons for this choice of the 2D semiconductor QR as down-conversion medium lies in the flexibility of changing the electronic spectrum by adopting the anharmonicity of the binding potential (see Sec. 4.1.1). A more realistic description that includes many interacting electrons and possibly even phononic excitations would be possible if we employ more efficient first-principle methods such as QEDFT (see Chap. 2.5.5) or QED-CC [15, 21]. Notwithstanding, the current level of description considered here already suffices to demonstrate the many details that become accessible with an ab-initio description of a down-conversion process. It is important to note that due to the rotational symmetry of the QR [161, 164, 167], a simple matter-only analysis would indicate that no standard down-conversion process takes place. This can be verified by considering the rotational symmetry of the eigenstates as only transitions that change the angular momentum by one (see Sec. 4.1.1) are dipole allowed, thus, a process as indicated in Fig. (16.b) is not dipole allowed. This also becomes evident in the second-order non-linear susceptibility, which is negligible in this case [159]. However, since we do not decouple light and matter, we observe that such a parametric process still takes place. The efficiency and the details of the ensuing down-conversion process will then depend mainly on the details of the photonic environment.

The photonic system is considered to be a multi-mode environment in which total control of the polarization, the frequency and the coupling strength of some of its modes can be attained. Specifically, we assume that we can manipulate three of these cavity modes at will, while the rest of the continuum of modes remains largely unchanged. These three relevant modes are associated with the vector potentials $\hat{\mathbf{A}}_1$, $\hat{\mathbf{A}}_2$ and $\hat{\mathbf{A}}_3$ which are given as in Eq. (50). We choose the field $\hat{\mathbf{A}}_1$ as the input (pump) mode with frequency ω_1, polarization direction $\mathbf{e}_1$ and coupling strength λ_1, and $\hat{\mathbf{A}}_2$ and $\hat{\mathbf{A}}_3$ as the vector potentials of the output (signal) modes with corresponding frequencies, polarizations and coupling strengths. The setup of the coupled matter-photon system is depicted in Fig. (16.a), such that only the x and y polarization directions are relevant and couple to the QR. Furthermore, the coordinate system is chosen such that $\hat{\mathbf{A}}_1 = \hat{A}_1\mathbf{e}_x$, $\hat{\mathbf{A}}_2 = \hat{A}_2(-\sin\theta_2\mathbf{e}_x + \cos\theta_2\mathbf{e}_y)$ and $\hat{\mathbf{A}}_3 = \hat{A}_3(\sin\theta_3\mathbf{e}_x + \cos\theta_3\mathbf{e}_y)$,

where θ_2 and θ_3 are the angles the respective polarization vectors makes with the coordinate system. Considering this possible setup, we can connect the change in coupling strength of the coupled electron-photon system to a change in the length of the cavity L and thus the mode volume, i.e., $\lambda = \sqrt{2/\epsilon L}$ where the dielectric permittivity of the GaAs semiconductor QR is $\epsilon = 12.7\epsilon_0$ and for simplicity of the coupled system, we assume that all three modes have the same coupling strength λ. While in the linear-response calculations (see Chap. 3.6.3) we sampled thousands of photon modes to compute the lifetimes and account for dissipation, here we treat the continuum of modes differently. That is, the rest of the continuum of modes (i.e. excluding the relevant modes) that account for dissipation and decoherence are subsumed, on the one hand, in the effective mass of the QR particle while the modes that constitute the linewidth of the enhanced modes are treated explicitly [18, 20]. The Hamiltonian for such coupled system is given in the following form

$$\hat{H} = \hat{H}_S + \hat{H}_B + \hat{H}_{SB}\,. \tag{333}$$

Here, the internal system Hamiltonian describing the down-conversion process is

$$\begin{aligned}\hat{H}_S = \hat{H}_{2D} + \hat{H}_1 + \hat{H}_2 + \hat{H}_3 - \frac{e}{m}\hat{A}_1\hat{p}_x \\ - \frac{e}{m}\left[\hat{A}_2\left(-\hat{p}_x\sin(\theta_2) + \hat{p}_y\cos(\theta_2)\right) + \hat{A}_3\left(\hat{p}_x\sin(\theta_3) + \hat{p}_y\cos(\theta_3)\right)\right] \\ + \frac{e^2}{2m}\left[\hat{A}_1^2+\hat{A}_2^2+\hat{A}_3^2-2\hat{A}_2\hat{A}_1\sin(\theta_2)-2\hat{A}_3\hat{A}_1\sin(\theta_3)+2\hat{A}_3\hat{A}_2\cos(\theta_2+\theta_3)\right],\end{aligned} \tag{334}$$

and the bath including system-bath coupling that constitute the rest of the $(M-3)$ modes in Eq. (333) are

$$\hat{H}_B = \sum_{\alpha=4}^{M}\hbar\omega_\alpha\left(\hat{a}_\alpha^\dagger\hat{a}_\alpha + \frac{1}{2}\right),\ \hat{H}_{SB} = \sum_{\alpha=4}^{M}\left[-\frac{e}{m}\hat{\mathbf{A}}_\alpha\cdot\hat{\mathbf{p}} + \frac{e^2}{2m}\left(2\hat{\mathbf{A}}_1+2\hat{\mathbf{A}}_2+2\hat{\mathbf{A}}_3+\sum_{\beta=4}^{M}\hat{\mathbf{A}}_\beta\right)\cdot\hat{\mathbf{A}}_\alpha\right],$$

where $\hat{\mathbf{p}} = \hat{p}_x\mathbf{e}_x + \hat{p}_y\mathbf{e}_y$ is the momentum operator of the 2D QR. The bare Hamiltonian $\hat{H}_{2D}$ of the matter subsystem is given in Eq. (332) and $\hat{H}_\alpha$ with $\alpha = 1,2,3$ are the photonic Hamiltonians of the selected modes having the form of Eq. (38). Here, the last two terms of Eq. (333) constitutes the active photonic bath of the system and its coupling to the internal system. The photonic bath is sampled with $(M-3) = M_{70} = 70$ bath modes that are treated in photon Fock number states together with the three relevant modes. The vector potential of the bath modes is $\hat{\mathbf{A}}_\alpha = \lambda'_\alpha\mathbf{e}_\alpha\sqrt{\frac{\hbar}{2\omega_\alpha}}\left(\hat{a}_\alpha + \hat{a}_\alpha^\dagger\right)$ where λ'_α is the coupling of the bath modes.

For the case of the non-degenerate two-photon down-conversion, we select the frequency of mode 1 in resonance with the dipole-allowed transition between the ground- and eleventh-excited state ($|\varphi_1^0\rangle \leftrightarrow |\varphi_7^1\rangle$) of the QR, which has energy $\hbar\omega_1 = 24.65$ meV, and choose the signal mode 2 with energy $\hbar\omega_2 = 1.36$ meV to be resonant with the tenth- and eleventh-excited states ($|\varphi_7^1\rangle \leftrightarrow |\varphi_6^0\rangle$) and finally the signal mode 3 with energy $\hbar\omega_3 = 23.29$ meV resonant with the ground- and tenth-excited state ($|\varphi_6^0\rangle \leftrightarrow |\varphi_1^0\rangle$). It is important to emphasize that the transition in resonance with mode 3 is not dipole allowed, since only states that differ by exactly one in their angular quantum number have a non-zero dipole transition element (see Chap. 4.1.1 for details). However, as a result of treating light and matter fully coupled we will still find

a down-conversion process in our ab-initio simulation. As a result the emission of a photon into mode 2 through radiative decay will differ from that of mode 3 due to the different dipole matrix elements involved (see Tab. (2)). This resonant coupling of the three modes to the energy levels of the QR are depicted in Fig. (16.b), however, noting here that the full spectrum of the QR is considered for a first-principles description of the down-conversion process. In Sec. 4.1.7, we make a comparison with an a priori restriction to only a few energy levels of the QR which shows how certain observables are not well captured if the number of states is not sufficiently large.

Before performing the time-evolution of the coupled system described by Eq. (333) and in majority of the simulations Eq. (334), we fix the polarization directions of the input and output modes in order to maximize the photon-pair generation. We choose the mixing angles $\theta_2 = \theta_3 = 90^\circ$ such that both fields of the signal modes are horizontally polarized as $\hat{\mathbf{A}}_2 = -\hat{A}_2\mathbf{e}_x$ and $\hat{\mathbf{A}}_3 = \hat{A}_3\mathbf{e}_x$. This choice results in maximization of the cross-talk of the interference terms of Eq. (334) since the sines and cosine of the mixing angles become one (see the detailed investigation in Sec. 4.2.1). Furthermore, the down-conversion process obeys the energy and momentum conservation of the photonic system $\hbar\omega_1 = \hbar\omega_2 + \hbar\omega_3$ and $\hbar\mathbf{k}_1 = \hbar\mathbf{k}_2 + \hbar\mathbf{k}_3$, respectively.

4.1.3 SIMULATION AND CHARACTERIZATION OF THE DOWN-CONVERSION

With the setup of the down-conversion scheme as described in the previous section, we now describe how we solve the problem and the observables considered to characterize properties of the down-conversion process.

4.1.3.1 *Time-evolution of the down-conversion process*

We investigate the down-conversion process of the coupled matter-photon system in detail by performing the time evolution of different initial states $|\Psi_{\text{in}}(0)\rangle$. This is achieved by explicitly propagating the time-dependent Schrödinger equation of Eq. (6) in one case with the Hamiltonian of Eq. (333) and in the other cases with the Hamiltonian of Eq. (334). As initial states, we consider in the following a factorizable product states of the form $|\Psi_{\text{in}}(0)\rangle = |\varphi_1^0\rangle|\phi_1\rangle|0_2\rangle|0_3\rangle\ldots|0_M\rangle$, where $|\varphi_1^0\rangle$ is the ground-state of the uncoupled QR and $|0_\alpha\rangle$ is the zero-photon state of mode α. For the pump mode $\alpha = 1$, we will consider two different initial states. The first choice is the simplest and ideal case in which $|\phi_1\rangle = |1_1\rangle$ is just a single-photon Fock state. The choice of this initial state is motivated by the fact that we can interpret the down-conversion process in the usual way as turning one photon into two with lower frequencies. The second choice of the initial state that will be mostly used throughout this chapter is a coherent state $|\phi_1\rangle = |\xi_1\rangle = e^{-|\xi_1|^2/2}\sum_{n_1=0}^{\infty}\left(\xi_1^{n_1}/\sqrt{n_1!}\right)|n_1\rangle$ where ξ_1 is the amplitude and $|n_1\rangle$ the Fock number states of mode 1. This implies that we have on average $|\xi_1|^2$ photons at the beginning in the input mode. By increasing $|\xi_1|^2 \gg 1$ we approach a classical laser field with a large number of photons. Furthermore, we consider this limit where the initially populated mode is replaced by an external classical laser field, in Sec. 4.1.6. It is important to note that changing the initial state to the correlated ground-state of the coupled system and then using an external pump

field to populate mode 1 leads to qualitatively similar results as will be shown in Sec. 4.1.6.

The time-dependent Schrödinger equation of the coupled system for all the different cases is solved with a Lanczos propagation scheme [168]. To represent the effective electron on a two-dimensional uniform real-space grid, we choose $N_x = N_y = 127$ grid points (implying 127^2 states are taken into account and treated explicitly) with grid spacing $\Delta x = \Delta y = 0.7052$ nm while applying an eighth-order finite-difference scheme for the gradient and Laplacian operators. In some cases, for comparison or numerical efficiency we represent the matter subsystem by its truncated uncoupled eigenstate basis instead of the real-space grid. This results to using only a few electronic states as the usual few-levels approximation (see Chap. C.1). We represent the photon modes in basis of Fock number states for the different fields and descriptions. We treat the photon subspace for the different cases as follows

- In Sec. 4.1.4.1, for each of the modes 1, 2, and 3 we include three photon Fock states which are the zero-photon, one-photon and two-photon states. To treat the photon bath consisting of $M - 3 = M_{70} = 70$ modes numerically exactly, we truncate the Fock space and consider only the vacuum state, the M_{70} one-photon states, and the $(M_{70}^2 + M_{70})/2$ two-photon states as in Ref. [91]. In only this simulation, do we consider for the matter subsystem the first 12 electronic states in Fig. (16.a) up to the state with energy 58.54 meV.
- In Sec. 4.1.4.2, we sample 20 Fock states for each of the modes 1, 2, and 3.
- In Secs. 4.1.6, till the end, we sample 30 photon Fock states for the individual modes 1, 2, and 3. The choice of 30 photon Fock states is to well represent the coherent state.

For the coupled electron-photon space, we explicitly construct matrix representations for all operators and the expectation value for observables of interest are computed for a time step of $\Delta t = 0.029$ fs of the time-evolved wavefunction.

4.1.3.2 *Characterization of the down-conversion process*

To characterize the down-conversion process in the time-evolution as described above, we compute several photonic observables. The mean photon occupation $n_1 = \langle \hat{a}_1^\dagger \hat{a}_1 \rangle$ of the pump mode is computed to contrast the amount of photonic occupation in the down-converted signal modes $n_2 = \langle \hat{a}_2^\dagger \hat{a}_2 \rangle$ and $n_3 = \langle \hat{a}_3^\dagger \hat{a}_3 \rangle$. Also we compute the population of the photon Fock-states defined by $P_{n_\alpha} = |\langle \hat{n}_\alpha | \Psi \rangle|^2$. The population of the single-, two- and three-photon Fock states, i.e., $|\langle 1_\alpha | \Psi(t) \rangle|^2$, $|\langle 2_\alpha | \Psi(t) \rangle|^2$ and $|\langle 3_\alpha | \Psi(t) \rangle|^2$ for $\alpha = 1, 2, 3$ are computed in order to identify the standard PDC process.

An important characteristic of the down-converted photon is the photon statistics which can be determined by computing the Mandel Q_α parameter [169] defined as

$$Q_\alpha = \frac{\langle \hat{a}_\alpha^\dagger \hat{a}_\alpha^\dagger \hat{a}_\alpha \hat{a}_\alpha \rangle - \langle \hat{a}_\alpha^\dagger \hat{a}_\alpha \rangle^2}{\langle \hat{a}_\alpha^\dagger \hat{a}_\alpha \rangle}, \tag{335}$$

which measures the deviation of the photon statistics from a Poisson distribution and thus is a measure for the quantum nature of the photonic subsystem. For a field with

non-classical properties, the range of values lies between $-1 \leq Q_\alpha < 0$ which is sub-Poissonian statistics (antibunching behavior). Fields with super-Poissonian statistics (bunching behavior) have $Q_\alpha > 0$ and for a coherent state with Poissonian statistics, $Q_\alpha = 0$ [33].

Besides the statistical properties of the fields, we consider the cross-correlation between the photon modes when they interact with a matter system. In accordance to this, the second-order cross-correlation function (intensity correlations) of a multi-mode field is defined by

$$g^{(2)}_{\alpha\beta} = \frac{\langle \hat{a}^\dagger_\alpha \hat{a}_\alpha \hat{a}^\dagger_\beta \hat{a}_\beta \rangle}{\langle \hat{a}^\dagger_\alpha \hat{a}_\alpha \rangle \langle \hat{a}^\dagger_\beta \hat{a}_\beta \rangle}. \tag{336}$$

The correlation function takes values greater than one for correlated modes. For uncorrelated modes, it is equal to one and it takes values smaller than one if the modes are anti-correlated [33, 35, 170]. We compute this observable as a measure of correlation between the relevant modes.

In addition, we compute the purity γ_α of the modes $\alpha = 1, 2, 3$ given in Eq. (386). If the purity is equal to one, the system can be expressed as a factorizable state of the individual photonic subsystems and that of the QR. If the purity is smaller than one, implies a non-factorizable state which indicates correlation (entanglement) between subsystems.

We note that we included the pump mode $\alpha = 1$ in the above observables. Properties of the pump mode are not usually accessible since it is treated only as a classical external observable which is not a dynamical part of the coupled system [154, 155]. However, since we treat both the modes and the electronic system fully quantized, these observables become accessible on this level of theory.

4.1.4 SINGLE INPUT-PHOTON DOWN-CONVERSION AND TEMPORAL CONTROL

With the down-conversion scheme and time-evolution as discussed in the previous section, we can now investigate the PDC process. In this section we consider the ideal case were the input mode 1 is occupied by a single photon, the coupling between light and matter is weak such that the usual non-linear optics considerations apply and we have a strongly anharmonic QR such that a few-level approximation is reasonable. The input state is $|\phi_1\rangle = |1_1\rangle$ and we fix a small coupling strength of $\lambda = 0.014$ and use an anharmonicity of $V_0 = 200$ meV (see Sec. 4.1.1 for details on the QR). To account for dissipation and decoherence as described by Eq. (333), we include M_{70} bath modes with polarizations equally aligned as the modes 1, 2, 3, otherwise, these bath modes would just couple more weakly. The M_{70} sampled bath modes are equally spaced and have energy ranges around the energies of $\hbar\omega_1$, $\hbar\omega_2$, $\hbar\omega_3$. For the resonant energy $\hbar\omega_2$, 20 bath modes are sampled which have energies that ranges from $\hbar\omega_{B_2} = [0.113, 4.521]$ meV and for $\hbar\omega_2$ and $\hbar\omega_3$ the combined energy range is $\hbar\omega_{B_{13}} = [11.303, 27.128]$ meV for which 50 bath modes are sampled with equal spacing $\hbar\Delta\omega = 0.25$ meV. The coupling strength of the bath modes is chosen to be $\lambda' = 0.007$. In the following, we present the time evolution for the combined system and bath (i.e. Eq. (333)) and system only (i.e. Eq. (334)). For the simulation including

the bath, we compute observables only for the relevant three modes while the bath modes that contribute to the lineshape serve just as dissipation and decoherence channels (similar to Chap. 3.6.5).

4.1.4.1 *Dissipation and coherence time*

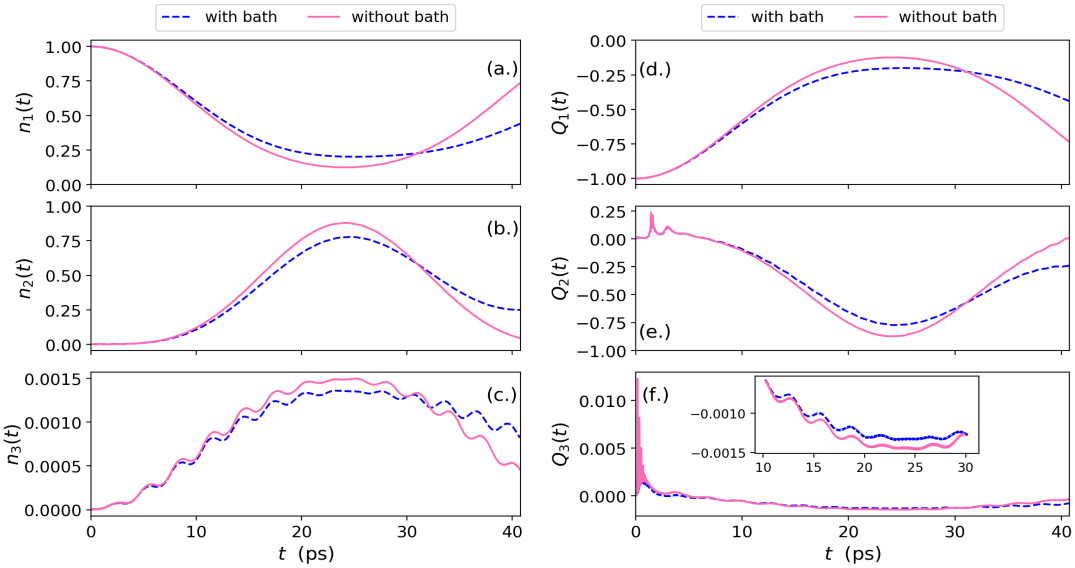

Figure 17: Comparison of the down-conversion for coupling to a photon bath and without photon bath. Panels (a.)-(c.) and (d.)-(e.) shows respectively the photon occupations and Mandel Q_α's of the pump and signal modes for weak coupling $\lambda = 0.014$ and bath coupling $\lambda' = 0.007$. The coherent simulation without the bath modes (solid pink line) agrees qualitatively with the simulation including the bath modes (dashed blue line) and only differs towards the end of the simulation, i.e., the end of the chosen coherence time.

We now consider the influence of the sampled bath modes on the down-conversion process. From the effective coupling $g_\alpha = \lambda\sqrt{\hbar/2\omega_\alpha}$, since $\omega_1 > \omega_2, \omega_3$ this implies $g_1 < g_2, g_3$. Therefore, for both cases the active electron in the excited state $|\varphi_7^1\rangle$ preferably relaxes by cascaded emission into signal modes 2 and 3. This is evident from Eq. (385) as the coupling strength is proportional to the square root of the spontaneous decay rate. In this case we expect that the signal modes 2 and 3 will get populated once the initial single-photon in the pump mode 1 interacts with the QR. This shows that in an ab-initio description of the PDC process, the effective coupling g_α plays an important role and the bare electronic dipole-transition elements are no longer the only major contribution to the process. This is evident since mode 3 is still populated even though the dipole moment of the transition is effectively zero (see Tab. (2.a) for value).

This becomes evident as shown in Fig. (17.a), where the mode occupations for the input and two signal modes become populated for both situations. Qualitatively, both simulations show a similar behavior with the main difference that the down-conversion from the input pump mode 1 into the signal modes is less effective for the simulation that includes the bath modes and the maximum of the down-converted

number of photons (i.e. amplitude of $n_2(t)$ and $n_3(t)$) occur slightly later. We note that propagating for a longer time, the simulation with bath modes will differ more strongly. Also, for a simulation time that is not too long to encounter the unphysical revival time due to having only a finite number of modes [171], the photon occupations would eventually relax to the ones of the coupled matter-photon ground-state (see Chap. 3.6.3). In the weak coupling case considered here, the occupations for the signal modes are effectively zero and at this point the photons are considered emitted. Our numerical setup does not simulate the full emission process, thus, to account for the emitted photons we assume that the maximum amount of photon occupation observed in the signal modes corresponds to what would be detected outside of the system. We note that the simulation that includes the bath modes do not change the maximum photon occupations strongly even for this weak coupling case where the bath contributes considerably. This implies that the simulation without the bath is a justified approximation provided we do not go beyond the coherence time of roughly 40 picoseconds (ps). Coherence time as utilized here means the time interval in which the bath-free (fully coherent) simulation is a good approximation to the simulation that includes the bath. It is important to note that increasing the coupling to the bath modes (stronger dissipation) the coherence time would be shorter, however, coupling stronger to the input and signal modes while keeping the bath modes fixed the coherence times would be longer. This highlights how to potentially obtain longer coherence times. Simulating explicitly $(70 + 3)$ modes coupled to the electronic system is numerically very expensive and would not allow for all the different cases of the down-conversion processes that we investigate in this chapter. To fairly compare all the different cases that we will investigate below, we therefore consider all the simulations without coupling to the bath modes and choose a coherence time of about 40 ps. We chose this number since QRs are known to have long coherence times on the order of ps, after which other dissipation channels destroy the coherence [161]. This analysis circumvents the use of (numerically expensive) non-unitary master-equation approaches to approximately treat the effect of the photon bath modes on the internal system [172] or to keep the bath explicitly as done above in our following considerations [2].

Since an important feature of the down-conversion process is the character of the generated photons, we consider the Mandel Q_α parameter (see Eq. (335)) to determine the statistics of the down converted photons. In Fig. (17.b), we observe that both simulations agree qualitatively and remain close for the simulated 40 ps. This demonstrates that the bath-free simulations capture qualitatively more complex properties of the generated photons. Since we will consider strong coupling to the relevant photon modes, the influence of the bath modes in these simulations will become less important. This as well holds true when we consider many input photons and classical external pumping.

2 As a side remark, we could avoid solving here the explicit correlated wavefunction by employing QEDFT. This can be achieved by sampling the photon bath with thousands of modes and employ the time-propagation method of QEDFT (see Chap. 3.5.3 for details) which includes all orders of the response. We will then only need to extract the desired order. However, since we have only the pRPA contribution of the v_{Pxc} potential, some observables such as the Mandel Q_α parameter will not be captured at this level of approximation.

4.1.4.2 *Temporal control of down-converted photons*

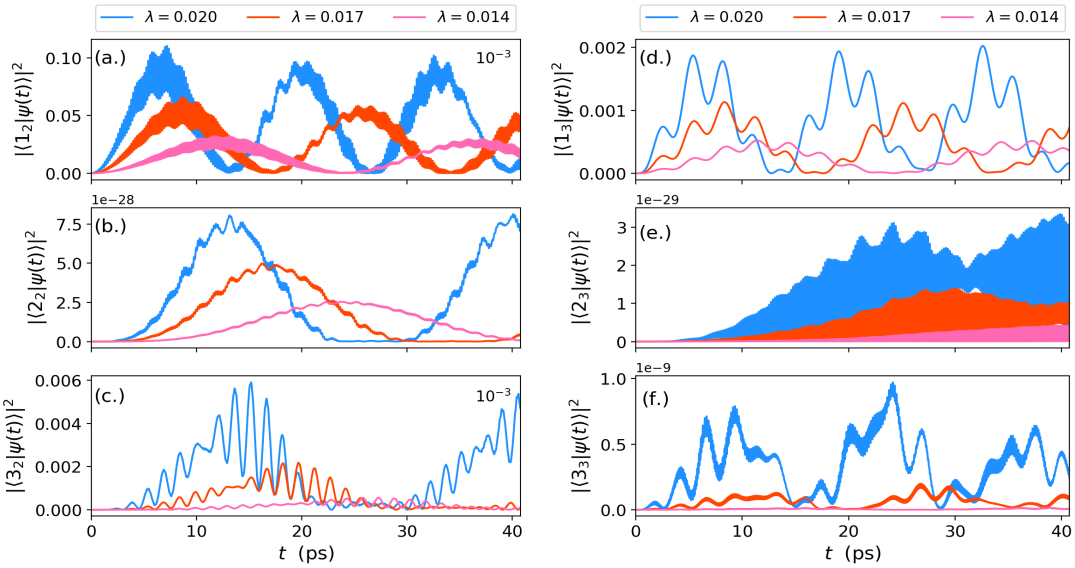

Figure 18: Real-time Fock state populations of the one-, two- and three-photon Fock states of signal modes 2 and 3 from weak (pink solid line) to ultra-strong coupling (blue line). In panels (a.)-(c.) and (d.)-(f.) of the respective modes 2 and 3, the one-photon Fock state dominates for a single photon in the input mode therefore signifying single-photon down-conversion in this modes.

In the previous section, we showed how the initially excited pump field with mode occupation of 1 populates the signal fields as their mode occupations become non-zero through out the 40 ps time evolution. However, this does not necessarily imply that two photons with energies $\hbar\omega_2$ and $\hbar\omega_3$ have been down-converted from a single photon of energy $\hbar\omega_1$. In order to make such analysis we need to compute the populations of the different Fock number states in each of the relevant modes. This is necessary because it could be that also the 2 and 3 photon states are populated in the down-conversion process. This then implies that higher-order processes play a role that would not be easily identifiable as a PDC process. To identify the down-conversion process we calculate the populations $|\langle \hat{n}_\alpha | \Psi \rangle|^2$ where we consider the populations of the one- up to the three-photon Fock states. In Fig. (18) we find that the process is indeed a PDC process since only the one-photon states have significant population throughout the simulation for the down-converted photons. Increasing the coupling strength from the weak to the ultra-strong coupling regime does not imply a priori that only the single-photon processes is still dominant and no higher-order (multi-level/multi-photon) contributions become important. The coupling λ is varied by changing the effective cavity length L (see also Fig. (16.a)) which also leads to modified effective coupling strengths g_α (see Tab. 3 for detail values), while the bare dipole transition elements stay unchanged. In Fig. (19.c) we find that the amount of photons in the signal modes can be increased considerably by increasing the coupling strength. This highlights that the effective coupling strength plays an important role for the efficiency of the PDC process in an ab-initio description. This also illustrates how strongly light and matter mix and how the matter-only eigen-

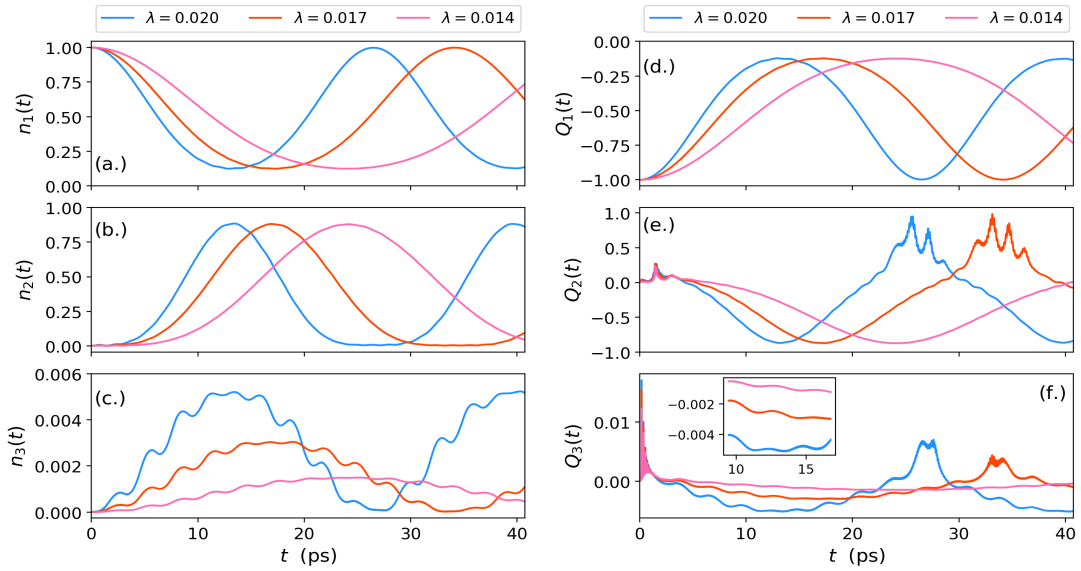

Figure 19: Photon occupations and Mandel Q_α shown in real-time for the input mode $n_1(t)$ initially in a single-photon Fock state from weak to ultra-strong coupling. (a.) shows the loss of occupation in mode 1 as it is down-converted into signal photons $n_2(t)$ and $n_3(t)$ in (b.) and (c.), respectively. The panels (d.) show the photon statistics as mode 1 has sub-Poissonian photon statistics for the entire evolution, (e.) strong anti-bunching as well as bunching features of signal mode 2 and (c.) mode 3 is close to a coherent state throughout the PDC process. In all cases the coupling strength shifts the appearance of the different features to earlier times.

states hybridize with the photon states to create new pathways potentially beneficial for the PDC process. This has been demonstrated in several works [13, 27] where the vacuum field of the modes can break the rotational symmetry and therefore g_α can be increased by changing the photonic environment. We note that even though the dipole moments are not the only quantity that describes how light and matter interact in this coupling regime, they however provide an intuitive picture for the PDC process. Also, the coupling g_α can be increased irrespective of a weak dipole moment (see Eq. (384)) by changing the photonic environment (decreasing length L) and with this the photon-photon couplings $g_1 * g_2, g_1 * g_3, g_2 * g_3$ between the modes increases. These terms arise due to the induced diamagnetic currents and are an often disregarded but yet are important contribution in many light-matter phenomena [43, 44, 102]. Also they are necessary for boundedness of the Pauli-Fierz Hamiltonian in dipole approximation as discussed in Chap. 3.1.

We now highlight an important effect that arises by varying from weak to the ultra-strong coupling regime. In Figs. (18) and (19), we consistently observe that for stronger couplings, the down-conversion of photons occurs at earlier times. Taking note of the coherence time of 40 ps, we can potentially overcome the undesired dissipative processes by strong and ultra-strong coupling. Formulated differently, by shifting the creation of the down-converted photons to earlier times by coupling stronger, while the coupled system is still coherent gets rid off undesired dissipative processes that is expected to show up after the coherence time. Interestingly this feature also shows up in other observables such as non-classicality and entanglement of the photons. Take for example the non-classicality of the different photon modes

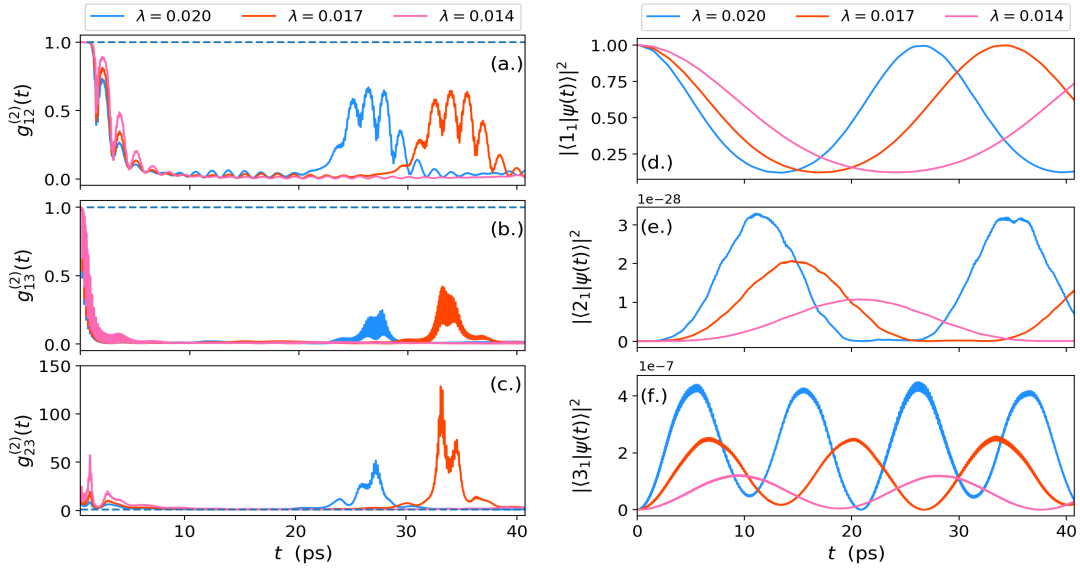

Figure 20: The real-time cross-correlation between the pump and signal modes for the input single-photon Fock state. The dashed line indicates when the modes are correlated (above the dashed line) or anti-correlated (below the dashed line). Panels (a.) and (b.) show that the pump and signal modes 2 and 3 are anti-correlated. (c.) The down-converted photons of modes 2 and 3 are correlated for the whole evolution. In panels (d.) to (f.), the single-photon Fock state of the input mode is shown to have significant population when compared to the two- and three-photon Fock states.

by considering the Mandel Q_α parameter. In Fig. (19.b), we also find that the time of appearance of non-classical features can be controlled by the coupling strength, i.e., varying from the weak to ultra-strong coupling regime. This feature carries on to the intensity cross-correlation functions (see Fig. (20.a-c)) as they show how the photon in mode 1 is anti-correlated with respect to the signal modes, while the signal modes are strongly correlated for the entire time-evolution. It is important to note that the single-photon Fock state of the input mode is the dominant contribution in the down-conversion as it is shown to have significant population when compared to the two- and three-photon Fock states as in Fig. (20.d-f). This becomes evident by contrasting Figs. (19.a-c) and (20.d-f), respectively. Even though the emission of the down-converted photons from the photonic environment is not modeled here, we expect that controlling the timing of the generation process of the down-converted photons by varying the coupling strength will have a direct impact on the features of the emitted photons. This is expected for a simple description of an instantaneous emission where the features of the generated signal photons are carried over to the emitted signal photons. It is still not certain whether these features are only there for the ideal and in practice highly-demanding choice of a single photon in mode 1 and whether also the temporal control of these features is lost with another initial state or when the pump mode is replaced by a classical external pump field, i.e., a laser. In the next section, this question is clarified by replacing the input mode initially in a single-photon Fock state by a field in a coherent state.

Coupling	weak	strong	ultra-strong
L (μm)	100	50	30
λ	0.014	0.020	0.026
g_1	0.00675	0.00954	0.01232
g_2	0.02875	0.04065	0.05249
g_3	0.00694	0.00981	0.01267
$g_1 * g_2$	0.00019	0.00039	0.00065
$g_1 * g_3$	0.00005	0.00009	0.00016
$g_2 * g_3$	0.00020	0.00040	0.00067

Table 3: The electron-photon coupling strengths by varying the cavity length/mode volume. The coupling strengths $g_\alpha = \lambda\sqrt{\hbar/2\omega_\alpha}$ are different for coupling to different different modes of frequency ω_α. Decreasing the cavity length L increases the coupling strengths g_α and their respective products. The coupling strengths are given in scaled effective atomic units as presented in Chap. 4.1.1.

4.1.5 INPUT MODE IN A COHERENT STATE

In the previous section, we investigated the PDC process using a single-photon Fock state as input field (mode 1). In reality, generating a single photon in a specific mode is highly challenging, and due to the usually low efficiency of the PDC process it is also not easy to observe such a process. So in practice, the number of photons in the pump field has to be increased to observe any down-converted photons. This implies that more than one photon is in the pump mode 1 at the initial time, however, it is not clear how this will change the main features observed for the single-photon input mode case above. Thus, we now consider how a change in the initial state influences the different observables.

Now, the pump mode is initially prepared in a coherent state $|\phi_1\rangle = |\xi_1\rangle$ and thus, its vector potential has the strength $\langle\xi_1|\hat{A}_1|\xi_1\rangle = \lambda\sqrt{2\hbar/\omega_1}|\xi_1|$ while that of the signal modes are zero at the beginning. We choose the amplitude $\xi_1 = 2$ such that the mean photon number $n_1(0) = \langle\hat{a}_1^\dagger\hat{a}_1\rangle = |\xi_1|^2 = 4$ at the initial time. This choice just slightly changes the occupation at the initial time and is already sufficient to no longer identify in a simple manner the usual PDC as one photon being down-converted to two photons, as we now have many photon states that mix. In Fig. (21), we find that the two- and three-photon states are also relatively strongly occupied. This is evident in Fig. (21.a & b) in which the second-Fock state populations are an order of magnitude larger than the ones of the single-photon Fock states. The second-Fock state of mode 3 in Fig. (21.e) is weakly populated due to coupling to a non-dipole allowed transition. We find changes in the total mode occupations as can be seen in Fig. (22.a-c). Comparing to the one-photon case in Fig. (19.a-c.), we observe that the mode occupations qualitatively remain the same and also the feature of faster down-conversion for stronger coupling is retained. We however observe changes in the photon statistics especially for the input mode 1 when compared to the single-photon

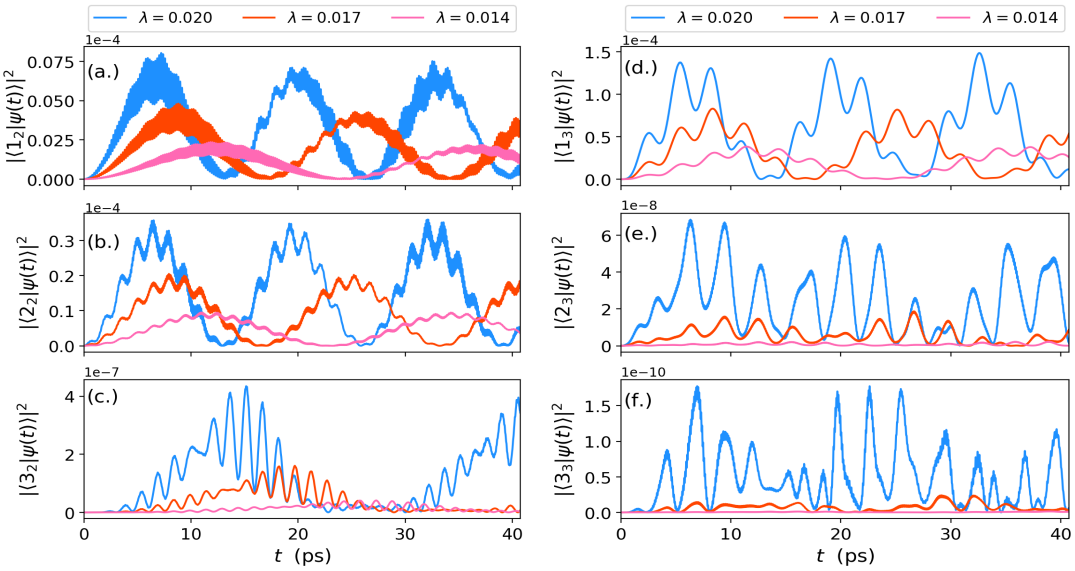

Figure 21: Real-time Fock state populations of the signal mode 2 and 3 from weak to ultra-strong coupling for the input coherent state. For mode 2, the two-photon Fock state in (b.) is mostly populated in comparison to the one- and three-photon Fock states in (a.) and (c.), respectively. For mode 3, in panel (d.) the one-photon Fock-state is mostly populated compared to the two- and three-photon Fock states in (e.) and (f.), respectively.

case(see Fig. (19) and (22)). As shown in Fig. (22.d-f), the anti-bunching behavior of mode 2 is increased and mode 3 becomes non-classical for a short time and later shows classical features.

Furthermore in Fig. (23.a,b), we observe a switching between anti-correlation and correlation in time. This change can be justified since we have now several photons in the initial state and the simple picture of one photon annihilated in mode 1 and one photon created in mode 2 and 3 respectively, is no longer straightforward. Simultaneously, the down-converted photons remain correlated throughout as in Fig. (23.c). Conservation of energy and momentum in this cascaded process leads to correlations, implying energy-time entanglement [173] which is important for on-demand generation of entangled photon pairs [148, 149]. This interpretation becomes more clear when we consider the purity γ_α to account for the measure of entanglement in the present case. We show in Fig. (23.d-f) the different modes start out uncorrelated (as $\gamma_\alpha = 1$) and become entangled over time since $\gamma_\alpha(t) < 1$. The entanglement and its time profile can equally be controlled by the coupling strength and pushed to earlier times as well.

So far, we have highlighted new possibilities in the down-conversion process that arise due to treating both the light and matter on an equal quantized footing. For example, we showed how the down-conversion process can be influenced by manipulating the photonic environment (increasing coupling strength) to have faster down-conversion that can overcome decoherence effects. Also, we showed new observables that become accessible due to this level of theory like the mode occupation (e.g. Fig. (22.a)), photon statistics (e.g. Fig. (22.d)), purity measure (e.g. Fig. (23.d)) of the pump mode as well as cross-correlation between the pump and signal modes (e.g.

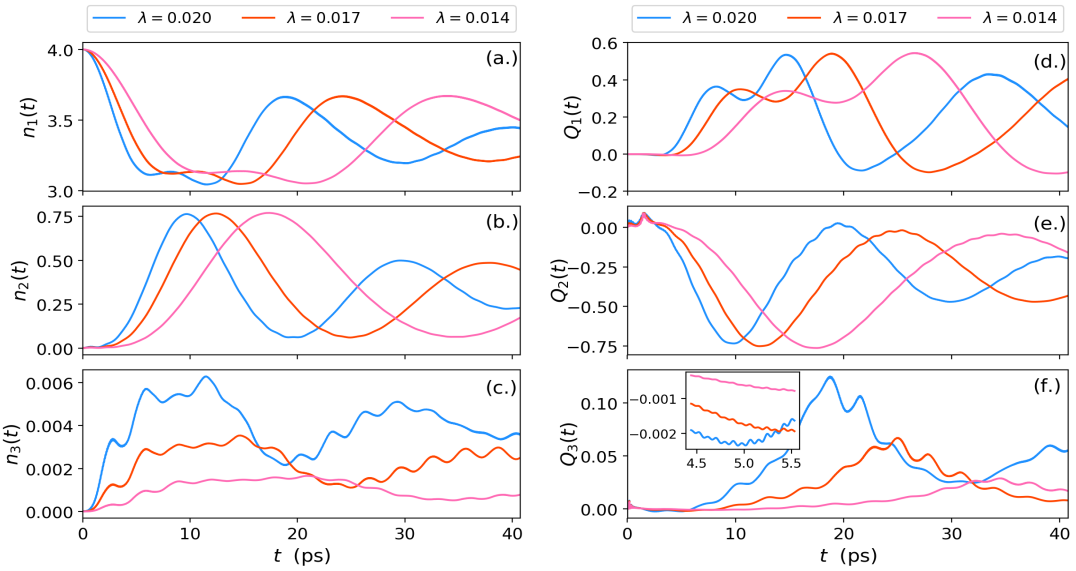

Figure 22: The real-time photon occupations and Mandel Q_α of the input mode $n_1(t)$ initially in a coherent state shown from weak to ultra-strong coupling. (a.) photons from $n_1(t)$ are down-converted into signal photons $n_2(t)$ and $n_3(t)$ in (b.) and (c.), respectively. The photon statistics of the down-conversion shows that mode 1 varies from fields with Poissonian, super-Poissonian and sub-Poissonian statistics as in (d.), strong anti-bunching feature for mode 2 as in (e.) and (c.) shows the emitted photon in mode 3 is non-classical for a brief time interval with maximum non-classicality of $Q_3 = -0.0025$ at $t = 4.93$ (ultra-strong coupling) ps as shown in the inset. In all cases the coupling strength shifts the appearance of the different features to earlier times.

Fig. (23.a and b)). We observed that the main features of the down-converted photons are qualitatively similar when the input mode is populated with a single-photon Fock state or a coherent state with few photons. We now want to investigate whether these features are affected when we drive the coupled system with an external classical field or external current. This is important in this case since it will show that our results are robust and do not depend on small details of the setup.

4.1.6 CLASSICAL INPUT FIELDS

Now, to investigate the down-conversion process from the coupled system with an external classical field, we have two possible choices from an ab-initio perspective. In one case the external field couples to the matter subsystem and its induced currents generate photons in the respective signal modes and in the other case an external current that couples directly to the input mode can be used to excite the mode and the down-conversion occurs. These descriptions are similar to that of the linear-response in Chap. 3.2.1 with the difference that these external perturbing fields can be strong such that perturbation theory becomes insufficient. Physically these alternatives should not be too different since they can be connected to each other through Maxwell's equation (see Chap. 3.4 for details). To investigate how these two approaches affect the down-conversion, we in the following consider both cases.

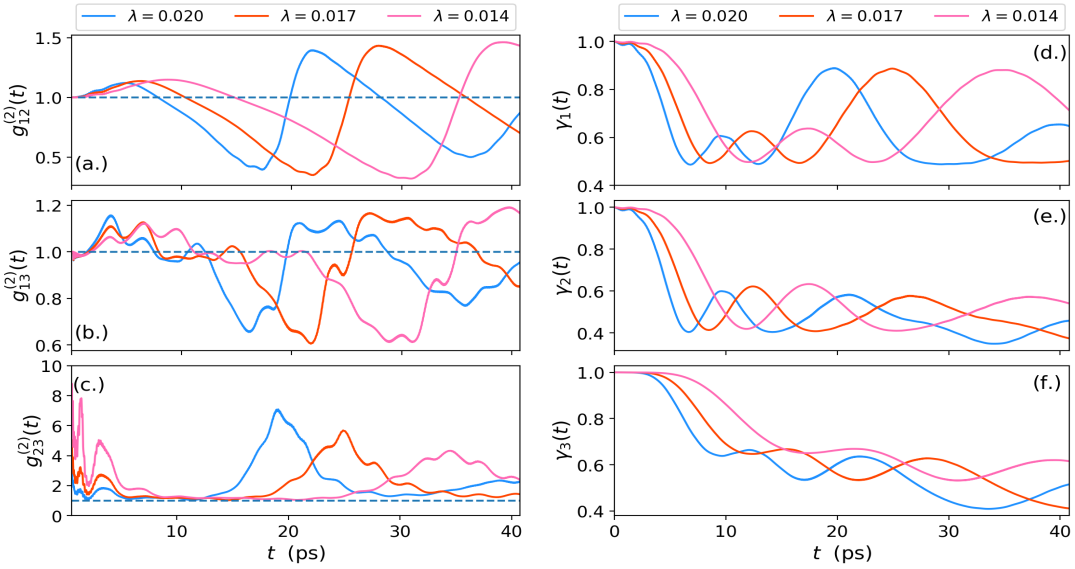

Figure 23: Real-time cross-correlation between the pump and signal modes and their individual purity measures. The dashed line in (a.)-(c.) indicates when the modes are correlated (above the dashed line) and anti-correlated (below the dashed line). In panels (a.) and (b.) we have correlation and anti-correlation between the pump and signal photons at different times. (c.) The generated photon pairs of modes 2 and 3 are time-entangled for the whole evolution. In (c.), we disregard the time interval between $t = 0$ and $t = 0.58$ ps due to finite numerical precision. For the three modes in panels (d.)-(f.), signal mode 2 is most entangled, signal mode 3 is intermediate, and pump mode 1 is least entangled. In addition, by increasing the coupling from weak to ultra-strong not only changes the entanglement profile but also makes the modes more entangled.

We first start with the common approach which is choosing some external electromagnetic field that drives the matter subsystem. This approach is often considered to avoid the need to have three explicit photon modes [155, 174, 175]. This is done in practice by replacing the pump mode 1 by a classical external field and keep the rest of the system's Hamiltonian the same. This is achieved by considering the solution of the mode-resolved Maxwell's equation in Eq. (72) and the Hamiltonian becomes

$$\begin{aligned}\hat{H}'_S(t) = \hat{H}_{2D} + \hat{H}_2 + \hat{H}_3 + \frac{e^2}{2m}\left[\hat{A}_2^2 + \hat{A}_3^2 + 2\hat{A}_3\hat{A}_2\cos(\theta_2+\theta_3)\right] \\ - \frac{e}{m}\left[\hat{A}_2\left(-\hat{p}_x\sin\theta_2 + \hat{p}_y\cos\theta_2\right) + \hat{A}_3\left(\hat{p}_x\sin\theta_3 + \hat{p}_y\cos\theta_3\right)\right] \\ - \frac{e}{m}A_1(t)\,\hat{p}_x + \frac{e^2}{2m}\left(A_1^2(t) - 2A_1(t)\hat{A}_2\sin\theta_2 - 2A_1(t)\hat{A}_3\cos\theta_3\right). \quad (337)\end{aligned}$$

Here, $A_1(t) = \lambda_1 q_1(t)$ is of the form of Eq. (72) and the external pulse employed here corresponds to the classical field induced by the below defined external source term for the photon field in the case that mode 1 would be uncoupled. For a simple comparison we therefore choose the weak coupling regime of Tab. (3) in the following, otherwise, the form of the external pulse will have to be adapted to expect a reasonable agreement. We note that as a result of treating mode 1 as an external classical field the corresponding observables of this mode become inaccessible in a direct way.

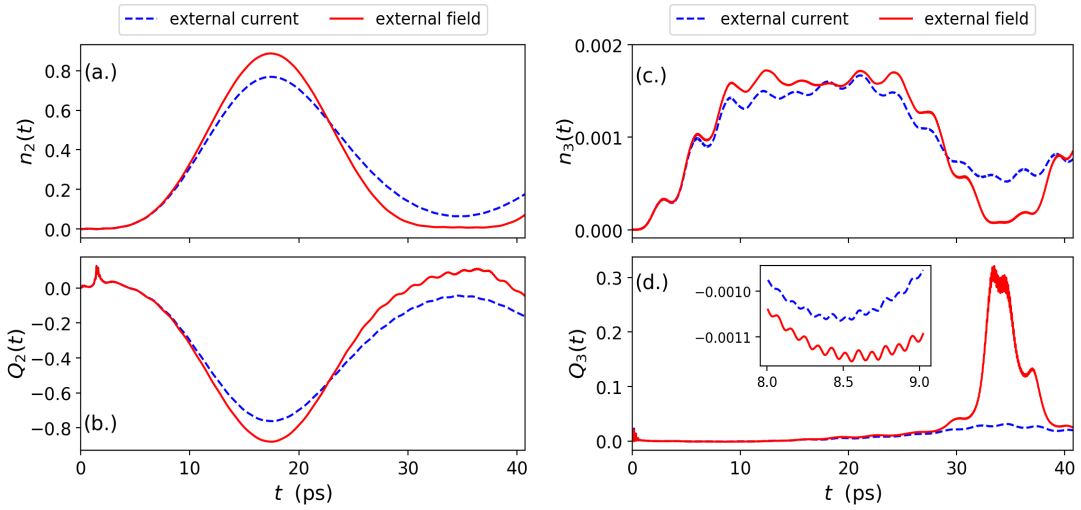

Figure 24: Comparison of the two different external drivings for weak electron-photon coupling $\lambda = 0.014$. In red an external laser pulse is used, and in blue an external current is used to pump mode 1 directly. The pump pulse and the pump current are chosen to be connected via Maxwell's equations such that for weak coupling both lead to similar effects.

In the second approach the input mode 1 is directly excited by an external field, i.e., a source term for the photons (similar as in Chap. 3.2.1). This approach still allows one to investigate properties of the input mode 1. The corresponding Hamiltonian becomes

$$\hat{H}_S(t) = \hat{H}_S + \hat{A}_1 \cdot j_1(t). \tag{338}$$

The external current is an envelope Gaussian field of the following form $j_1(t) = j_1 \exp\left(-(t-t_0)^2/\tau^2\right) \sin(\omega_1 t)$. We choose the parameters of the Gaussian pulse such that at time $t = 0.23$ ps, the pump mode is driven to an excited state with on average $n_1(0) = 4$ photons. We observe that through Maxwell's equation both approaches can be connected to each other through the solution of Eq. (72) (see Chap. 2.3.1.1 for details). For both approaches, the initial state is chosen to be a non-factorizable ground-state of the time-independent parts of the respective Hamiltonians.

In Fig. (24.a,b) we compare both approaches of external driving and find that they both agree qualitatively for the mode occupations and for the Mandel Q_α parameters. However, we find that at later times for Q_3 that they can differ strongly. Next, comparing the external current case to the case of no external driving (i.e. using input mode in a coherent state) and having 4 photons in mode 1 at $t = 0$ instead (discussed in Sec. 4.1.5), we find that the chosen external current qualitatively reproduces this case for the photon occupations and Mandel Q_α as shown in Fig. (25).

From these results, we can conclude that our down-conversion scheme is relatively robust since it qualitatively reproduces the same results when we use as input field; an external classical field or external current or when we use a coherent state.

4.1.7 COMPARISON TO STANDARD APPROXIMATIONS

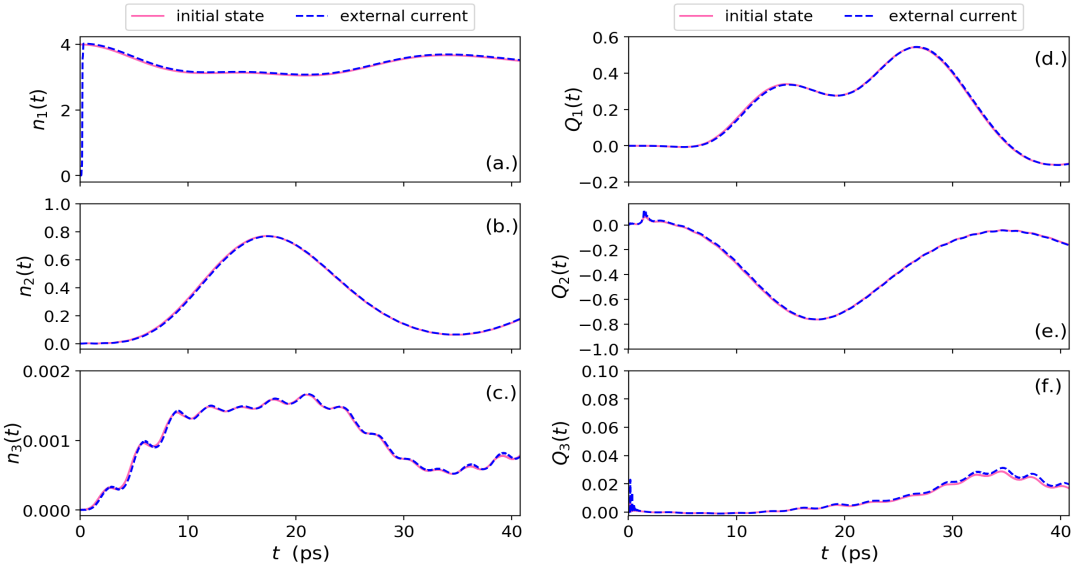

Figure 25: Comparison between an initial coherent state with on average of 4 photons (discussed in detail in Sec. 4.1.5) and an external current that simulates the creation of these 4 photons for weak coupling $\lambda = 0.014$. In (a.) at $t = 0.23$ ps, 4 photons are readily excited by the external current $j_1(t)$. The external current and initial state are qualitatively the same for the entire profile of the mode occupations and Mandel Q_α for panels (a.)-(f.).

We have so far presented the down-conversion from an ab-initio description of light-matter interaction from the weak to the ultra-strong coupling regime. However, it is important to contrast this description (ab-initio theory of strong light-matter interaction) to standard approaches employed to theoretically investigate the down-conversion process. Such a comparison is expected to highlight shortcomings of these approaches in some situations since the level of theory considered in these approaches can be deduced from the non-relativistic QED description (see Chap. 2.2 for details). As most of the observables in the down-conversion as described above stay relatively unchanged, the question arises is it possible to capture these effects also with standard approaches? The different approaches are the above mentioned quantum-optical method based on the few-level approximation and semi-classical approaches which is employed in non-linear optics.

The few-level approximation considers only a few relevant matter states in contrast to the large amount of states that are usually considered in ab-initio simulations [176]. In an ab-initio simulation, one considers as many states as possible until either the observables of interest or even the full wavefunction does not change. Ignoring the issue of the convergence of the basis-set, one can rather consider only a few "relevant" matter states, which can be determined from the Hamiltonian given in Chap. 4.1.7. An application of the few-level approximation (i.e. the Rabi and Jaynes-Cummings models) is discussed in the linear-response regime in Chap. 3.6.1.1. In this section, the four highlighted energy levels shown in Fig. (16.b) are considered which by simple energy arguments are the most relevant states for the down-conversion process considered here. Applying such a simplification to the electronic subsystem discards the possibilities of the existence of other hybridized polariton and virtual states that

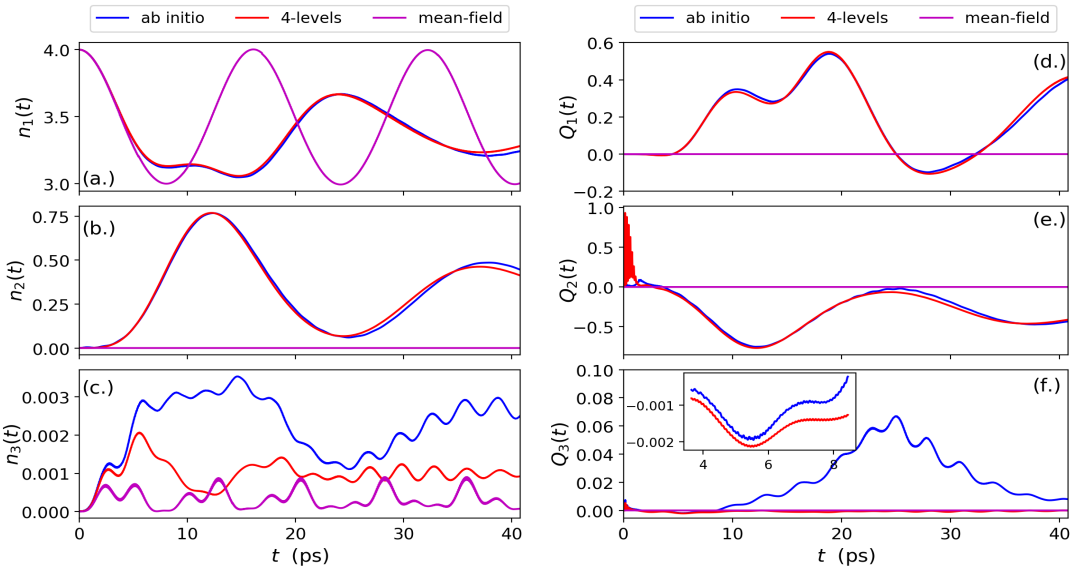

Figure 26: Performance of few-level and Maxwell-Schrödinger approximation in comparison to the numerically exact electron-photon case. In (a.) and (b.) the few-level approximation is relatively accurate while the Maxwell-Schrödinger approximation is qualitatively correct only up to $t = 5$ ps. In (c.) both approximations are qualitatively off and do not capture the occupation of mode 3. While the few-level approximation captures the Mandel Q_1 in (d.) quite well, it is wrong initially for Q_2 in (e.) and wrong for Q_3 in (f.). As expected, the Maxwell-Schrödinger approximation does not capture the quantum features of the photon field in (d.)-(e.).

occur in an ab-initio treatment when the quantized field is coupled to the full matter subsystem. The few-level approximation considered here differs from the usual few-level approximations [156, 176] since we include the mode-mode interactions that arise from the diamagnetic term. Ignoring these terms will lead to results that differ since part of the full current in a matter-photon system is eliminated

For non-linear optics, the semi-classical approximation (see Chap. 2.3 for details) is employed and the focus is on, for example, non-linear matter-only response functions. However, for the two-photon down-conversion considered here with the QR as medium the second-order non-linear susceptibility is zero [159] at the employed frequencies and thus no further conclusions could be drawn. We therefore go beyond the usual semi-classical approximation (see Chap. 2.3.1) and employ an adapted Maxwell-Schrödinger approximation [85], which is an approximation commonly used in the field of non-linear optics. This approximation replaces the quantized photon field by its mean-field expression such that the problem reduces to solving self-consistently the Maxwell's equation coupled to a Schrödinger Hamiltonian (see Chap. 2.3.1 for details). In the case of Eq. (334), this leads to a set of coupled non-linear equations

$$\begin{aligned} i\hbar\frac{\partial}{\partial t}\varphi(\mathbf{r},t) &= \hat{H}_{\mathrm{MS}}([q_\alpha],t)\varphi(\mathbf{r},t)\,, \\ \left(\frac{\partial^2}{\partial t^2}+\omega_\alpha^2\right)q_\alpha(t) &= j_\alpha([\mathbf{p},q_\alpha],t)\,. \end{aligned} \tag{339}$$

Where $\varphi(\mathbf{r},t)$ is the wavefunction of the matter subsystem and the Maxwell-Schrödinger Hamiltonian is

$$\hat{H}_{\mathrm{MS}}([q_\alpha];t) = \hat{H}_{\mathrm{2D}} - \frac{e\lambda_1}{m} q_1(t)\hat{p}_x - \frac{e}{m}\left[\lambda_2 q_2(t)\left(-\hat{p}_x\sin\theta_2 + \hat{p}_y\cos\theta_2\right) + \lambda_3 q_3(t)\left(\hat{p}_x\sin\theta_3 + \hat{p}_y\cos\theta_3\right)\right].$$

The current $j_\alpha(t)$ that self-consistently couples the mode-resolved Maxwell fields to the electronic subsystem are given explicitly as

$$\begin{aligned}
j_1([\mathbf{p},q_\alpha]) &= \frac{e\lambda_1}{m}p_x(t) + \frac{e^2}{m}\left[-\lambda_1^2 q_1(t) + \lambda_2\lambda_1 q_2(t)\sin\theta_2 + \lambda_3\lambda_1 q_3(t)\sin\theta_3\right],\\
j_2([\mathbf{p},q_\alpha]) &= \frac{e\lambda_2}{m^*}(-p_x(t)\sin\theta_2 + p_y(t)\cos\theta_2)\\
&\quad + \frac{e^2}{m}\left[-\lambda_2^2 q_2(t) + \lambda_2\lambda_1 q_1(t)\sin\theta_2 - \lambda_2\lambda_3 q_3(t)\cos(\theta_2+\theta_3)\right],\\
j_3([\mathbf{p},q_\alpha]) &= \frac{e\lambda_3}{m}(p_x(t)\sin\theta_3 + p_y(t)\cos\theta_3)\\
&\quad + \frac{e^2}{m}\left[-\lambda_3^2 q_3(t) + \lambda_3\lambda_1 q_1(t)\sin\theta_2 - \lambda_3\lambda_2 q_2(t)\cos(\theta_2+\theta_3)\right].
\end{aligned}$$

Here we have included in the Maxwell-Schrödinger approximation also the mean-field mode-mode interactions (and with this the diamagnetic current). Ignoring these terms, as usually done makes the Maxwell-Schrödinger approximation less accurate. As a side remark, the Maxwell-Schrödinger approximation is similar to the pRPA employed in Chap. 3.5.4 since the pRPA neglects all xc contributions of the explicit matter-photon interaction terms. Therefore, the Maxwell-Schrödinger can be viewed as the simplest approximation that can be used within QEDFT. If one was to employ QEDFT, only the electron density and the expectation value of the displacement coordinate are directly accessible and all other observables attain a non-trivial form in terms of these quantities [12, 13, 22, 91].

Although the PDC is well described for the weak-coupling situation considered here, in the strong-coupling case where hybrid light-matter states emerge, it is expected to be less reliable. An example of this is the case of the linear-response in the ultra-strong coupling regime where the Rabi splitting becomes less reliable for the pRPA (see Chap. 3.6.1.2 and Fig. (6) for details). In Fig. (26) we depict a comparison of the down-conversion process in the strong coupling regime (i.e. $\lambda = 0.017$) of the few-levels and Maxwell-Schrödinger approximation to the exact solution. In this few-photon strong-coupling limit, the Maxwell-Schrödinger approximation fails for all the observables shown. Since the quantum features of the electromagnetic field are essential for describing the down-conversion process [153], the Maxwell-Schrödinger theory (mean-field-type approach) is incapable of capturing these features. Nevertheless, if the number of photons are increased the Maxwell-Schrödinger theory becomes much more accurate such that in the limit of arbitrarily many photons the full ab-initio theory becomes essentially equivalent to the Maxwell-Schrödinger theory. Therefore, this level of theory can be used to assess how increasing the number of input photons affects the down-conversion process (see Sec. 4.2.3).

Also, in Fig. (26.e,f) we observe that the usual few-level approximation is not completely reliable as well. The reason in this case is due to the non-dipole allowed

transition in resonance with mode 3. And in this case many more levels that would have had a contribution to the down-conversion into mode 3 have been eliminated. This highlights that reducing the matter system to just a few electronic states leads to less accurate results.

4.2 OPTIMIZATION OF THE DOWN-CONVERSION: THE DEGENERATE CASE

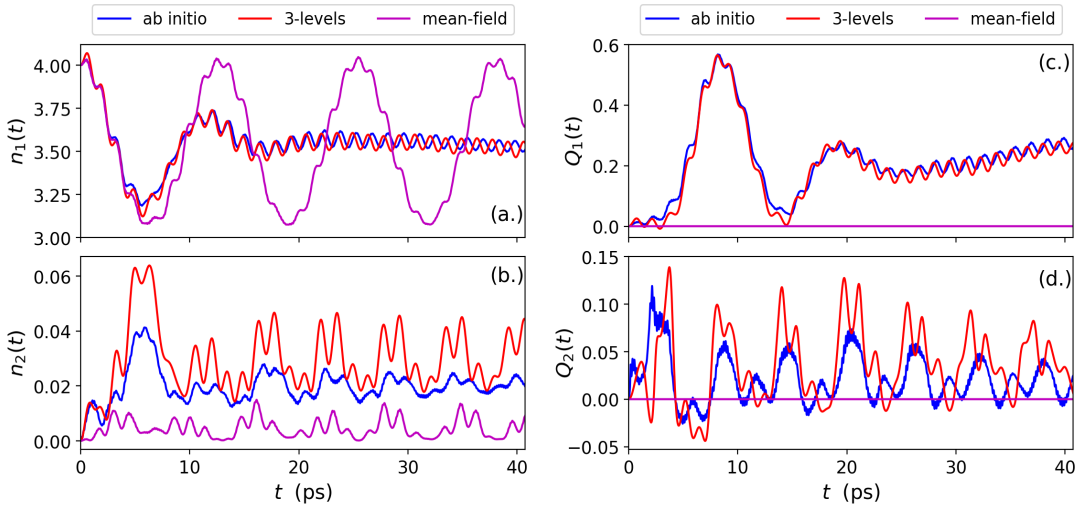

Figure 27: Example of the degenerate two-photon down-conversion process in the strong coupling regime ($\lambda = 0.017$) and for a mixing angle of $\theta_1 = 60°$. (a.) The 3-level approximation qualitatively captures the full dynamics of $n_1(t)$, while the Maxwell-Schrödinger description deviates around $t = 5$ ps for the entire dynamics. (b.) Associated $n_2(t)$ of down-converted photons where both approximations are off from the ab-initio result. (c.) The 3-level approximation qualitatively captures the full dynamics of $Q_1(t)$, while the mean-field is zero for the full simulation by construction. (d.) The 3-levels and Maxwell-Schrödinger approximations are off for the complete time evolution.

In the previous sections, we investigated the down-conversion process from an ab-initio light-matter description and showed that for stronger coupling the down-conversion of photons can be pushed to occur at earlier times which can potentially help to overcome dissipation and decoherence. Also we showed that the features of the down-converted photons are qualitatively similar irrespective of how we pump the system, i.e., either with an external classical field or external current or initial states (one-photon and coherent state). We now want to further explore the proposed cavity down-conversion setup to find an optimal setting for generating, on one hand, an efficient polariton-mediated down-conversion process, and on the other hand, non-classical and controlled down-converted photons. Non-classical down-converted photons as used here is identified by the minimum negative value of the Mandel Q_α parameter. Such a polariton mediated down-conversion will highlight new possibilities of defining novel photon sources such as an N-photon gun.

For this investigation, we consider the degenerate down-conversion case, i.e., mode 2 and 3 have the same frequency. Due to the degeneracy in energy, we decouple signal

mode 3 from Eq. (334) and the down-converted photons now populate only mode 2. The polarization of signal mode 2 is set as $\hat{\mathbf{A}}_2 = \hat{A}_2 \mathbf{e}_y$ by choosing $\theta_2 = 0°$ and changing the polarization of the pump field to $\hat{\mathbf{A}}_1 = \hat{A}_1(\cos\theta_1 \mathbf{e}_x + \sin\theta_1 \mathbf{e}_y)$ where θ_1 is the mixing angle between the photonic and electronic subsystems. The Hamiltonian of Eq. (334) now reduces to the two-mode electron-photon Hamiltonian

$$\hat{H}_D = \hat{H}_{2D} + \hat{H}_1 + \hat{H}_2 - \frac{e}{m}\hat{A}_1\left(\hat{p}_x \cos\theta_1 + \hat{p}_y \sin\theta_1\right) - \frac{e}{m}\hat{A}_2\hat{p}_y + \frac{e^2}{2m}\left[\hat{A}_1^2 + \hat{A}_2^2 + 2\hat{A}_1\hat{A}_2 \sin(\theta_1)\right]. \tag{340}$$

Since we showed that increasing the coupling strength pushes the down-conversion process to earlier times, here we consider its maximal efficiency and minimum Mandel Q_α parameter in mode 2. To find the optimal setup, we will vary the polarization directions (see Sec. 4.2.1), the anharmonicity of the binding potential of the QR (see Sec. 4.2.2), and the coupling strength as well as the number of input photons (see Sec. 4.2.3). In order to judge the efficiency of the down-conversion we consider the maximal amount of mode occupation $n_2^{(\max)}$ (except of in Sec. 4.2.3 where we take a more general definition) over the range of the first 40 ps. For the non-classicality we determine the smallest value of $Q_2^{(\min)}$ over the same time interval.

We simulate the time-evolution dynamics of the ab-initio system, the three-level approximation and the self-consistent Maxwell-Schrödinger approximation in the strong-coupling regime ($\lambda = 0.017$). The initial state is a factorizable product state of the electron in its ground-state, mode 2 in its vacuum state and the pump mode 1 is a coherent state with $n_1(0) = 4$ photons (i.e. amplitude $\xi_1 = 2$). For degenerate two-photon generation considered here, the pump field with energy $\hbar\omega_1 = 1.413$ meV drives resonantly the transition between the ground- and first-excited state $|\varphi_1^0\rangle \leftrightarrow |\varphi_2^1\rangle$, which populates the state $|\varphi_2^1\rangle$. The energy of the signal mode $\hbar\omega_2 = 0.706$ meV is half that of the transition $|\varphi_1^0\rangle \leftrightarrow |\varphi_2^1\rangle$ which indicates a two-photon process. As the coupling $g_1 = 0.0398$ of the pump mode is less than the coupling $g_2 = 0.0563$ of the signal mode, the electron in the first-excited state $|\varphi_2^1\rangle$ preferably relaxes to the ground-state through a two-photon emission channel via a virtual state. From a standard perspective, this process should be very inefficient if one looks only at the dipole moments that are involved. However, as we will show that tuning the frequency of the signal mode in resonance to a virtual state leads to the creation of hybrid light-matter states that can efficiently mediate the down-conversion of the input photons.

In Fig. (27), we show the results for photon occupations and Mandel Q_α parameters of the pump photon for a mode-mixing angle $\theta_1 = 60°$ and the degenerate down-converted photons in signal mode 2. Some details for the ab-initio results of the profile $n_1(t)$ show that at $t = 5.61$ ps, 0.82 of a photon is annihilated by an absorption process to promote the electron to the state $|\varphi_2^1\rangle$. At a later time $t = 5.84$ ps, the electron subsequently relaxes to the ground-state via the virtual state by emitting two photons with maximum mode occupation $n_2 = 0.041$. This apparent weak profile for $n_2(t)$ is due to emission via virtual states and can be increased by increasing the effective coupling strength. For the photon statistics, the pump field starts out in a coherent state and leads to a field with super-Poissonian statistics (see Fig. (27.c)) while that of the generated photon pair varies between a field with bunching and

anti-bunching features at different times, with the minimal value of $Q_2 = -0.0199$ at $t = 4.94$ ps (see Fig. (27.d)). Now comparing the few-levels approximation (in this case we only take three states into account) to the ab-initio case, we find in Fig. (27.a,b) that it is relatively accurate, while the Maxwell-Schrödinger performance is qualitatively correct only up to $t = 5$ ps and by construction it remains a coherent field for the entire evolution with constant $Q_1 = 0$. Both approximations deviate from the ab-initio result in Fig. (27.b,d). We observe that the three-level approximation consistently overestimates the down-conversion efficiency including the varying statistics of the photons in mode 2 (due to reducing the matter to three-levels), the Maxwell-Schrödinger approximation under-estimates these quantities. We note that for the Mandel Q_α parameter this is by design and for the down-conversion efficiency the Maxwell-Schrödinger neglects all the correlation between light and matter that becomes beneficial in the strong coupling regime.

This ab-initio down-conversion scheme is indeed an inverse second-harmonic generation by coupling the signal mode to a virtual state at half the energy of the first degenerate excited state $|\varphi_2^1\rangle$. This is, however, not the only case. We show the case of the third-, fourth- up to eleventh-photon generation (see Sec. 4.3) thereby introducing the concept of inverse high harmonic generation for realizing an $N-$photon gun. The system can be tuned in an experimentally realizable way such that this setup can potentially be used as an $N-$photon source with highly non-classical properties. In the following section, we discuss the optimization for the inverse second-harmonic generation process.

4.2.1 OPTIMIZATION OF FIELD POLARIZATION

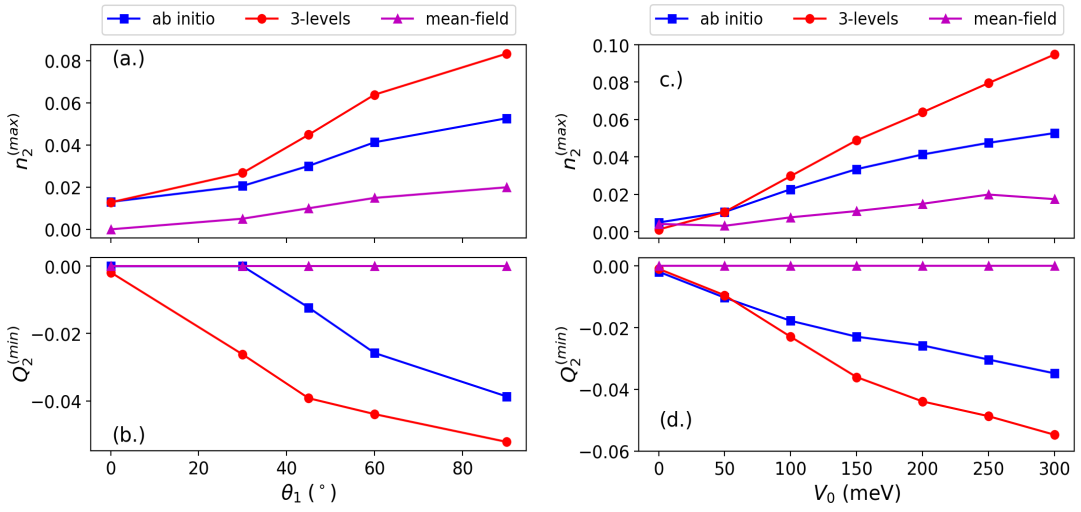

Figure 28: (a.) The influence of the interference term in photon-pair generation by varying the mixing angle θ_1. Increasing θ_1 increases the photon occupation. The 3-levels and Maxwell-Schrödinger approximations are off from the exact results. (b.) Increasing the mixing angle θ_1 results in increasing sub-Poissonian statistics (anti-bunching) of the down-converted photons.

θ_1 (°)	Exact $n_2^{(\max)}$	Exact $Q_2^{(\min)}$
0	0.0130	0.0
30	0.0206	0.0
45	0.0301	−0.0123
60	0.0413	−0.0258
90	0.0527	−0.0387

Table 4: The numerically exact real-space values for maximum $n_2^{(\max)}$ and minimum Mandel $Q_2^{(\min)}$ for different mixing angles. Increasing θ_1 increases $n_2^{(\max)}$ and decreases $Q_2^{(\min)}$.

First, we consider which relative polarization is most efficient to obtain a large n_2 and simultaneously minimizes Q_2 (most negative value for antibunching). In our setup this implies that we consider the mixing angle θ_1 and the contribution of the interference term $2\hat{A}_1\hat{A}_2\sin(\theta_1)$. To investigate this we perform the time-propagation for different mixing angles $\theta_1 = 0°, 30°, 45°, 60°, 90°$ for the coupling ($\lambda = 0.017$) and choose as the input mode 1 in a coherent state with $\xi_1 = 2$ and set $V_0 = 200$ meV. In Fig. (28.a) we observe that for $\theta_1 = 0°$, where the polarization of pump and signal modes are perpendicular, we obtain the smallest value of $n_2 = 0.013$ when compared to all the cases with different mixing angels. The mean photon occupation of the signal mode $n_2(t)$ is shown to increase with increasing angles due to the fact that $2\hat{A}_1\hat{A}_2\sin(\theta_1)$ becomes larger. For $\theta_1 = 90°$ we find the highest down-conversion of photons as we obtain $n_2^{(\max)} = 0.0527$ since $\sin(\theta_1) = 1$ and the polarization of both modes are parallel with momenta contribution only in the y-axis (i.e., $\hat{p}_y \neq 0$ while $\hat{p}_x = 0$). In Fig. (28.b), the Mandel $Q_2(t)$ for $\theta_1 = 90°$ shows the highest non-classical (anti-bunching) features of the down-converted photons as $Q_2^{(\min)} = -0.0387$. For the angles $\theta_1 = 0°, 30°, 45°, 60°, 90°$, the values of $n_2^{(\max)}$ and $Q_2^{(\min)}$ are given in Tab. (4). In Fig. (28.a,b) both the three-levels and Maxwell-Schrödinger approximations deviate from the ab-initio results, however provide upper and lower bounds. Although the Maxwell-Schrödinger [85] accounts for the mixing angle, it fails to capture the induced correlations between the pump and signal modes, highlighting that an efficient down-conversion process is driven in this strong-coupling case by the quantum correlations between the different modes and the matter system. The three-level approximation, on the other hand, overestimate these quantum correlations.

4.2.2 OPTIMIZATION OF THE MATTER SPECTRUM

Next, we investigate the influence of the anharmonicity (controlled by potential parameter V_0) of the electronic subsystem on the down-conversion process. The pump mode 1 is chosen to be in a coherent state with on average $n_1(0) = 4$ photons, assume strong coupling ($\lambda = 0.017$) and set the mixing angle $\theta_1 = 60°$ such that both momentum components of the electronic system are non-zero (i.e., $\hat{p}_x \neq 0$ and $\hat{p}_y \neq 0$). The

V_0 (meV)	$\hbar\omega_1$ (meV)	$\hbar\omega_2$ (meV)	Exact $n_2^{(\max)}$	Exact $Q_2^{(\min)}$
0.0	10.00	5.00	0.0049	−0.0019
50.0	3.121	1.560	0.0105	−0.0103
100.0	1.924	0.962	0.0227	−0.0178
150.0	1.580	0.790	0.0334	−0.0229
200.0	1.413	0.706	0.0413	−0.0258
250.0	1.311	0.655	0.0475	−0.0303
300.0	1.239	0.619	0.0527	−0.0348

Table 5: The pump energies for resonant coupling of the electron ground-state and first excited state and corresponding down-converted energies of the signal field for different values of V_0. The numerically exact real-space values for maximum $n_2^{(\max)}$ and minimum $Q_2^{(\min)}$.

potential parameter is varied as $V_0 = 0, 50, 100, 150, 200, 250, 300$ meV (see Fig. (14.b)) which changes the transition energies between states from harmonic (all have the same transition energy) to anharmonic (different transitions have different energies). In Tab. (5), the transition energies from the electronic ground-state to the first excited state that the pump energy is resonant to and its down-converted energies are shown. Also, increasing V_0 also increases the transition dipoles (see Tab. (2.b)) of the electronic system which leads to a stronger coupling between light and matter as the coupling parameter is proportional to the transition dipoles as given explicitly in Eq. (385).

In Fig. (28.c,d), we find that with an increasing V_0 the maximum photon occupation $n_2^{(\max)}$ also increases. Simultaneously, the character of the generated photon pairs become increasingly anti-bunched as $Q_2^{(\min)}$ is shown to become more negative. These interesting features result from (i.) the increasing dipole moments due to reducing the width of the QR for increasing V_0 and (ii.) an increase in the effective coupling strength due to the reduced scaling of the transition energies (see Tab. (5)) as the effective coupling is related to the frequency by $g_\alpha = \lambda\sqrt{\hbar/2\omega_\alpha}$. We find that the three-level approximation for $V_0 = 0$ meV fails, because more than just three energy levels are important when all electronic transitions have the same energy and a few specific transitions cannot be separated. When the system becomes strongly anharmonic and hence a separation between states is more reasonable, the three-level approximation strongly overestimates the results. We still find that the Maxwell-Schrödinger approximation consistently under-estimates the results.

4.2.3 OPTIMIZATION OF THE COUPLING AND THE INPUT FIELD

Finally, we consider the influence of the coupling alongside the strength of the pump field on the efficiency of the down-conversion process. When we increase the number of photons in the input mode 1, this leads to the generation of more photons

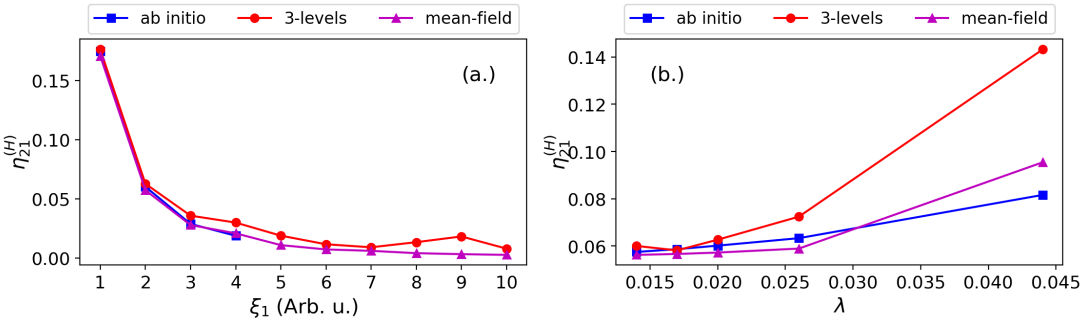

Figure 29: (a.) Comparison of the down-conversion efficiency for the 3-levels and mean-field approximations of the real-space numerically exact coupled electron-photon system for increasing input mode 1 amplitude ξ_1. For the exact system, we vary $\xi_1 = 1, 2, 3, 4$ because of the large dimensionality. (b.) Increasing efficiency for increasing λ for the 3-level and mean-field approximations of the real-space coupled system.

in signal mode 2 (see Sec. 4.3). Therefore, there is the need of a way to judge the efficiency of the down-conversion. To measure the efficiency, we choose the ratio of the photon energy of down-converted photons to the photon energy of the pump field, i.e., $\eta_{21}^{(H)} = \max(H_2(t)/H_1(t_0))$. In this definition, simply increasing the input field does not directly lead to a higher efficiency. To perform the different simulations, we choose a mixing angle of $\theta_1 = 60°$, a binding potential strength of $V_0 = 200$ meV, a coupling strength of $\lambda = 0.017$ and then different initial states for mode 1 by scanning $\xi_1 = 1, 2, 3, ..., 10$ such that the input field has $n_1(0) = 1, 4, 9, ..., 100$ photons at the initial time.

The results for this calculation is given in Fig. (29.a). We find that by increasing the strength of the pump field via the amplitude ξ_1 the efficiency of the down-conversion decreases. The ab-initio simulation for such large number of photons becomes numerically very expensive due to a large number of Fock states that has to be included to correctly describe the different coherent states for larger amplitudes. Therefore, we extrapolate by using the three-level and the Maxwell-Schrödinger approximations. As is expected, for increasing amount of photons in the pump mode 1 the Maxwell-Schrödinger theory becomes increasingly accurate and in the limit of very large photon numbers it should become exact (in the case of weak coupling). Since the GaAs semiconductor QR can only convert a finite amount of photons in the considered 40 ps, in this limit $\eta_{21}^{(H)}$ goes to zero. On the contrary, by fixing the amplitude of the input mode to $\xi_1 = 2$ with $n_1(0) = 4$ photons, but rather increase the coupling strength $\lambda = 0.014, 0.017, 0.019, 0.026, 0.044$, we see that the efficiency increases as shown in Fig. (29.b). However, both approximations are shown to overestimate the efficiency for large λ. We note that for very large coupling strengths, the quantum correlations no longer provide a higher down-conversion rate but rather the shear strength of the coupling terms that dominates. Therefore, by controlling the photonic environment to reach the ultra-strong coupling limit, the degenerate two-photon down-conversion is strongly enhanced.

So far, we presented the possibilities that arise if we do not make the initial assumption to treat light and matter separately. Our numerical simulations of non-relativistic QED showed how novel hybrid light-matter states (polaritons) are created that can act

as pathways in a photon down-conversion process. We studied the case of inverse second-harmonic generation by coupling the signal mode to a virtual state half the energy of a chosen excited state and optimized the down-conversion scheme to gain an efficient down-conversion. In the following, we explore this polariton-mediated down-conversion scheme to realize and N-photon source.

4.3 INVERSE HARMONIC GENERATION: AN N-PHOTON SOURCE

In this section we further explore this polariton-mediated down-conversion scheme to realize an N-photon source. This is motivated by the growing range of quantum applications which makes it increasingly important to diversify the available quantum sources of photons. The quest for such photon sources has been achieved in a cavity QED setting by employing a few-levels approximation [177]. Since in Sec. 4.2, the inverse second-harmonic generation involving virtual (and polariton) states was shown to be efficient (even more so with stronger coupling), this makes it a viable scheme for realizing an N-photon source. Since the few-level and Maxwell-Schrödinger approximations were shown to not be absolutely reliable for down-conversions involving virtual states (see Sec. 4.2), we will not consider these approximations here. We investigate such a down-conversion process with the same cavity setup as in Fig. (16.a).

The N-photon down-conversion presented here is the degenerate case (i.e. degeneracy in energy). Therefore, in a similar way to the degenerate two-photon down-conversion in Sec. 4.2, all the signal modes for each of the respective Nth-photon down-conversions (described by a Hamiltonian Eq. (49)) will populate just a single signal mode (here denoted signal mode 2). This reduces the parameter space and in this case the Hamiltonian simplifies to the two-mode electron-photon Hamiltonian of Eq. (340). We consider the optimized setup deduced in Sec. 4.2, therefore, the potential strength parameter is $V_0 = 200$ meV (suitable anharmonicity), $\theta_1 = 90^\circ$ (pump and signal modes are parallel) and $\lambda = 0.017$. The Hamiltonian in this case further simplifies to

$$\hat{H}_{ND} = \hat{H}_{2D} + \hat{H}_1 + \hat{H}_2 - \frac{e}{m}\left[\hat{A}_1 + \hat{A}_2\right]\hat{p}_y + \frac{e^2}{2m}\left[\hat{A}_1^2 + \hat{A}_2^2 + 2\hat{A}_1\hat{A}_2\right]. \tag{341}$$

As in the previous sections, mode 1 is the input pump mode and the vector potential has the explicit form $\hat{A}_\alpha = \lambda\hat{q}_\alpha$ with $\alpha = 1, 2$ where the coupling λ is assumed to be equal for both modes. While in the previous sections we were interested in the efficiency of the down-conversion process and the non-classical properties of the generated photons. Here, the focus is mainly on how efficient is it to generate N-photons via coupling the signal mode to virtual and potentially polaritonic states for increasing N. In the following, we consider the consecutive $N =$ 2-, 3-, 4-,...,11-photon down-conversions.

The down-conversion scheme is as follows. The active electron initially in the ground-state $|\varphi_1^0\rangle$ is promoted to the excited state $|\varphi_7^1\rangle$ of energy $\hbar\omega_1 = 24.65$ meV by the pump field. For the different degenerate down-conversions, the signal mode is: one-half (2-photon down-conversion), one-third (3-photon down-conversion), one-fourth (4-photon down-conversion) up to one-eleventh (11-photon down-conversion) the energy of the excited state ($|\varphi_7^1\rangle$ at energy $\hbar\omega_1 = 24.65$ meV), respectively (see

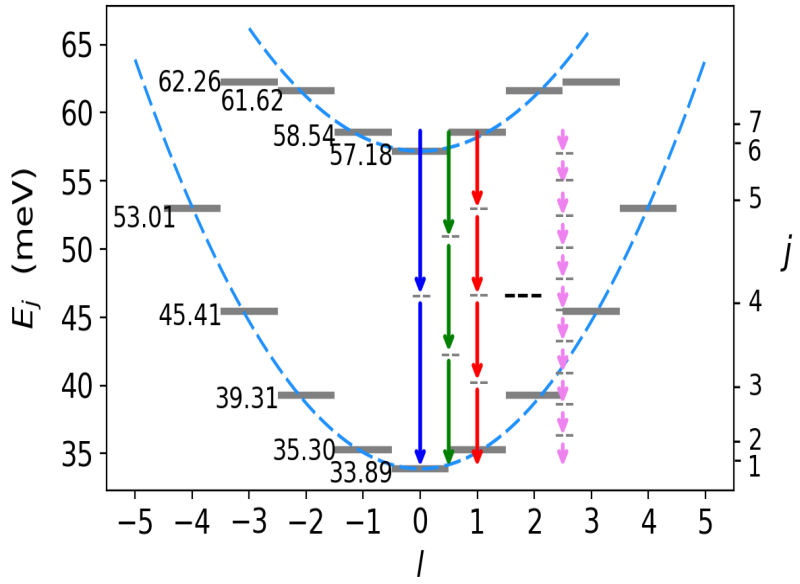

Figure 30: Illustration of an N-photon down-conversion scheme. The active electron in the excited-states $|\psi_7^{-1,1}\rangle$ relaxes to the ground-state $|\psi_1^0\rangle$ via virtual states (gray dashed lines) to which the signal mode couples to. The energy of the signal mode for the different down-conversions is chosen to be: one-half (2-photon down-conversion blue), one-third (3-photon down-conversion green), one-fourth (4-photon down-conversion red) up to one-eleventh (11-photon down-conversion violet) the energy of the excited state.

Fig. (30) for down-conversion scheme). Such down-conversion scheme represents an inverse (high-) harmonic generation via virtual and potentially polaritonic states and the energies for all the down-converted photons are given in Tab. (6). For all these cases, the effective coupling of the pump mode is $g_1 = 0.0095$ while that for the different down-conversions are determined from $g_2 = \lambda\sqrt{\hbar/2\omega_2}$ where $\omega_2 = \omega_1/N$ with $N = 2, 3, 4, ..., 11$. For $N \geq 2$ the effective coupling $g_1 < g_2$, thus the electron in the excited state $|\varphi_7^1\rangle$ will relax to the ground-state via virtual states thereby generating N-photon into the signal mode. The down-conversion scheme obeys the respective energy and momentum conservations in the photonic subspace given by $\hbar\omega_1 = N\hbar\omega_2$ and $\hbar\mathbf{k}_1 = N\hbar\mathbf{k}_2$, where $N = 2, 3, 4, ..., 11, ...$.

To simulate such an N-photon down-conversion, we numerically solve the time-dependent Schrödinger equation (6) with the Hamiltonian of Eq. (341). Since the computed observables in the time-evolution were shown to be robust to whether the system is driven by an external field or by a chosen initial state with same number of photon (see Sec. 4.1.6 and Fig. (25)), we consider here a factorizable initial state of the form $|\Psi_{\text{in}}(0)\rangle = |\varphi_1^0\rangle|\phi_1\rangle|0_2\rangle$, where the signal mode is the vacuum state $|0_2\rangle$ and the pump mode is a coherent state $|\phi_1\rangle = |\xi_1\rangle$. At the initial time the input mode is a field in a coherent state with amplitude $\xi_1 = 2$ with on average $n_1(0) = 4$ photons. The expectation values of the photon number operator for the time-evolved wavefunction is computed, i.e., $n_\alpha = \langle \hat{a}_\alpha^\dagger \hat{a}_\alpha \rangle$. This quantity indicates how much photons have been down-converted from the pump to the signal mode.

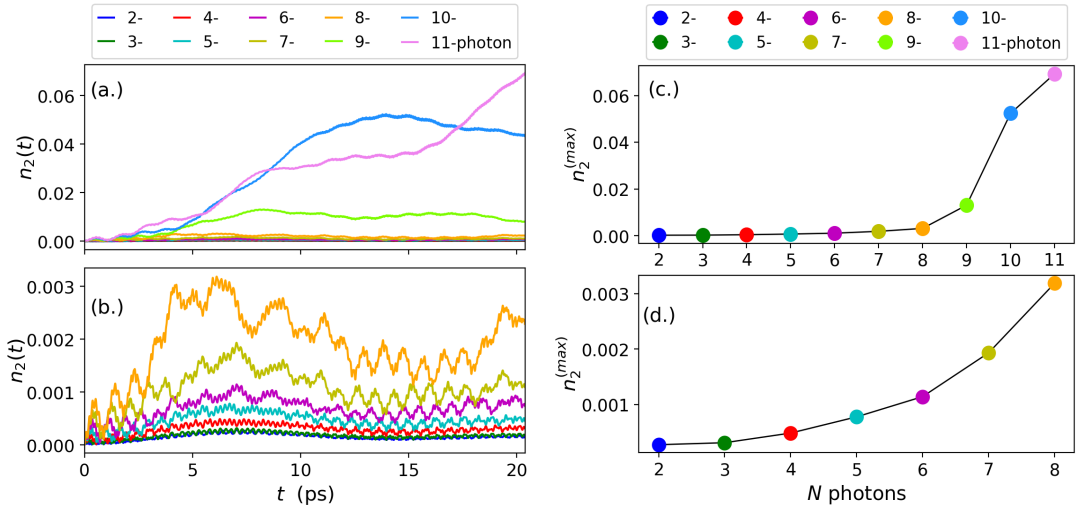

Figure 31: (a.) Real-time photon occupation of the signal mode showing the profiles for two- up to eleven-photon down-conversions for $\xi_1 = 2$. The maximum amplitude of the photon occupations $n_2(t)$ increase with increasing order N. (b.) A zoom-in view of (a.) showing the profile of the two- to eighth-photon down-conversions with the same increasing trend. Panel (c.) shows the maximum $n_2^{(\max)}$ for each of the N-photon down-conversions for the evolved time in panel (a.). Panel (d.) shows a zoom-in view of (c.) showing the $n_2^{(\max)}$ of the two- up to eighth-photon down-conversions.

In Fig. (31.a) we show the real-time photon occupations of the signal modes for all the $N = 2, 3, 4, ..., 11$-photon down-conversions for up to $t = 20$ ps. The amplitude (amount of down-converted photons) of $n_2(t)$ is shown to increase for increasing N. Fig. (31.b) is a zoom-in view for $N = 2$ up to $N = 8$ photon down-conversions which show clearly the increasing trend for the amount of down-converted photons. The $N = 9, 10, 11$ photon down-conversions are shown to have significant down-converted photons when compared to the others. This can be attributed to the fact that their energies (see Tab. (6)) are close enough to resonance to the dipole-allowed transition $|\varphi_1^0\rangle \leftrightarrow |\varphi_2^{-1,1}\rangle$ with energy $\hbar\omega_{12} = 1.41$ meV and potentially polaritonic states (as discussed in Sec. 4.3.1). This increase in the occupation for these down-conversions will not be captured if we employed the few-levels approximation that considered just the two states to which the pump mode is resonant to (i.e. $|\varphi_1^0\rangle \leftrightarrow |\varphi_7^{-1,1}\rangle$). Also in Fig. (31.c) we plot the maximal amount of the mode occupation $n_2^{(\max)}$ obtained for the 20 ps time-evolution for the different down-conversion cases. The maximum mode occupation $n_2^{(\max)}$ is shown to increase for increasing order of N. The zoom-in view of Fig. (31.d) shows an approximate quadratic increase for $N = 2$ up to $N = 8$ of the different down-conversions. The mode occupation $n_1(t)$ of the pump modes are all qualitatively the same for all the down-conversions (see Fig. (32.a)) up to around 7 ps where they start to differ strongly for higher N. The loss of photons from $n_1(t)$ after $t = 7$ ps is shown to be consistent with the increase in $n_2(t)$ for the $N = 9, 10, 11$-photon down-conversions. The non-classical properties

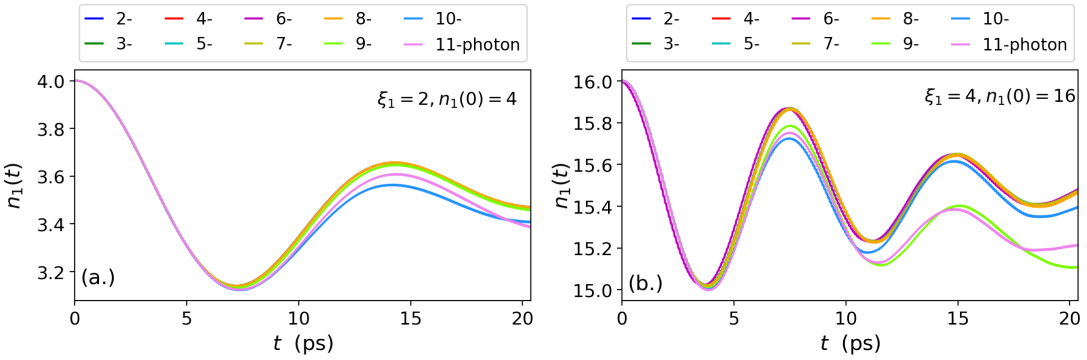

Figure 32: Real-time photon occupation of the pump mode for 2-,3-,4-,...,11-photon down-conversions. Panel (a.) shows the occupation when the amplitude of the coherent state of the pump field is $\xi_1 = 2$ with $n_1(0) = 4$ photons. Panel (b.) shows the occupation for the case $\xi_1 = 4$ with $n_1(0) = 16$ photons.

of the down-converted photons such as antibunching feature can be computed using the generalized Mandel $Q_\alpha^{(N)}$ parameter [169, 178] given by

$$Q_\alpha^{(N)} = \frac{\langle (\Delta n_\alpha)^N \rangle - \langle \hat{n}_\alpha \rangle}{\langle \hat{n}_\alpha \rangle}. \tag{342}$$

The interpretation of the photon statistics obtained from Eq. (342) is the same as that of Eq. (335). That is, for all $N \geq 2$, a field with non-classical properties, the range of values lies between $-1 \leq Q_\alpha^{(N)} < 0$ which is sub-Poissonian statistics (antibunching behavior). Fields with super-Poissonian statistics (bunching behavior) have $Q_\alpha^{(N)} > 0$ and for a coherent state with Poissonian statistics, $Q_\alpha^{(N)} = 0$. In Sec. 4.3.1, we compute the third-order Mandel $Q_\alpha^{(3)}$ parameter for the three-photon down-conversion as an example case to study the non-classicality of the down-converted photons.

From the results of Fig. (31), we can conclude that the down-conversion can be tuned with the system parameters (e.g. frequency of signal mode 2) so that the down-conversion scheme behaves as a laser or as an N-photon gun [177]. Interestingly, the higher-order down-conversions are shown to be more efficient than the lower ones which makes it a viable source for an N-photon gun. The increase of the efficiency is due to two reasons (i.) near-resonance conditions to a dipole-allowed transition and (ii.) for smaller frequencies the effective coupling g_2 increases. Of course, one cannot just increase the coupling arbitrary by reducing the frequency to zero because there is a natural renormalization in the lower frequency, which appears as an intrinsic frequency cutoff [41, 43]. A careful analysis shows that this intrinsic cutoff, which depends on the number of particles, makes sure that no infrared divergence appears. However, if this natural renormalization of the frequencies is not taken properly into account, such an unphysical divergence appears.

Next, we investigate the influence of a stronger input field on the down-conversion while the system parameters are kept the same. For this we follow closely the results of Sec. 4.2.3 and choose an amplitude of the pump field to be $\xi_1 = 4$ such that the field has on average $n_1(0) = |\xi_1|^2 = 16$ photons at the initial time. In Fig. (32.b), we show the mode occupations of the pump mode for $N = 2, 3, 4, ..., 11$. Similar to the case with $\xi_1 = 2$, the occupations $n_1(t)$ are qualitatively the same up to around

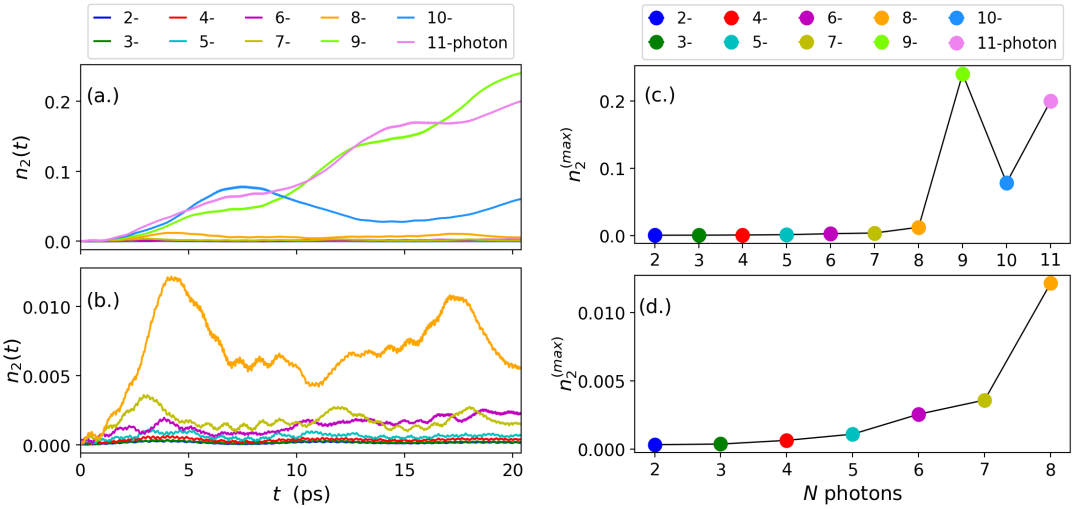

Figure 33: (a.) Real-time photon occupation of the signal mode showing the profiles for two- to eleven-photon down-conversions for $\xi_1 = 4$. The maximum amplitude of the photon occupations $n_2(t)$ increase with increasing order N. (b.) A zoom-in view of (a.) showing the profile of the two- to eighth-photon down-conversions with the same increasing trend. Panel (c.) shows the maximum $n_2^{(\max)}$ for each of the N-photon down-conversions for the evolved time in panel (a.). Panel (d.) shows a zoom-in view of (c.) showing the $n_2^{(\max)}$ of the two- to eighth-photon down-conversions. The $N = 9$-photon down-conversion is shown to increase significantly compared to the case with $\xi_1 = 2$.

$t = 4$ ps except for $N = 6$ and afterwards they start to differ for $N \geq 9$. Also, we plot the mode occupations $n_2(t)$ in Fig. (33). We observe that the amount of down-converted photons in the signal modes have increased when compared to Fig. (31) where $\xi_1 = 2$ and also the trend of increasing $n_2(t)$ for increasing N still holds (see Tab. (6)) except for $N = 9$. Such an increase in the occupation of the signal mode is due to stronger pumping and this is in agreement with the case of three-photon PDC using a flux-pumped superconducting parametric cavity where they observed that increasing the strength of the pump field increases the brightness of the triplet source [179]. Analogous to this observation, we see a similar increase in our case for $N = 3$ and for higher N-photon down-conversions (see Tab. (6)). Therefore, our ab-initio results serve as a generalization of this effect to higher-order down-conversions. In addition, we observe by comparing Fig. (33.a) to (31.a) that the down-conversion can be pushed to occur at earlier times similar to Sec. 4.1, however here for stronger pumping. This implies a suitable choice of the strength of the input field and strong coupling will potentially overcome detrimental decoherence effects.

The non-classical properties of the down-converted photons are usually of importance due to their applications in quantum-information processing [139, 140]. In the following, we consider the $N = 3$ down-conversion and show that the down-converted photons have strong non-classical properties.

$N-$ photon	$\hbar\omega_2$ (meV)	$n_2^{(\max)}$ for $\xi_1 = 2$	$n_2^{(\max)}$ for $\xi_1 = 4$
2	12.32657	0.00027956	0.00032736
3	8.21771	0.00031508	0.00037502
4	6.16328	0.00048875	0.00064416
5	4.93063	0.00078086	0.00109885
6	4.10886	0.00114483	0.00255912
7	3.52188	0.00193335	0.00359964
8	3.08164	0.00318637	0.01215882
9	2.73924	0.01312342	0.24051696
10	2.46531	0.05239264	0.07836939
11	2.24119	0.06927053	0.20012262

Table 6: The energies of the down-converted photons for different inverse harmonic generations. Accompanying the energies are the maximum photon occupation of the signal mode for a time-evolution of 20 ps for $\xi_1 = 2$ and $\xi_1 = 4$. The energy of the pump mode is $\hbar\omega_1 = 24.65$ meV.

4.3.1 THREE-PHOTON DOWN-CONVERSION IN STRONG COUPLING

In the previous section we demonstrated how to realize an N-photon source by coupling the signal mode to virtual states and potentially polaritonic states. This novel down-conversion scheme highlighted new possibilities that become available when we treat light and matter on an equal quantized footing, as the strong coupling regime presented the possibility of polariton-mediated N-photon down-conversion by coupling to virtual states. These down-conversion pathways will not be available if one considers just classical fields that couples to the matter subsystem as in a non-linear optics approach. In this section, we want to investigate the non-classical properties of the down-converted photons since they are of importance in a down-conversion process. As an example, we study the case of three-photon down-conversion.

We consider the 3-photon down-conversion case in Sec. 4.3 but for non-degenerate three-photon down-conversion via coupling to selected electronic states. We do this to investigate how the efficiency of the down-conversion increases when dipole-allowed transitions are involved. This will also validate our prediction in Sec. 4.3 where for $N = 9, 10, 11$ the efficiency of the down-conversion increased considerably due to near resonance condition with the dipole-allowed transition $|\varphi_1^0\rangle \leftrightarrow |\varphi_2^{-1,1}\rangle$. We note that the current study of three-photon down-conversion is also motivated by applications in which PDC leads to the creation of entangled photon triplets which serves as a source for generating three-photon entangled states such as Greenberger-Horne-Zeilinger states [180], as well as heralded entangled triplets [181]. A widespread and common technique for realizing three-photon generation is by means of a *cascaded* PDC. This is an approach in non-linear optics where one of the photons from a primary PDC process is used to pump a secondary down-conversion source leading to the generation of polarization entangled photon triplets [180–183]. This approach usually results in low conversion efficiency and scalability, which limits its applica-

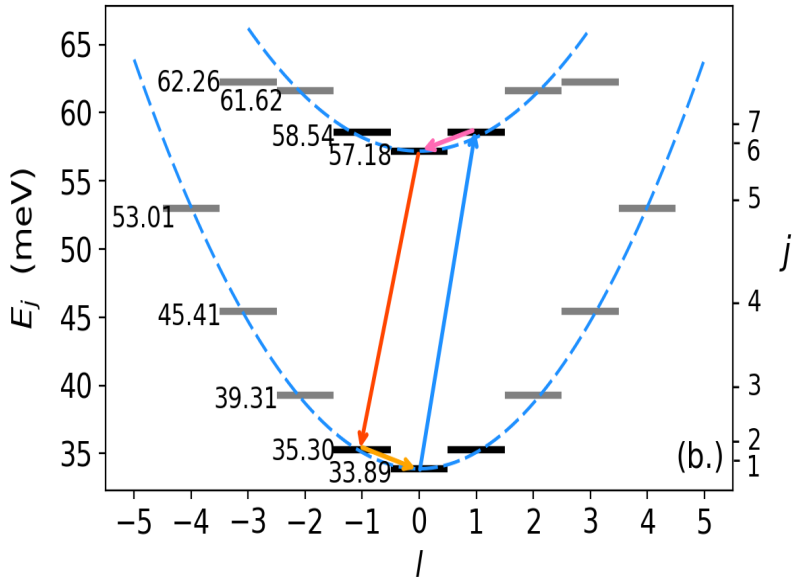

Figure 34: Resonant coupling to specific energy-levels (dark-shaded) for cascaded three-photon down-conversion. The pump mode (light blue) drives resonantly the transition $|\psi_1^0\rangle \leftrightarrow |\psi_7^{-1,1}\rangle$ while the signal modes couple resonantly $|\psi_6^0\rangle \leftrightarrow |\psi_7^{-1,1}\rangle$ (red for mode 2), $|\psi_6^0\rangle \leftrightarrow |\psi_2^{-1,1}\rangle$ (pink for mode 3) and $|\psi_1^0\rangle \leftrightarrow |\psi_2^{-1,1}\rangle$ (orange for mode 4).

tion [181]. We showed in Sec. 4.1.4.2 that by manipulating the photonic environment we can control the down-conversion features such as efficiency, non-classicality and earlier down-conversion times by stronger coupling. Therefore, our ab-initio simulation of quantum light-matter interaction for a three-photon down-conversion will present a way to overcome limitations in this process by changing the photonic environment. To investigate the three-photon down-conversion we employ the same cavity setup as in Fig. (16.a). Since we want to investigate the efficiency of the down-conversion due to resonant coupling to dipole-allowed transitions, we explicitly describe three signal modes together with the pump mode. The schematic for the resonant coupling of all four modes is shown in Fig. (34). Still working in the dipole approximation, the Pauli-Fierz Hamiltonian for this setting is given by

$$\begin{aligned}\hat{H}_{3D} = \hat{H}_{2D} + \hat{H}_1 + \hat{H}_2 + \hat{H}_3 + \hat{H}_4 - \frac{e}{m}\left[\hat{A}_1 + \hat{A}_2 - \hat{A}_3 + \hat{A}_4\right]\hat{p}_y \\ + \frac{e^2}{2m}\left[\hat{A}_1^2 + \hat{A}_2^2 + \hat{A}_3^2 + \hat{A}_4^2 + 2\hat{A}_1\hat{A}_2 - 2\hat{A}_1\hat{A}_3 + 2\hat{A}_1\hat{A}_4\right. \\ \left. -2\hat{A}_2\hat{A}_3 - 2\hat{A}_2\hat{A}_4 - 2\hat{A}_3\hat{A}_4\right] . \end{aligned} \tag{343}$$

The above Hamiltonian is similar to Eq. (341) but here the three signal modes are included explicitly, where $\hat{H}_{2D}$ is the bare Hamiltonian of the matter subsystem given in Eq. (332) and $\hat{p}_y$ is the y-component of the momentum operator of the 2D QR. The photonic Hamiltonians $\hat{H}_\alpha$ of the selected modes have the form of Eq. (38) and the vector potentials are $\hat{A}_\alpha = \lambda\hat{q}_\alpha$ where $\alpha = 1,2,3,4$ and we assume equal coupling for the all modes $\lambda_\alpha = \lambda$.

We now outline the optimizations and specifics applied here based on the observations in Sec. 4.2. In analogy to the two-photon non-degenerate case (see Sec. 4.1),

mode 1 is the pump mode while modes 2, 3, 4 are the signal modes. Based on the optimization of the field polarizations and matter subsystem (see Secs. 4.2.1 and 4.2.2), we choose the polarization of the selected cavity modes to be $\hat{\mathbf{A}}_1 = \hat{A}_1\mathbf{e}_x$, $\hat{\mathbf{A}}_2 = \hat{A}_2\mathbf{e}_x$, $\hat{\mathbf{A}}_3 = -\hat{A}_3\mathbf{e}_x$ and $\hat{\mathbf{A}}_4 = \hat{A}_4\mathbf{e}_x$ as they maximize the mode-mode interaction terms due to the diamagnetic contribution and the potential strength parameter is $V_0 = 200$ meV. Also, since increasing the coupling strength increases the efficiency of the down-conversion and as well push the down-conversion events to earlier times with potential to overcome decoherence effects (see Secs. 4.2.3 and 4.1.4.2), we hereby choose the strong coupling regime where $\lambda = 0.017$. Based on previous considerations were the bath modes were shown to not affect strongly the down-conversion efficiency (see Sec. 4.1.4.1 and Fig. (17)), we assume that the bath modes will not be important here. Also, since we consider strong coupling we expect that the bath modes are less important.

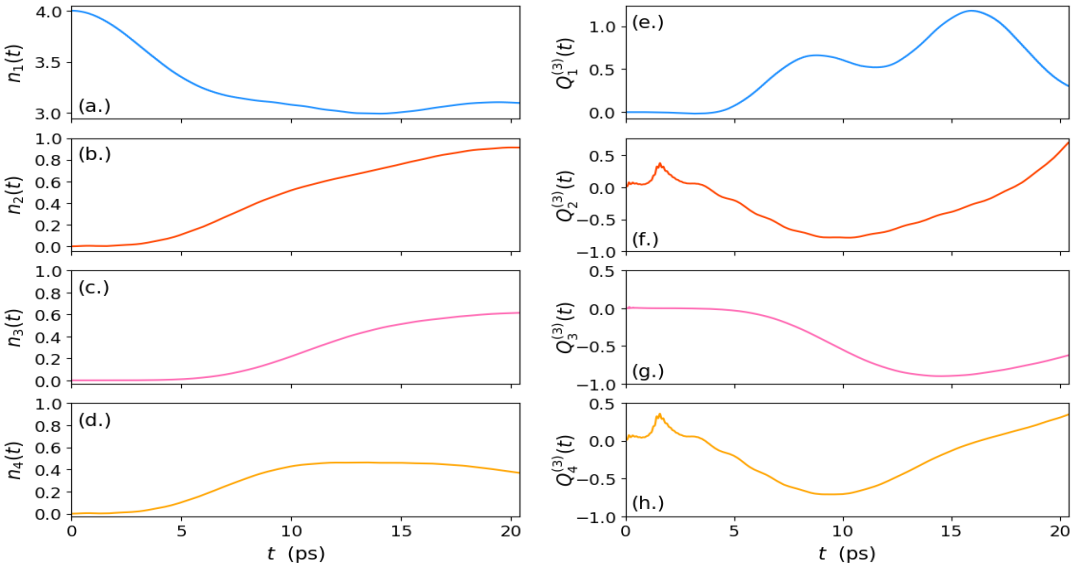

Figure 35: Real-time photon occupations and Mandel $Q_\alpha^{(3)}$ parameters for three-photon down-conversion. Panel (a.) shows how the occupation from the input field is down-converted to the signal modes which have significant occupations in panels (b.)-(d.). Panels (e.)-(h.) shows the photon statistics of the pump (mainly bunched) and signal modes (mainly anti-bunched).

Contrary to the case of non-degenerate two-photon down-conversion discussed in Sec. 4.1.5 where one of the signal modes was less efficient due to coupling resonantly to a non-dipole allowed transition, we find here that we can couple all the signal modes to dipole-allowed transitions. This is because between the ground-state $|\psi_1^0\rangle$ and excited state $|\psi_7^1\rangle$, we can find three electronic transitions (dipole-allowed) that change their angular momentum $|l|$ by a value of one (see Fig. (34)). Therefore, we prepare pump mode 1 (input field) in a coherent state with amplitude $\xi_1 = 2$ such that there are $n_1 = 4$ photons in the initial pulse while the signal modes are in the vacuum state. The pump field drives resonantly the electronic transition $|\varphi_1^0\rangle \leftrightarrow |\varphi_7^1\rangle$ of energy $\hbar\omega_1 = 24.65$ meV. The signal modes are chosen such that mode 2 is resonant with the transition $|\varphi_7^1\rangle \leftrightarrow |\varphi_6^0\rangle$ of energy $\hbar\omega_2 = 1.36$ meV, mode 3 is resonant with the transition $|\varphi_6^0\rangle \leftrightarrow |\varphi_2^1\rangle$ of energy $\hbar\omega_3 = 21.88$ meV and mode 4 is resonant with

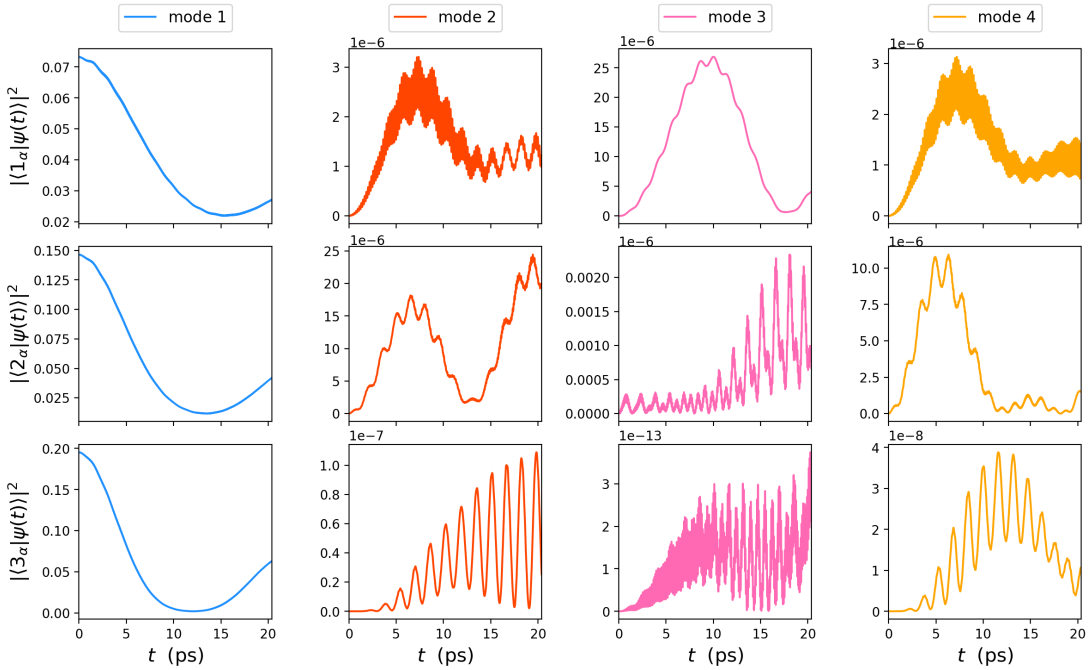

Figure 36: One-, two-, and three-photon Fock state populations for pump and signal modes. The two-photon Fock states of the signal modes is most populated when compared to the one- and three-photon Fock states except for mode 3 for the time-evolution shown.

the transition $|\varphi_2^1\rangle \leftrightarrow |\varphi_1^0\rangle$ of energy $\hbar\omega_4 = 1.41$ meV. Such a scheme hereby forms an atomic cascade of the form $|\varphi_7^1\rangle \rightarrow |\varphi_6^0\rangle \rightarrow |\varphi_2^1\rangle \rightarrow |\varphi_1^0\rangle$ (see Fig. (34)). The effective coupling $g_\alpha = \lambda\sqrt{\hbar/2\omega_\alpha}$ for each of the modes are $g_1 = 0.0095$, $g_2 = 0.0407$, $g_3 = 0.0101$ and $g_4 = 0.0398$. Since the coupling g_1 of the pump mode is smaller in comparison to that of the signal modes g_2, g_3, g_4, the electron in the excited state $|\varphi_7^1\rangle$ preferably relaxes to the ground-state by cascaded emission of three photons into signal modes 2, 3 and 4, respectively. The three-photon generation into signal photons obeys the energy and momentum conservations in the photonic subspace given by $\hbar\omega_1 = \hbar\omega_2 + \hbar\omega_3 + \hbar\omega_4$ and $\hbar\mathbf{k}_1 = \hbar\mathbf{k}_2 + \hbar\mathbf{k}_3 + \hbar\mathbf{k}_4$, respectively.

We simulate the time-evolution dynamics of the three-photon down-conversion by explicitly propagating the time-dependent Schrödinger equation of Eq. (6) with the Hamiltonian of Eq. (343). The initial state is a factorizable product state $|\Psi_{\text{in}}(0)\rangle = |\varphi_1^0\rangle|\xi_1\rangle|0_2\rangle|0_3\rangle|0_4\rangle$ where $|\varphi_1^0\rangle$, $|0_2\rangle$, $|0_3\rangle$ and $|0_4\rangle$ are the ground-state and vacuum states of the electronic and photonic subsystems, respectively, while the state $|\xi_1\rangle$ of the pump mode is a coherent state. We note that we could increase the amplitude ξ_1 to obtain more photons in the signal mode as discussed in Sec. 4.3. However, since we want to compare to the case in Sec. 4.3 how coupling resonantly to dipole-allowed transitions influences the efficiency of the down-conversion, we choose the amplitude $\xi_1 = 2$. The expectation value of observables of interest for the time-propagation are computed for each time step, $\Delta t = 0.029$ fs, of the time-evolved wavefunction. We consider the time-evolution up to 20 ps. This choice is based on arguments in Sec. 4.1.4.1 where it is expected that the system stays coherent for up to 40 ps and by

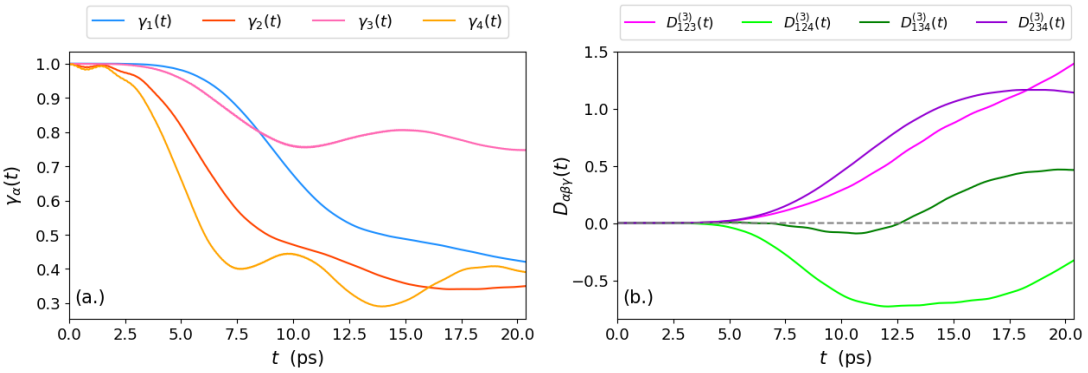

Figure 37: (a.) Purity of the pump and signal modes showing how each modes become entangled after $t > 0$ in real-time. (b.) Shows the third-order cross-correlation between the pump and signal modes. Gray dashed line indicates when the modes are correlated ($D_{\alpha\beta\gamma} > 0$), anti-correlated ($D_{\alpha\beta\gamma} < 0$) or uncorrelated ($D_{\alpha\beta\gamma} = 0$).

increasing the coupling strength, one expects to have the maximum down-conversion at an earlier time (see Fig. (19.b,c) for increasing λ).

To monitor the absorbed and emitted photons from the cascade, we compute the real-time photon occupations of the pump $n_1 = \langle \hat{a}_1^\dagger \hat{a}_1 \rangle$ and down-converted signal modes $n_2 = \langle \hat{a}_2^\dagger \hat{a}_2 \rangle$, $n_3 = \langle \hat{a}_3^\dagger \hat{a}_3 \rangle$ and $n_4 = \langle \hat{a}_4^\dagger \hat{a}_4 \rangle$. In Fig. (35.a-d) we show the mode occupations of the pump and signal modes as photons are down-converted from the pump mode to the signal modes. All signal modes are shown to have significant photon occupations which can be attributed to the dipole-allowed transitions that these modes are resonant with. This validates our prediction in Sec. 4.3 that for near resonance (and in this case resonant) conditions with the dipole-allowed transitions $|\varphi_1^0\rangle \leftrightarrow |\varphi_2^{-1,1}\rangle$ the efficiency of the down-conversion for $N = 9, 10, 11$ increased considerably. The efficient down-conversion is also accredited to the optimized setup employed here that maximized the contributions coming from the mode-mode interactions of the diamagnetic term. Put together, this ensures an efficient three-photon generation in an ab-initio cavity controlled down-conversion setting. We note that while the down-converted photons are split between three modes similar to Ref. [179], these photons can be generated in a single mode (see Sec. 4.3 for $N = 3$ and Ref. [179]). It is interesting to characterize the state of the generated photons. Since this is a third-order process, we compute the third-order Mandel $Q_\alpha^{(3)}$ parameter deduced from Eq. (342) and given as

$$Q_\alpha^{(3)} = \frac{(\Delta n_\alpha)^3 - \langle \hat{n}_\alpha \rangle}{\langle \hat{n}_\alpha \rangle}, \tag{344}$$

where deviation of the third-moment from the mean is given explicitly as $(\Delta n_\alpha)^3 - \langle \hat{n}_\alpha \rangle = \langle \hat{a}_\alpha^\dagger \hat{a}_\alpha^\dagger \hat{a}_\alpha^\dagger \hat{a}_\alpha \hat{a}_\alpha \hat{a}_\alpha \rangle - 3\langle \hat{a}_\alpha^\dagger \hat{a}_\alpha \rangle \langle \hat{a}_\alpha^\dagger \hat{a}_\alpha^\dagger \hat{a}_\alpha \hat{a}_\alpha \rangle + 3\langle \hat{a}_\alpha^\dagger \hat{a}_\alpha^\dagger \hat{a}_\alpha \hat{a}_\alpha \rangle - 3\langle \hat{a}_\alpha^\dagger \hat{a}_\alpha \rangle^2 + 2\langle \hat{a}_\alpha^\dagger \hat{a}_\alpha \rangle^3$. In Fig. (35.e-h) we show $Q_\alpha^{(3)}(t)$ for all the modes. The photon statistics of the signal modes shows that the down-converted photons are non-classical (anti-bunched) while the pump mode has a classical features (bunched) for most of the time-evolution shown. From this result, we can predict that for higher-order down-conversions (as considered in Sec. 4.3) the photon statistics of the down-converted photons (computed using Eq. (342) for different N) will have stronger antibunching features when

the signal modes are resonant to dipole-allowed transitions. The non-classical features of the down-converted photons are particularly of interest since they are used for quantum information processing [184]. We equally show the one-, two- and three-photon Fock state populations of the pump and signal fields in Fig. (36). Here we highlight for the case of the signal modes that the two-photon Fock states are most populated when compared to the one- and three-photon Fock states except for mode 3. This observation is similar to the non-degenerate case in Fig. (21) where it becomes difficult to identify in a simple manner the photon down-conversion process as a single photon being down-converted to three photons since we have many photon states that mix.

Finally, we investigate the entanglement and cross-correlation between the down-converted signal modes and as well the pump mode. We characterize the individual entanglement of the photonic subsystems by computing the purity γ_α where $\alpha = 1, 2, 3, 4$ (see Eq. (386)). In Fig. (37.a), we show the purity results of the pump and signal modes as they all start out uncorrelated (since $\gamma_\alpha = 1$) and for the entire time-evolution, in order of most entangled (minimum γ_α) are $\gamma_4 < \gamma_2 < \gamma_1 < \gamma_2$. Since the purity $\gamma_\alpha < 1$ for all modes, this implies that the initial uncorrelated state at $t = 0$ becomes correlated at a later time as the wavefunction is non-separable thus specifying entanglement in the system. Also, cross-correlations between the down-converted photons is also a desired non-classical feature. To investigate for mode-mode correlation between the pump and signal modes, we compute the third-order cross-correlation function which we define as

$$g^{(3)}_{\alpha\beta\gamma} = \frac{\langle \hat{a}^\dagger_\alpha \hat{a}_\alpha \hat{a}^\dagger_\beta \hat{a}_\beta \hat{a}^\dagger_\gamma \hat{a}_\gamma \rangle}{\langle \hat{a}^\dagger_\alpha \hat{a}_\alpha \rangle \langle \hat{a}^\dagger_\beta \hat{a}_\beta \rangle \langle \hat{a}^\dagger_\gamma \hat{a}_\gamma \rangle} \,. \tag{345}$$

The above expression has the same interpretation as the second-order cross-correlation function of Eq. (336). The correlation function $D^{(3)}_{\alpha\beta\gamma}$ is related to the third-order cross-correlation by $D^{(3)}_{\alpha\beta\gamma} = \langle \hat{n}_\alpha \rangle \langle \hat{n}_\beta \rangle \langle \hat{n}_\gamma \rangle \left(g^{(3)}_{\alpha\beta\gamma} - 1 \right)$. The correlation function $D^{(3)}_{\alpha\beta\gamma}$ takes values greater than zero for correlated modes. For uncorrelated modes, it is equal to zero and it takes values less than zero if the modes are anti-correlated. In Fig. (37.b), we show that all the modes are uncorrelated up to $t = 3.97$ ps. From there on, the photon modes show varying temporal correlation and anti-correlation. The modes specified by the correlation function $D^{(3)}_{134}$ vary between anti-correlated and correlated while the correlation function $D^{(3)}_{124}$ is anti-correlated for the remainder of the simulation. Interestingly, the correlation function $D^{(3)}_{234}$ for the down-converted signal photons is correlated for the remainder of the simulation, also with correlation function $D^{(3)}_{123}$. This is a desired feature usually observed for three-photon down-conversion [180–182, 185, 186].

To conclude, we found that our cavity-controlled first-principles description of the down-conversion process can be used to achieve an N-photon source via coupling the signal mode to virtual and potentially polaritonic states. The efficiency can be increased when the signal mode(s) is close to resonance with a dipole-allowed transition or when it resonantly couples. To study the non-classical character of the down-converted photons, we considered the case $N = 3$ and showed that the down-converted photons have strong non-classical features of antibuching, cross-correlation and entanglement. The cavity-controlled down-conversion scheme made accessible

new observable quantities due to quantized light-matter interaction. We expect that for higher-order down-conversions, the down-converted photons will have such non-classical properties as well.

4.4 SUMMARY

In summary, we highlighted the details that become accessible and controllable for a photon down-conversion process when light and matter are treated on an equal quantized footing within an ab-initio light-matter simulation. We showed that by manipulating the photonic environment to attain stronger coupling, the down-conversion can be pushed to occur at earlier times potentially overcoming detrimental decoherence effects. Also, we highlighted that the quantized light-matter description of the down-conversion process makes accessible novel observables that are not usually observed in the usual down-conversion, such as occupation, photon statistics and entanglement of the pump mode as well as cross-correlation between the pump and signal modes. In addition, we highlighted that by coupling the signal mode(s) to virtual and polaritonic states, we can engineer new down-conversion pathways and the efficiency of the process can be increased by increasing the coupling strength. With this, we proposed a polariton-mediated down-conversion scheme to realize an N-photon gun (source). Comparing to other approaches employed to investigate the down-conversion process, we showed cases where the usual descriptions that utilizes the few-level approximation (quantum optics approach) and Maxwell Schrödinger approximation (non-linear optics approach) become less accurate. This finding supports the need for an ab-initio description of the down-conversion process.

Part V

CONCLUSION

5

SUMMARY, CONCLUSION AND OUTLOOK

In the course of this thesis, we presented an ab-initio description of coupled light-matter systems in the linear response regime and beyond the linear response regime. These first-principles descriptions are capable of describing experimental observations that shows how properties of matter can be controlled and modified on the nanoscale by coupling to photons in high-Q optical cavities or plasmonic devices. For the case of the linear response regime, existing standard ab-initio methods that do not include the photon field in their description are not capable of capturing features of strong light-matter interaction. By introducing the linear-response regime of coupled matter-photon systems where strong light-matter coupling is usually identified by linear spectroscopy, the methods developed in this thesis were shown to capture excited-states properties of strongly coupled light-matter systems as polaritonic peaks emerge in the absorption spectra. Such modified spectra are usually observed in experiments by coupling resonantly a photon mode to an electronic excitation [90]. In most of such strong coupling experiments, the focus is usually on how the photon field changes the matter properties and less on the effects of how the matter subsystem changes the photon field. Looking at the problem in this way misses out on interesting effects that show up in the photonic subsystem especially since there is a self-consistent interaction between both matter and photon in this coupling regime. In light of this, we computed the spectrum of the displacement field and observed features of strong coupling (polaritonic peaks) that indicate the cross-talk between both subsystems. This highlights that novel linear spectroscopic observables can be accessed that give a detail understanding of how light and matter interact and also entails that the Maxwell's equation in matter get modified due to this self-consistent cross-talk. These results change the perspective of strong-light matter interaction as well as open up new possibilities to be investigated. For example, we showed how to compute the lifetimes from first-principles in a non-perturbative way of not only electronic excited-states but also that of polaritonic states by sampling the photon bath. This is important because the lifetimes of these states are usually computed with perturbative Wigner-Weisskopf theory which is less accurate in some cases as we showed in Chap. 3.6.5. As the ab-initio description allows to sample the photon bath densely with thousands of photon modes, this allows us to investigate non-standard situations. For example, we showed how one can achieve a transition from Lorentzian to Fano lineshapes by strongly coupling to the continuum. Standard matter-only methods such as those employed in electronic-structure or quantum chemistry cannot capture this important feature. This example makes a good case as to why standard matter-only methods need further development to include the contributions of the photon field as in the case of QEDFT and QED-CC. Our ab-initio results are an important first step for treating excited-states properties of coupled matter-photon systems. At present, QEDFT which scales well with the coupled system size is still at its infancy stage as it has been applied to static situations [17] or very simple time-dependent problems [12, 13, 22, 91]. Since we have developed in this thesis a linear-response

formulation and numerical methods within the framework of QEDFT which is sufficient for many interesting observables that identify features of strong light-matter coupling, this puts QEDFT at the spotlight for several different applications. The QEDFT linear-response methods are gaining recognition as they have been applied to different situations of strong-light matter coupling [19, 20, 23, 47] and have potential to unravel new interesting chemical and physical effects.

As QEDFT is exact to all orders, some of the numerical methods (e.g. Sternheimer method) developed in this thesis can be extended beyond the linear response regime. Going beyond the linear-response regime of strong light-matter coupling using QEDFT is a topic under consideration now since there is high potential for new findings. In order for us to get a detailed understanding of non-linear processes in the strong light-matter coupling regime, we considered the paradigmatic case of non-linear optics and quantum optics for photon down-conversion process from an ab-initio perspective when light and matter are treated on an equal level of theory. This was motivated by the growing range of quantum applications which makes it increasingly important to diversify the available quantum sources of photons [177]. In this study we found that coupling strongly to a photonic environment opens new possibilities that would not be captured with the standard approaches. For example, we showed that coupling the signal mode to virtual or non-dipole allowed states creates new pathways for photon down-conversion and with this a novel source of photons (photon gun) with non-classical properties. This highlights a new possibility of engineering photon sources in non-linear processes using hybrid light-matter states (polaritons) in which the efficiency of the down-conversion can be controlled in an experimentally realizable way by varying the photonic environment. Such a down-conversion will not be possible using a non-linear optics approach and with a quantum optics approach, it becomes less accurate. Another new possibility is the potential to overcome the undesired detrimental effects of decoherence by strong coupling, since it causes the down-conversion of photons to occur at earlier times when the system is expected to stay coherent. This ab-initio study of the down-conversion for strong light-matter interaction also highlighted novel observables of the subsystem that become accessible due to the quantized treatment of the coupled system. The standard approaches do not capture this new possibilities because they treat light and matter differently. The results of the down-conversion processes together with the linear-response studies highlight how not only the matter properties get modified but also how the photon field gets modified due to the self-consistent interaction between the coupled system at this level of theory. This opens up new possibilities that can be investigated for coupled light-matter systems.

Outlook. In Chap. 3.6.4 we showed the shift in peak position (Lamb shift) due to coupling to a continuum of photon modes. Such a shift is usually dealt with by renormalizing the bare mass in non-relativistic QED. To get an in-depth understanding of how this is done for bound systems, we will investigate such a renormalization procedure using a numerically exactly solvable system of a hydrogen atom coupled to a continuum of photon modes. The focus will be on the ground-state properties since the ground-state is in this case the only eigenstate of the coupled system while the excited states of the matter subsystem turn into resonances. This investigation is expected to layout the foundation of ab-initio mass renormalization theory for bound systems. Next, the linear-response framework of QEDFT has been shown in this thesis

and in other works [18, 20, 23] to correctly capture modifications of excited-states properties of correlated electron-photon systems. In the growing field of polaritonic chemistry, vibrational effects have been shown to play a critical role in chemical reactions. For instance, it has been demonstrated that a vibrational mode can be altered by strong light-matter coupling which influences the reactions potentially allowing for site-selective chemistry [187]. To capture such effects, QEDFT was recently extended to include the nuclear dynamics [47]. Simulating the coupled problem is time consuming due to the different time scales of the subsystems. Therefore, the electron-photon linear-response methods introduced in this thesis that work in frequency space become preferable for this study. We will extend these linear-response methods to treat coupled electron-nuclear-photon problems. This will allow for efficient ab-initio studies of excited-states phenomena of strong vibrational coupled matter-photon systems. For example, we can investigate in detail whether collective coupling implies local modifications of chemical properties that scale with the ensemble size [23]. This allows us to pose questions as to how does collective strong coupling in this setting affect the potential energy surfaces and in what way will this modify chemical properties? This level of theory and computational scheme further opens new avenues in first-principles studies such as determining lifetimes for the excited-states of molecular systems since the nuclei are now included and plays an important role in the relaxation process.

For the proposed ab-initio down-conversion scheme, we can explore going beyond the restriction to a single active electron to include an ensemble of quantum rings or a general many-electron system. In such a treatment, one will expect that the total number of down-converted photons can be efficiently increased. Such setups can be accessed with, for instance, using the time-propagation method of QEDFT and polaritonic coupled cluster [15]. Such investigation can provide not only qualitative results but also a quantitative prediction how hybrid light-matter states can generate photons on demand. In certain cases, one can even include the nanophotonic structure as part of the simulation and model the full emission process [85]. The results of this thesis demonstrate that the design of efficient photon sources is a very interesting working avenue for the emerging field of ab-initio light-matter interactions. We envision that the methods presented in this thesis can be used to complement experimental observations in polaritonic chemistry and material sciences and even propose new avenues of research and observables to investigate.

Part VI

APPENDIX

A

SUPPORTING RESULTS OF THE LINEAR-RESPONSE IN NON-RELATIVISTIC QED

In this appendix, we give supporting details to the results of Chap. 3. The results presented here are: verification of the reformulation of the response functions of non-relativistic QED to the framework of QEDFT, an alternative derivation of the frequency-dependent Sternheimer equations for electron-photon coupled systems and the derivation of oscillator strengths for the electron-photon Casida method.

A.1 VERIFICATION OF THE RESPONSE FUNCTIONS

In this section, we show how the Mxc kernels defined in Eqs. (223)-(226) reproduce the response functions of the interacting system. We first express the response functions of Eqs.(227), (229), (232) and (234) derived within the linear-response framework of QEDFT in the following way

$$\chi^n_n = \chi^n_{n,s} + \chi^n_{n,s} f^n_{\mathrm{Mxc}} \chi^n_n + \chi^n_{n,s} \sum_\alpha f^{q_\alpha}_{\mathrm{Mxc}} \chi^{q_\alpha}_n \,, \tag{346}$$

$$\chi^n_{q_\alpha} = \chi^n_{n,s} \sum_{\alpha'} f^{q_{\alpha'}}_{\mathrm{Mxc}}\, \chi^{q_{\alpha'}}_{q_\alpha} + \chi^n_{n,s} f^n_{\mathrm{Mxc}}\, \chi^n_{q_\alpha} \,, \tag{347}$$

$$\chi^{q_\alpha}_{q_{\alpha'}} = \chi^{q_\alpha}_{q_{\alpha,s}} + \sum_\beta \sum_{\beta'} \chi^{q_\alpha}_{q_{\beta,s}} g^{q_{\beta'}}_{\mathrm{Mxc}} \chi^{q_{\beta'}}_{q_\alpha} + \sum_\beta \chi^{q_\alpha}_{q_{\beta,s}} g^{n_\beta}_{\mathrm{Mxc}} \chi^n_{q_{\alpha'}} \tag{348}$$

$$\chi^{q_\alpha}_n = \sum_\beta \sum_{\beta'} \chi^{q_\alpha}_{q_{\beta,s}} g^{q_{\beta'}}_{\mathrm{Mxc}} \chi^{q_{\beta'}}_n + \sum_\beta \chi^{q_\alpha}_{q_{\beta,s}} g^{n_\beta}_{\mathrm{Mxc}} \chi^n_n \,, \tag{349}$$

where integration over space and time is implied as in Eqs. (227), (229), (232) and (234). Starting with χ^n_n, we substitute the expression of f^n_{Mxc} and $f^{q_\alpha}_{\mathrm{Mxc}}$ given in the respective Eqs. (223) and (224) into Eq. (346) to obtain

$$\begin{aligned}
\chi^n_n &= \frac{\delta n[v_s]}{\delta v_s} + \frac{\delta n[v_s]}{\delta v_s} \left(\frac{\delta v_s[n]}{\delta n} - \frac{\delta v[n,q_\alpha]}{\delta n} \right) \frac{\delta n[v,j_\alpha]}{\delta v} \\
&\quad + \frac{\delta n[v_s]}{\delta v_s} \sum_\alpha \left(- \frac{\delta v[n,q_\alpha]}{\delta q_\alpha} \right) \frac{\delta q_\alpha[v,j_\alpha]}{\delta v} \\
&= \frac{\delta n[v_s]}{\delta v_s} + \frac{\delta n[v_s]}{\delta v_s} \frac{\delta v_s[n]}{\delta n} \frac{\delta n[v,j_\alpha]}{\delta v} \\
&\quad - \frac{\delta n[v_s]}{\delta v_s} \underbrace{\left(\frac{\delta v[n,q_\alpha]}{\delta n} \frac{\delta n[v,j_\alpha]}{\delta v} + \sum_\alpha \frac{\delta v[n,q_\alpha]}{\delta q_\alpha} \frac{\delta q_\alpha[v,j_\alpha]}{\delta v} \right)}_{\delta v[n,q_\alpha]/\delta v = \delta(\mathbf{x}-\mathbf{r}')\delta(\tau-t')} \\
&= \frac{\delta n[v_s]}{\delta v_s} + \frac{\delta n[v,j_\alpha]}{\delta v} - \frac{\delta n[v_s]}{\delta v_s} \\
&= \frac{\delta n[v,j_\alpha]}{\delta v} \,.
\end{aligned} \tag{350}$$

We see from Eq. (350) that we obtain the interacting density-density response function. Note that we used in Eq. (350) the functional derivative formalism discussed

in Chap. 3.2.2. Next, we consider $\chi^{n}_{q_\alpha}$ and substitute the expression of f^{n}_{Mxc} and $f^{q_\alpha}_{\mathrm{Mxc}}$ given in the respective Eqs. (223) and (224) into Eq. (347) which yields

$$\begin{aligned}
\chi^{n}_{q_\alpha} &= \frac{\delta n[v_s]}{\delta v_s}\left(\frac{\delta v_s[n]}{\delta n} - \frac{\delta v[n,q_\alpha]}{\delta n}\right)\frac{\delta n[v,j_\alpha]}{\delta j_\alpha} + \frac{\delta n[v_s]}{\delta v_s}\sum_{\alpha'}\left(-\frac{\delta v[n,q_\alpha]}{\delta q_{\alpha'}}\right)\frac{\delta q_{\alpha'}[v,j_\alpha]}{\delta j_\alpha} \\
&= \frac{\delta n[v_s]}{\delta v_s}\frac{\delta v_s[n]}{\delta n}\frac{\delta n[v,j_\alpha]}{\delta j_\alpha} - \frac{\delta n[v_s]}{\delta v_s}\underbrace{\left(\frac{\delta v[n,q_\alpha]}{\delta n}\frac{\delta n[v,j_\alpha]}{\delta j_\alpha} + \sum_{\alpha'}\frac{\delta v[n,q_\alpha]}{\delta q_{\alpha'}}\frac{\delta q_{\alpha'}[v,j_\alpha]}{\delta j_\alpha}\right)}_{\delta v[n,q_\alpha]/\delta j_\alpha = 0} \\
&= \frac{\delta n[v,j_\alpha]}{\delta j_\alpha}\,. \qquad (351)
\end{aligned}$$

We also see from Eq. (351) that we obtain the interacting density-photon response function. Now we consider the photon-photon response function $\chi^{q_\alpha}_{q_{\alpha'}}$ and substitute the expression of $g^{n_\beta}_{\mathrm{Mxc}}$ and $g^{q_\alpha}_{\mathrm{Mxc}}$ given in Eqs. (225) and (226) into Eq. (348) to obtain

$$\begin{aligned}
\chi^{q_\alpha}_{q_{\alpha'}} &= \frac{q_\alpha[j_{\alpha,s}]}{j_{\alpha,s}} + \sum_{\beta}\sum_{\beta'}\frac{\delta q_\alpha[j_{\alpha,s}]}{\delta j_{\beta,s}}\left(\frac{\delta j_{\beta,s}[q_\alpha]}{\delta q_{\beta'}} - \frac{\delta j_\beta[n,q_\alpha]}{\delta q_{\beta'}}\right)\frac{\delta q_{\beta'}[v,j_\alpha]}{\delta j_{\alpha'}} \\
&\quad + \sum_{\beta}\frac{\delta q_\alpha[j_{\alpha,s}]}{\delta j_{\beta,s}}\left(-\frac{\delta j_\beta[n,q_\alpha]}{\delta n}\right)\frac{\delta n[v,j_\alpha]}{\delta j_{\alpha'}} \\
&= \frac{q_\alpha[j_{\alpha,s}]}{j_{\alpha,s}} + \sum_{\beta}\sum_{\beta'}\frac{\delta q_\alpha[j_{\alpha,s}]}{\delta j_{\beta,s}}\frac{\delta j_{\beta,s}[q_\alpha]}{\delta q_{\beta'}}\frac{\delta q_{\beta'}[v,j_\alpha]}{\delta j_{\alpha'}} \\
&\quad - \sum_{\beta}\frac{\delta q_\alpha[j_{\alpha,s}]}{\delta j_{\beta,s}}\underbrace{\left(\sum_{\beta'}\frac{\delta j_\beta[n,q_\alpha]}{\delta q_{\beta'}}\frac{\delta q_{\beta'}[v,j_\alpha]}{\delta j_{\alpha'}} + \frac{\delta j_\beta[n,q_\alpha]}{\delta n}\frac{\delta n[v,j_\alpha]}{\delta j_{\alpha'}}\right)}_{\delta j_\beta[n,q_\alpha]/\delta j_{\alpha'} = \delta_{\beta\alpha'}} \\
&= \frac{\delta q_\alpha[v,j_\alpha]}{\delta j_{\alpha'}}\,. \qquad (352)
\end{aligned}$$

From Eq. (352) we see that we obtain the interacting photon-photon response function. Finally, we consider the photon-density response function $\chi^{q_\alpha}_{n}$ and substitute the expression of $g^{n_\beta}_{\mathrm{Mxc}}$ and $g^{q_\alpha}_{\mathrm{Mxc}}$ given in Eqs. (225) and (226) into Eq. (349) to obtain

$$\begin{aligned}
\chi^{q_\alpha}_{n} &= \sum_{\beta}\sum_{\beta'}\frac{\delta q_\alpha[j_{\alpha,s}]}{\delta j_{\beta,s}}\left(\frac{\delta j_{\beta,s}[q_\alpha]}{\delta q_{\beta'}} - \frac{\delta j_\beta[n,q_\alpha]}{\delta q_{\beta'}}\right)\frac{\delta q_{\beta'}[v,j_\alpha]}{\delta v} \\
&\quad + \sum_{\beta}\frac{\delta q_\alpha[j_{\alpha,s}]}{\delta j_{\beta,s}}\left(-\frac{\delta j_\beta[n,q_\alpha]}{\delta n}\right)\frac{\delta n[v,j_\alpha]}{\delta v} \\
&= \sum_{\beta}\sum_{\beta'}\frac{\delta q_\alpha[j_{\alpha,s}]}{\delta j_{\beta,s}}\frac{\delta j_{\beta,s}[q_\alpha]}{\delta q_{\beta'}}\frac{\delta q_{\beta'}[v,j_\alpha]}{\delta v} \\
&\quad - \sum_{\beta}\frac{\delta q[j_{\alpha,s}]}{\delta j_{\beta,s}}\underbrace{\left(\sum_{\beta'}\frac{\delta j_\beta[n,q_\alpha]}{\delta q_{\beta'}}\frac{\delta q_{\beta'}[v,j_\alpha]}{\delta v} + \frac{\delta j_\beta[n,q_\alpha]}{\delta n}\frac{\delta n[v,j_\alpha]}{\delta v}\right)}_{\delta j_\alpha[n,q_\alpha]/\delta v = 0} \\
&= \frac{\delta q_\alpha[v,j_\alpha]}{\delta v}\,. \qquad (353)
\end{aligned}$$

We also see from Eq. (353) that we obtain the interacting photon-density response function. This validates our linear-response formulation of QEDFT which expresses the interacting response function in terms of the non-interacting and interacting response functions and Mxc kernels.

A.2 ALTERNATE DERIVATION OF THE FREQUENCY-DEPENDENT STERNHEIMER EQUATIONS

In this section, we present a derivation of the frequency-dependent Sternheimer equation for electron-photon systems that includes the projector operator into the subspace of ground-state KS orbitals as in the electron-only Sternheimer derivations presented in Refs. [83, 117]. Our derivation is restricted to the frequency space as in Chap. 3.5.2. In an alternate derivation of the frequency-dependent Sternheimer equations, we could have instead of defining the orbitals $\varphi^{(\pm)}_{k,v}(\mathbf{r},\omega)$ in Eq. (300), defined the orbitals $\tilde{\varphi}^{(\pm)}_{k,v}(\mathbf{r},\omega)$ [53]. By substituting Eq. (265) into Eq. (256), the density response $\delta n_v(\mathbf{r},\omega)$ can be expressed in terms of the orbitals $\tilde{\varphi}^{(\pm)}_{k,v}(\mathbf{r},\omega)$ as follows

$$\delta n_v(\mathbf{r},\omega) = \sum_{k=1}^{N_e} \left[\varphi^*_k(\mathbf{r}) \tilde{\varphi}^{(+)}_{k,v}(\mathbf{r},\omega) + \varphi_k(\mathbf{r}) \left[\tilde{\varphi}^{(-)}_{k,v}(\mathbf{r},\omega) \right]^* \right]. \tag{354}$$

The first-order responses of the perturbed KS orbitals $\tilde{\varphi}^{(\pm)}_{k,v}(\mathbf{r},\omega)$ are given by

$$\tilde{\varphi}^{(+)}_{k,v}(\mathbf{r},\omega) = \int d^3\mathbf{r}' \sum_{l=N_e+1}^{\infty} \frac{\varphi_l(\mathbf{r})\varphi^*_l(\mathbf{r}')\varphi_k(\mathbf{r}')}{\omega - (\epsilon_l - \epsilon_k) + i\eta} \delta v_{\mathrm{KS},v}(\mathbf{r}',\omega), \tag{355}$$

$$\tilde{\varphi}^{(-)}_{k,v}(\mathbf{r},\omega) = -\int d^3\mathbf{r}' \sum_{l=N_e+1}^{\infty} \frac{\varphi_l(\mathbf{r})\varphi^*_l(\mathbf{r}')\varphi^*_k(\mathbf{r}')}{\omega + (\epsilon_l - \epsilon_k) + i\eta} \delta v_{\mathrm{KS},v}(\mathbf{r}',\omega). \tag{356}$$

Following similar steps as in Chap. 3.5.2, Eqs. (355) and (356) can be multiplied through with $\left(\omega - \hat{h} + \epsilon_k + i\eta\right)$ and $\left(\omega + \hat{h} - \epsilon_k + i\eta\right)$, respectively resulting to

$$\begin{aligned}
\left(\omega - \hat{h} + \epsilon_k + i\eta\right) \tilde{\varphi}^{(+)}_{k,v}(\mathbf{r},\omega) = \int d^3\mathbf{r}' \sum_{l=N_e+1}^{\infty} \left(\omega - \hat{h} + \epsilon_k + i\eta\right) \\
\times \frac{\varphi_l(\mathbf{r})\varphi^*_l(\mathbf{r}')\varphi_k(\mathbf{r}')}{\omega - (\epsilon_l - \epsilon_k) + i\eta} \delta v_{\mathrm{KS},v}(\mathbf{r}',\omega), \\
\left(\omega + \hat{h} - \epsilon_k + i\eta\right) \tilde{\varphi}^{(-)}_{k,v}(\mathbf{r},\omega) = -\int d^3\mathbf{r}' \sum_{l=N_e+1}^{\infty} \left(\omega + \hat{h} - \epsilon_k + i\eta\right) \\
\times \frac{\varphi_l(\mathbf{r}')\varphi^*_l(\mathbf{r})\varphi^*_k(\mathbf{r}')}{\omega + (\epsilon_l - \epsilon_k) + i\eta} \delta v_{\mathrm{KS},v}(\mathbf{r}',\omega).
\end{aligned}$$

The above equations now simplify to have the following forms

$$\left(\omega - \hat{h} + \epsilon_k + i\eta\right) \tilde{\varphi}^{(+)}_{k,v}(\mathbf{r},\omega) = \int d^3\mathbf{r}' \sum_{l=N_e+1}^{\infty} \varphi_l(\mathbf{r})\varphi^*_l(\mathbf{r}')\varphi_k(\mathbf{r}')\delta v_{\mathrm{KS},v}(\mathbf{r}',\omega), \tag{357}$$

$$\left(\omega + \hat{h} - \epsilon_k + i\eta\right) \tilde{\varphi}^{(-)}_{k,v}(\mathbf{r},\omega) = -\int d^3\mathbf{r}' \sum_{l=N_e+1}^{\infty} \varphi_l(\mathbf{r}')\varphi^*_l(\mathbf{r})\varphi^*_k(\mathbf{r}')\delta v_{\mathrm{KS},v}(\mathbf{r}',\omega). \tag{358}$$

Equations (357) and (358) can be further transformed by using the resolution of the identity for KS orbitals, i.e., $\sum_{l=1}^{\infty} \varphi_l(\mathbf{r})\varphi_l^*(\mathbf{r}') = \delta(\mathbf{r}-\mathbf{r}')$. With this expression, the summation over unoccupied orbitals can be replaced by the closure relation

$$\sum_{l=N_e+1}^{\infty} \varphi_l(\mathbf{r})\varphi_l^*(\mathbf{r}') = \delta(\mathbf{r}-\mathbf{r}') - \sum_{k=1}^{N_e} \varphi_k(\mathbf{r})\varphi_k^*(\mathbf{r}'),$$

which circumvents the infinite sum over ground-state KS orbitals to equations of the form

$$\begin{aligned}\left(\omega - \hat{h} + \epsilon_k + i\eta\right)\tilde{\varphi}_{k,v}^{(+)}(\mathbf{r},\omega) = \int d^3\mathbf{r}' \left(\delta(\mathbf{r}-\mathbf{r}') - \sum_{k=1}^{N_e}\varphi_k(\mathbf{r})\varphi_k^*(\mathbf{r}')\right) \\ \times \varphi_k(\mathbf{r}')\delta v_{\mathrm{KS},v}(\mathbf{r}',\omega), \qquad (359)\\ \left(\omega + \hat{h} - \epsilon_k + i\eta\right)\tilde{\varphi}_{k,v}^{(-)}(\mathbf{r},\omega) = -\int d^3\mathbf{r}' \left(\delta(\mathbf{r}-\mathbf{r}') - \sum_{k=1}^{N_e}\varphi_k(\mathbf{r})\varphi_k^*(\mathbf{r}')\right) \\ \times \varphi_k^*(\mathbf{r}')\delta v_{\mathrm{KS},v}(\mathbf{r}',\omega). \qquad (360)\end{aligned}$$

Simplifying the integral of Eqs. (359) and (360) leads to the frequency-dependent Sternheimer equation of the form

$$\left(\omega - \hat{h} + \epsilon_k + i\eta\right)\tilde{\varphi}_{k,v}^{(+)}(\mathbf{r},\omega) = \hat{\mathrm{P}}_c\ \varphi_k(\mathbf{r})\delta v_{\mathrm{KS},v}(\mathbf{r},\omega), \qquad (361)$$

$$\left(\omega + \hat{h} - \epsilon_k + i\eta\right)\tilde{\varphi}_{k,v}^{(-)}(\mathbf{r},\omega) = -\hat{\mathrm{P}}_c\ \varphi_k^*(\mathbf{r})\delta v_{\mathrm{KS},v}(\mathbf{r},\omega). \qquad (362)$$

where $\hat{\mathrm{P}}_c = \hat{\mathbb{1}} - \sum_{k=1}^{N_e}\varphi_k(\mathbf{r})\varphi_k^*(\mathbf{r})$ is the projector operator to the unoccupied KS ground-state. The photonic contribution to the Sternheimer equation have the same form as in Eqs. (307)-(309). A similar derivation that yields Sterheimer equations with projector operators as in Eqs. (361) and (362) can be derived for the density response $\delta n_j(\mathbf{r},\omega)$ to an external charge current $\delta j_\alpha(\omega)$.

A.3 OSCILLATOR STRENGTH FOR ELECTRON-PHOTON CASIDA METHOD

In this section, we derive the expression for computing the oscillator strengths by using the eigenvectors of the pseudo-eigenvalue problem of Eqs. (295) and (296). We first focus on the linear density response due to a perturbation from an external potential $\delta v(\mathbf{r},\omega)$. From Eq. (291), we multiply out the matrix to get the following form

$$\begin{aligned} L\mathbf{X}_v + K\mathbf{Y}_v + M(\mathbf{A}_v + \mathbf{B}_v) - \omega\mathbf{X}_1 &= -v,\\ K\mathbf{X}_v + L\mathbf{Y}_v + M(\mathbf{A}_v + \mathbf{B}_v) + \omega\mathbf{Y}_1 &= -v,\\ N(\mathbf{X}_v + \mathbf{Y}_v) + \omega_\alpha\mathbf{A}_v - \omega\mathbf{A}_v &= 0,\\ N(\mathbf{X}_v + \mathbf{Y}_v) + \omega_\alpha\mathbf{B}_v + \omega\mathbf{B}_v &= 0,\end{aligned} \qquad (363)$$

or equivalently

$$\begin{aligned} (L+K)(\mathbf{X}_v + \mathbf{Y}_v) + 2M(\mathbf{A}_v + \mathbf{B}_v) - \omega(\mathbf{X}_v - \mathbf{Y}_v) &= -2v,\\ (L-K)(\mathbf{X}_v - \mathbf{Y}_v) - \omega(\mathbf{X}_v + \mathbf{Y}_v) &= 0,\\ 2N(\mathbf{X}_v + \mathbf{Y}_v) + \omega_\alpha(\mathbf{A}_v + \mathbf{B}_v) - \omega(\mathbf{A}_v - \mathbf{B}_v) &= 0,\\ \omega_\alpha(\mathbf{A}_v - \mathbf{B}_v) - \omega(\mathbf{A}_v + \mathbf{B}_v) &= 0.\end{aligned} \qquad (364)$$

Here, the frequency-dependence of these matrices and potentials are dropped for notational simplicity. From here on we set $S = L - K$, the above pair of equations now becomes

$$S(L+K)\mathbf{E}_v + 2SM\mathbf{P}_v - \omega^2\mathbf{E}_v = -2S\boldsymbol{v},$$
$$2\omega_\alpha N\mathbf{E}_v + \omega_\alpha^2\mathbf{P}_v - \omega^2\mathbf{P}_v = 0,$$

where the new eigenvectors are $\mathbf{E}_v = \mathbf{X}_v + \mathbf{Y}_v$ and $\mathbf{P}_v = \mathbf{A}_v + \mathbf{B}_v$. The above equation can be written in matrix form as

$$\left[\begin{pmatrix} S(L+K) & 2SM \\ 2\omega_\alpha N & \omega_\alpha^2 \end{pmatrix} - \omega^2 \begin{pmatrix} 1 & 0 \\ 0 & 1 \end{pmatrix}\right] \begin{pmatrix} \mathbf{E}_v \\ \mathbf{P}_v \end{pmatrix} = - \begin{pmatrix} 2S\boldsymbol{v} \\ 0 \end{pmatrix}. \tag{365}$$

We make the nonlinear eigenvalue problem Hermitian and obtain

$$\left[C - \omega^2\mathbb{1}\right] \begin{pmatrix} N^{1/2}S^{-1/2}\mathbf{E}_v \\ M^{1/2}\omega_\alpha^{-1/2}\mathbf{P}_v \end{pmatrix} = - \begin{pmatrix} 2N^{1/2}S^{1/2}\boldsymbol{v} \\ 0 \end{pmatrix}, \tag{366}$$

where $C = \begin{pmatrix} U & V \\ V^\dagger & \omega_\alpha^2 \end{pmatrix}$. We determine the eigenvectors given to be

$$\mathbf{E}_v = -2S^{1/2}\left[C - \omega^2\mathbb{1}\right]^{-1} S^{1/2}\boldsymbol{v}, \tag{367}$$
$$\mathbf{P}_v = -2\omega_\alpha^{1/2}M^{-1/2}\left[C - \omega^2\mathbb{1}\right]^{-1} N^{1/2}S^{1/2}\boldsymbol{v}. \tag{368}$$

When $\mathbf{Z}_I$ is normalized, we can use the spectral expansion to get

$$\left[C - \omega^2\mathbb{1}\right]^{-1} = \sum_I \frac{\mathbf{Z}_I\mathbf{Z}_I^\dagger}{(\Omega_I^2 - \omega^2)}, \quad \text{where} \quad \mathbf{Z}_I = \begin{pmatrix} \mathbf{E}_{vI} \\ \mathbf{P}_{vI} \end{pmatrix}. \tag{369}$$

A.3.1 OSCILLATOR STRENGTH FOR THE DENSITY-DENSITY RESPONSE FUNCTION

For determining the expression of the oscillator strength for the linear density-density response function due to an external potential $\delta v(\mathbf{r}, \omega)$, we make use of the formula for the polarizability tensor. The dynamic polarizability tensor first given in Eq. (329) can also be expresses as

$$\alpha_{\mu\nu}(\omega) = \int d^3\mathbf{r}\ \mathbf{r}_\mu \frac{\delta n(\mathbf{r}, \omega)}{\delta E_\nu(\omega)}, \tag{370}$$

with $\mu, \nu = (1, 2, 3)$ denoting all three spatial directions. By substituting Eq. (367) in Eq. (267) and using the above Eq. (370) yields

$$\alpha_{\mu\nu}(\omega) = \sum_I \frac{2\mathbf{r}_\mu^\dagger S^{1/2}\mathbf{Z}_I\mathbf{Z}_I^\dagger S^{1/2}\mathbf{r}_\nu}{\Omega_I^2 - \omega^2}, \tag{371}$$

where $\mathbf{r}_\mu^\dagger = \int d^3\mathbf{r}\ \mathbf{r}_\mu \sum_{i,a} \Phi_{ia}^*(\mathbf{r})$ and the transition density is defined as $\Phi_{ia}(\mathbf{r}) = \varphi_i^*(\mathbf{r})\varphi_a(\mathbf{r})$ in terms of KS orbitals. It can be verified that $\mathbf{r}_\mu^\dagger S^{1/2}\mathbf{Z}_I = \omega_I^{1/2}\langle\Psi_0|\mathbf{r}_\mu|\Psi_I\rangle$ and the oscillator strength [53, 84] is given by

$$f_I = \frac{2}{3}\sum_{\mu=1}^{3} \left|\mathbf{Z}_I^\dagger S^{1/2}\mathbf{r}_\mu\right|^2 = \frac{2}{3}\omega_I \sum_{\mu=1}^{3} \left|\langle\Psi_0|er_\mu|\Psi_I\rangle\right|^2 \tag{372}$$

Also, in the case of the Casida method within QEDFT the oscillator strength satisfy the Thomas-Reiche-Kuhn sum rule (also known as f-sum rule), i.e. $\sum_I f_I = N_e$, where N is the total number of electrons in the system. The oscillator strength can be linked to the dipole strength function as given in Eq. (318) and integrates according to the f-sum rule to the total number of electrons.

A.3.2 OSCILLATOR STRENGTH FOR THE PHOTON-MATTER RESPONSE FUNCTION

Next, we compute the oscillator strength for the photon-density response function of the photon coordinate $q_{\alpha,v}(\omega)$ due to an external potential $\delta v(\mathbf{r},\omega)$. We substitute the expression of the spectral expansion of Eq. (369) in Eq. (368) and by substituting $\mathbf{P}_v$ in Eq. (266) yields

$$\delta q_{\alpha,v}(\omega) = \sum_I \left\{ \frac{2\omega_\alpha^{1/2} M^{-1/2} \mathbf{Z}_I \mathbf{Z}_I^\dagger N^{1/2} S^{1/2}}{(\omega^2 - \Omega_I^2)} \right\} v(\omega).$$

The oscillator strength for the response $q_{\alpha,v}(\omega)$ is given by the numerator of the above equation

$$f_{qn}^{I,\alpha} = 2\omega_\alpha^{1/2} M^{-1/2} \mathbf{Z}_I \mathbf{Z}_I^\dagger N^{1/2} S^{1/2}. \tag{373}$$

Also, from Eq. (258) and using the Lehmann representation of the response function $\chi_n^{q_\alpha}(\mathbf{r}',\omega)$ of Eq. (219) the response $\delta q_{\alpha,v}(\omega)$ is given by

$$\delta q_{\alpha,v}(\omega) = \int d^3\mathbf{r}' \sum_{k=0} \left[\frac{2\Omega_k \langle \Psi_0 | \hat{q}_\alpha | \Psi_k \rangle \langle \Psi_k | \hat{n}(\mathbf{r}') | \Psi_0 \rangle}{\omega^2 - \Omega_k^2} \right] \delta v(\mathbf{r}',\omega)\,.$$

The oscillator strength of Eq. (373) can be expressed as matrix elements of the internal pair $(\hat{n}(\mathbf{r}), \hat{q}_\alpha)$ and is related to the oscillator strength of Eq. (373) as

$$f_{\alpha,k}(\mathbf{r}') = 2\Omega_k \langle \Psi_0 | \hat{q}_\alpha | \Psi_k \rangle \langle \Psi_k | \hat{n}(\mathbf{r}') | \Psi_0 \rangle \equiv f_{qn}^{I,\alpha}\,. \tag{374}$$

A.3.3 OSCILLATOR STRENGTH FOR THE MATTER-PHOTON RESPONSE FUNCTION

Following similar steps of Eqs. (363)-(368), we obtain the new eigenvectors

$$\mathbf{E}_j = -2S^{1/2} N^{-1/2} \left[C - \omega^2 \mathbb{1} \right]^{-1} M^{1/2} \omega_\alpha^{1/2} j_\alpha, \tag{375}$$

$$\mathbf{P}_j = -2\omega_\alpha^{1/2} \left[C - \omega^2 \mathbb{1} \right]^{-1} \omega_\alpha^{1/2} j_\alpha, \tag{376}$$

where $\mathbf{E}_j = \mathbf{X}_j + \mathbf{Y}_j$ and $\mathbf{P}_j = \mathbf{A}_j + \mathbf{B}_j$ and $\mathbf{j}_\alpha(\omega) = \frac{1}{2\omega_\alpha} j_\alpha(\omega)$. Next, by substituting the spectral expansion Eq. (369) in Eq. (375) and further substituting in Eq. (270) yields

$$\delta n_j(\mathbf{r},\omega) = 2 \sum_I \sum_{ia} \frac{\Phi_{ia} S^{1/2} N^{-1/2} \mathbf{Z}_I \mathbf{Z}_I^\dagger M^{1/2} \omega_\alpha^{1/2} \Phi_{ai}}{(\omega^2 - \Omega_I^2)} j_\alpha(\omega),$$

and the oscillator strength is given by

$$f_{nq}^{I,\alpha} = 2 \sum_{ia} \Phi_{ia} S^{1/2} N^{-1/2} \mathbf{Z}_I \mathbf{Z}_I^\dagger M^{1/2} \omega_\alpha^{1/2} \Phi_{ia}\,. \tag{377}$$

From Eq. (257) and using the Lehmann representation of the response function $\chi^{n}_{q_\alpha}(\mathbf{r},\omega)$ of Eq. (218), the response $\delta n_j(\mathbf{r},\omega)$ is given by

$$\delta n_j(\mathbf{r},\omega) = \sum_{\alpha}\sum_{k=0}\left[\frac{2\Omega_k\langle\Psi_0|\hat{n}(\mathbf{r})|\Psi_k\rangle\langle\Psi_k|\hat{q}_\alpha|\Psi_0\rangle}{\omega^2-\Omega_k^2}\right]\frac{\delta j_\alpha(\omega)}{\omega_\alpha}.$$

Similarly, the oscillator strength of Eq. (377) can be related to oscillator strength in terms of the matrix elements of the internal pair $(\hat{n}(\mathbf{r}),\hat{q}_\alpha)$ as

$$f_{k,\alpha}(\mathbf{r}) = 2\Omega_k\langle\Psi_0|\hat{n}(\mathbf{r})|\Psi_k\rangle\langle\Psi_k|\hat{q}_\alpha|\Psi_0\rangle \equiv f^{I,\alpha}_{nq}\,. \tag{378}$$

A.3.4 OSCILLATOR STRENGTH FOR THE PHOTON-PHOTON RESPONSE FUNCTION

Finally, we derive the oscillator strength for the photon-photon response function of the photon coordinate $q_{\alpha,j}(\omega)$ due to an external charge current $\delta j_\alpha(\omega)$. First, we define a collective photon coordinate for the α modes as $Q = \sum_\alpha q_\alpha$ (in analogy with $\mathbf{R} = \sum_i e\mathbf{r}_i$). Assuming the collective photon coordinate Q is Taylor expandable, we deduce to first-order the "*displacement field polarizability*" in frequency space as

$$\beta_\alpha(\omega) = \sum_{\alpha'}\frac{1}{\omega_{\alpha'}}\frac{\delta q_\alpha(\omega)}{\delta j_{\alpha'}(\omega)}. \tag{379}$$

By substituting Eq. (376) in Eq. (270) and using the spectral expansion, we obtain

$$\delta q_{\alpha,j}(\omega) = -\sum_I \frac{2\omega_\alpha^{1/2}\mathbf{Z}_I\mathbf{Z}_I^\dagger\omega_\alpha^{1/2}}{\left(\Omega_I^2-\omega^2\right)}j_\alpha.$$

From the above equation, we deduce that

$$\beta_\alpha(\omega) = -\sum_I \frac{\omega_\alpha^{1/2}\mathbf{Z}_I\mathbf{Z}_I^\dagger\omega_\alpha^{1/2}}{\left(\Omega_I^2-\omega^2\right)}\,. \tag{380}$$

Equation (380) is the *displacement field polarizability* analogous to the atomic polarizability tensor of Eq. (371) and the oscillator strength is given by

$$f_{I,\alpha} = \omega_\alpha^{1/2}\mathbf{Z}_I\mathbf{Z}_I^\dagger\omega_\alpha^{1/2}\,. \tag{381}$$

B

DRESSED SPECTRA AND NUMERICAL DETAILS OF COMPUTATIONS

In this section, we present the dressed spectra obtained for a molecule coupled to a photon mode using the frequency-dependent Sterneimer method for electron-photon coupled systems and we also outline the numerical details employed in Chap. 3.

B.1 NUMERICAL DETAILS OF COMPUTATIONS

B.1.1 THE BENZENE MOLECULE

To calculate the electronic structure of the benzene (C_6H_6) molecule, we follow closely the setup of Ref. [120]. Thus, we use a cylindric real space grid of 8 Å length with the radius of 6 Å in the x-y plane, and a spacing of $\Delta x = \Delta y = \Delta z = 0.22$ Å. For the benzene nuclear structure, we use the CC bond length of 1.396 Å, and CH bond length of 1.083 Å. We explicitly describe the 30 valence electrons in our calculations that amounts to 15 doubly occupied Kohn-Sham orbitals, while the core atoms are considered implicitly by LDA Troullier-Martins pseudopotentials [188]. The Casida method requires unoccupied orbitals, thus in the excited state manifold, we include 500 unoccupied states in the pseudo-eigenvalue calculation. This number amounts to $30 \times 500 = 7500$ pairs of occupied-unoccupied states. For the Sternheimer and time-propagation methods, just the 15 doubly occupied orbitals are used in this method. Furthermore, to describe the electron-electron and electron-photon interaction in the response functions, we apply the approximations given in Eq. (298).

B.1.2 THE NAPHTHALENE MOLECULE

To numerical treat the naphthalene ($C_{10}H_8$) molecule, the electronic structure of the naphthalene molecule is computed using a cylindrical real space grid of 8 Å length with the radius of 6 Å in the x-y plane and a spacing $\Delta x = \Delta y = \Delta z = 0.22$ Å. The core electrons of the carbon and hydrogen atoms are described using LDA Troullier-Martins pseudopotentials [188] and the 48 valence electrons are explicitly described in our calculations amounting to 24 doubly occupied KS orbitals. Since the time-propagation method considers only occupied orbitals, in this case only the 24 doubly occupied orbitals are explicitly propagated as in Eq. (177).

B.2 DRESSED AND NOVEL PHOTONIC OBSERVABLE

We are interested in the excited-state properties of the azulene ($C_{10}H_8$) molecule confined within a photonic environment. The observable of interest usually measured in experiments is the photo-absorption cross-section given by the formula in Eq. (317). Here we will show from our ab-initio theory that the spectrum gets modified when

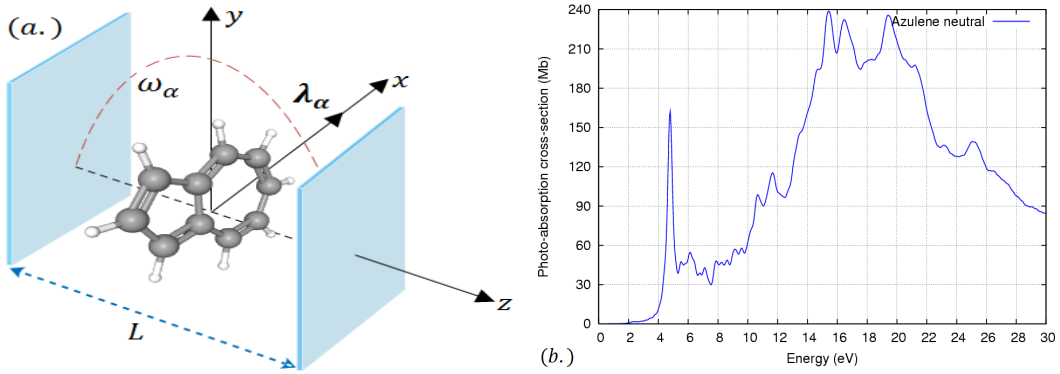

Figure 38: (a.) Schematic setup of an azulene molecule confined within an optical cavity. The cavity field is polarized along the $x-$axis and the photon propagation vector is along the cavity length L. (b.) Reference photo-absorption cross-section spectrum of a neutral azulene molecule in free space computed with TDDFT [122] showing the $\Pi - \Pi^*$ transition at roughly 4.825 eV. The units of the absorption cross-sections is in megabarns ($1\text{Mb} = 10^{-18}\text{cm}^2$).

it strongly interacts with photons. In addition, we show a new observable that is photonic in nature that becomes accessible when light and matter strongly couple. We compute these spectra using the Sternheimer method formulated within linear-response QEDFT discussed in Chap. 3.5.2.

We start by computing the electronic structure of the azulene ($C_{10}H_8$) molecule. The azulene molecule is a bicyclic, nonbenzenoid aromatic hydrocarbon and is an isomer of the naphthalene molecule [189] studied in Chap. 3.6.2. The electronic structure of the azulene molecule is computed using a cylindrical real space grid of 8 Å length with the radius of 6 Å in the x-y plane and a spacings $\Delta x = \Delta y = \Delta z = 0.22$ Å. The core electrons of the carbon and hydrogen atoms are described using LDA Troullier-Martins pseudopotentials [188]. Therefore, the 48 valence electrons are explicitly described in our calculations amounting to 24 doubly occupied KS orbitals. Since the Sternheimer method considers only occupied orbitals, therefore, only the 24 occupied orbitals are used in the computation with the Sternheimer method. The molecule is then confined within an optical cavity of length L and the photon field is polarized along the x-direction with a coupling strength λ_α as shown in Fig. (38.a).

Before showing the results, we first show a reference calculation of the photo-absorption cross-section of the azulene molecule in free space (in the absence of the cavity) using TDDFT [122, 190] as in Fig. (38.b). We find the $\Pi \rightarrow \Pi^*$ electronic transitions in the ultraviolet region of the spectrum at around 4.825 eV. Next, for the situation were the azulene molecule is confined in the cavity, we tune the mode frequency resonant to the peak arising due to the $\Pi - \Pi^*$ transition, that is, $\hbar\omega_\alpha = 4.825$ eV. We now solve the coupled electron-photon Sternheimer equations (300) and (305)-(309) and obtain the photo-absorption cross-section using Eq. (317) only for one component of the polarizabilty tensor, that is, $\alpha_{xx}(\omega)$ as well as the photon coordinate.

In Fig. (38), we show the changes in the photo-absorption cross-section and the imaginary part of the photon coordinate (displacement field) of the azulene molecule coupled to a single photon mode in an optical cavity. First, the coupling strength is set to zero ($\lambda_\alpha = 0$) implying a free space situation as the $\Pi - \Pi^*$ transition occurring at

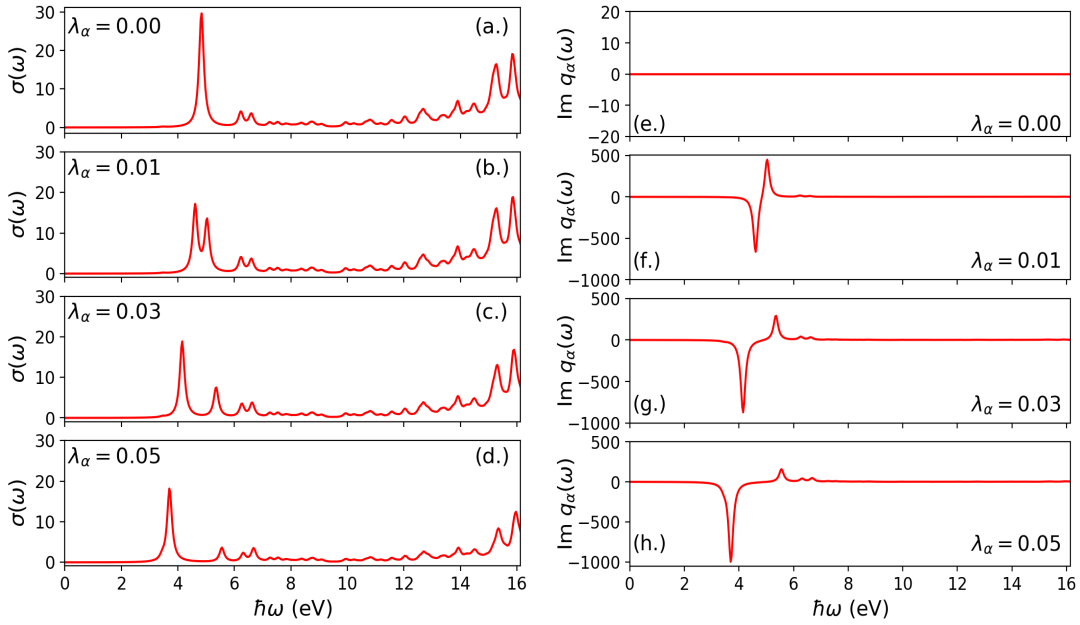

Figure 39: Photo-absorption cross-section and imaginary part of photon coordinate of an azulene molecule confined in an optical cavity. Panel (a.) shows the spectrum of the azulene molecule in free space (i.e. $\lambda_\alpha = 0$) with $\Pi - \Pi^*$ transition at around 4.8 eV. Increasing the coupling strength continuously as in (b.), (c.) and (d.) leads to a splitting of the peak into lower and upper polariton branches that drift apart for increasing λ_α. Panel (e.) has no response as the photons are decoupled. Coupling the photons and increasing the coupling leads to lower and upper polaritonic peaks in the photonic spectrum as in (f.), (g.), (h.).

4.825 eV is captured as depicted in Fig. (39.a). Next, switching on the coupling ($\lambda_\alpha = 0.01$) of the molecule to the cavity mode results to a splitting of the $\Pi - \Pi^*$ transition peak into lower and upper polariton branches as shown in Fig. (39.b). These new peaks are a result of the hybridization of electronic and photonic degrees. Increasing the coupling strength λ_α as in Fig. (39.c,d) further increases the Rabi splitting as light and matter strongly couple. In our description of light-matter interaction, the photon field is quantized and is a dynamical part of the coupled system. This means we can also compute spectral properties of the photon field due to perturbing the electronic system. If we do not couple to the photons (i.e. $\lambda_\alpha = 0$), we obtain the spectrum of Fig. (39.e) showing no response of the photonic subsystem. However, coupling to the photons (i.e. $\lambda_\alpha > 0$) shows novel spectra features that indicate cross-talk between the coupled electronic and photonic subsystems as lower and upper polaritonic peaks emerge as shown in Fig. (39.f,g,h). We observe negative and positive peaks as discussed in Chap. 3.6.2.

In this example, we showed how the molecular subsystem changes due to hybridization with the photon field and also a new observable that become accessible in strong light-matter coupled systems. This open new avenues that can potentially lead to novel linear spectroscopy.

C

ENERGY BASIS AND THE DENSITY MATRIX

This appendix presents the energy basis description of coupled matter-photon systems and the one-body reduced density matrix for the matter-photon systems.

C.1 THE ENERGY BASIS DESCRIPTION OF COUPLED MATTER-PHOTON SYSTEMS

An exact solution of the coupled matter-photon problem even in the dipole approximation described by either of the Hamiltonians of Eqs. (49) and (55) is not feasible except for very small systems [23]. This calls for further approximations to significantly scale-down the degrees of freedom of the coupled problem. A common way to achieve this is to use instead of the full electronic space just a few number of a-priori chosen "relevant states" that couple to the photons [100]. This is common to the field of quantum optics were the electronic space is reduce to a single two-level or collective two-levels [101, 191, 192]. In Chap. 3.6.1 such a two-level system coupled to one photon mode is employed to highlight in a simple way how excited-state properties of coupled electron-photon systems get modified. Also, more than two electronic energy levels can be employed. To do this, one needs to first obtain the electronic spectrum (eigenenergies and eigenstates) from an ab-initio electronic structure method. In the next step, these quantities are used as input parameters in the coupled matter-photon Hamiltonian. Such a procedure will be later applied in Chap. 4.1.7, hence, this section presents how to set up the energy basis description of coupled matter-photon systems.

This representation is derived by assuming that one has access to all electronic eigenenergies E_i and eigenstates $|\psi_i\rangle$ of the matter system and using the completeness relation $\sum_{i=1}^{\infty} |\psi_i\rangle\langle\psi_i| = \hat{\mathbb{1}}$, the operators of the matter system can be expressed as [33]

$$\hat{H}_{\mathrm{el}} = \sum_{i=1} \hbar\omega_i |\psi_i\rangle\langle\psi_i|, \quad \hat{\mathbf{p}} = \sum_{i=1}\sum_{j=1} \langle\psi_i|\hat{\mathbf{p}}|\psi_j\rangle |\psi_i\rangle\langle\psi_j|, \quad \hat{\mathbf{R}} = \sum_{i=1}\sum_{j=1} \langle\psi_i|\hat{\mathbf{R}}|\psi_j\rangle |\psi_i\rangle\langle\psi_j|,$$

where the indices i, j runs over the number of electronic states considered, $\hat{\mathbf{p}} = \sum_{l=1}^{N_e} \hat{\mathbf{p}}_l$ and the diagonal representation of $\hat{H}_{\mathrm{el}}$ was obtained from $\hat{H}_{\mathrm{el}} = \hat{T}_e + \hat{W}_{ee} + \hat{V}_{eN}$. Substituting the above expressions into Eqs. (49) and (55) gives the velocity and length gauge Hamiltonians in energy basis

$$\hat{H}_V^{(E)} = \sum_{i=1} \hbar\omega_i |\psi_i\rangle\langle\psi_i| - \frac{e}{m}\hat{\mathbf{A}} \cdot \sum_{i=1}\sum_{j=1} \langle\psi_i|\hat{\mathbf{p}}|\psi_j\rangle |\psi_i\rangle\langle\psi_j| + \frac{e^2}{2m}\hat{\mathbf{A}}^2 + \hat{H}_{pt}\,, \tag{382}$$

$$\hat{H}_L^{(E)} = \sum_{i=1} \hbar\omega_i |\psi_i\rangle\langle\psi_i| + \frac{1}{2}\sum_{\alpha=1}^{M} \left[\hat{p}_\alpha^2 + \omega_\alpha^2 \left(\hat{q}_\alpha - \frac{\boldsymbol{\lambda}_\alpha}{\omega_\alpha} \cdot \sum_{i=1}^{N}\sum_{j=1} \langle\psi_i|\hat{\mathbf{R}}|\psi_j\rangle |\psi_i\rangle\langle\psi_j| \right)^2 \right]. \tag{383}$$

From Eqs. (382) and (383), the expression of the electron-photon bilinear interaction term is given explicitly as

$$\hat{H}_V^{(int)} = -\frac{e}{m}\sum_{i=1}\sum_{j=1}\sum_{\alpha=1}^{M}\sqrt{\frac{\hbar}{2\omega_\alpha}}\left(\hat{a}_\alpha + \hat{a}_\alpha^\dagger\right)\boldsymbol{\lambda}_\alpha\cdot\langle\psi_i|\hat{\mathbf{p}}|\psi_j\rangle|\psi_i\rangle\langle\psi_j|\,,$$

$$\hat{H}_L^{(int)} = -\sum_{i=1}\sum_{j=1}\sum_{\alpha=1}^{M}\omega_\alpha\sqrt{\frac{\hbar}{2\omega_\alpha}}\left(\hat{a}_\alpha + \hat{a}_\alpha^\dagger\right)\boldsymbol{\lambda}_\alpha\cdot\langle\psi_i|\hat{\mathbf{R}}|\psi_j\rangle|\psi_i\rangle\langle\psi_j|\,.$$

Using the above two equations, one defines the expression for the electron-photon coupling of the velocity and length gauge Hamiltonians given by

$$g_{\alpha,V}^{(ij)} = \frac{e}{m}\sqrt{\frac{\hbar}{\epsilon_0\omega_\alpha V}}\langle\psi_i|\mathbf{e}_\alpha\cdot\hat{\mathbf{p}}|\psi_j\rangle \quad\text{and}\quad g_{\alpha,L}^{(ij)} = \sqrt{\frac{\hbar\omega_\alpha}{\epsilon_0 V}}\langle\psi_i|\mathbf{e}_\alpha\cdot\hat{\mathbf{R}}|\psi_j\rangle\,, \tag{384}$$

where $\boldsymbol{\lambda}_\alpha = \sqrt{2/\epsilon_0 V}\mathbf{e}_\alpha$ was used. From Eq. (384), the electron-photon couplings can be increased by reducing the quantization volume V. Also, the coupling can be increased in cases where the transition dipole (momentum) matrix elements can be increased by varying the binding potential $\hat{V}_{eN}$ (see example in Chap. 4.1.1).

For free space radiation of coupled electron-photon systems for a single particle, the coupling term is related to the radiative decay rate γ_{ij} between two states by [193]

$$g_{\alpha,V}^{(ij)} = \left(\frac{3\hbar^2c^3}{\omega_\alpha\omega_{ij}\epsilon_0 V}\gamma_{ij}\right)^{1/2}, \tag{385}$$

where the relation between the radiative decay rate and the transition dipole matrix elements $\gamma_{ij} = \frac{\omega_{ij}^3|\langle\psi_i|\hat{\mathbf{R}}|\psi_j\rangle|^2}{3\pi\epsilon_0 c^3}$ was used in obtaining Eq. (385). Here, the coupling strength is directly proportional to the square root of the radiative decay rate. From the energy basis representation, simplified models that utilize just a few "relevant states" (few-levels approximation) can be deduce. Although these simplified quantum optical models are able to describe in some cases the emerging physical effects, in other cases they are less accurate as discussed in Chap. 4.1.7.

C.2 THE DENSITY MATRIX AND PURITY

To quantify features of entanglement in the matter-photon coupled system, it is appropriate to compute the purity. This can be done by defining appropriate one-body reduced density matrices for the individual subsystems [194, 195]. For the case of the matter-photon system, the one-body reduced density matrices of the entire electronic and photonic subsystems are given respectively by

$$\gamma_{\text{el}}(\underline{\mathbf{r}},\underline{\mathbf{r}}') = \int d\underline{q}\,\Psi(\underline{\mathbf{r}},\underline{q})\Psi^*(\underline{\mathbf{r}}',\underline{q})\,,$$

$$\gamma_{\text{pt}}(\underline{q},\underline{q}') = \int d^3\underline{\mathbf{r}}\,\Psi(\underline{\mathbf{r}},\underline{q})\Psi^*(\underline{\mathbf{r}},\underline{q}')\,,$$

where the notation $\underline{\mathbf{r}} = (\mathbf{r}_1,...,\mathbf{r}_{N_e})$ and $\underline{q} = (q_1,...,q_M)$. The normalization of these reduced density matrices can be chosen to be equal to one, such that the following holds

$$\text{Tr}(|\Psi\rangle\langle\Psi^*|) = \text{Tr}(\gamma_{\text{el}}) = \text{Tr}(\gamma_{\text{pt}}) = 1\,.$$

From this normalization, the reduced density matrices can be used to compute the purity of the subsystems by requiring

$$\mathrm{Tr}\left(\gamma_{\mathrm{el}}^2\right) = \mathrm{Tr}(\gamma_{\mathrm{pt}}^2) = 1\,. \tag{386}$$

The purity is obtained by tracing over the square of the one-body reduced density matrix of the respective subsystems. If the purity is equal to one, the system can be expressed as a factorizable state of the subsystems and the rest of the coupled matter-photon system. If the purity is smaller than one, implies a non-factorizable state, which indicates entanglement between the subsystems. It is also possible to determine the purity of the constituents of individual subsystems. Consider the case of computing the purity of each of the M photon modes. In this case, the one-body reduced density matrices of these individual M modes are

$$\begin{aligned}
\gamma_1(q_1, q_1') &= \iiint d^3\underline{\mathbf{r}}\, dq_2\, dq_3 \ldots \int dq_M \Psi(\underline{\mathbf{r}}, q_1, q_2, q_3, \ldots, q_M)\Psi^*(\underline{\mathbf{r}}, q_1', q_2, q_3, \ldots, q_M),\\
\gamma_2(q_2, q_2') &= \iiint d^3\mathbf{r}\, dq_1\, dq_3 \ldots \int dq_M \Psi(\underline{\mathbf{r}}, q_1, q_2, q_3, \ldots, q_M)\Psi^*(\underline{\mathbf{r}}, q_1, q_2', q_3, \ldots, q_M),\\
\gamma_3(q_3, q_3') &= \iiint d^3\underline{\mathbf{r}}\, dq_1\, dq_2 \ldots \int dq_M \Psi(\underline{\mathbf{r}}, q_1, q_2, q_3, \ldots, q_M)\Psi^*(\underline{\mathbf{r}}, q_1, q_2, q_3', \ldots, , q_M),\\
&\vdots\\
\gamma_M(q_M, q_M') &= \iiint d^3\underline{\mathbf{r}}\, dq_1\, dq_2 \ldots \int dq_{M-1} \Psi(\underline{\mathbf{r}}, q_1, q_2, q_3, \ldots, q_M)\Psi^*(\underline{\mathbf{r}}, q_1, q_2, q_3, \ldots, , q_M').
\end{aligned}$$

Where $\gamma_1(q_1, q_1')$, $\gamma_2(q_2, q_2')$, $\gamma_3(q_3, q_3')$, ..., $\gamma_M(q_M, q_M')$ are respectively the one-body reduced density matrices of the photonic subsystems. From Eq. (386), the purity of the photon modes can be determined.

D

NUMERICAL IMPLEMENTATION

In this section, we outline the numerical implementations used in this thesis and also the code development that lead to the results presented in this work. The results presented in this thesis are based on *ab initio* model and real systems calculations. The model systems considered in this thesis were treated numerically with a Python code of our group called LIBQED which Heiko Appel, Sebastian Ohlmann, Mary-Leena Tchenkoue and for the most part myself built from scratch. The real systems were treated by the real-space Octopus code (`https://octopus-code.org/`).

D.1 MODEL SYSTEMS WITH LIBQED

In order to treat numerically the model systems considered in this thesis, we developed the calculation modes listed below in LIBQED. LIBQED is an efficiently parallelized Python code that treats numerically exactly matter-photon coupled systems (or the decoupled subsystems) using a real-space basis set. It is well suited to treat model systems in one- and two-dimension but it is not restricted only to model systems since the calculation modes 1 to 6 can be used to treat small three-dimensional system, for example, the Helium atom.

1. **Calculation Modes: td, tp :** These run modes (**td** or **tp**) performs a time-propagation of Eq. (6) for a given time-independent (or time-dependent) Hamiltonian for a given initial state. As propagators, we've implemented the Lanczos propagator, 4th order Runge-Kutta, and the "enforced time-reversal symmetry" based on the exponential midpoint rule.

2. **Calculation Mode: gs :** Here an imaginary time-propagation is performed that determines the ground-state of an arbitrary system for a guess of the initial state. The propagators mentioned above can be used.

3. **Calculation Modes: ed, td_ed :** The **ed** calculation mode diagonalizes the time-independent Schrödinger equation (7) by calling Eigenvalue SoLvers for Petaflop-Applications (ELPA) and outputs the full spectrum (eigenvalues and eigenvectors). The Hamiltonian matrix is distributed in block-cyclic fashion for diagonalization. The **td_ed** mode first performs an exact diagonalization as the run mode **ed** and then performs a time-propagation using the spectrum results.

4. **CalculationMode: ms :** performs a Maxwell-Schrödinger time-propagation of the forms (velocity and length gauge) presented in Chap. 2.3.1. It uses the propagators described above.

5. **CalculationMode: dft :** this performs a ground-state calculation for electron-only one-dimensional systems discussed in Chap. 2.5.1.1.

6. **CalculationMode: stern:** when specified, it performs the Sternheimer calculation for the electron-only case or electron-photon Sternheimer for one-dimensional

systems in Chap. 3.5.2 coupled to photons. We've implemented the biconjugate gradient stabilized method to solve the Sternheimer equations.

D.2 REAL SYSTEMS WITH OCTOPUS

The real system calculations presented in Chap. 3.6 were obtained using the real-space OCTOPUS code [83, 120, 121]. The real-space OCTOPUS code already had the implementation of the three linear-response methods (Casida, Sternheimer, time-propagation) that treated only the interacting many-electron systems. The numerical implementation of the extension of these linear response methods to treat matter-photon coupled systems was carried out by Johannes Flick, Davis Welakuh, Sebastian Olhmann and Heiko Appel. The Casida method was implemented by Johannes Flick and massively parallelized by Sebastian Olhmann. The Sternheimer method was implemented by Davis Welakuh and Heiko Appel oversaw this implementation. The time-propagation method was independently implemented by Johannes Flick and Davis Welakuh. In the following we mention a few useful details about this implementations, for example, to perform linear response calculations of matter-photon coupled systems using this methods, the flag "EnablePhotons" should be set to "yes".

1. **CalculationMode: casida :** This calculation mode performs an exact diagonalization of Eq. (295) and outputs the eigenvalues (transition energies), eigenvectors (eigenstates) and the norm of these eigenstates. For larger matrices, the diagonalization is done in parallel using ScaLAPACK or ELPA.

2. **CalculationMode: em_resp :** Here a self-consistency calculation of the Sternheimer equations of Eqs. (305)-(306) together with Eq. (260) and Eqs. (308)-(309) is performed to obtain the frequency-dependent linear density response and photon coordinate. Both parameters η and η' are necessary to obtain the complex density and photon coordinate and we suggest using $\eta' = 0.001$ eV.

3. **CalculationMode: td :** Equally, a self-consistency calculation of the Maxwell-KS system given by Eqs. (177) and (178) are evolved in time to obtain the time-dependent density response (or dipole) and photon coordinate. In practice, Eq. (178) is replaced by Eq. (179) for faster propagation.

BIBLIOGRAPHY

[1] James A. Hutchison, Tal Schwartz, Cyriaque Genet, Eloïse Devaux, and Thomas W. Ebbesen. "Modifying Chemical Landscapes by Coupling to Vacuum Fields." In: *Angew. Chem. Int. Ed.* 51.7 (2012), pp. 1592–1596. ISSN: 1521-3773. DOI: 10.1002/anie.201107033 (cit. on pp. 3, 51).

[2] David M. Coles, Niccolo Somaschi, Paolo Michetti, Caspar Clark, Pavlos G. Lagoudakis, Pavlos G. Savvidis, and David G. Lidzey. "Polariton-mediated energy transfer between organic dyes in a strongly coupled optical microcavity." In: *Nature Materials* 13.7 (May 2014), pp. 712–719. DOI: 10.1038/nmat3950 (cit. on pp. 3, 56).

[3] Xiaolan Zhong, Thibault Chervy, Lei Zhang, Anoop Thomas, Jino George, Cyriaque Genet, James A. Hutchison, and Thomas W. Ebbesen. "Energy Transfer between Spatially Separated Entangled Molecules." In: *Ang. Chem. Int. Ed.* 56.31 (July 2017), pp. 9034–9038. DOI: 10.1002/anie.201703539 (cit. on pp. 3, 56).

[4] E. Orgiu et al. "Conductivity in organic semiconductors hybridized with the vacuum field." In: *Nature Mater.* 14.11 (Sept. 2015), pp. 1123–1129. DOI: 10.1038/nmat4392 (cit. on p. 3).

[5] Daqing Wang, Hrishikesh Kelkar, Diego Martin-Cano, Dominik Rattenbacher, Alexey Shkarin, Tobias Utikal, Stephan Götzinger, and Vahid Sandoghdar. "Turning a molecule into a coherent two-level quantum system." In: *Nature Physics* 15 (Feb. 2019), pp. 483–489. DOI: 10.1038/s41567-019-0436-5 (cit. on p. 3).

[6] Kenji Hirai, James A. Hutchison, and Hiroshi Uji-i. "Recent Progress in Vibropolaritonic Chemistry." In: *ChemPlusChem* 85.9 (Sept. 2020), pp. 1981–1988. DOI: 10.1002/cplu.202000411 (cit. on p. 3).

[7] W. Pauli and M. Fierz. "Zur Theorie der Emission langwelliger Lichtquanten." In: *Nuovo Cim.* 15 (1938), pp. 167–188. DOI: 10.1007/BF02958939 (cit. on pp. 3, 9).

[8] Michael Ruggenthaler, Nicolas Tancogne-Dejean, Johannes Flick, Heiko Appel, and Angel Rubio. "From a quantum-electrodynamical light-matter description to novel spectroscopies." In: *Nature Reviews Chemistry* 2.3 (Mar. 2018), p. 0118. DOI: 10.1038/s41570-018-0118 (cit. on pp. 3, 9, 19, 86).

[9] Walter Kohn. "Nobel Lecture: Electronic structure of matter-wave functions and density functionals." In: *Rev. Mod. Phys.* 71 (1999), p. 1253. DOI: 10.1103/RevModPhys.71.1253 (cit. on pp. 3, 27, 28).

[10] Trygve Helgaker, Poul Jorgensen, and Jeppe Olsen. *Molecular Electronic-Structure Theory*. John Wiley and Sons Ltd, 2000. DOI: 10.1002/9781119019572 (cit. on pp. 3, 11).

[11] Monika Rodney J. Bartlett and Monika Musiał. "Coupled-cluster theory in quantum chemistry." In: *Rev. Mod. Phys.* 79 (1 Feb. 2007), pp. 291–352. DOI: 10.1103/RevModPhys.79.291 (cit. on p. 3).

[12] Michael Ruggenthaler, Johannes Flick, Camilla Pellegrini, Heiko Appel, Ilya V. Tokatly, and Angel Rubio. "Quantum-electrodynamical density-functional theory: Bridging quantum optics and electronic-structure theory." In: *Phys. Rev. A* 90 (1 July 2014), p. 012508. DOI: 10.1103/PhysRevA.90.012508 (cit. on pp. 4, 27, 43, 45, 51, 85, 86, 127, 149).

[13] Johannes Flick, Michael Ruggenthaler, Heiko Appel, and Angel Rubio. "Kohn-Sham approach to quantum electrodynamical density-functional theory: Exact time-dependent effective potentials in real space." In: *Proc. Natl. Acad. Sci. U. S. A.* 112.50 (2015), pp. 15285–15290. DOI: 10.1073/pnas.1518224112 (cit. on pp. 4, 18, 20, 45, 51, 109, 118, 127, 149).

[14] Michael Ruggenthaler. "Ground-State Quantum-Electrodynamical Density-Functional Theory." In: *ArXiv e-prints* (Sept. 2017). arXiv: 1509.01417 [quant-ph] (cit. on pp. 4, 27, 40–42, 45, 52).

[15] Tor S. Haugland, Enrico Ronca, Eirik F. Kjonstad, Angel Rubio, and Henrik Koch. "Coupled Cluster Theory for Molecular Polaritons: Changing Ground and Excited States." In: *Phys. Rev. X* 10.4 (Dec. 2020), p. 041043. DOI: 10.1103/PhysRevX.10.041043 (cit. on pp. 4, 110, 151).

[16] Uliana Mordovina, Callum Bungey, Heiko Appel, Peter J. Knowles, Angel Rubio, and Frederick R. Manby. "Polaritonic coupled-cluster theory." In: *Phys. Rev. Research* 2 (June 2020), p. 023262. DOI: 10.1103/PhysRevResearch.2.023262 (cit. on p. 4).

[17] Johannes Flick, Christian Schäfer, Michael Ruggenthaler, Heiko Appel, and Angel Rubio. "Ab Initio Optimized Effective Potentials for Real Molecules in Optical Cavities: Photon Contributions to the Molecular Ground State." In: *ACS Photonics* 5.3 (2018), pp. 992–1005. DOI: 10.1021/acsphotonics.7b01279 (cit. on pp. 4, 51, 149).

[18] Johannes Flick, Davis M. Welakuh, Michael Ruggenthaler, Heiko Appel, and Angel Rubio. "Light-Matter Response in Nonrelativistic Quantum Electrodynamics." In: *ACS Photonics* 6.11 (2019), pp. 2757–2778. DOI: 10.1021/acsphotonics.9b00768 (cit. on pp. 4, 43, 45, 47, 52, 72, 111, 151).

[19] Johannes Flick and Prineha Narang. "Ab initio polaritonic potential-energy surfaces for excited-state nanophotonics and polaritonic chemistry." In: *J. Chem. Phys.* 153 (2020), p. 094116. DOI: 10.1063/5.0021033 (cit. on pp. 4, 150).

[20] Derek S. Wang, Tomáš Neuman, Johannes Flick, and Prineha Narang. "Light-matter interaction of a molecule in a dissipative cavity from first principles." In: *J. Chem. Phys.* 154 (Mar. 2021), p. 104109. DOI: 10.1063/5.0036283 (cit. on pp. 4, 99, 111, 150, 151).

[21] Tor S. Haugland, Christian Schäfer, Enrico Ronca, Angel Rubio, and Henrik Koch. "Intermolecular interactions in optical cavities: an ab initio QED study." In: *J. Chem. Phys.* 154 (Mar. 2021), p. 094113. DOI: 10.1063/5.0039256 (cit. on pp. 4, 110).

[22] Camilla Pellegrini, Johannes Flick, Ilya V. Tokatly, Heiko Appel, and Angel Rubio. "Optimized Effective Potential for Quantum Electrodynamical Time-Dependent Density Functional Theory." In: *Phys. Rev. Lett.* 115 (9 Aug. 2015), p. 093001. DOI: 10.1103/PhysRevLett.115.093001 (cit. on pp. 4, 51, 85, 86, 127, 149).

[23] Dominik Sidler, Christian Schäfer, Michael Ruggenthaler, and Angel Rubio. "Polaritonic Chemistry: Collective Strong Coupling Implies Strong Local Modification of Chemical Properties." In: *J. Phys. Chem. Lett.* 12 (2021), pp. 508–516. DOI: 10.1021/acs.jpclett.0c03436 (cit. on pp. 4, 150, 151, 167).

[24] Walter Greiner and Joachim Reinhardt. *Field quantization*. Springer-Verlag Berlin Heidelberg, 1996. DOI: 10.1007/978-3-642-61485-9 (cit. on p. 9).

[25] Hans A. Bethe and Edwin E. Salpeter. *Quantum Mechanics of One- and Two-Electron Atoms*. Springer-Verlag Berlin, Heidelberg, 1957. DOI: 10.1007/978-3-662-12869-5 (cit. on pp. 9, 97).

[26] M. Born and R. Oppenheimer. "Zur Quantentheorie der Molekeln." In: *Ann. Phys.* 389.20 (1927), pp. 457–484. ISSN: 1521-3889. DOI: 10.1002/andp.19273892002 (cit. on p. 9).

[27] Christian Schäfer, Michael Ruggenthaler, and Angel Rubio. "Ab initio nonrelativistic quantum electrodynamics: Bridging quantum chemistry and quantum optics from weak to strong coupling." In: *Phys. Rev. A* 98 (2018), p. 043801. DOI: 10.1103/PhysRevA.98.043801 (cit. on pp. 9, 83, 118).

[28] Claude Cohen-Tannoudji, Jacques Dupont-Roc, and Gilbert Grynberg. *Photons and Atoms: Introduction to Quantum Electrodynamics*. John Wiley and Sons, Inc., 1989. DOI: 10.1002/9783527618422 (cit. on pp. 9, 17).

[29] D. P. Craig and T. Thirunamachandran. *Molecular Quantum Electrodynamics: An Introduction to Radiation-molecule Interactions*. Dover Books on Chemistry Series. Dover Publications, 1998. ISBN: 9780486402147. URL: https://store.doverpublications.com/0486402142.html (cit. on pp. 9, 12).

[30] Erwin Schrödinger. "An Undulatory Theory of the Mechanics of Atoms and Molecules." In: *Phys. Rev.* 28 (1926), p. 1049. DOI: 10.1103/PhysRev.28.1049 (cit. on p. 10).

[31] Gianluca Stefanucci and Robert van Leeuwen. *Nonequilibrium Many-Body Theory of Quantum Systems: A Modern Introduction*. Cambridge University Press, 2013. DOI: 10.1017/CBO9781139023979 (cit. on p. 11).

[32] David A. Mazziotti. "Two-Electron Reduced Density Matrix as the Basic Variable in Many-Electron Quantum Chemistry and Physics." In: *Chem. Rev.* 112.1 (Aug. 2012), pp. 244–262. DOI: 10.1021/cr2000493 (cit. on p. 11).

[33] Rodney Loudon. *The Quantum Theory of Light*. Oxford University Press, 2000. URL: https://global.oup.com/academic/product/the-quantum-theory-of-light-9780198501763?cc=de&lang=en& (cit. on pp. 12, 14, 114, 167).

[34] Peter W. Milonni. *The Quantum Vacuum: An Introduction to Quantum Electrodynamics*. Academic Press, Boston, 1993 (cit. on pp. 14, 15).

[35] C. C. Gerry and P. L. Knight. *Introductory Quantum Optics*. Cambridge University Press, 2005. DOI: 10.1017/CBO9780511791239 (cit. on pp. 14, 114).

[36] Gilbert Grynberg, Alain Aspect, and Claude Fabre. *Introduction to Quantum Optics From Semi-classical Approach to Quantized Light*. Cambridge University Press, New York, 2010. DOI: 10.1017/CBO9780511778261 (cit. on pp. 14, 17, 22, 53, 85).

[37] D. F. Walls and Gerard J. Milburn. *Quantum Optics*. Springer-Verlag Berlin Heidelberg, 1994. DOI: 10.1007/978-3-540-28574-8 (cit. on p. 14).

[38] Daniel Adam Steck. *Quantum and Atom Optics*. available online at http://steck.us/teaching, 2015. URL: http://atomoptics-nas.uoregon.edu/~dsteck/teaching/quantum-optics/quantum-optics-notes.pdf (cit. on pp. 15, 18).

[39] Iwo Białynicki-Birula Zofia Białynicka-Birula. *QED: Quantum theory of the electromagnetic field*. Ed. by Bob D. Guenther. Encyclopedia of Modern Optics (Elsevier, Amsterdam), 2004. DOI: 10.1016/C2013-0-10071-2 (cit. on p. 15).

[40] K. Kakazu and Y. S. Kim. "Quantization of electromagnetic fields in cavities and spontaneous emission." In: *Phys. Rev. A* 50 (Aug. 1994), p. 1830. DOI: 10.1103/PhysRevA.50.1830 (cit. on p. 15).

[41] Herbert Spohn. *Dynamics of charged particles and their radiation field*. Cambridge university press, 2004. DOI: 10.1017/CBO9780511535178 (cit. on pp. 16, 17, 28, 52, 96, 98, 137).

[42] Farhad H. M. Faisal. *Theory of Multiphoton Processes*. Berlin: Springer US, 1987. DOI: 10.1007/978-1-4899-1977-9 (cit. on pp. 16, 17, 53).

[43] Vasil Rokaj, Michael Ruggenthaler, Florian G. Eich, and Angel Rubio. "The Free Electron Gas in Cavity Quantum Electrodynamics." In: *arXiv:2006.09236* (2020) (cit. on pp. 17, 98, 118, 137).

[44] Vasil Rokaj, Davis M. Welakuh, Michael Ruggenthaler, and Angel Rubio. "Light-matter interaction in the long-wavelength limit: no ground-state without dipole self-energy." In: *J. Phys. B: At. Mol. Opt. Phys.* 51.3 (Jan. 2018), p. 034005. DOI: 10.1088/1361-6455/aa9c99 (cit. on pp. 18, 23, 52–56, 85, 118).

[45] A. D. Bandrauk, F. Fillion-Gourdeau, and E. Lorin. "Atoms and molecules in intense laser fields: gauge invariance of theory and models." In: *J. Phys. B: At. Mol. Opt. Phys.* 46 (2013), p. 153001. DOI: 10.1088/0953-4075/46/15/153001 (cit. on p. 18).

[46] Ilya V. Tokatly. "Time-Dependent Density Functional Theory for Many-Electron Systems Interacting with Cavity Photons." In: *Phys. Rev. Lett.* 110 (23 June 2013), p. 233001. DOI: 10.1103/PhysRevLett.110.233001 (cit. on pp. 21, 43, 45).

[47] Johannes Flick and Prineha Narang. "Cavity-Correlated Electron-Nuclear Dynamics from First Principles." In: *Phys. Rev. Lett.* 121 (2018), p. 113002. DOI: 10.1103/PhysRevLett.121.113002 (cit. on pp. 21, 80, 92, 150, 151).

[48] Tai L. Chow. *Mathematical Methods for Physicists: A Concise Introduction*. Cambridge University Press, 2000. DOI: 10.1017/CBO9780511755781 (cit. on pp. 21, 22).

[49] Marlan Scully and Muhammad Suhail Zubairy. *Quantum Optics*. Cambridge University Press, 1997. DOI: 10.1017/CBO9780511813993 (cit. on pp. 22, 23, 85).

[50] Ryogo Kubo. "Statistical-Mechanical Theory of Irreversible Processes. I. General Theory and Simple Applications to Magnetic and Conduction Problems." In: *J. Phys. Soc. Jpn.* 12 (1957), pp. 570–586. DOI: 10.1143/JPSJ.12.570 (cit. on p. 23).

[51] Alexander Fetter and John Dirk Walecka. *Quantum theory of many-particle systems*. Courier Corporation, 2003. URL: https://store.doverpublications.com/0486428273.html (cit. on p. 23).

[52] Philippe Blanchard and Erwin Brüning. *Mathematical Methods in Physics: Distributions, Hilbert Space Operators, Variational Methods, and Applications in Quantum Physics*. Vol. 69. Birkhäuser, 2015. DOI: 10.1007/978-3-319-14045-2 (cit. on p. 25).

[53] Carsten A. Ullrich. *Time-dependent density-functional theory: concepts and applications*. OUP Oxford, 2011. DOI: 10.1093/acprof:oso/9780199563029.001.0001 (cit. on pp. 26, 32, 34, 76, 77, 157, 159).

[54] Harry Lehmann. "Über Eigenschaften von Ausbreitungsfunktionen und Renormierungskonstanten quantisierter Felder." In: *Nuovo Cimento II* 11 (1954), 342–357. DOI: 10.1007/BF02783624 (cit. on p. 26).

[55] Eberhard Engel Reiner M. Dreizler. *Density Functional Theory: An Advanced Course*. Theoretical and Mathematical Physics. Springer-Verlag Berlin Heidelberg, 2011. ISBN: 9783642140907. DOI: 10.1007/978-3-642-14090-7 (cit. on pp. 27, 28).

[56] M. Marques, N. Maitra, F. Nogueira, E. Gross, and A. Rubio. *Fundamentals of Time-Dependent Density Functional Theory*. Lecture Notes in Physics, Springer Berlin Heidelberg, 2012. URL: https://www.springer.com/gp/book/9783642235177 (cit. on pp. 27, 32).

[57] Viraht Sahni. *Quantal Density Functional Theory*. Springer-Verlag Berlin Heidelberg, 2016. DOI: 10.1007/978-3-662-09624-6 (cit. on p. 28).

[58] Klaus Capelle. "A bird's-eye view of density-functional theory." In: *Braz. J. Phys.* 36.4a (2006), pp. 1318–1343. DOI: 10.1590/S0103-97332006000700035 (cit. on pp. 28, 29).

[59] Helmut Eschrig. *The Fundamentals of Density Functional Theory (Teubner Texte zur Physik)*. Vieweg and Teubner Verlag, Wiesbaden, 1996. DOI: 10.1007/978-3-322-97620-8 (cit. on p. 28).

[60] P. Hohenberg and W. Kohn. "Inhomogeneous Electron Gas." In: *Phys. Rev.* 136 (3B Nov. 1964), pp. 864–871. DOI: 10.1103/PhysRev.136.B864 (cit. on pp. 28, 29).

[61] Mel Levy. "Universal variational functionals of electron densities, first-order density matrices, and natural spin-orbitals and solution of the v-representability problem." In: *Proc. Natl. Acad. Sci. USA* 76.12 (1979), pp. 6062–6065. DOI: 10.1073/pnas.76.12.6062 (cit. on pp. 29, 52).

[62] Walter Kohn. "v-Representability and Density Functional Theory." In: *Phys. Rev. Lett.* 51.17 (Oct. 1983), pp. 1596–1598. DOI: 10.1103/PhysRevLett.51.1596 (cit. on p. 29).

[63] Mel Levy. "Electron densities in search of Hamiltonians." In: *Phys. Rev. A* 26.3 (Sept. 1982), pp. 1200–1208. DOI: 10.1103/PhysRevA.26.1200 (cit. on p. 29).

[64] W. Kohn and L. J. Sham. "Self-Consistent Equations Including Exchange and Correlation Effects." In: *Phys. Rev.* 140 (4A Nov. 1965), A1133–A1138. DOI: 10.1103/PhysRev.140.A1133 (cit. on pp. 30, 32, 82).

[65] Michael Ruggenthaler, Markus Penz, and Robert van Leeuwen. "Existence, uniqueness, and construction of the density-potential mapping in time-dependent density-functional theory." In: *J. Phys.: Condens. Matter* 27.20 (2015), p. 203202. DOI: 10.1088/0953-8984/27/20/203202 (cit. on pp. 30, 36, 45, 46).

[66] Miguel A.L. Marques, Micael J.T. Oliveira, and Tobias Burnus. "Libxc: A library of exchange and correlation functionals for density functional theory." In: *Computer Physics Communications* 183.10 (2012), pp. 2272 –2281. ISSN: 0010-4655. DOI: 10.1016/j.cpc.2012.05.007 (cit. on p. 32).

[67] John P. Perdew and Alex Zunger. "Self-interaction correction to density-functional approximations for many-electron systems." In: *Phys. Rev. B* 23 (10 May 1981), pp. 5048–5079. DOI: 10.1103/PhysRevB.23.5048 (cit. on pp. 32, 82).

[68] Axel D. Becke. "Density-functional exchange-energy approximation with correct asymptotic behavior." In: *Phys. Rev. A* 38 (1988), p. 3098. DOI: 10.1103/PhysRevA.38.3098 (cit. on p. 32).

[69] John P. Perdew and Yue Wang. "Accurate and simple analytic representation of the electron-gas correlation energy." In: *Phys. Rev. B* 45 (1992), p. 13244. DOI: 10.1103/PhysRevB.45.13244 (cit. on p. 32).

[70] John P. Perdew, Kieron Burke, and Matthias Ernzerhof. "Generalized Gradient Approximation Made Simple." In: *Phys. Rev. Lett.* 77 (18 Oct. 1996), pp. 3865–3868. DOI: 10.1103/PhysRevLett.77.3865 (cit. on p. 32).

[71] C. A. Ullrich, U. J. Gossmann, and E. K. U. Gross. "Time-Dependent Optimized Effective Potential." In: *Phys. Rev. Lett.* 74 (1995), p. 872. DOI: 10.1103/PhysRevLett.74.872 (cit. on p. 32).

[72] Stephan Kümmel and John P. Perdew. "Optimized effective potential made simple: Orbital functionals, orbital shifts, and the exact Kohn-Sham exchange potential." In: *Phys. Rev. B* 68 (3 July 2003), p. 035103. DOI: 10.1103/PhysRevB.68.035103 (cit. on p. 32).

[73] John P. Perdew and Matthias Ernzerhof. "Rationale for mixing exact exchange with density functional approximations." In: *J. Chem. Phys.* 105 (1996), p. 9982. DOI: 10.1063/1.472933 (cit. on p. 32).

[74] Erich Runge and E. K. U. Gross. "Density-Functional Theory for Time-Dependent Systems." In: *Phys. Rev. Lett.* 52 (12 Mar. 1984), pp. 997–1000. DOI: 10.1103/PhysRevLett.52.997 (cit. on pp. 32, 34, 35).

[75] Eberhard K. U. Gross, E. Runge, and O. Heinonen. *Many-Particle Theory*. Adam Hilger, 1991. ISBN: 9780750300728. URL: http://books.google.de/books?id=F6VfQgAACAAJ (cit. on p. 32).

[76] Silvana Botti, Arno Schindlmayr, Rodolfo Del Sole, and Lucia Reining. "Time-dependent density-functional theory for extended systems." In: *Rep. Prog. Phys.* 70 (2007), p. 357. DOI: doi:10.1088/0034-4885/70/3/R02 (cit. on p. 32).

[77] I. V. Tokatly. "Quantum many-body dynamics in a Lagrangian frame: I. Equations of motion and conservation laws." In: *Phys. Rev. B* 71 (Apr. 2005), p. 165104. DOI: 10.1103/PhysRevB.71.165104 (cit. on p. 33).

[78] Ilya V. Tokatly. "Quantum many-body dynamics in a Lagrangian frame: II. Geometric formulation of time-dependent density functional theory." In: *Phys. Rev. B* 71 (16 Apr. 2005), p. 165105. DOI: 10.1103/PhysRevB.71.165105 (cit. on p. 33).

[79] Neepa T. Maitra, Kieron Burke, and Chris Woodward. "Memory in Time-Dependent Density Functional Theory." In: *Phys. Rev. Lett.* 89 (2 June 2002), p. 023002. DOI: 10.1103/PhysRevLett.89.023002 (cit. on pp. 36, 46).

[80] M. Petersilka, U. J. Gossmann, and E. K. U. Gross. "Excitation Energies from Time-Dependent Density-Functional Theory." In: *Phys. Rev. Lett.* 76 (8 Feb. 1996), pp. 1212–1215. DOI: 10.1103/PhysRevLett.76.1212 (cit. on pp. 38, 39).

[81] M. Ruggenthaler, S. E. B. Nielsen, and R. van Leeuwen. "Analytic density functionals with initial-state dependence and memory." In: *Phys. Rev. A* 88 (Aug. 2013), p. 022512. DOI: 10.1103/PhysRevA.88.022512 (cit. on p. 39).

[82] K. Yabana and G. F. Bertsch. "Time-dependent local-density approximation in real time: Application to conjugated molecules." In: *International Journal of Quantum Chemistry* 75.1 (1999), pp. 55–66. ISSN: 1097-461X. DOI: 10.1002/(SICI)1097-461X(1999)75:1<55::AID-QUA6>3.0.CO;2-K (cit. on pp. 39, 40, 80–82).

[83] Xavier Andrade, Silvana Botti, Miguel A. L. Marques, and Angel Rubio. "Time-dependent density functional theory scheme for efficient calculations of dynamic (hyper)polarizabilities." In: *J. Chem. Phys.* 126 (May 2007), p. 184106. DOI: 10.1063/1.2733666 (cit. on pp. 39, 77, 80, 81, 157, 172).

[84] Mark E. Casida. "Time-Dependent Density Functional Response Theory of Molecular Systems: Theory, Computational Methods, and Functionals." In: *Recent Developments and Applications of Modern Density Functional Theory*. Ed. by J. M. Seminario. Elsevier, Amsterdam, 1996. DOI: 10.1142/9789812830586_0005 (cit. on pp. 39, 40, 71, 76, 159).

[85] René Jestädt, Michael Ruggenthaler, Micael J. T. Oliveira, Angel Rubio, and Heiko Appel. "Light-matter interactions within the Ehrenfest-Maxwell-Pauli-Kohn-Sham framework: fundamentals, implementation, and nano-optical applications." In: *Advances in Physics* 68 (2020), pp. 225–333. DOI: 10.1080/00018732.2019.1695875 (cit. on pp. 43, 126, 131, 151).

[86] A. K. Rajagopal. "Time-dependent functional theory of coupled electron and electromagnetic fields in condensed-matter systems." In: *Phys. Rev. A* 50 (1994), p. 3759. DOI: 10.1103/PhysRevA.50.3759 (cit. on p. 43).

[87] M. Ruggenthaler, F. Mackenroth, and D. Bauer. "Time-dependent Kohn-Sham approach to quantum electrodynamics." In: *Phys. Rev. A* 84 (4 Oct. 2011), p. 042107. DOI: 10.1103/PhysRevA.84.042107 (cit. on p. 43).

[88] M. Ruggenthaler and R. van Leeuwen. "Global fixed-point proof of time-dependent density-functional theory." In: *EPL* 95.1 (2011), p. 13001. DOI: 10.1209/0295-5075/95/13001 (cit. on p. 45).

[89] Thomas W. Ebbesen. "Hybrid Light-Matter States in a Molecular and Material Science Perspective." In: *Acc. Chem. Res.* 49.11 (Nov. 2016), pp. 2403–2412. DOI: 10.1021/acs.accounts.6b00295 (cit. on p. 51).

[90] Kati Stranius, Manuel Hertzog, and Karl Börjesson. "Selective manipulation of electronically excited states through strong light-matter interactions." In: *Nature Communications* 9 (June 2018), p. 2273. DOI: 10.1038/s41467-018-04736-1 (cit. on pp. 51, 90, 149).

[91] Johannes Flick, Michael Ruggenthaler, Heiko Appel, and Angel Rubio. "Atoms and molecules in cavities, from weak to strong coupling in quantum-electrodynamics (QED) chemistry." In: *Proceedings of the National Academy of Sciences* 114.12 (2017), pp. 3026–3034. DOI: 10.1073/pnas.1615509114 (cit. on pp. 51, 94, 113, 127, 149).

[92] Elliott H. Lieb. *The Stability of Matter: From Atoms to Stars*. Ed. by Walter Thirring. Springer, Berlin, Heidelberg, 2005. DOI: 10.1007/b138553 (cit. on p. 52).

[93] Javier Galego, Claudia Climent, Francisco J. Garcia-Vidal, and Johannes Feist. "Cavity Casimir-Polder Forces and Their Effects in Ground-State Chemical Reactivity." In: *Phys. Rev. X* 9 (June 2019), p. 021057. DOI: 10.1103/PhysRevX.9.021057 (cit. on p. 52).

[94] Nicholas Rivera, Johannes Flick, and Prineha Narang. "Variational Theory of Nonrelativistic Quantum Electrodynamics." In: *Phys. Rev. Lett.* 122 (May 2019), p. 193603. DOI: 10.1103/PhysRevLett.122.193603 (cit. on p. 52).

[95] Tosio Kato. *Perturbation Theory for Linear Operators*. Springer-Verlag Berlin Heidelberg, 1980. DOI: 10.1007/978-3-642-66282-9 (cit. on p. 52).

[96] Philippe Blanchard and Erwin Brüning. *Mathematical Methods in Physics*. Birkhäuser, 2003. URL: https://www.springer.com/de/book/9783319140445 (cit. on p. 52).

[97] Gerald Teschl. *Mathematical Methods in Quantum Mechanics: With Applications to Schrödinger Operators*. Vol. 157. American Mathematical Soc., 2014 (cit. on pp. 52, 54).

[98] I. I. Rabi. "Space Quantization in a Gyrating Magnetic Field." In: *Phys. Rev.* 51 (8 Apr. 1937), pp. 652–654. DOI: 10.1103/PhysRev.51.652 (cit. on pp. 53, 85).

[99] D. Braak. "Integrability of the Rabi Model." In: *Phys. Rev. Lett.* 107 (10 Aug. 2011), p. 100401. DOI: 10.1103/PhysRevLett.107.100401 (cit. on pp. 53, 85).

[100] Bruce W. Shore and Peter L. Knight. "The Jaynes-Cummings Model." In: *Journal of Modern Optics* 40.7 (1993), pp. 1195–1238. DOI: 10.1080/09500349314551321 (cit. on pp. 53, 85, 167).

[101] Barry M. Garraway. "The Dicke model in quantum optics: Dicke model revisited." In: *Philosophical Transactions of the Royal Society of London A: Mathematical, Physical and Engineering Sciences* 369.1939 (2011), pp. 1137–1155. ISSN: 1364-503X. DOI: 10.1098/rsta.2010.0333 (cit. on pp. 53, 85, 167).

[102] Christian Schäfer, Michael Ruggenthaler, Vasil Rokaj, and Angel Rubio. "Relevance of the Quadratic Diamagnetic and Self-Polarization Terms in Cavity Quantum Electrodynamics." In: *ACS Photonics* 7.4 (Feb. 2020), pp. 975–990. DOI: 10.1021/acsphotonics.9b01649 (cit. on pp. 55, 56, 118).

[103] H. Ehrenreich. "Electromagnetic transport in solids: optical properties and plasma effects." In: *The Optical Properties of Solids*. 1966, p. 106 (cit. on p. 69).

[104] W. Luis Mochán and Rubén G. Barrera. "Electromagnetic response of systems with spatial fluctuations. I. General formalism." In: *Phys. Rev. B* 32.8 (1985), p. 4984. DOI: 10.1103/PhysRevB.32.4984 (cit. on p. 69).

[105] Jeffery J. Maki, Michelle S. Malcuit, J. E. Sipe, and Robert W. Boyd. "Linear and nonlinear optical measurements of the Lorentz local field." In: *Phys. Rev. Lett.* 67.8 (1991), p. 972. DOI: 10.1103/PhysRevLett.67.972 (cit. on p. 69).

[106] Eleonora Luppi, Hannes Hübener, and Valérie Véniard. "Ab initio second-order nonlinear optics in solids: Second-harmonic generation spectroscopy from time-dependent density-functional theory." In: *Phys. Rev. B* 82 (23 Dec. 2010), p. 235201. DOI: 10.1103/PhysRevB.82.235201 (cit. on pp. 69, 71).

[107] A. Di Piazza, C. Müller, K. Z. Hatsagortsyan, and C. H. Keitel. "Extremely high-intensity laser interactions with fundamental quantum systems." In: *Rev. Mod. Phys.* 84.3 (2012), p. 1177. DOI: 10.1103/RevModPhys.84.1177 (cit. on p. 70).

[108] Ofer Firstenberg, Thibault Peyronel, Qi-Yu Liang, Alexey V. Gorshkov, Mikhail D. Lukin, and Vladan Vuletic. "Attractive photons in a quantum nonlinear medium." In: *Nature* 502.7469 (Sept. 2013), pp. 71–75. DOI: 10.1038/nature12512 (cit. on p. 71).

[109] R. Sternheimer. "On Nuclear Quadrupole Moments." In: *Phys. Rev.* 84 (2 Oct. 1951), pp. 244–253. DOI: 10.1103/PhysRev.84.244 (cit. on p. 77).

[110] Stefano Baroni, Paolo Giannozzi, and Andrea Testa. "Green's-function approach to linear response in solids." In: *Phys. Rev. Lett.* 58 (1987), p. 1861. DOI: 10.1103/PhysRevLett.58.1861 (cit. on p. 77).

[111] Stefano Baroni, Stefano de Gironcoli, Andrea Dal Corso, and Paolo Giannozzi. "Phonons and related crystal properties from density-functional perturbation theory." In: *Rev. Mod. Phys.* 73 (2 July 2001), pp. 515–562. DOI: 10.1103/RevModPhys.73.515 (cit. on p. 77).

[112] Feliciano Giustino, Marvin L. Cohen, and Steven G. Louie. "GW method with the self-consistent Sternheimer equation." In: *Phys. Rev. B* 81 (11 Mar. 2010), p. 115105. DOI: 10.1103/PhysRevB.81.115105 (cit. on p. 77).

[113] Hannes Hübener and Feliciano Giustino. "Time-dependent density-functional theory using atomic orbitals and the self-consistent Sternheimer equation." In: *Phys. Rev. B* 89 (2014), p. 085129. DOI: 10.1103/PhysRevB.89.085129 (cit. on p. 77).

[114] Hannes Hübener and Feliciano Giustino. "Linear optical response of finite systemsusing multishift linear system solvers." In: *J. Chem. Phys.* 141 (2014), p. 044117. DOI: 10.1063/1.4890736 (cit. on p. 77).

[115] G. Senatore and K. R. Subbaswamy. "Hyperpolarizabilities of closed-shell atoms and ions in the local-density approximation." In: *Phys. Rev. A* 34 (1986), p. 3619. DOI: 10.1103/PhysRevA.34.3619 (cit. on p. 77).

[116] J.-I. Iwata and K. Yabana. "Real-space computation of dynamic hyperpolarizabilities." In: *J. Chem. Phys.* 115 (2001), p. 8773. DOI: 10.1063/1.1411996 (cit. on p. 77).

[117] Fabian Hofmann, Ingo Schelter, and Stephan Kümmel. "Linear response time-dependent density functional theory without unoccupied states: The Kohn-Sham-Sternheimer scheme revisited." In: *J. Chem. Phys.* 149 (2018), p. 024105. DOI: 10.1063/1.5030652 (cit. on pp. 77, 80, 157).

[118] K. Yabana and G. F. Bertsch. "Application of the time-dependent local density approximation to optical activity." In: *Phys. Rev. A* 60 (1999), p. 1271. DOI: 10.1103/PhysRevA.60.1271 (cit. on pp. 80–82, 92).

[119] K. Yabana and G. F. Bertsch. "Time-dependent local-density approximation in real time." In: *Phys. Rev. B* 54 (1996), p. 4484. DOI: 10.1103/physrevb.54.4484 (cit. on pp. 80, 81).

[120] Miguel A. L. Marques, Alberto Castro, George F. Bertsch, and Angel Rubio. "Octopus: a first-principles tool for excited electron-ion dynamics." In: *Computer Physics Communications* 151.1 (2003), pp. 60 –78. ISSN: 0010-4655. DOI: 10.1016/S0010-4655(02)00686-0 (cit. on pp. 81–83, 163, 172).

[121] Xavier Andrade et al. "Real-space grids and the Octopus code as tools for the development of new simulation approaches for electronic systems." In: *Phys. Chem. Chem. Phys.* 17.47 (2015), pp. 31371–31396. DOI: 10.1039/C5CP00351B (cit. on pp. 81, 172).

[122] G. Malloci, C. Joblin, and G. Mulas. "On-line database of the spectral properties of polycyclic aromatic hydrocarbons." In: *Chem. Phys.* 332 (2007), pp. 353–359. DOI: 10.1016/j.chemphys.2007.01.001 (cit. on pp. 82, 90, 91, 164).

[123] A. Shalabney, J. George, J. Hutchison, G. Pupillo, C. Genet, and T. W. Ebbesen. "Coherent coupling of molecular resonators with a microcavity mode." In: *Nat. Commun.* 6 (Feb. 2015), p. 5981. DOI: 10.1038/ncomms6981 (cit. on p. 83).

[124] Jino George, Thibault Chervy, Atef Shalabney, Eloïse Devaux, Hidefumi Hiura, Cyriaque Genet, and Thomas W. Ebbesen. "Multiple Rabi Splittings under Ultrastrong Vibrational Coupling." In: *Phys. Rev. Lett.* 117 (15 Oct. 2016), p. 153601. DOI: 10.1103/PhysRevLett.117.153601 (cit. on p. 83).

[125] J. Q. You and Franco Nori. "Atomic physics and quantum optics using superconducting circuits." In: *Nature* 474 (June 2011), pp. 589–597. DOI: 10.1038/nature10122 (cit. on p. 85).

[126] I. Thanopulos, E. Paspalakis, and Z. Kisc. "Laser-driven coherent manipulation of molecular chirality." In: *Chem. Phys. Lett.* 390 (2004), pp. 228–235. DOI: 10.1016/j.cplett.2004.03.129 (cit. on p. 85).

[127] Tanja Dimitrov, Johannes Flick, Michael Ruggenthaler, and Angel Rubio. "Exact functionals for correlated electron-photon systems." In: *New J. Phys.* 19 (Sept. 2017), p. 113036. DOI: 10.1088/1367-2630/aa8f09 (cit. on p. 85).

[128] Pierre Meystre and Murray Sargent. *Elements of Quantum Optics*. Springer-Verlag Berlin Heidelberg, 2007. DOI: 10.1007/978-3-540-74211-1 (cit. on p. 86).

[129] G. Malloci, G. Mulas, and C. Joblin. "Electronic absorption spectra of PAHs up to vacuum UV." In: *Astron. Astrophys.* 426 (2004), pp. 105–117. DOI: 10.1051/0004-6361:20040541 (cit. on pp. 90, 91).

[130] K. Yabana, T. Nakatsukasa, J.-I. Iwata, and G. F. Bertsch. "Real-time, real-space implementation of the linear response time-dependent density-functional theory." In: *Phys. stat. sol. (b)* 243.5 (2006), pp. 1121–1138. DOI: 10.1002/pssb.200642005 (cit. on p. 92).

[131] Joaquim Jornet-Somoza and Irina Lebedeva. "Real-Time Propagation TDDFT and Density Analysis for Exciton Coupling Calculations in Large Systems." In: *J. Chem. Theory Comput.* 15 (2019), pp. 3743–3754. DOI: 10.1021/acs.jctc.9b00209 (cit. on p. 92).

[132] V. Weisskopf and E. Wigner. "Berechnung der natürlichen Linienbreite auf Grund der Diracschen Lichttheorie." In: *Zeitschrift für Physik* 63 (1930), pp. 54–73. DOI: 10.1007/BF01336768 (cit. on pp. 94, 95, 98).

[133] V. Buzek, G. Drobny, Min Gyu Kim, M. Havukainen, and P. L. Knight. "Numerical simulations of atomic decay in cavities and material media." In: *Phys. Rev. A* 60 (1 July 1999), pp. 582–592. DOI: 10.1103/PhysRevA.60.582 (cit. on p. 95).

[134] P. W. Milonni. "Semiclassical and quantum-electrodynamical approaches in nonrelativistic radiation theory." In: *Physics Reports* 25.1 (1976), pp. 1 –81. ISSN: 0370-1573. DOI: 10.1016/0370-1573(76)90037-5 (cit. on p. 95).

[135] Franz Mandl and Graham Shaw. *Quantum Field Theory*. Wiley, 2010 (cit. on p. 97).

[136] Rohit Chikkaraddy, Bart de Nijs, Felix Benz, Steven J. Barrow, Oren A. Scherman, Edina Rosta, Angela Demetriadou, Peter Fox, Ortwin Hess, and Jeremy J. Baumberg. "Single-molecule strong coupling at room temperature in plasmonic nanocavities." In: *Nature* 535.7610 (June 2016), pp. 127–130. DOI: 10.1038/nature17974 (cit. on p. 99).

[137] Ugo Fano. "Sullo spettro di assorbimento dei gas nobili presso il limite dello spettro d'arco." In: *Nuovo Cimento* 12 (1935), pp. 154–161. DOI: 10.1007/BF02958288 (cit. on p. 100).

[138] Christian Ott, Andreas Kaldun, Philipp Raith, Kristina Meyer, Martin Laux, Jörg Evers, Christoph H. Keitel, Chris H. Greene, and Thomas Pfeifer. "Lorentz Meets Fano in Spectral Line Shapes: A Universal Phase and Its Laser Control." In: *Science* 340.6133 (May 2013), pp. 716–720. DOI: 10.1126/science.1234407 (cit. on p. 100).

[139] Jeremy L. O'Brien, Akira Furusawa, and Jelena Vuckovic. "Photonic quantum technologies." In: *Nature Photon.* 3 (2009), pp. 687–695. DOI: 10.1038/nphoton.2009.229 (cit. on pp. 105, 138).

[140] Shi-Biao Zheng and Guang-Can Guo. "Efficient Scheme for Two-Atom Entanglement and Quantum Information Processing in Cavity QED." In: *Phys. Rev. Lett.* 85 (2000), p. 2392. DOI: 10.1103/PhysRevLett.85.2392 (cit. on pp. 105, 138).

[141] Thomas Jennewein, Christoph Simon, Gregor Weihs, Harald Weinfurter, and Anton Zeilinger. "Quantum cryptography with entangled photons." In: *Phys. Rev. Lett.* 84 (2000), p. 4729. DOI: 10.1103/PhysRevLett.84.4729 (cit. on p. 105).

[142] D. Boschi, S. Brancaa, F. De Martini, L. Hardy, and S. Popescu. "Experimental realization of teleporting an unknown pure quantum state via dual classical and Einstein-Podolsky-Rosen channels." In: *Phys. Rev. Lett.* 80 (1998), p. 1121. DOI: 10.1103/PhysRevLett.80.1121 (cit. on p. 105).

[143] Robert W. Boyd. *Nonlinear Optics*. Academic, New York, 1992. URL: https://www.elsevier.com/books/nonlinear-optics/boyd/978-0-12-369470-6 (cit. on p. 105).

[144] P. Evans, R. Bennink, W. Grice, T. Humble, and J. Schaake. "Bright Source of Spectrally UncorrelatedPolarization-Entangled Photons with Nearly Single-Mode Emission." In: *Phys. Rev. Lett.* 105 (2010), p. 253601. DOI: 10.1103/PhysRevLett.105.253601 (cit. on p. 105).

[145] N. Bruno, A. Martin, T. Guerreiro, B. Sanguinetti, and R. T. Thew. "Pulsed source of spectrally uncorrelatedand indistinguishable photons at telecomwavelengths." In: *Opt. Express* 22 (2014), p. 17246. DOI: 10.1364/OE.22.017246 (cit. on p. 105).

[146] N. Akopian, N. H. Lindner, E. Poem, Y. Berlatzky, J. Avron, D. Gershoni, B. D. Gerardot, and P. M. Petroff. "Entangled photon pairs from semiconductor quantum dots." In: *Phys. Rev. Lett.* 96 (Apr. 2006), p. 130501. DOI: 10.1103/PhysRevLett.96.130501 (cit. on p. 105).

[147] P. K. Pathak and S. Hughes. "Coherent generation of time-bin entangled photon pairs using the biexciton cascade and cavity-assisted piecewise adiabatic passage." In: *Phys. Rev. B* 83 (2011), p. 245301. DOI: 10.1103/PhysRevB.83.245301 (cit. on p. 105).

[148] Adrien Dousse, Jan Suffczynski, Alexios Beveratos, Olivier Krebs, Aristide Lemaitre, Isabelle Sagnes, Jacqueline Bloch, Paul Voisin, and Pascale Senellart. "Ultrabright source of entangled photon pairs." In: *Nature* 466 (2019), pp. 217–220. DOI: 10.1038/nature09148 (cit. on pp. 105, 121).

[149] M. Müller, S. Bounouar, K. D. Jöns, M. Glässl, and P. Michler. "On-demand generation of indistinguishable polarization-entangled photon pairs." In: *Nat. Photonics* 8 (2014), pp. 224–228. DOI: 10.1038/nphoton.2013.377 (cit. on pp. 105, 121).

[150] Juan B. Pérez-Sánchez and Joel Yuen-Zhou. "Polariton Assisted Down-Conversion of Photons via Nonadiabatic Molecular Dynamics: A Molecular Dynamical Casimir Effect." In: *J. Phys. Chem. Lett.* 11.1 (2020), pp. 152–159. DOI: 10.1021/acs.jpclett.9b02870 (cit. on p. 105).

[151] Baleegh Abdo, Katrina Sliwa, Flavius Schackert, Nicolas Bergeal, Michael Hatridge, Luigi Frunzio, A. Douglas Stone, and Michel Devoret. "Full Coherent Frequency Conversion between Two Propagating Microwave Modes." In: *Phys. Rev. Lett.* 110 (Apr. 2013), p. 173902. DOI: 10.1103/PhysRevLett.110.173902 (cit. on p. 105).

[152] Archana Kamal, Ananda Roy, John Clarke, and Michel H. Devoret. "Asymmetric Frequency Conversion in Nonlinear Systems Driven by a Biharmonic Pump." In: *Phys. Rev. Lett.* 113 (2014), p. 247003. DOI: 10.1103/PhysRevLett.113.247003 (cit. on p. 105).

[153] Christophe Couteau. "Spontaneous parametric down-conversion." In: *Contemporary Physics* 59.3 (Mar. 2018), pp. 291–304. DOI: 10.1080/00107514.2018.1488463 (cit. on pp. 105, 127).

[154] E. Sánchez-Burillo, L. Martín-Moreno, J. J. Garcia-Ripoll, and D. Zueco. "Full two-photon down-conversion of a single photon." In: *Phys. Rev. A.* 94 (2016), p. 053814. DOI: 10.1103/PhysRevA.94.053814 (cit. on pp. 105, 114).

[155] Yue Chang, Alejandro González-Tudela, Carlos Sánchez Munoz, Carlos Navarrete-Benlloch, and Tao Shi. "Deterministic Down-Converter and Continuous Photon-Pair Source within the Bad-Cavity Limit." In: *Phys. Rev. Lett.* 117 (2016), p. 203602. DOI: 10.1103/PhysRevLett.117.203602 (cit. on pp. 105, 114, 123).

[156] Anton Frisk Kockum, Vincenzo Macri, Luigi Garziano, Salvatore Savasta, and Franco Nori. "Frequency conversion in ultrastrong cavity QED." In: *Scientific Reports* 7 (2017), p. 5313. DOI: 10.1038/s41598-017-04225-3 (cit. on pp. 105, 126).

[157] C. J. Villas-Boas, N. G. de Almeida, R. M. Serra, and M. H. Y. Moussa. "Squeezing arbitrary cavity-field states through their interaction with a single driven atom." In: *Phys. Rev. A* 68 (2003), 061801(R). DOI: 10.1103/PhysRevA.68.061801 (cit. on p. 105).

[158] R. M. Serra, C. J. Villas-Boas, N. G. de Almeida, and M. H. Y. Moussa. "Frequency up- and down-conversions in two-mode cavity quantum electrodynamics." In: *Phys. Rev. A* 71 (2005), p. 045802. DOI: 10.1103/PhysRevA.71.045802 (cit. on p. 105).

[159] Carlos M. Duque, Miguel E. Mora-Ramos, and Carlos A. Duque. "Quantum disc plus inverse square potential. An analytical model for two-dimensional quantum rings: Study of nonlinear optical properties." In: *Ann. Phys.* 524.6-7 (July 2012), pp. 327–337. DOI: 10.1002/andp.201200055 (cit. on pp. 106, 110, 126).

[160] E. Räsänen, A. Castro, J. Werschnik, A. Rubio, and E. K. U. Gross. "Optimal Control of Quantum Rings by Terahertz Laser Pulses." In: *Phys. Rev. Lett.* 98 (15 Apr. 2007), p. 157404. DOI: 10.1103/PhysRevLett.98.157404 (cit. on pp. 106, 108, 109).

[161] Vladimir M. Fomin. *Physics of Quantum Rings*. Springer-Verlag Berlin Heidelberg, 2018. DOI: 10.1007/978-3-642-39197-2 (cit. on pp. 106–108, 110, 116).

[162] M. Abbarchi, C. A. Mastrandrea, A. Vinattieri, S. Sanguinetti, T. Mano, T. Kuroda, N. Koguchi, K. Sakoda, and M. Gurioli. "Photon antibunching in double quantum ring structures." In: *Phys. Rev. B* 79 (2009), p. 085308. DOI: 10.1103/PhysRevB.79.085308 (cit. on p. 106).

[163] Davis M. Welakuh, Michael Ruggenthaler, Mary-Leena M. Tchenkoue, Heiko Appel, and Angel Rubio. "Down-conversion processes in ab-initio non-relativistic quantum electrodynamics." In: *arxiv* (2021) (cit. on p. 106).

[164] Nicolai F. Hartmann, Matthew Otten, Igor Fedin, Dmitri Talapin, Moritz Cygorek, Pawel Hawrylak, Marek Korkusinski, Stephen Gray, Achim Hartschuh, and Xuedan Ma. "Uniaxial transition dipole moments in semiconductor quantum rings caused by broken rotational symmetry." In: *Nat. Commun.* 10 (2019), p. 3253. DOI: 10.1038/s41467-019-11225-6 (cit. on pp. 107, 110).

[165] A. Fuhrer, S. Lüscher, T. Ihn, T. Heinzel, K. Ensslin, W. Wegscheider, and M. Bichler. "Energy spectra of quantum rings." In: *Nature* 413 (2001), pp. 822–825. DOI: 10.1038/35101552 (cit. on p. 107).

[166] Thomas Ihn, Andreas Fuhrer, Lorenz Meier, Martin Sigrist, and Klaus Ensslin. "Quantum physics in quantum rings." In: *Europhysics News* 36.3 (2005), pp. 78–71. DOI: 10.1051/epn:2005302 (cit. on p. 107).

[167] J. A. Vinasco, A. Radu, E. Kasapoglu, R. L. Restrepo, A. L. Morales, E. Feddi, M. E. Mora-Ramos, and C. A. Duque. "Effects of Geometry on the Electronic Properties of Semiconductor Elliptical Quantum Rings." In: *Scientific Reports* 8 (2018), p. 13299. DOI: 10.1038/s41598-018-31512-4 (cit. on p. 110).

[168] Marlis Hochbruck and Christian Lubich. "On Krylov subspace approximations to the matrix exponential operator." In: *SIAM J. Numer. Anal.* 34 (1997), pp. 1911–1925. DOI: 10.1137/S0036142995280572 (cit. on p. 113).

[169] L. Mandel. "Sub-Poissonian photon statistics in resonance fluorescence." In: *Opt. Lett.* 4.7 (July 1979), pp. 205–207. DOI: 10.1364/OL.4.000205 (cit. on pp. 113, 137).

[170] J. K. Kalaga, A. Kowalewska-Kudlaszyk, W. Leonski, and A. Barasinski. "Quantum correlations and entanglement in a model comprised of a short chain of nonlinear oscillators." In: *Phys. Rev. A* 94 (2016), p. 032304. DOI: 10.1103/PhysRevA.94.032304 (cit. on p. 114).

[171] P. Bocchieri and A. Loinger. "Quantum Recurrence Theorem." In: *Phys. Rev.* 107 (1957), p. 337. DOI: 10.1103/PhysRev.107.337 (cit. on p. 116).

[172] Heinz-Peter Breuer and Francesco Petruccione. *The Theory of Open Quantum Systems*. Oxford University Press, 2007. DOI: 10.1093/acprof:oso/9780199213900.001.0001 (cit. on p. 116).

[173] Ashok Muthukrishnan, Girish S. Agarwal, and Marlan O. Scully. "Inducing Disallowed Two-Atom Transitions with Temporally Entangled Photons." In: *Phys. Rev. Lett.* 93 (2004), p. 093002. DOI: 10.1103/PhysRevLett.93.093002 (cit. on p. 121).

[174] Yu xi Liu, J. Q. You, L. F. Wei, C. P. Sun, and Franco Nori. "Optical Selection Rules and Phase-Dependent Adiabatic State Controlin a Superconducting Quantum Circuit." In: *Phys. Rev. Lett.* 95 (2005), p. 087001. DOI: 10.1103/PhysRevLett.95.087001 (cit. on p. 123).

[175] Yu xi Liu, Hui-Chen Sun, Z. H. Peng, Adam Miranowicz, J. S. Tsai, and Franco Nori. "Controllable microwave three-wavemixing via a single three-levelsuperconducting quantum circuit." In: *Scientific Reports* 4 (2014), p. 7289. DOI: 10.1038/srep07289 (cit. on p. 123).

[176] Omar Di Stefano, Alessio Settineri, Vincenzo Macrì, Luigi Garziano, Roberto Stassi, Salvatore Savasta, and Franco Nori. "Resolution of gauge ambiguities in ultrastrong-coupling cavity quantum electrodynamics." In: *Nature Physics* 15 (2019), pp. 803–808. DOI: 10.1038/s41567-019-0534-4 (cit. on pp. 125, 126).

[177] C. Sánchez Munoz, E. del Valle, A. González Tudela, K. Müller, S. Lichtmannecker, M. Kaniber, C. Tejedor, J. J. Finley, and F. P. Laussy. "Emitters of N-photon bundles." In: *Nature Photonics* 8 (June 2014), pp. 550–555. DOI: 10.1038/nphoton.2014.114 (cit. on pp. 134, 137, 150).

[178] G. Callsen et al. "Noncommutative q-photon-added coherent states." In: *Phys. Rev. A* 93 (2016), p. 053824. DOI: 10.1103/PhysRevA.93.053824 (cit. on p. 137).

[179] C.W. Sandbo Chang, Carlos Sabín, P. Forn-Diaz, Fernando Quijandria, A.M. Vadiraj, I. Nsanzineza, G. Johansson, and C.M. Wilson. "Observation of Three-Photon Spontaneous Parametric Down-Conversion in a Superconducting Parametric Cavity." In: *Phys. Rev. X* 10 (2020), p. 011011. DOI: 10.1103/PhysRevX.10.011011 (cit. on pp. 138, 143).

[180] Sascha Agne, Thomas Kauten, Jeongwan Jin, Evan Meyer-Scott, and Jeff Z. Salvail. "Observation of Genuine Three-Photon Interference." In: *Phys. Rev. Lett.* 118 (Apr. 2017), p. 153602. DOI: 10.1103/PhysRevLett.118.153602 (cit. on pp. 139, 144).

[181] Deny R. Hamel, Lynden K. Shalm, Hannes Hübel, Aaron J. Miller, Francesco Marsili, Varun B. Verma, Richard P. Mirin, Sae Woo Nam, Kevin J. Resch, and Thomas Jennewein. "Direct generation of three-photon polarization entanglement." In: *Nature Photonics* 8 (2014), pp. 80–807. DOI: 10.1038/nphoton.2014.218 (cit. on pp. 139, 140, 144).

[182] Hannes Hübel, Deny R. Hamel, Alessandro Fedrizzi, Sven Ramelow, Kevin J. Resch, and Thomas Jennewein. "Direct generation of photon triplets using cascaded photon-pair sources." In: *Nature* 466 (2010), pp. 466, DOI: 10.1038/nature09175 (cit. on pp. 139, 144).

[183] L. K. Shalm, D. R. Hamel, Z. Yan, C. Simon, K. J. Resch, and T. Jennewein. "Three-photon energy-time entanglement." In: *Nature Physics* 9 (Nov. 2013), pp. 19–22. DOI: 10.1038/nphys2492 (cit. on p. 139).

[184] Sergei Slussarenko and Geoff J. Pryde. "Photonic quantum information processing: A concise review." In: *Appl. Phys. Rev* 6.4 (Oct. 2019), p. 041303. DOI: 10.1063/1.5115814 (cit. on p. 144).

[185] Milad Khoshnegar et al. "A solid state source of photon triplets basedon quantum dot molecules." In: *Nat. Commun.* 8 (2017), p. 15716. DOI: 10.1038/ncomms15716 (cit. on p. 144).

[186] J. Persson, T. Aichele, V. Zwiller, L. Samuelson, and O. Benson. "Three-photon cascade from single self-assembled InP quantum dots." In: *Phys. Rev. B* 69 (2004), p. 233314. DOI: 10.1103/PhysRevB.69.233314 (cit. on p. 144).

[187] Anoop Thomas et al. "Ground-State Chemical Reactivity under Vibrational Coupling to the Vacuum Electromagnetic Field." In: *Angewandte Chemie International Edition* 55.38 (2016), pp. 11462–11466. ISSN: 1521-3773. DOI: 10.1002/anie.201605504 (cit. on p. 151).

[188] N. Troullier and José L. Martins. "Efficient pseudopotentials for plane-wave calculations." In: *Phys. Rev. B* 43 (3 Jan. 1991), pp. 1993–2006. DOI: 10.1103/PhysRevB.43.1993 (cit. on pp. 163, 164).

[189] Paul Cowper, Adam Pockett, Gabriele Kociok-Köhn, Petra J.Cameron, and Simon E. Lewis. "Azulene-Thiophene-Cyanoacrylic acid dyes with donor-π-acceptor structures. Synthesis, characterisation and evaluation in dye-sensitized solar cells." In: *Tetrahedron* 4.22 (2018), pp. 2775–2786. DOI: 10.1016/j.tet.2018.04.043 (cit. on p. 164).

[190] G. Malloci, G. Mulas, G. Cappellini, V. Fiorentini, and I. Porceddu. "Theoretical electron affinities of PAHs and electronic absorption spectra of their mono-anions." In: *Astron. Astrophys.* 432 (2005), pp. 585–594. DOI: 10.1051/0004-6361:20042246 (cit. on p. 164).

[191] Michael Tavis and Frederick W. Cummings. "Exact Solution for an N-Molecule–Radiation-Field Hamiltonian." In: *Phys. Rev.* 170 (June 1968), pp. 379–384. DOI: 10.1103/PhysRev.170.379 (cit. on p. 167).

[192] R. H. Dicke. "Coherence in Spontaneous Radiation Processes." In: *Phys. Rev.* 93 (Jan. 1954), p. 99. DOI: 10.1103/PhysRev.93.99 (cit. on p. 167).

[193] Kwang Jun Ahn. "Temporal dynamics of zero-delay second order correlation function and spectral entanglement of two photons emitted from ladder-type atomic three-level systems." In: *Optics Express* 28.2 (Jan. 2020), pp. 1790–1804. DOI: 10.1364/OE.382498 (cit. on p. 168).

[194] Christian Schäfer, Michael Ruggenthaler, Heiko Appel, and Angel Rubio. "Modification of excitation and charge transfer in cavity quantum-electrodynamical chemistry." In: *PNAS* 116.11 (Mar. 2019), pp. 4883–4892. DOI: 10.1073/pnas.1814178116 (cit. on p. 168).

[195] Florian Buchholz, Iris Theophilou, S. E. B. Nielsen, Michael Ruggenthaler, and Angel Rubio. "Reduced Density-Matrix Approach to Strong Matter-Photon Interaction." In: *ACS Photonics* 11 (2019), p. 2694. DOI: 10.1021/acsphotonics.9b00648 (cit. on p. 168).

LIST OF FIGURES

LIST OF TABLES

LIST OF ACRONYMS

ALDA adiabatic local-density approximation

DFT density-functional theory

ELPA Eigenvalue SoLvers for Petaflop-Applications

EOM equation of motion

GaAs gallium arsenide

HEG homogeneous electron gas

HK Hohenberg-Kohn

Hxc Hartree exchange-correlation

KS Kohn-Sham

LDA local-density approximation

Mxc mean-field exchange-correlation

OEP optimized effective potential

PDC parametric down-conversion

pRPA photon random-phase approximation

QED quantum electrodynamics

QED-CC quantum electrodynamics coupled cluster theory

QEDFT quantum electrodynamical density-functional theory

QR quantum ring

RG Runge-Gross

RWA rotating-wave approximation

TDDFT time-dependent density-functional theory

xc exchange-correlation

LIST OF PUBLICATIONS

The following publications are part of this thesis:

[1] Vasil Rokaj, Davis M. Welakuh, Michael Ruggenthaler and Angel Rubio. *Light-matter interaction in the long-wavelength limit: no ground-state without dipole self-energy*, J. Phys. B: At. Mol. Opt. Phys. **51**, 034005 (2018) doi:10.1088/1361-6455/aa9c99 .

[2] Johannes Flick, Davis M. Welakuh, Michael Ruggenthaler, Heiko Appel and Angel Rubio. *Light-Matter Response in Nonrelativistic Quantum Electrodynamics*, ACS Photonics 6, 11, 2757-2778 doi:10.1021/acsphotonics.9b00768.

[3] Davis M. Welakuh, Michael Ruggenthaler, Mary-Leena M. Tchenkoue, Heiko Appel and Angel Rubio. *Down-conversion processes in ab-initio non-relativistic quantum electrodynamics*, Submitted to Physical Review Research. arXiv:2103.06947.

[4] Davis M. Welakuh, Michael Ruggenthaler, Heiko Appel and Angel Rubio. *Inverse (high-) harmonic generation in non-relativistic quantum electrodynamics*, In preparation.

[5] Davis M. Welakuh, Johannes Flick, Heiko Appel, Michael Ruggenthaler and Angel Rubio. *Frequency-dependent Sternheimer linear-response formalism for light-matter coupled systems*, In preparation.

LIST OF TALKS AND POSTERS AT CONFERENCES

List of talks presented at conferences:

[1] The APS March Meeting
Boston, Massachusetts USA, March 2019

[2] Mini-symposium: Extensions to DFT
Amsterdam, Netherlands July 2018

[3] The 15th ETSF Young Researchers' Meeting
Hamburg, Germany, June 2018

[4] The APS March Meeting
Los Angeles, California USA, March 2018

[5] IMPRS-UFAST Candidate Workshop
Hamburg, Germany, April 2016

List of posters presented at conferences:

[1] Scientific Advisory Board Meeting
Hamburg, Germany, January 2019

[2] XXV International Summer School "Nicolas Cabrera"
Miraflores de la Sierra, Madrid, Spain, September 2018

[3] Strong Coupling with Organic Molecules (SCOM)
Eindhoven, Netherlands, April 2018

ACKNOWLEDGMENTS

This work is a collaborative effort, and I will like to thank the people involved for their assistance and encouragement throughout my PhD graduate program. First and foremost, I would like to thank my advisor, Angel Rubio for his support and guidance in my work, his insight into physical problems, and his enthusiasm for scientific work. I also want to thank him for giving me so many opportunities to grow as an academic, sending me to conferences early and often. I'm grateful to have been in his group from which I gained much needed experiences and skills. Secondly, I will like to immensely thank Michael Ruggenthaler and Heiko Appel for having guided me in the theoretical and computational aspect, respectively, that was needed to bring this thesis to fruition. The time Michael put into teaching me DFT, TDDFT and QEDFT to name a few was a great experience as well as the time Heiko put into advancing my computing skills to what it is today is something I'll always carry on. I'm grateful for the skills I learned from both of you.

Also, I want thank Johannes Flick for the much needed scientific discussion through weekly Zoom meetings and exchange of ideas and collaboration. Much thanks goes to Sebastian Ohlmann not only for the help with the efficient massive parallel implementation of our LIBQED code and OCTOPUS electron-photon Casida, but also for his patients to walk me through the problems I faced with OCTOPUS on the clusters. Also, I will like to thank Nicolas Tancogne-Dejean, Arunangshu Debnath and Florian Buchholz for fruitful scientific discussions. Thanks also goes to Vasil Rokaj for our many scientific discussions and also for out of science activities, discussions, get-together on planned social events which were all the time full of fun. Along the same lines, thanks goes to Mary-Leena Tchenkoue for all the discussions and remembrance of home and experiences we have shared. It was quite a long and enjoyable experience. Vasil Rokaj together with my office mates Fabio Covito and Gabriel Topp made the PhD program experience the most fun with our time-to-time kicker and soccer games to take our minds off scientific thoughts, for this, I am grateful.

In addition, I will like to thank all the members of the Theory Department, IMPRS throughout my time at the MPSD who helped me one way or the other. Your time, assistance and advice no doubt helped me in some way to during my PhD program.

Finally, I want to thank my family Andrew Welakuh, Edna Welakuh, Carolin Perkuhn, Petronilla Fruasaha, John T. Ndefru and the rest of my family for all the love and support given to me throughout my PhD program.

COLOPHON

This document was typeset using `classicthesis`.
The plots have been created using python 2.7.13. with matplotlib and SciPy, GIMP, and EdrawMax

Final Version as of June 14, 2021 .